THE UNIVERSITY *of* EDINBURGH

Anti-inflammatory mechanisms of the neutrophil-released antimicrobial peptide α-defensins

Gareth Hugh Tomlinson

PhD

The University of Edinburgh

2014

Abstract

Tissue homeostasis is necessary for optimal organ functioning. The onset of tissue trauma compromises the homeostatic environment resulting in widespread cell death with the likelihood of exposure to invading micro-organisms. Early stage elimination of microbes and immunomodulation is co-ordinated by leukocytes of the innate immune system of which neutrophils and macrophages play a pivotal role. Leukocyte-released pro-inflammatory factors are vital in the containment of infection but bring with it a degree of collateral tissue destruction. Thus cascading stages during inflammation must be tightly regulated to bring about timely tissue regeneration and regained homeostasis. However, chronic inflammatory diseases e.g. rheumatoid arthritis highlights the existence of defective regulation at numerous stages during this transition, often leading to debilitating disease progression.

Recently published findings by our research group identified the anti-inflammatory properties of α-defensin - an anti-microbial peptide released from dying human neutrophils - on stimulated macrophages. Thus the main objective of my research was to gain an understanding into the molecular actions of α-defensins which inhibit the macrophage inflammatory potential. Strong evidence supported the propensity of α-defensins to inhibit both intracellular and secreted protein synthesis, as assessed by *de novo* ^{35}S-radiolabeled Methionine incorporation. Inhibition was not attributed to endoplasmic reticulum stress events, a common diagnosis in the regulation of global translation. Supporting evidence using cell-free systems identified a fundamental block in translation with the inclusion of α-defensin. Biochemical studies linked the ability of α-defensin to bind non-specifically to oligonucleotide sequences. This binding potential was also demonstrated on ribosomal RNA (rRNA), impeding its migration through electrophoretic gels. Immunocytochemical assays proposed an emerging suggestion of α-defensins in macrophages concentrated in close proximity to ribosomes around the perinuclear region. Evidence of suggested defensin/ribosome accumulation after 24hrs after treatment were attempted but to date remained unconfirmed. Attempts to determine the fate of these proposed accumulations were inconclusive, assessed by autophagy assays and ribosome semi-quantitation.

This thesis describes for the first time an enhanced understanding into the intracellular inhibitory mechanisms of α-defensins on macrophages and possibly other cell types. Understanding the molecular impact of α-defensins provide key insights into this novel inflammatory regulator, with the potential to be utilized in future immunotherapies.

Declaration

This thesis has been solely composed by myself and comprises my own original research, except where explicitly acknowledged in the text. No part of this work has been submitted for any other degree or professional qualification.

Date: 18 September, 2013 _____

Gareth Hugh Tomlinson

Acknowledgements

I would like to thank Dr Mohini Gray for her advice, support and encouragement during my years of study. I would also like to thank my second supervisor, Professor Adriano Rossi, for his supportive role of catch-up meetings, help with designing the calcium assays, proofreading this thesis and our general corridor conversations to check on my progress. I am most grateful for your time and advice.

A huge thank you goes to Dr Matthew Brook for his boundless time, input and commitment into helping me make this exciting project realise its potential. His 'big brother' role in the laboratory was immensely insightful and I have gained a great deal of knowledge and expertise in all things molecular biology. The same gratitude goes to Matt's colleague, Dr Richard Smith, again for providing a solid support base for the most technical aspects of this project. Their collaborative help, along with Dr Nicola Gray, was invaluable to the progress of this research.

This project would not have been possible without access to synthetic α-defensins, and for this I am extremely indebted to Professor Wuyuan Lu (University of Baltimore). I would also like to thank Katherine Miles for her sound advice with α-defensin experiments since she brought the project to the point where my research began. I would like to thank Professor Pieter Hiemstra and Emily van't Wout for their help with the ER stress data, and Drs Andrew Childs and Hazel Kinnel for their assistance with qPCR. A big thank you goes to Jana Ovciarikova for her huge effort and commitment during her Masters project dealing with autophagy, and Dr Kanchan Phadwal for her expertise on this topic as well.

Finally, I would not be in this position today if it were not for those who never stopped believing in me, no matter where it took me and no matter how many more thousands of miles came between us. To my dear family in South Africa, especially my loving parents, Frances and Gerald Tomlinson; words are not enough to express my gratitude for your guidance and values that make me the person that I am today. To my sister and brother, Melissa and Darren, having you both in Scotland

supporting me has been just the best thing a brother could ask for while undertaking something as important to me as this PhD. And to my fiancée, Ana-Maria Banu; you were the person that I confided in after a long day (and often evenings) at the lab. Your support never failed me, it never let me down, and always made me determined to keep pursuing my goals and dreams. You are the person that I can always count on and I look forward to our life together in Toronto.

Contents

Page

Abbreviations

^{35}S-Met	^{35}S-radiolabeled methionine
β-gal	β-galactosidase
BiP	Immunoglobulin binding protein
BMDMs	Bone marrow-derived macrophages
Ca^{2+}	Calcium ions
CHOP	C/EBP-homologous protein
CI	CD40L/IFN-γ
DAPI	(4′,6-Diamidino-2-phenylindole dihydrochloride)
EGTA	(Ethylene glycol-bis(2-aminoethylether)-*N,N,N',N'*-tetraacetic acid)
eIF	Eukaryotic initiation factor
EMSA	Electrophoretic mobility shift assay
GDP	Guanosine diphosphate
GTP	Guanosine triphosphate
HMDMs	Human monocyte-derived macrophages
HNP	Human Neutrophil Peptide
IFN-γ	Interferon gamma
IL	Interleukin
IP	Immunoprecipitation
kDa	Kilodalton
LC3B	Microtubule-associate protein light chain 3 beta
LHNP	Linearized Human Neutrophil Peptide
LPS	Lipopolysaccharide
Luc	Luciferase
m7G	m7G (5')ppp(5')G RNA cap structure
Me-Ile20-HNP	Methylated isoleucine residue 20-HNP
mRNA	Messenger ribonucleic acid
NN	Necrotic neutrophils supernatant
PABP1	Poly(A)-binding protein 1
PBMCs	Peripheral blood mononuclear cells
PMNs	Polymorphonuclear leukocytes
pmol	Picomole
Poly A	Adenine oligonucleotide
Poly C	Cysteine oligonucleotide
Poly U	Uracil oligonucleotide
RNA	Ribonucleic acid
rps20	Ribosomal protein S20
rRNA	ribosomal ribonucleic acid
SAC	*Staphylococcus aureus* Cowan strain
SDS-PAGE	Sodium dodecyl sulphate polyacrylamide gel electrophoresis
TG	Thapsigargin
TNF-α	Tumour necrosis factor alpha
W26A	HNP1 analogue; alanine-substituted for tryptophan at residue 26

XBP-1	X-box binding protein 1

List of Tables

List of Figures

Appendix Figures

Chapter 1

1 Introduction

Inflammation regulation is critical to tissue homeostasis within an organism. Functioning as a defensive mechanism to combat the invasion of various pathogens that bridge the epithelial barrier upon tissue trauma, inflammation is the host's first line of defence in eliminating potentially fatal infections. The complex inflammatory cascade is a series of stages, triggers, stop signals, go signals, all being orchestrated in very tight time constraints. Premature inflammation termination might leave the host susceptible to lingering infection with the risk of sepsis. The prolonging of inflammation brings with it the risk of extensive tissue damage with possible organ failure. It is imperative to the host that this delicate balance remains tightly regulated.

The many examples of chronic inflammatory disorders in humans are testament to the need for tight regulation as persistent inflammatory events can indeed cause greater harm than the initial triggering event itself[1]. Current trends in inflammation research aim to gain a better understanding of the intricacies surrounding the inflammatory pathway to identify key regulators, which could serve as potential new therapies. This need is particularly applicable to autoimmune disease research. In many instances the cause for disease onset is poorly understood while costs to governmental health services continue to escalate. For example, estimates show costs to the UK's NHS in alleviating symptoms of rheumatoid arthritis amount to £560 million annually (correct as of 2009)[2].

While scientific research continues to further understand disease onset and progression, new therapeutics are continuously being researched and developed to replace ineffective or costly treatments, or those with long term side effects. Identifying new modulators of inflammation that can supersede current treatment is pivotal to the improvement of human health care.

1.1 Inflammation during injury

Innate immunity forms the first line of defence

The role of the innate immune system is crucial to host survival. This is evident in the fact that even simpler life forms possess an innate immune system in one form or another. Innate immunity is a system designed to discriminate species self from infectious nonself[3], and serves as an initial pathogen recognition, response and elimination system comprised of modulatory cells and proteins. In evolutionary terms, it can thus be appreciated that the inclusion or adaptation to elicit some form of host response to invading microbes was essential to species survival. As a result, it is no surprise that innate host defence in vertebrates is generally a well conserved response system[4].

In mammals, initial detection of foreign invaders is by localised tissue-resident sentinel cells, mainly mast cells and macrophages. Recognition of characteristic pathogen components known as Pathogen Associated Molecular Patterns (PAMPs) include bacterial products such as the cell membrane endotoxin lipopolysaccharide (LPS), flagellin, lipoteichoic acid, and peptidoglycan. Viral products such double stranded RNA (dsRNA) or unmethylated CpG motifs are also recognized within the infected cell through intracellular PAMPs[5]. In addition, sites of tissue trauma will result in the unregulated dying of cells (necrosis), releasing Danger Associated Molecular Patterns (DAMPS) into the extracellular matrix. These include heat shock proteins, DNA, RNA, HMGB1 (high mobility group box 1) and purine metabolites[6,7]. Sentinel cells detect these various stimuli through a variety of outer membrane and intracellular Pattern Recognition Receptors (PRRs), including the family of Toll-Like Receptors (TLRs)[3]. These recognition patterns will activate a complex network of cell transduction pathways, activating transcription factors resulting in the synthesis and secretion of a multitude of defence molecules and cytokines which act as cell activators and chemoattractants (chemokines)[8]. The main function of released chemoattractants is in orchestration of the inflammatory response cascade, which will result in enhanced infiltration of activated leukocytes as further reinforcement. Neutrophils are regarded as the foot soldiers of the immune system, which are one of the earliest arriving leukocytes to further the counter-offensive[9].

Neutrophils are essential inflammatory cells

Mature neutrophils are developed over 10-14 days in the bone marrow from multipotent progenitor cells by the process of granulopoiesis[10]. These polymorphonuclear leukocytes (PMNs) are released into the bloodstream where they circulate under a resting phase in the absence of extracellular stimuli for 1-5 days before undergoing programmed cell death known as apoptosis[11]. Early pathogen detection by mast cells releases neutrophil activating and recruiting factors histamine and eicosanoids (e.g. leukotrienes and prostaglandin D2)[1]. Activated macrophages meanwhile secrete neutrophil activating and recruitment factors such as tumour necrosis factor (TNF), GM-CSF (granulocyte macrophage colony-stimulating factor) and interleukin (IL)-8. Subsequently, increased amounts of neutrophils are released from the bone marrow while the endothelium near sites of local inflammation become leaky to fluid as well as sticky for leukocytes, facilitated by increased expression of leukocyte-endothelial cell adhesion molecules[12,13]. As a result, rolling neutrophils (and other leukocytes) are tethered to the endothelial barrier, then tightly adhere and subsequently enter the tissues through the process of diapedesis.

Activated neutrophils undergo degranulation and massive respiratory burst and begin to actively phagocytose microorgansims, the rate of which is enhanced by opsonisation of particles by immunoglobulins or complement fragments[14-16]. Foreign particles sequestered in phagosomes are eliminated by activated products of neutrophil respiratory burst. This includes killing by oxidants (e.g. hydrogen peroxide, hypohalites and chloramines), mediated through the opening of intracellular ion channels as well as the activation NADPH oxidase to generate the production of these oxidative compounds collectively known as ROS (Reactive Oxygen Species)[1].

In addition to oxidative killing mechanisms, neutrophils release an arsenal of antimicrobial proteins that are harboured with four types of storage granules. These granules develop during maturation within the bone marrow with each granule protein facilitating a specific antimicrobial function[16]. The first of these granules are the azurophil granules, which consist of Azurocidin, α-defensins (cationic

antimicrobial peptides) and the serine proteases Cathepsin G, Elastase and Proteinase 3. These agents have a direct impact in the killing and digestion of pathogens when the azurophil granules fuse with phagosomes[12]. In addition, specific granules contain the Cathelicidin LL37/hCAP18 cationic peptide, which in addition to having direct microbicidal activity against a broad spectrum of pathogens, serves to activate both neutrophils and monocytes[17,18]. They also act as chemoattractants to neutrophils, monocytes and T cells through interactions with a PRR known as formyl peptide receptor-like 1 (FPRL1)[19].

Furthermore specific (secondary) granules contain Pentraxin 3 (PTX3) which possess opsonin-like activity[20], and Lactoferrin, which when released upon cell apoptosis, selectively inhibits granulocyte migration through interaction with cell adhesion and motility signalling pathways[21]. Lastly, gelatinase granules contain Arginase I which undergo exocytosis when activated by azurophil contents and act to suppress the immune response by inhibiting T cell proliferation[22]. As powerful as neutrophil respiratory burst is at eliminating pathogens, these released products contribute extensively to the destruction of surrounding tissue. This is deemed a necessary collateral damage for overall host survival but does require very tight regulation.

In addition to this function, neutrophils play an integral part in shaping the extracellular matrix by acting as paracrine modulators. Before the 1990s the paradigm existed that neutrophils were terminally differentiated cells with minimal protein synthesis, having synthesized a complete set of required proteins during maturation within the bone marrow. Subsequently, studies now show that activated neutrophils are indeed effectors cells, releasing a plethora of active compounds as summarised in Table 1.1[23,24].

Table 1.1: Immunomodulatory factors released from neutrophils

Pro-inflammatory cytokines	IL-1α, IL-1β, IL-6‡, IL-7, IL-9‡, IL-16‡, IL-17A‡, IL17F‡, IL-18, MIF
Anti-inflammatory cytokines	IL-1RA, IL-4, TGF-β1, TGF-β2
Immunoregulatory cytokines	IFN-γ‡, IL-12, IL-23
Colony-stimulating factors	G-CSF, M-CSF‡, GM-CSF‡, IL-3‡
Other cytokines	Amphiregulin, midkine, oncostatin M, PBEF
CXC-chemokines	CXCL1, CXCL2, CXCL3, CXCL4, CXCL5, CXCL6, CXCL8, CXCL9, CXCL10, CXCL11
CC-chemokines	CCL2 CCL3 CCL4 CCL17 CCL19 CCL20 CCL22
Angiogenic and fibrogenic factors	HB-EGF, HGF, FGF_2, TGF-α, VEGF, prokineticin 2
TNF superfamily members	APRIL, BAFF, CD30L, CD95L, RANKL, TNF, TRAIL
Antimicrobial peptides (in humans)	Azurocidin, α-defensins (Human Neutrophil Peptide 1 - 4, Cathelicidin (hCAP-18/LL-37)

‡ Denotes controversial data for human neutrophils at present

The synthesis and release of these modulators are regulated at the intracellular level depending on the current physiological state of the inflammatory environment. These levels of regulation are largely at the stage of mRNA transcription, governed by cell surface receptors and signal transduction pathways in response to external stimuli, and also at the levels of post transcriptional regulation[25,26]. In addition regulation at the stage of protein secretion has been published in the case of TNF superfamily proteins BAFF and APRIL, where they are stored in pools and secreted in response to secretagogues such as TNF-α, complement component C5a and other chemotactic factors[27].

The functions of neutrophils have been extended further. Over the past decade interest has been heightened in the ability of neutrophils to exhibit extracellular microbicidal properties by way of 'casting' NETs (Neutrophil Extracellular Traps)[28]. Extracellular traps are comprised of nuclear components (DNA, histones), which are

laced with proteins originating from azurophilic, secondary and tertiary granules. These proteins are involved in direct microbial recognition (e.g. PTX3), possess antimicrobial activity (e.g. LL-37, myeloperoxidase) and tissue remodelling (e.g. elastase and MMP9) capabilities. NETs have been demonstrated to trap a multitude of pathogens for killing by granule protein-mediated killing, such as *Staphylococcus aureus*, *Shigella flexneri*, *Salmonella typhimurium*[28]. Simon *et al.* (2013)[29] references a number of observations that suggest NETs are the product of viable, motile neutrophils, requiring energy once activated to rapidly (within 5-10min) eject DNA. Up until very recently it was widely regarded that dying neutrophils undergo a specialised form of death that differed from necrosis and apoptosis, termed NETosis. However, as highlighted in Simon *et al.* (2009), this release of DNA from dying neutrophils has only been observed in PMA (phorbyl-12-myristate-13-acetate) treated neutrophils thus far and remains a controversial subject.

As effective as NETs are considered in the elimination of microorganisms, studies have identified the contribution of NETs to enhanced inflammation in chronic autoimmune disorders. Patients with systemic lupus erythematosus (SLE) demonstrate B cell generation of autoantibodies to released ribonucleoproteins (RNPs) and LL-37, resulting in plasmacytoid dendritic cell (pDC) activation and subsequent IFN-α release[30].

One other notable mention of recent interest is the discovery of a cell's ability to produce extracellular vesicles (EVs) as a means of intercellular communication. EVs are commonly between 30nm to 1μm in diameter with the vesicles >100nm in size referred to as exosomes while larger vesicles are known as ectosomes, microvesicles or microparticles. Apoptotic bodies are also classified under the general terminology of EVs. They are formed by way of shedding or budding from the plasma membrane[31], although they are considered difficult to confidently identify using current techniques (flow cytometry, light scattering and electron microscopy)[32].It is considered that most cells produce EVs comprised of varying amount of membrane and cytoplasmic rich constituents. EVs are reportedly to have number of functions depending on the type of cell that they originate from[16]. PMN-derived EVs have been isolated from healthy blood donors and have been shown to upregulate

endothelial cell expression of IL-6, IL-8 and ICAM-1 *in vitro* [33]. Neutrophil-derived EVs have been suggested to possess antibacterial properties as published recently by Timar *et al.* (2013)[16]. EVs generated after exposure to opsonised zymosan or whole bacteria were able to inhibit *S. aureus* growth and form aggregates with the bacteria. This was compared to EVs generated from neutrophils in complement-depleted serum and in the presence of TNF-α. This study suggests the possibility that the antimicrobial effect of neutrophils may be far-reaching.

It is clearly evident how essential neutrophils are to the host's innate immune response. This is highlighted by defective neutrophil disorders such as chronic neutropenia, leukocyte adhesion deficiency syndrome and chronic granulomatous disease[34-36].

Antimicrobial actions of α-defensins within neutrophils

As briefly mentioned, essential to the elimination of invading pathogens by neutrophils are the actions of antimicrobial peptides harboured within storage granules. Antimicrobial peptides form part of the host's innate defence system against a broad range of bacterial, fungal and viral pathogens. These peptides, fewer than 100 amino acids in length, are widely expressed in organisms ranging from plants and insects to mammals[37].

A key constituent of the neutrophil-containing antimicrobial peptide arsenal is a family of small peptides known as α-defensins, approximately 3-5kDa in size (Figure 1.1). This subfamily form part of a structurally similar family divided into α-, β- and θ-defensins, with θ-defensins present in certain non-human primates[38]. α- and β-defensins are similar in that they are largely comprised of a core, triple-stranded β-sheet structure stabilized by three intramolecular disulphide bonds between six conserved cysteines. They differ in the length of peptide segments between these six cysteine amino acids[39]. Within humans, α-defensin isoforms consist of Human Neutrophil Peptide (HNP) 1-4 contained within neutrophils azurophil granules, and HD-5 and -6 abundantly expressed in intestinal Paneth cells. β-defensins are located mostly on epithelial surfaces and secretory glands[40]. The six α-defensin peptides are

encoded by five DEFA genes, with the proteolytic removal of amino acids on HNP1 (DEFA1) or HNP3 (DEFA3) forming HNP2[41]. It is widely thought that α-defensin genes ascended from the genes of β-defensins, given the abundance of β-defensin genes present throughout the evolutionary tree compared to α-defensin genes found exclusively in mammals[42]. Defensins are cationic antimicrobial peptides due to excess arginine and lysine expression but do vary in charge number. In addition to their cationicity they are amphipathic, having both hydrophobic as well as hydrophobic portions.

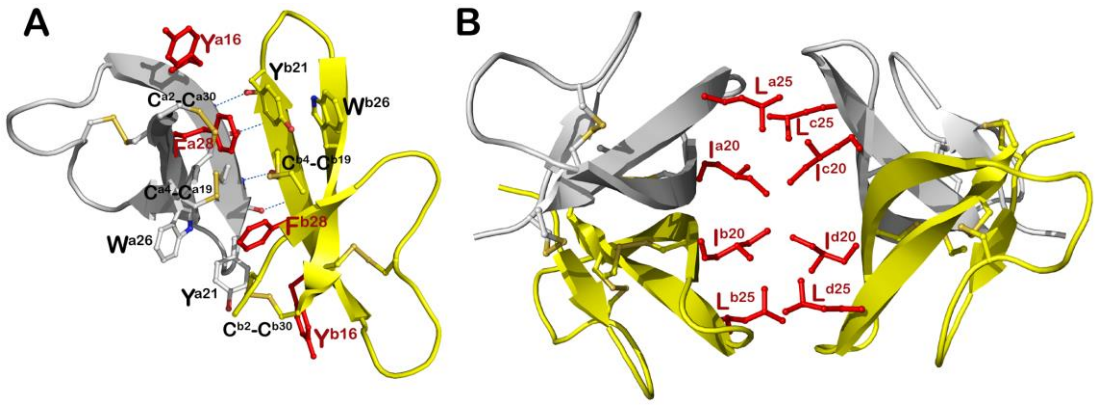

Figure 1.1: Quaternary structure of wild type HNP1

The crystal structure of the dimeric (**A**) and tetrameric (**B**) assembly of Human Neutrophil Peptide-1 (HNP1). Disulphide bonds as well as residues involved in oligomerization are shown as balls and sticks and reciprocal main chain hydrogen bonds are shown as blue dashes[43].

The antimicrobial mechanisms of α-defensins have been extensively studied[44]. Within human neutrophils, azurophil granules fuse with phagosomes containing captured microbes. It is thought that released antimicrobial peptides initially make contact by binding to the outer microbial membrane through electrostatic interactions[45]. Through their amphipathic and lectin-like properties they are then able to insert themselves within the outer membrane lipid bilayer, with their hydrophilic portions associating with the hydrophilic outer heads while utilizing its hydrophobic portion to embed itself amongst the hydrophobic tail portion of the cell wall. This

membrane association creates pores of macromolecule size, which permits leakage of intracellular components and cell lysis. In addition, pores allow α-defensins to enter and target other intracellular components, resulting in DNA, RNA and protein synthesis inhibition[46]. A collapse in membrane potential has also been reported to occur as well the formation of voltage gated channels, resulting in intracellular ion imbalances[47]. HNP1-3 comprises of 5-7% of the total amount of protein within human PMNs, and between 35-50% within azurophil granules with much less abundance of HNP4[48]. α-Defensins also display potent anti-viral activity as demonstrated in the prevention of HIV-1 entry into cells through direct binding to viral glycoproteins[49,50]. Their aggregation with Influenza A virus has also been shown to mediate neutrophil uptake, as well as prevent Adenovirus capsid disassembly required for infection[51,52]. In addition, they have demonstrated an ability to neutralize a large number of bacterial toxins including *Staphylococcus aureus* and anthrax lethal factor[53-55], as well as prevent synthesis of bacterial cell wall precursor lipid II[56]. α-Defensins have also been shown to induce IL-8 secretion in intestinal epithelial cells[57]. The property of hydrophobicity with the ability to form canonical dimers and even quaternary structures are essential to their antimicrobial functions as elegantly studied and published by the Professor Wuyuan Lu research group by the single point substitution of key amino acids[58,59]. Further immunomodulatory properties of α-defensins will be introduced later in this chapter and in Chapter 3.

Macrophages: sentinel cells in immunity

At sites of inflamed tissue, recruited neutrophils engage in complex bidirectional cellular crosstalk with macrophages, dendritic cells, natural killer cells, lymphocytes and mesenchyme stem cells[24]. The state of neutrophil activity plays a pivotal role in the macrophage physiology, which are key immune effector cells in the initiation, propagation and resolution of inflammation. Macrophages are derived from hematopoietic granulocyte-monocyte progenitor cells within the bone marrow and enter the blood stream as monocytes and differentiate into macrophages or immature dendritic cells upon tissue entry[60,61]. Under resting state tissue-resident macrophages fulfil 'housekeeping' duties, clearing cellular debris and apoptotic cells by phagocytosis whilst remaining inactivated [62].

In response to tissue trauma macrophages become classically activated – designated as phenotype 'M1' - by released DAMPs, cytokines and exogenous PAMPs recognised by TLRs, intracellular pattern-recognition receptors and interleukin 1 receptor (IL1-R). Most inflammatory signal transduction takes place via the adaptor molecule myeloid differentiation primary response gene 88 (MyD88) and downstream signalling via the Nuclear Factor Kappa B (NFκB) and the Mitogen-Activated Protein Kinase (MAPK) signalling pathways[63-65]. Subsequently-activated transcription factors upregulate gene expression of proteases, eicosanoids, pro-inflammatory cytokines (e.g. TNF-α, IL-12, IL-23), and reactive oxygen and nitrogen intermediates (ROIs and RNI, respectively)[1]. Activated macrophages also display an increased phagocytic capacity for invading microbes. By processing their components for antigen presentation to T-cells together with dendritic cells (DCs), they provide a critical link to the adaptive immune system.

The M2 macrophage classification or 'alternatively' activated macrophages broadly classifies a range of other macrophage phenotypes. These are defined by the subtypes M2a (after exposure to IL-4 and/or IL-13), M2b (immune complexes in combination with IL-1β or LPS) and M2c (IL-10, TGF-β or glucocorticoids)[66]. In general, alternatively activated macrophages are associated with response to parasitic infections (M2a)[67], producing anti-inflammatory IL-10 and TGF-β with abrogated IL-12. They are therefore regarded as being immunosuppressive in function.

In a recent review of macrophage phenotyping, Mosser and Edwards (2008)[68] suggested that macrophages are more accurately characterised as having a degree of phenotypic plasticity as opposed to being solely classical or alternatively activated. Instead, they suggest that macrophages should be interchangeably grouped according to their function as either being involved in host defence, wound healing or immune regulation. Indeed in the rapidly changing tissue environment that is a milieu of cytokines, chemokines and tissue growth factors, it would seem feasible that macrophages should be considered readily adaptable to change and shape its function accordingly. Macrophage plasticity highlights how critical these cells are at

controlling inflammation from the point of initial infiltration to the eventual resolution and tissue regeneration.

1.2 Inflammation regulation

Leukocytes and their role in inflammation clearly benefit the host in providing protection against infections and avoiding often fatal septicaemia through multiple organ failure. As a consequence of defective inflammation regulation, chronic inflammation can often lead to extensive tissue damage. In severe cases of chronic inflammatory disorders such as rheumatoid arthritis, it can often result in chronic pain, permanent disfiguration and debilitation as a result of irreversible tissue and joint destruction[69]. Not only is inflammation pathophysiology detrimental in chronic inflammatory diseases, it has also been implicated in the progression of other disease states including Alzheimer's[70], diabetes[71], cancers[72] and cardiovascular diseases[73]. Thus it is imperative to the host that the inflammatory event, when required, be effective in its function while transitioning (when appropriate) to bring about tissue regeneration and eventual tissue homeostasis. For this to occur, inflammation must be tightly regulated.

The regulation of inflammation is diverse and complex process, occurring at multiple stages during the inflammatory cascade. Neutrophils play a role in early stage checkpoints with one such mechanism involving switching from the production of pro-inflammatory lipid autocoids such as leukotrienes and prostaglandins to anti-inflammatory lipoxins, a distinct lipoxygenase-derived eicosanoids that carry stop signals for inflammation[74]. For example, Lipoxin A_4 inhibits further neutrophil migration mediated through formyl peptide 1 receptor (FPR-1) and also initiates non-phlogistic recruitment of monocytes and phagocytosis of apoptotic neutrophils by macrophages[75]. Efferocytosis brings with it the release of resolvins and protectins from neutrophils[76]. These mediators bring about pro-resolving actions in neutrophils (tissue infiltration inhibition), macrophages (non-phlogistic phagocytosis of apoptotic neutrophils), dendritic cells (blocks IL-12 production) and T cells (CCR5 upregulation, inhibition of TNF-α, IFN-γ) amongst other functions[75].

Clearance of apoptotic neutrophils is an anti-inflammatory event

The clearance of cells dying by programmed cell death was previously considered as a very low impact event in shaping tissue homeostasis. Indeed the engulfment and elimination of these no longer required cells by phagocytes was considered to be a refuse and recycling process without much consequence. Besides normal cell turnover under homeostatic conditions, apoptosis occurs during times of infection, wound healing and in disease states[77]. Over the last decade extensive research has shown that timely removal of apoptotic bodies by phagocytes dampens inflammation and promotes pro-resolution. Clearance of neutrophil corpses no longer required during the inflammatory cascade have a direct bearing on the physiological state of phagocytes[78]. Apoptotic neutrophil clearance by macrophages brought about a release of anti-inflammatory TGF-β, prostaglandin E2 and platelet-activating factor (PAF) which were found to mediate the decrease in inflammatory cytokines GM-CSF, IL-1β, IL-8 and TNF-α[79]. In addition ingestion of apoptotic cells by immature DCs alters their maturation while promoting TGB-β secretion and induces tolerogenic CD4+Foxp3+ regulatory T cells[80]. Ingestion of circulating apoptotic leukocyte ingestion by splenic marginal zone DCs lead to decreased mRNA levels of IL-1α, IL-1β, IL-6, IL-12p70 and TNF-α[81].

Studies have suggested the involvement of two key factors mediating this effect. The first is by the release of 'find me' signals by apoptotic cells, which are recognised by receptors on scavenger cells and direct their migration. To date four released signals and their associate receptors have been identified: lysophosphatidylcholine (LPC) and G2A, fractalkine (CX_3CL1) and CX_3CR1, sphingosine 1-phosphate (S1P) and $S1P_{1\text{-}5}$, and lastly the nucleotides ATP and UTP with P2Y[82]. The second factor is through the receptor-mediated recognition of 'eat me' signals presented on the surface of apoptotic cells. Most notably is the recognition of membrane translocated phosphatidylserine (PtdSer) by phagocytic receptors including TIM4, BAI1, RAGE and stabilin-2[9]. While debate continues as to whether presented PtdSer alone is sufficient to mediate receptor interaction and uptake by phagocytes, it is appreciated that PtdSer does play an integral part together with currently unidentified signals and receptor interactions which orchestrate this event. What is known is that the

activation of PtdSerR triggers the release of TGF-β[83]. Fadok *et al.* (2001)[84] found that membranes of lysed neutrophils were able to suppress the expression of pro-inflammatory mediators and upregulate TGF-β, believed to be PtdSer-mediated.

While timely apoptotic cell clearance shapes the tissue environment, impaired clearance leads to gradual accumulation in the tissue. In some cases this can lead to a decrease in self-tolerance with the production of autoantibodies as seen with the onset of SLE[85,86].

Dying neutrophils release anti-inflammatory α-defensins

Inflamed tissue brings with it large scale uncontrolled cell death and the release of DAMPs from necrotic cells, ultimately leading to further macrophage activation. Neutrophils dying by necrosis are widely regarded as inflammatory through the release of danger signals, of which serine proteases and elastase are key contributors[84]. However not all cellular components released from dying neutrophils are inflammatory to macrophages and do quite the opposite, perhaps acting as a counteroffensive to an overly exaggerated inflammatory response.

The inhibitory effect of α-defensins on pro-inflammatory macrophages was published by the Dr Mohini Gray lab group[87] and forms the groundwork to the research in this thesis. This paper showed for the first time that apoptotic human neutrophils release soluble factor/s that significantly attenuate secreted TNF-α in classically activated human monocyte derived macrophages (HMDMs) *in vitro*. This was achieved by the use of a Transwell system to separate apoptotic cells from macrophages and also by ultracentrifugation to clear soluble contents of apoptotic bodies. Crucially this effect was independent of both direct cell contact with macrophages and the anti-inflammatory modulator TGF-β.

More striking were the anti-inflammatory soluble contents of neutrophils that were made necrotic by freeze/thawing were cleared of their membrane components by ultracentrifugation, yet these resulting neutrophil supernatants were profoundly inhibitory (12×10^6 neutrophils; containing 8-15 ±0.45μg/mL HNP1-3). Titrated

amounts of these necrotic neutrophil supernatants were found to significantly attenuate a multitude of pro-inflammatory mediators, notably cytokines TNF-α, IL-1β, IL-6 and IL-8 as well as the ROS agent nitric oxide. Interestingly these also lead to a decrease in the anti-inflammatory IL-10. This effect remained exclusive to human neutrophils as human thymocytes and murine neutrophils (which lack α-defensin) displayed no anti-inflammatory effect on macrophages.

Through extensive testing neutrophil lysates were depleted of α-defensins by non-specific hydrophobic protein depletion using a bead depletion assay. Resulting electrophoretic protein gels identified α-defensins as a prominent protein band removed from these fractions. Confirmation of the key modulatory role of α-defensins was confirmed when hydrophobic protein-depleted fractions, which had subsequently lost its anti-inflammatory potential, regained this property when purified α-defensins were added back at physiological concentrations. The anti-inflammatory effects of purified, neutrophil-derived as well as synthetic HNP on pro-inflammatory HMDMs in cell culture experiments reiterated the direct immunomodulatory properties of this peptide. Crucially it was found that neutrophils in culture display a gradual release of HNP1-3 over 24hrs, peaking at 9hrs. These studies also highlighted structural importance of HNP function, as the linearised and $_{D}$-enantiomer peptide form showed no inhibitory effect. Furthermore the human cathelicidin LL-37 was tested with no effects on secreted TNF-α observed. It is worth noting that, contrary to this finding, a number of other publications have reported on the ability of LL-37 to reduce TNF-α and NO production in bone marrow derived macrophages (BMDMs) and tissue macrophages both *in vitro* and *in vivo*[88].

Importantly the effect of α-defensins was not attributed to a decrease in macrophage viability. In fact macrophages in culture exposed to α-defensins for 1hr or 24hrs, and then allowed to rest in culture, gradually restored their full propensity to produce TNF-α upon LPS activation after 20hrs and 72hrs respectively. Whilst the capability of HNP treated macrophages to produce cytokines was limited, functionally, HMDMs remained capable of eliminating live (and dead) *Pseudomonas auruginosa*

in culture and showed enhanced phagocytosis of fluorescent beads compared to untreated cells.

In vivo, mice infected with *Salmonella enterica* were administered with necrotic human neutrophil supernatants and after seven days showed a reduction in serum TNF-α concentration as well as fewer bacterial colonies from lysed splenocytes when plated onto agar. The therapeutic effect of α-defensin in a sterile inflammatory model was also demonstrated; mice induced with peritonitis by thioglycolate injection alongside HNP1 or necrotic human neutrophil supernatants showed a reduction in infiltrating GR-1^+ neutrophils and F4/80^+ macrophages.

And finally, in a clinical setting, studies from synovial fluid extracted from rheumatoid arthritis patients undergoing arthrocentesis have been reported to contain high concentrations of α-defensins in the range of 3 – 25μg/mL, with a mean of 12.4μg/mL.

1.3 Key concepts

Within this thesis, key research concepts pertaining to the role of α-defensins were performed. Of note, the role of autophagy, classical activation of macrophages via the TLR7/8 agonist R848, and Rheumatoid Arthritis with the potential involvement of α-defensins. These three concepts will be briefly introduced.

1.3.1 Autophagy

Autophagy ('self-eating') is largely defined as a catabolic process whereby cellular components are digested by lysosomes for metabolic recycling (Figure 1.2). In addition to homeostatic organelle turnover, the onset of autophagy can occur as a consequence to nutrient deprivation, infection as well as regulation of the innate immune response[89-91]. A major subtype of autophagy, termed macroautophagy is generally defined as a process where cellular components are compartmentalised into phagosomes followed by fusion with lysosomes for degradation during periods of nutrient starvation. Macroautophagy (hereafter referred to as autophagy) in this regard is a useful method of recycling when required, but is also recognised as an

immune-related response in the degradation of intracellular bacteria and viruses (xenography) as well as in the general turnover of excess, damaged or dysfunctional organelles[89,90,92].

One of the most common markers for monitoring autophagy in mammalian cells is the conversion and incorporation of soluble LC3B-I (microtubule-associated protein light chain 3, homolog B) situated within the cytoplasm to lipid-bound LC3B-II, which is conjugated with phosphatidylethanolamine (PE). LC3B-II thus forms part of the autophagosome containing sequestered macromolecules after which these vesicles fuse with lysosomes (autophagolysomes) and are degraded[93,94]. Interestingly, an abnormality of key autophagy proteins within murine intestinal Paneth cells has been linked to an increased susceptibility to Crohn's disease as a result of defective exocytosis of granule proteins[95]. In addition, defective cellular autophagy is implicated in pathophysiological processes that include neurodegenerative and metabolic disorders, cancers, cardiovascular and pulmonary diseases[96].

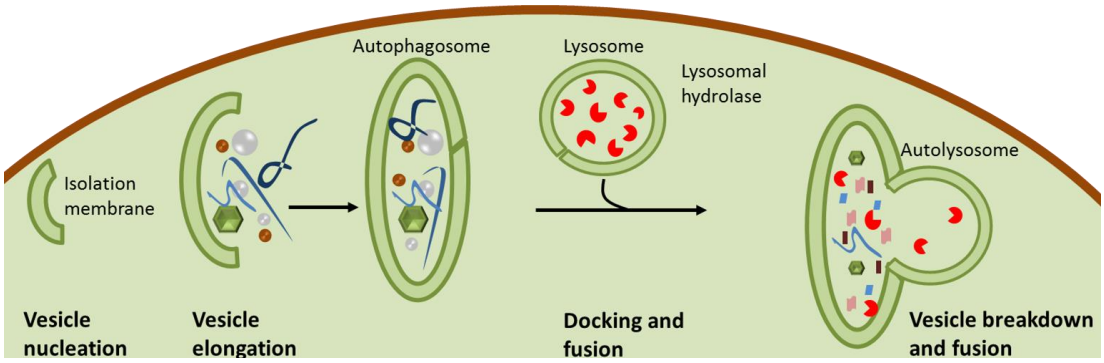

Figure 1.2: Overview of the autophagy pathway

The development of an autophagosome forms from membrane formation and extension, followed by envelopment of cellular organelles to be degraded. The lysosome containing hydrolases fuse to form the autolysosome for the catalytic digestion.

1.3.2 Macrophage activation through R848 stimulation

Imperative to the research investigating the effects of α-defensins on macrophages was their means of 'classical' activation by TLRs. These pattern recognition receptors are grouped by their preferences for conserved structural motifs of pathogens. Specifically TLR 3, 7, 8 and 9 located on the membranes of endosomes are able to recognize and respond to viral infections through the recognition of genomic DNA or RNA[97]. The activation of TLR 7/8 is notably in response to single stranded RNA viruses (ssRNA40), for example retroviruses including Human Immunodeficiency Virus -1 (HIV-1) and the influenza virus[98,99]. Macrophage and dendritic cell response to TLR7/8 activation is through signaling via the NF-κB pathway resulting in the production of inflammatory cytokines including TNF-α[100](Figure 1.3).

R848 is an amidazoquinoline compound with potent anti-viral activity that activates immune cells via TLR7/8 through the MyD88-dependent signalling pathway and NF-κB activation[101,102]. Not only was R848 selected as the ideal choice of agonist for macrophage activation against viral infection, but the hindrance of this activation pathway by α-defensins had implications against potential protection against autoimmunity. In particular, self-RNA and DNA can inappropriately be recognized by TLR7 (and TLR9). As a consequence, this self-directed immune response can lead to the development of autoimmune disorders such as systemic lupus erythematosus (SLE)[103].

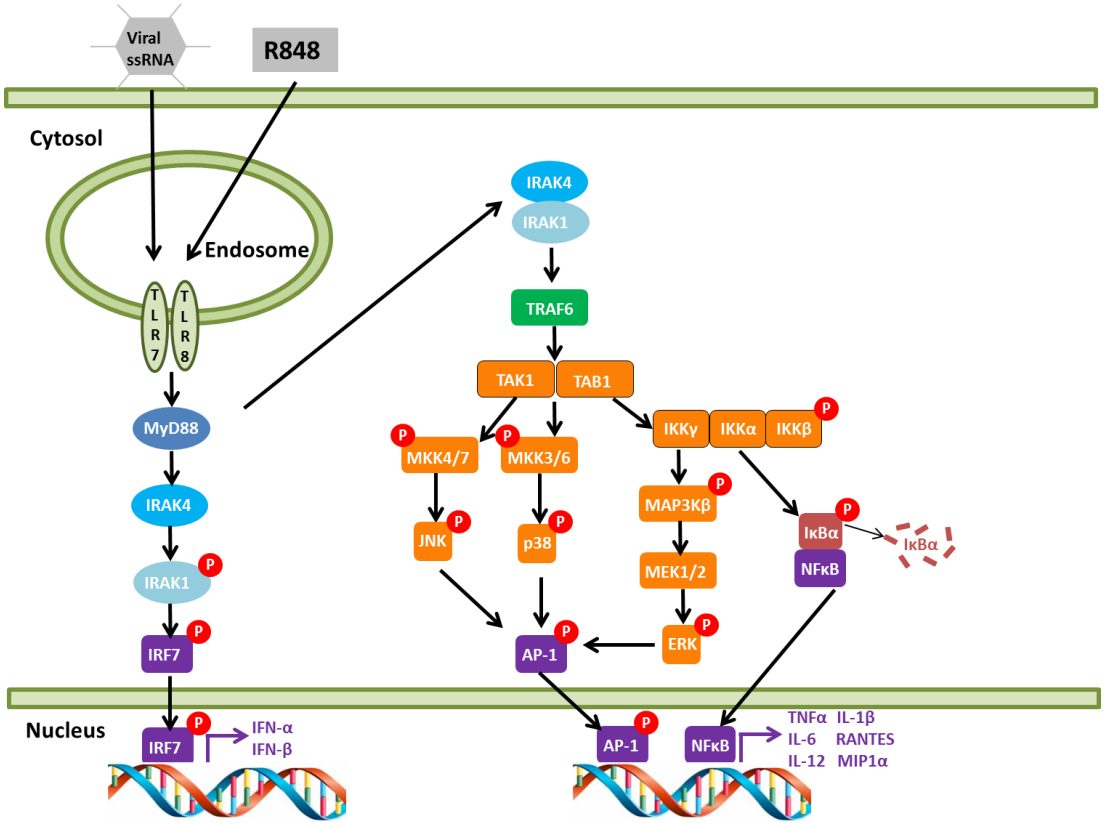

Figure 1.3: R848 activation of the TLR7/8 signalling pathway

The activation of toll-like receptors (TLRs) 7 and 8 (TLRs) by R848 and viral ssRNA. Activation leads to signaling via the MyD88-dependent pathway. Generation of interferon-α and -β gene expression is the result of activated IRAK4 (interleukin-1 receptor-associated kinase) phosphorylation of IRAK1, followed by phosphorylation of transcription factor interferon regulatory factor 7 (IFR7). IRAK4/1 activation also results in activation of TRAF6 (TNF receptor associated factor) and downstream protein kinase TAK1 and TAB1, resulting in the activation of the Mitogen Activated Protein kinase (MAPK) and NF-κB signaling pathway. Phosphorylation of ERK (extracellular signal-regulated kinase), JNK (c-jun N-terminal kinases) and p38 lead to the phosphorylation and nucleus translocation of transcription factor AP-1 (activator protein-1), inducing pro-inflammatory mediator gene expression. In addition, phosphorylation of IKKβ activates the IκBα/NFκB complex, resulting in the release and translocation of NFκB (and proteolytic degradation of IκBα). Activated NFκB promotes the gene expression of pro-inflammatory mediators for downstream protein synthesis and secretion.

1.3.3 Rheumatoid Arthritis

In addition to the potential influence of α-defensins in SLE, direct influences of dying neutrophils and the release of α-defensins on the counter-development of Rheumatoid arthritis (RA) are proposed and discussed throughout this thesis. RA is a chronic, progressive and systemic inflammatory disorder affecting approximately 1-2% of the population. RA is a debilitating disease and is characterised by chronic joint pain, inflammation and disability as a result of cartilage and bone destruction[69]. Although the direct cause of RA remains unknown, evidence has linked the onset to genetic and environmental factors, with genome-wide analysis relating immune regulatory factors strongly to disease onset[104,105].

Key to the development of RA is the increase in rheumatoid factor within the joint synovium, which is a high-affinity autoantibody against the Fc portion of immunoglobulins[69]. Measured rheumatoid factor within the vasculature has been a long-standing test used by rheumatologists to diagnose RA. Complement activation is also implicated in the initial pathogenesis of RA, triggering subsequent activation of resident leukocytes within the synovial fluid, notably synovial fibroblasts and resident macrophages[106]. Activation of these cells results in the release of pro-inflammatory cytokines including TNF-α, IL-1 and IL-6, as well as mediators of vascular growth (e.g. VEGF)[107,108]. VEGF-induced angiogenesis results in increased trafficking of activated leukocytes, particularly neutrophils which are one of the earliest and influential inflammatory cells to infiltrate the synovium[109,110]. Cartilage-degrading factors such as released matrix metalloproteinases (MMPs) contribute to pannus formation and resultant cartilage erosion. Continued cartilage erosion exposes bone to inflammatory cells and subsequent activation of osteoclasts and chondrocytes, further contributing to the heightened inflammatory state that destroys cartilage and bone through the release of MMPs[111]. Notably excessive TNF-α and RANKL co-stimulate osteoclastogenesis of monocytes within the bone marrow, resulting in precursor osteoclast development and maturation into osteoclasts, resulting in bone resorption[112].

Ultimately RA results in irreversible cartilage damage and joint space narrowing. Thus it is the importance of TNF-α activity within RA joints that has spurned the clinical development of anti-TNF-α biologics as a therapeutic agent in the prevention of disease progression[113,114].

1.4 Aims of this thesis

The aims of this thesis were to elucidate the mechanistic actions of α-defensins on macrophages. At the point of undertaking this project, very little was established into the molecular mechanisms underlying the inhibitory actions of this peptide. In the paper published by the Dr Mohini Gray group on defensins, it was established that the effect was not due to the prevention of inflammatory cytokine exocytosis. This finding contradicted another report showing that α-defensins specifically blocked secretion of IL-1β (and not TNF-α) in LPS stimulated murine monocytes[115].

Given this information, pinpointing the underlying effects α-defensins in the complexities of cell biology was somewhat of an undertaking. In a cycle of trial and error, coupled with a continuous reassessment of the mechanistic hypothesis, a collection of evidence was puzzled together to characterize the inhibitory effects. Below is a summary from each chapter, highlighting the general studies performed and the working hypothesis where applicable.

Chapter 3

Initial investigations went into recapitulating the previously published anti-inflammatory effects of necrotic neutrophil supernatants on human macrophages. These effects were then extended to include purified HNP and single amino acid mutations thereof in order to identify the key functional components. The inhibitory actions of α-defensins on other cell types were studied. In addition, the potential wound healing effects of mouse macrophages treated with human necrotic neutrophil supernatants were assessed *in vivo*. The impact of α-defensins on inflammatory mRNA expression was also addressed in order to begin addressing the inhibitory mechanisms in HMDMs.

Chapter 4

Overall *de novo* protein synthesis of macrophages was assessed leading to the hypothesis of HNP-induced mRNA translation regulation caused by the onset of endoplasmic reticulum (ER) stress. Studies assessing key contributory factors involved in ER stress were carried out, namely: calcium homeostasis and upregulation of genes regulating translation initiation.

Chapter 5

The inhibitory actions of HNP on translation were examined in further detail, using cell-free systems and reporter mRNAs. Assays addressing the hypothesis of HNP binding to RNA were assessed using electrophoretic mobility shift assays (EMSAs) using synthesised oligonucleotide sequences as well as human macrophage-derived RNA (continued in chapter 6). The hypothesis was furthered to propose that HNP directly impaired ribosome function through direct binding to ribosomal RNA (rRNA). Macrophage polysome analysis was performed to pinpoint clues into the state of translating ribosomes in HNP-treated HMDMs *in vitro*.

Chapter 6

The ribosome binding hypothesis was further examined using immunocytochemistry to assess the co-localisation of HNP with ribosomes in HMDMs by confocal microscopy. Experiments were performed in an attempt to confirm HNP-ribosome binding hypothesis, namely by immunoprecipitation and ultracentrifugation. The fate of the suggested HNP-bound ribosomes was addressed by studying the involvement of autophagy.

Chapter 2

2 Materials and Methods

2.1 Reagents

Reagents were purchased from Sigma Aldrich (St Louis, U.S.A) unless otherwise stated.

2.2 Cell culture

2.2.1 Human Monocyte Derived Macrophage (HMDM) derivation

Peripheral Blood Mononuclear Cells (PBMCs) were purified from whole blood obtained from healthy donors within the Centre for Inflammation Research (REC reference number 08/S1103/03) or from blood obtained from buffy coats obtained from the NHS Blood Transfusion Unit (Lauriston Place, Edinburgh). Buffy coats were obtained normally 2-3 days after donation having been kept at room temperature in the interim period at the blood transfusion centre. Cells were isolated using dextran sedimentation and a Percoll gradient accordingly to Haslett *et al.* (1985)[116]: 4mL 3.8% sodium citrate was added to 50mL of blood to prevent coagulation during preparation. Plasma, separated from remaining blood volume by centrifugation (Rotina 420R, Hettich, Tuttlingen, Germany), was cleared of aggregated platelets by the addition of 200μL 1M calcium chloride ($CaCl_2$) in 10mL glass tubes. This serum would be retained for inclusion in cell culture medium. Leukocytes were separated from red blood cells by the addition of 6% dextran (Pharmocosmos; Holbaek, Denmark) and removed for Percoll (GE Healthcare; Waukesha, U.S.A) gradient separation. Following centrifugation cell pellets were mixed with 55% (v/v) Percoll solution and layered onto 68% and 81% (v/v) Percoll gradients. Centrifugation was performed at 720 × g for 20min with no rotor acceleration or deceleration to separate PBMCs from polymorphonuclear leukocytes (PMNs). PBMCs were aspirated, washed twice in 1xPBS (PAA Laboratories, Pasching, Austria) and counted using a cell counting chamber (Hawksley; Sussex, U.K). PBMCs were seeded at 4×10^6 cells/mL in Iscove's Modified Dulbecco's Medium (IMDM) supplemented with 2mM $_L$-glutamine, 100U(units)/mL penicillin

and 0.1mg/mL streptomycin (all PAA Laboratories GmbH) in cultured in T75cm^2 flasks (Corning Inc,; Corning, U.S.A).

Flasks were incubated (SANYO Electric Biomedical, Osaka, Japan) for 1hr at 37°C, 5% CO_2 (carbon dioxide), 80% humidity which are the standard incubation conditions for the remainder of this thesis. Media and non-adherent cells were then aspirated and supplemented IMDM containing 10% (v/v) heat-inactivated autologous serum (referred to as 'complete IMDM'). Note that for buffy coat-derived cell culture IMDM was supplemented with heat-inactivated Fetal Bovine Serum (FBS, BioSera; Ringmer, East Sussex, UK). Culture media was replaced every three days. On day six adherent Human Monocyte Derived Macrophages (HMDMs) were lifted off flasks using 1x Cell Dissociation Solution (Sigma) with gentle scraping, counted, and seeded in flat bottomed 96-well culture plates (Corning Inc.) at 20 000 cells/well (unless otherwise stated) the day before commencing experiments. All cell culture experiments were performed in serum-free culture media unless stated otherwise. In addition HMDMs from fresh donations were used unless mentioned otherwise.

2.2.2 Generation of human necrotic neutrophils (NN)

Fresh neutrophils were obtained from the above-mentioned protocol. Neutrophils were seeded in serum free IMDM at 50 × 10^6cells/mL and made necrotic by freeze/thawing five times on dry ice. Cell volume was then centrifuged at 100 000 × g using the S100-AT6 fixed angle rotor and the RC M150 GX ultracentrifuge (Thermo Scientific Sorvall, Waltham, U.S.A) for 60min at 4°C. Supernatants were removed from discarded pellet and used directly in cell culture assays (abbreviated as 'NN').

2.2.3 Bone Marrow Derived Macrophages (BMDMs)

Bone marrow was harvested from murine femur and tibia bones by aseptic flushing using a 19G needle containing DMEM F12 Glutamax™ (Gibco/Life Technologies, Carlsbad, U.S.A) supplemented with 20% (v/v) sterile-filtered L929 cell culture supernatant (produced in-house), 10% FBS and 100U/mL penicillin and 0.1mg/mL streptomycin. Cells were incubated in a humidified incubator at 37°C, 5% CO_2 in Teflon® pots with ¼ volume culture media replaced on Days 3 and 5. Mature

BMDMs were used between days 7-10. Where appropriate, BMDMs were stimulated with FGK-45 and murine IFN-γ (PeproTech, Rocky Hill, U.S.A).

BMDMs obtained from mice containing a Tristetraprolin protein knockout ($TTP^{-/-}$) on a C57 BL/6 background were kindly donated by Dr Jonathan Dean (Department of Medicine, Imperial College London) and cultured as described above.

2.2.4 Cell lines

THP-1 monocytic cell line: Low passage number THP-1 cells (P26) were obtained from Shalini Rajagopal from the Centre for Reproductive Health, Queen's Medical Research Institute, Edinburgh University. The suspension cells were maintained in cultured in flasks containing Dulbecco's Modified Eagle Medium (DMEM, PAA Laboratories) supplemented with 2mM $_L$-glutamine, 100U/mL penicillin, 0.1mg/mL streptomycin and 10% FBS (referred to as 'complete DMEM'). For passaging, a 1:10 split of cell suspension was performed every 3-4 days. Maturation into macrophages was performed by seeding cells into culture wells in complete DMEM containing 10ng/mL phorbol 12-myristate 13-acetate (PMA) as per recommended concentration[117]. Treated cells were incubated for 48hrs prior to being checked for adherence, followed by washing in 1× PBS (phosphate buffered saline) prior to use in experiments.

Mutu-1: The Burkitt lymphoma cell line Mutu-1 was received from Professor Chris Gregory (Centre for Inflammation Research, University of Edinburgh). Cell were grown in suspension and cultured in T25cm^2 flasks containing RPMI1640 supplemented with 2mM $_L$-glutamine, 100U/mL penicillin and 0.1mg/mL streptomycin and 10% FBS. Cells were passaged every 3-4 days. For experiments, cells were seeded in round-bottom 96 well plates at 20 000/well in 200μL culture media.

2.2.5 α-defensin peptides

Natural, purified HNP1-3 was purchased from Hycult Biotech (Uden, The Netherlands). Synthetic HNP1 was kindly supplied by Professor Wuyuan Lu

(University of Maryland School of Medicine, Baltimore, U.S.A). Mutant derivatives were also donated which included: LHNP1 (structurally linearized HNP1 by the substitution of cysteine amino acids with alanine), and W26A-HNP1 (tryptophan substitution with alanine at residue position 26). All peptides donated were prepared by solid-phase synthesis as described in Wu *et al.* (2004)[118]. These peptides were supplied in lyophilized form, with the exception of LHNP1 which was supplied in reconstituted form at a predetermined stock concentration. Upon receipt lyophilized peptides were weighed out in 1mg amounts using a microbalance (MT5, Mettler-Toledo, Greifensee, Switzerland) and reconstituted in sterile dH_2O (deionized H_2O) containing 0.01% acetic acid (VWR International, Radnor, U.S.A). Protein absorbance at A280nm was measured on a NanoDrop 1000 (Thermo Fisher Scientific) and used to calculate the molar (M) concentration of peptide using the Beer-Lambert law equation:

$$C = \frac{A}{\varepsilon \ell}$$

Where:
C is the peptide concentration (M).
A is the absorbance at A280nm.
ℓ is the path length (cm).
ε is defined as the molar extinction coefficient ($M^{-1}cm^{-1}$) calculated according to Pace *et al.* (1995)[119].

Quantitated protein concentrations were aliquoted into small volumes and vacuum dried for 1hr in an Alpha rotational vacuum concentrator (Martin Christ, Osterode am Harz, Germany). Aliquots were stored at -20°C until needed and reconstituted when required in sterile 0.01% acetic acid at desired stock concentration.

2.2.6 HMDM and THP-1 stimulants

Stimulants commonly used to stimulate primary cells and cell lines included the amidazoquinoline compound R848 purchased from Invivogen (Toulouse, France) and used at 1µg/mL unless otherwise stated. In addition, other stimulants used were: CD40L with 5ng/mL IFN-γ (PeproTech), Lipopolysaccharide from *Escherichia coli*

(LPS), Protein A from *Staphylococcus aureus* Cowan Strain (SAC), Peptidoglycan (PGN, Invivogen), Poly I:C (Invivogen) and CpG ODN 2006 (Hycult Biotech).

2.2.7 HNP1 treated POPC liposomes

5mg POPC liposomes (1-palmitoyle-2-oleoyl-sn-glycerol-3-phosphocholine; Avanti Polar Lipids Inc., Alabaster, U.S.A) were dissolved in 250µL chloroform within glass vials to obtain a clear lipid solution. Organic solvent was then evaporated with a steady stream of N_2 further dried by rotatory vacuum for 2hrs. Multilamellar vesicles (MLVs) were hydrated by dispersing dry lipid films in >18MΩ/cm (25°C) serum free IMDM media at a concentration of 10mg/mL with slight frequent agitation containing either 0% mol HNP1 (nil) or 2% mol HNP1 (i.e. 100ug HNP1 in 5mg POPC). Prior to treatment working concentrations of liposomes were aliquoted into eppendorf tubes and sonicated for 2min in a sonicating waterbath (Ultrawave, Cardiff, UK) at 37°C. Liposomes were pelleted by centrifugation at 3500 × g for 20min (4°C) and resuspended at working concentration required. HNP1 treated liposome volumes were used in downstream experiments with R848-stimulated HMDMs to assess the effect on secreted TNF-α.

2.3 Colourimetric assays

2.3.1 Enzyme Linked Immunosorbant Assay (ELISA)

This protocol describes the general method used to detect secreted cytokines from cell culture experiments. Human TNF-α, mouse IL-1β (donated by Dr Kevin Dhaliwal, Edinburgh University), human IL-6, IL-8, IL-10 (mouse and human) were purchased from R&D Systems (Minneapolis, U.S.A) and performed according to manufacturer's protocol and working concentrations. The assay was performed in 96 well EIA/RIA plates (Corning Life Sciences; New York, U.S.A) which were initially coated overnight in capture antibody. After washing the wells with 1× PBS/0.05% Tween-20, plates were patted dry and samples from cell culture supernatants were added to wells, diluted if necessary in 1× Reagent Diluent (R&D Systems) in a final volume of 50µL per well. Standards of known cytokine concentration were included on plates and a two-fold dilution series was performed in duplicate for comparison. Plates were incubated at room temperature for 1.5hrs after which wells were washed and incubated with detection antibody and incubated for 1hr at room temperature. Wells were washed and incubated with streptavidin HRP (horseradish peroxidase; dilution 1:200) for 30min in the dark at room temperature. After washing the wells

50µL of SureBlue™ TMB Microwell Peroxidase substrate (KPL Inc., Gaithersburg, Maryland, U.S.A) was added. After 10-15min and upon sample solution turning blue, the enzymatic reaction was stopped using 50µL 0.6N sulphuric acid and absorbance values were read at A450nm on a Synergy HT plate reader (Biotech, Winnoski, U.S.A) using Gen5 (version V.1.01.14) software from BioTek. The plate background absorbance was corrected by subtracting the absorbance readings at A570nm from the A450nm values. Absorbance readings from standards were plotted graphically using Microsoft Excel (Redmont, U.S.A) to obtain a line equation of absorbance versus protein concentration. This equation was then used to calculate the appropriate cytokine concentration of samples which were then plotted on a graph using GraphPad Prism software, V4 (GraphPad Software Inc.; San Diego, U.S.A).

2.3.2 Alamar Blue assay

alamarBLUE (AdB Serotec, Kidlington, UK) was added together with cells in culture media at a final volume of 10% (v/v) as per manufacturer's guidelines as a measure of cellular metabolic activity. At specified time points, the culture plate was read on a Synergy HT plate reader using Gen5 software at A570nm and A600nm. The percentage reduction of alamarBlue was calculated using the equation:

$$\% \text{ reduction of alamarBlue} = \frac{(O2 \times A1) - (O1 \times A2)}{(R1 \times N2) - (R2 \times N1)} \times 100$$

Where:

O1 = molar extinction coefficient (E) of oxidized alamarBlue (Blue) at A570nm (8056 $M^{-1}cm^{-1}$)

O2 = E of oxidized alamarBlue at A600nm (117216 $M^{-1}cm^{-1}$)

R1 = E of reduced alamarBlue (Red) at A570nm (155677 $M^{-1}cm^{-1}$)

R2 = E of reduced alamarBlue at A600nm (14652 $M^{-1}cm^{-1}$)

A1 = absorbance of test wells at A570nm

A2 = absorbance of test wells at A600nm

N1 = absorbance of negative control well (media plus alamarBlue but no cells) at A570nm

N2 = absorbance of negative control well (media plus alamarBlue but no cells) at A600nm

Absorbance readings were then plotted graphically using GraphPad Prism.

2.4 Protein purification and determination

Cells in culture plates were washed in 1× PBS and air-dried briefly before being lysed in 100µL lysis buffer (on ice) consisting of:

- 50mM Tris-HCl (pH7.5)
- 150mM NaCl (sodium chloride)
- 1% Triton X-100
- 0.5% Deoxycholic acid
- 0.1% SDS
- 1mM PMSF (phenylmethylsulfonyl fluoride)
- 1x Complete protease inhibitor cocktail with EDTA (Roche)
- 1mM NaF (Sodium Fluoride)
- 1mM Na_3VO_4 (Sodium Orthovanadate)

After 10min incubation on ice with intermittent pipetting, samples were centrifuged at 10 000 × g for 10min, 4°C after which supernatants were collected in fresh tubes. Protein concentrations were first quantitated using the Bio-Rad protein assay and if necessary, concentrated by precipitation and purified using either the ProteoExtract Protein Precipitation kit (Merck Millipore, Billerica, U.S.A) as per manufacturer's protocol or by Trichloroacetic acid (TCA) precipitation.

2.4.1 Bio-Rad protein assay

Protein determination of samples was performed using the DC Protein Assay kit (Bio-Rad, Hercules, California, U.S.A) which is based on the Lowry assay principle[120]. Samples containing cell lysates were diluted to suitable concentrations while a protein standard range using bovine serum albumin (BSA; VWR International) was obtained by a two-fold dilution series in a 96 well plate. The diluent used for samples as well as standards was the protein lysis buffer used

originally in each respective assay. 5µL of protein sample was then added to 25µL of Reagent A containing 2% (v/v) Reagent S (performed in triplicate). 200µL of Reagent B was then added to each well and incubated for 15min at room temperature with gentle rocking. Sample absorbance readings were then read at A750nm using the Synergy HT plate reader using Gen5 (version V.1.01.14) software. Absorbance readings from protein standards versus known protein concentrations were then plotted to obtain a line equation of the resulting plot. This equation was then used to calculate the protein concentration of samples for use in downstream applications.

2.4.2 Trichloroacetic acid (TCA) protein precipitation

One volume of 20% (v/v) TCA was added to one volume lysate, vortexed and incubated on ice for 1hr. Samples were then centrifuged using a bench top IEC MicroCL 17R (Thermo Scientific) centrifuge at 14 000 × g for 5min, 4°C after which TCA was aspirated and 100µL ice cold 20% (v/v) acetone (VWR International) was added to pellet and incubated for a further 30min on ice. Samples were again centrifuged at 14 000 × g for 5min, 4°C and supernatant aspirated. The acetone incubation step was repeated after which pellets were air dried for 5min at room temperature and 30µL of 1x Laemmli buffer [2% SDS, 10% Glycerol, 5% 2-mercaptoethanol, 0.002% Bromophenol Blue, 63mM Tris-HCl, pH6.8] was added to each sample. Tubes were incubated on a thermomixer (Eppendorf; Hamburg, Germany) at 75°C, 700rpm (revolutions per minute) for 1hr or until pellets were visibly solubilised.

2.5 Sodium Dodecyl Sulphate Polyacrylamide Gel Electrophoresis (SDS-PAGE) and Western Blotting

Protein samples were prepared for polyacrylamide gel electrophoresis by adding 2× Laemmli sample buffer to obtain a 1× dilution. Samples were heated for 5min at 95°C followed by 5min incubation on ice and brief centrifugation. Samples were loaded onto a NuPage Novex 10% Bis-Tris precast mini-gel within an XCell SureLock Mini-cell gel tank containing 1× NuPage MOPS SDS Running buffer (all purchased from Invitrogen/Life Technologies, Carlsbad, U.S.A). Gel tank was then connected to a power pack (PowerPac™ 300, Bio-Rad) and run at 100 volts (V) for approximately 2hrs.

Alternatively SDS-PAGE gels were made in-house using Sigma reagents. Two glass plates were assembled into the Bio-Rad gel loading cassette and running gel buffer (Table 2.1) was poured approximately up to 2cm from the top of the glass plates and left to set with dH_2O. Upon polymerisation, water was removed off and loading gel buffer (Table 2.2) was poured, gel comb inserted and left to set. Samples were loaded as before and run at 80V for 90mins.
For the approximate molecular weight determination of separated proteins, 10µL of 1× SeeBlue® Plus2 pre-stained protein standard (Invitrogen) was loaded in a well alongside samples.

Following electrophoresis, the proteins were transferred onto a Hybond-P PVDF (Polyvinylidene difluoride) membrane (GE Healthcare) pre-soaked in methanol. The gel/membrane was sandwiched between blotting paper (Bio-Rad) inserted into an XCell II Blot Module (Invitrogen) which was placed inside the XCell SureLock gel tank and filled with western transfer buffer [20% (v/v) methanol, 38.6mM glycine, 47.9mM Tris, 0.04% SDS]. The system was connected to a power pack and run at a constant current 1mA (milliamp)/cm^2 of gel surface area for 2hrs at room temperature, or alternatively overnight at 4°C. Protein transfer from gel to membrane was confirmed by the transfer of molecular weight standards. Membranes were then rinsed briefly in 1x TBS [20mM Tris, 150mM NaCl; pH7.4] and blocked overnight at 4°C in 1× TBS/0.1% Tween-20 containing 5% (w/v) milk powder (Marvel, Premier International Foods UK Ltd., St Albans, UK). Membranes were immunoblotted in 1× TBS/0.1% Tween20/1% BSA (unless otherwise stated) with antibodies stipulated in relevant results chapter for 2hrs at room temperature with rotation. As a loading control for protein amounts in each sample, membranes were also immunoblotted for polyclonal rabbit anti β-Actin (Abcam, Cambridge, UK) at a 1:5000 dilution. The membranes were then washed three times for 15min in 1× TBS/0.1% Tween20. The appropriate HRP-conjugated secondary antibody (Dako, Glostrup, Denmark) was diluted in 1× TBS/0.1% Tween20/1% BSA and membranes were incubated for 2hrs at room temperature. Following incubation, membranes were washed three times for 2min in 1× TBS/0.1% Tween20 and proteins were detected

by chemiluminescence using the West FEMTO substrate kit (Thermo Fisher Scientific) imaged on the VersaDoc™ Imaging System (Bio-Rad) using the Quantity One software program (version 4.5.0, Bio-Rad). Alternatively BioMax Light X-ray film was sandwiched with membranes in an X-ray film cassette (GE Healthcare) for 1-3 minutes followed by development using a Konica SRX -101A X-ray developer.

Table 2.5.1: Electrophoretic resolving gel buffer

Reagent	***Volumes (mL)***		
	10%	**12%**	**15%**
dH_2O	4.05	3.3	2.3
10% SDS	0.1	0.1	0.1
1.5M Tris-HCl, 0.4% SDS (pH8.8)	2.5	2.5	2.5
30% (v/v) acrylamide/bisacrylamide [37.5:1]	3.3	4	5
10% (w/v) ammonium persulphate	0.1	0.1	0.1
TEMED (N,N,N´,N´-tetramethylethylenediamine)	0.01	0.01	0.01

Table 2.5.2: Electrophoretic stacking gel buffer

Reagent	***Volumes (mL)***		
	10%	**12%**	**15%**
dH_2O	3.05	3.05	3.05
10% SDS	0.05	0.05	0.05
0.5M Tris-HCl, 0.4% SDS (pH8.8)	1.25	1.25	1.25
30% (v/v) acrylamide/bisacrylamide [37.5:1]	0.65	0.65	0.65
10% (w/v) ammonium persulphate	0.05	0.05	0.05
TEMED	0.01	0.01	0.01

2.6 Preparation of total RNA

2.6.1 Nuclease-free procedures

The use of sterile, nuclease-free dH_2O was used in all assays and was sourced either through suppliers (Sigma-Aldrich) or from dH_2O treated overnight in 0.1% DEPC (Diethyl pyrocarbonate) followed by autoclaving.

Pipette tips and eppendorf tubes used were purchased as sterile or autoclaved prior to use. Pipettes, work bench, gloves and general equipment were all sprayed with RNase AWAY (Sigma-Aldrich) prior to, and regularly throughout, work procedure.

2.6.2 RNA extraction

For RNA extraction from all biological material, two methods of RNA extraction were employed. Initial RNA extraction was performed using kits; namely the NucleoSpin RNA II (Macherey-Nagel, Dueren, Germany) and the ISOLATE RNA mini-kit (Bioline Reagents Ltd., London, UK) according to manufacturer's instructions

Alternatively samples were extracted using the TRIzol assay using TRI Reagent (Ambion/Life Technologies). 100µL TRI Reagent was added to washed cells in a monolayer or three volumes to samples in solution. After mixing and 5min incubation at room temperature, 1/3rd volume of chloroform was added, vortexed for 15sec and incubated on ice for 5min. Samples were centrifuged at 12 000 × g for 15min, 4°C and the aqueous top phase removed containing soluble RNA. In new tubes, 1/3rd volume 2-Propanol was added to solution together with 1µL of 20mg/mL glycogen (Invitrogen/Life Technologies) and left for 1hr at -20°C to precipitate. Samples were then centrifuged at 12 000 × g for 10min, 4°C after which the supernatant was aspirated and 100µL 80% ethanol (AnalaR NORMAPUR, VWR International) added to each sample. Tubes were pulse-vortexed and incubated at room temperature for 10min followed by centrifugation at 5000 × g, 5min, 4°C. Ethanol was removed and pellets air-dried for 5min and resuspended in 8µL nuclease free water.

Residual DNA was digested using the RQ1 RNase-free DNase kit (Promega; Madison, Wisconsin) where 1µL 10× RQ1 DNase Reaction Buffer was added together with 1µL (1U) RQ1 RNase-free DNase into sample tubes and incubated at 37°C, 30min. 1µL of RQ1 10× Stop Reaction Buffer was then added to samples and incubated at 65°C, 10min. 30µL nuclease free water and 55µL 2-Propanol was then added and tubes were incubated for 10min, room temperature. Samples were centrifuged at 12 000 × g, 15min, 4°C after which supernatant was aspirated and

100µL 80% ethanol added to the pellet. After 15min incubation at room temperature samples were centrifuged at 12 000 × g for 5min. Resultant pellet were air dried for 5min, room temperature after which RNA was re-solubilised in 15µL nuclease free water and stored at -80°C.

2.6.3 Quantitation of total RNA

RNA concentration was determined using the NanoDrop ND-1000 spectrophotometer using 2µL of sample (diluted 1 in 10). RNA purity was assessed by the A260:A280 absorbance ratios as well as at A260:230. Ratios above 1.9 and 2.0 respectively were considered to be pure RNA. In addition the quality of RNA was assessed on a 1% agarose gel. 0.5g SeaKem ® LE agarose powder (Lonza, Basel, Switzerland) was dissolved in 50mL 1×TBE [90mM Tris, 90mM Boric Acid, 2mM EDTA, pH8.0] in DEPC-dH_2O containing Gel Red nucleic acid stain (Biotium, Hayward, U.S.A), microwaved for 1min (LG Intellowave, Yeouido-dong, South Korea), and cooled to room temperature in a horizontal gel cast system. Volume for 500ng RNA was added to 6× blue/orange loading dye (Promega) to obtain a 1× dilution and loaded into wells. Gels were run for 20min at 100V in 1×TBE running buffer and RNA quality was assessed under UV light using the UVP transilluminator (Upland, U.S.A). Samples with clear, well separated 28S and 18S rRNA bands with no signs of degradation qualified for downstream applications.

2.7 Quantitave real-time Polymerase Chain Reaction (qPCR)

2.7.1 Reverse transcription reaction (RT-PCR)

Unless otherwise specified, 500ng total RNA was reverse transcribed into cDNA using the High Capacity cDNA reverse transcriptase kit (Applied Biosystems/Life Technologies) according to the following protocol. Samples were prepared on ice in 0.6mL thin-walled PCR tubes (Thermo Fisher Scientific) which contained the following:

Table 2.7.1: RT-PCR master mix reagents and volumes

Component	*Volume/Reaction (uL)*
10 x Reverse Transcription (RT) buffer	2.0
25 x dNTP mix (100mM)	0.8
10 x RT Random Primers	2.0
MultiScribe™ Reverse Transcriptase (50U/uL)	1.0
RNase inhibitor	1.0
Nuclease-free H_2O (Ambion)	3.2
Sample RNA	10.0

Reverse transcription was performed using the iCycler Thermal Cycler (Bio-Rad) with the recommended cycling conditions: annealing at 25°C for 10min, extension at 37°C for 120min, and denaturation at 85°C for 5min. Resulting cDNA was stored at -20°C until used.

2.7.2 qPCR by Taqman assay

qPCR was performed using the Taqman gene expression assay or by SYBR Green where indicated in individual chapters.

For the Taqman assay, from the original cDNA samples with a starting RNA amount of 500ng, a 1in50 dilution was made and 10µL was pipetted into a MicroAmp® Fast optical 96-well, 0.1mL reaction plate (Applied Biosystems/Life Technologies) in duplicate. A reaction master mix was made consisting of (volume per reaction well):

- 12.5µL 2x Taqman Universal PCR Master Mix
- 1.25µL 20x Taqman probe
- 1.25µL dH_2O

The gene expression assays were used for the analysis of human TNF-α (HS99999043_m1) and IL-10 (HS00272002_m1). In order to allow for the relative gene expression between cDNA samples, separate wells were set up to quantitate the endogenous control gene 18S rRNA. 2µL of diluted cDNA sample was added per well to which 15µL of a master mix was added consisting of (per well):

- 12.5µL 2x Taqman Universal PCR Master Mix
- 1.25µL 20x Eukaryotic 18S rRNA Endogenous control (FAM™/MGB probe)
- 9.25µL dH_2O

Plates were covered with MicroAmp® Optical adhesive film (Applied Bioscience/Life Technologies). After centrifugation at 450 × g, 30sec, 4°C the plate was run on a 7900HT Fast-Real Time System (Applied Biosystems/Life Technologies) using SDS software (v2.4, Applied Biosystems/Life Technologies) with the following PCR amplification conditions:

Temp (°C)	Time	No. of cycles
50	2min	x1
95	10min	x1
95	15sec	x40
60	1min	

Resulting threshold cycles (C_T) values were obtained from the amplification plot and the automated threshold line. Data was analysed using the comparative C_T method (also known as the delta-delta C_T), whereby the fold differences in gene expression between control and test samples (ΔC_T) was normalised to their respective ΔC_T of the 18S rRNA reference gene.

2.7.3 qPCR by SYBR Green

For gene expression using SYBR Green, 1µL cDNA was pipetted in triplicate into a MicroAmp® Fast 96-well reaction plate to which 9µL master mix was added consisting of:

- 5µL 2x Power SYBR Green Master Mix (Applied Biosystems)
- 0.2µL forward primer
- 0.2µL reverse primer
- 3.6µL dH_2O

Plates were sealed and prepared as before and run on the 7900HT Fast-Real Time System using the pre-set PCR amplification conditions:

Temp (°C)	Time	No. of cycles
50	2min	x1
95	10min	x1
95	15sec	x40
60	1min	

Each qPCR run was extended to include a dissociation step: 95°C for 15sec, 60°C for 15sec, 95°C for 15sec to generate a melting curve. The resulting melting curve was used to verify that only one product was generated during the PCR reaction.

For gene quantitation, a standard curve was generated from mRNA ranging from 2ng to 0.04pg in a 1 in 10; 1 in 2.5 sequential dilution series followed by RT-PCR to generate cDNA (performed using triplicate experimental repeats). The resulting C_T values from qPCR was used to generate an amplification slope for which a linear equation was generated using Microsoft Excel. This equation was used to plot known C_T values from experiments to quantitate starting gene amounts.

2.8 Immunocytochemistry

HMDMs were lifted by a non-enzymatic dissociation buffer (Sigma) and seeded on 13mm glass coverslips in culture overnight. Experiments were then performed with HNP1 or W26A at specified times. Media was removed and wells were washed with 1× PBS and fixed in 3% paraformaldehyde (PFA) for 20min at room temperature. PFA was quenched with 50mM glycine for 10min followed by 1× PBS washing and cells were permeabilized with 0.1% Triton X-100 for 4min. Cells were blocked for 1hr in 5% goat serum at room temperature followed by a 1hr incubation with primary antibody combinations in 1× PBS/0.1% Tween-20 at room temperature (listed in Table 2.4). After three washes cells were incubated with fluorochrome-conjugated secondary antibodies for 1hr at room temperature (listed in Table 2.5). Secondary antibodies used were affinity purified to react with IgG (immunoglobulin G) heavy and light chains. To minimize cross-reactivity, antibodies were adsorbed against IgGs from other commonly used host species. After washing nuclei were stained with 1μg/mL DAPI (4′,6-Diamidino-2-phenylindole dihydrochloride) and cover slips

were mounted onto glass slides using Mowiol mounting medium [9.6% (w/v) Mowiol 4-88, 24% (w/v) glycerol, 0.1M Tris-HCl, pH8.5]. Images were acquired on a Leica TCS SP5 (Leica Microsystems, Wetzlar, Germany) confocal laser scanning microscope with a fixed stage inverted microscope DMI6000CS, equipped with helium/neon lasers (633nm and 543nm), an argon laser (457-514nm), a diode laser (405nm) and a HCX PL APO 63x/1.33 NA oil immersion objective. The acquisition software used was the LAS AF software (Leica Microsystems) and images were acquired from fluorescent channels by sequential scanning to prevent crosstalk between channels. Obtained images were modified from 8-bit mode to RGB (red, green blue) using ImageJ (v1.37c, NIH) with resolution set to 600 dpi (dots per inch).

Table 2.8.1: Immunocytochemistry primary antibodies

Name	*Clone*	*Host*	*Supplier*	*Dilution*
HNP1-3	mono	Mouse	Hycult Biotech	1in100
Rps20	poly	Rabbit	Abcam	1in250
LC3B	mono	Mouse	nanoTools	10µg/mL

Table 2.8.2: Immunocytochemistry secondary antibodies

Name	*Host*	*Target*	*Supplier*	*Dilution*
Alexa Fluor® 647 (H+L) IgG	Goat	Rabbit	Invitrogen	1in400
Alexa Fluor® 555 (H+L) IgG	Goat	Mouse	Invitrogen	1in400
Alexa Fluor® 488 (H+L) IgG	Goat	Mouse	Invitrogen	1in400

2.8.1 Quantitative image analysis

2.8.1.1 Corrected Total Cell Fluorescence (CTCF)

To quantitate rsp20 fluorescence in HNP1 treated cells and controls, ten random field images were taken of cells at 24hrs without adjusting the settings on the confocal microscope between each slide. Using single fluorescent channel images obtained for rps20, three cells were chosen at random and a region was drawn around each cell to be measured using ImageJ software (v1.44p; National Institutes of Health, U.S.A). The Integrated Density (product of the mean grey value and area) was measured for each cell which was corrected for background fluorescence using the equation:

CTCF = Integrated Density – (Area of selected cell × mean fluorescence of three background readings)

The CTCF method was taken from Potapova *et al.* (2011)[121]. The means of the corrected cell fluorescence were calculated for each image and plotted graphically for comparison between treatments and statistical significance.

2.8.1.2 Pearson correlation coefficient

The Pearson correlation coefficient was applied to confocal images as a means to calculate the co-localisation of HNP1 and rps20 using ImageJ (v.1.37c) software. Single fluorescent channels for HNP1 and rps20 staining were converted from RGB colour to 8-bit greyscale and an automated Otsu Threshold setting was applied for each image. Correlation analysis was performed for both images resulting in a frequency scatter plot with tabulated Pearson correlation values. This was performed for ten random field images of each sample at 4hr and 24hr time points and plotted graphically for statistical significance.

2.9 ^{35}S-Methionine labelling

HMDMs were seeded at $1.2x10^5$ cells/well in 24 well culture plates and incubated in $_L$-methionine free DMEM (MP Biomedicals; Santa Ana, U.S.A) for 2hrs. At 2hrs supernatant was removed and, in triplicate, cells were treated with HNP1 (12.5 or 25µg/mL) alone or stimulated with CD40L and IFN-γ alongside untreated controls. Radiolabelled ^{35}S-Methionine (Perkin Elmer, Waltham, U.S.A) was added to media at 100µCi (microcurie)/mL and incubated for 4hrs and overnight. At time points culture media was collected for TNF-α ELISA and TCA protein precipitation. Protein pellets were resolubilised in 100uL 1× Laemmli buffer (Invitrogen/Life Technologies). Washed cells were lysed in 100µL 1× Laemmli buffer and purified by passing the lysate through an RNeasy Microkit filter column (Qiagen; Hilden, Germany). 25µL and 20µL of secreted and cellular fractions, respectively, were separated by SDS-PAGE using NuPage® Novex ® 4-12% Bis-Tris gradient gels (Invitrogen/Life Technologies) run at 200V. Gels were fixed for 15min in 50% methanol/10% acetic acid, rinsed and stained using Gelcode Blue (Thermo

Scientific; Waltham, U.S.A) overnight. After overnight destaining in dH_2O, gels were dried (Model 583, Bio-Rad) and visualised on an Image Scanner 3 (GE Healthcare, Waukesha, Wisconsin). Radioactive protein images were developed on a Phospho cassette (GE Healthcare) and visualised using a Typhoon 9400 imager (Amersham Biosciences; Piscataway, U.S.A). From phosphorimaging, total protein band volumes in gel lanes were semi-quantitated from images using ImageQuant TL 7.0 software (GE Healthcare), applying a rolling ball method set at '200' for lane background subtraction.

Radioactive proteins were also quantitated by scintillation counting by adding 10µL sample to 1mL Optiphase HiSafe 2 scintillation cocktail (Perkin Elmer). Radioactive emission was measured on a Wallac 1450 Micobeta TriLux liquid scintillation counter (Perkin Elmer).

2.10 *In vitro* translation

2.10.1 Plasmids and in vitro transcription

Derivation of plasmids expressing reporter mRNA were previously described for pCSFV-*lacZ*[122] and pT7-*Luc*[123]. Plasmids together with an aliquot of Chemically Competent Cells (*E.coli*, X01 Blue strain) was kindly donated by Dr Nicola Gray (Centre for Reproductive Health, University of Edinburgh) and thawed on ice. CCC cells were incubated with 0.5µg plasmid for 30min on ice followed by heat shock for 45sec at 42°C and returned to ice for 2min. Cells were incubated on agar culture plates containing 100µg/mL ampicillin overnight at 37°C in a humidified incubator. A single bacterial colony was picked and scaled up by incubation in 2mL Luria Broth (LB) containing 100µg/mL ampicillin for 5hrs at 37°C in an orbital incubator (Kallenkamp) at 200rpm. 50µL of culture was then added to 100mL LB broth (with 100µg/mL ampicillin) in an Erlenmeyer flask and further incubated. Bacterial culture was then centrifuged at 3000 × g for 10min at 4°C to obtain a cell pellet and plasmid DNA was extracted using the Endofree® Plasmid Maxi kit (Qiagen, Hilden, Germany) according to manufacturer's protocol. The resultant purified DNA concentration was determined using the Nanodrop1000 spectrophotometer (Thermo

Scientific) and purity was confirmed by the absorbance ratio at A260nm and A280nm.

2.10.2 DNA digestion

For both plasmids 10µg plasmid DNA was digested with 2µL of Bgl II restriction enzyme (Roche) in 10µL of 10x SuRE/cut Buffer M (Roche) in a total volume of 100µL. This mixture was incubated for 1hr at 37°C after which 0.5µL of restriction enzyme was added and further incubated for 30min at 37°C. Following incubation, the digested plasmid was purified using the Qiaprep® Miniprep kit by adding 5 volumes of buffer PB to 1 volume of DNA solution, added to Qiaprep spin columns and centrifuged for 1min at 3000xg. The flow through was discarded and columns were washed with 750µL buffer PE and centrifuged for 30s at 3000 × g, followed by a brief centrifugation at 14 000 × g for 1min to discard residual buffer. DNA was eluted by adding 50µL buffer EB, incubating for 1min and centrifuging for 1min at 3000 × g. Resultant DNA was measured on the NanoDrop 1000 (Thermo Scientific) to determine concentration and purity using the absorbance values at A260nm and A280nm.

2.10.3 In vitro transcription

Transcription was performed from digested plasmid DNA to yield reporter mRNA Luc-A0 (containing a gene for Luciferase expression) and CSFV-Gal (containing a gene for β-galactosidase expression). The following reagents were added in an RNase-free tube for the transcription of each mRNA transcript:

Table 2.10.1: *in vitro* transcription reagents (Luc-Ao mRNA)

Reagent	***Supplier***	***Vol (µL)***
T7 transcription buffer (5x)	Stratagene	l0.00
Dithiothreitol (DTT; 1mM)	Sigma	1.50
m7G (5')ppp(5')G RNA cap structure analogue (40mM)	New England Biolabs	8.75
Nucleic acid mix (Adenine, Uracil, Cytosine, 25mM)	GE Healthcare	2.00
Rnasin® RNase inhibitor (40U/µL)	Promega	2.50
T7 RNA polymerase	Agilent	3.00
DNA template	N/A	l7.50

Table 2.10.2: *in vitro* translation transcription reagents (CSFV-Gal mRNA)

Reagent	***Supplier***	***Vol (µL)***
SP6 transcription buffer (10x)	Stratagene	5.00
ApE (G'(5)ppp(5')A RNA cap structure analogue (40mM)	New England Biolabs	8.75
Nucleic acid mix (Adenine, Uracil, Cytosine, 25mM)	GE Healthcare	2.00
Rnasin® RNase inhibitor (40U/µL)	Promega	2.50
SP6 RNase polymerase	Roche	3.00
DNA template	N/A	23.75

Mixtures were incubated for 10min, 37°C after which 5µL of 10mM GTP (GE Healthcare) was added. The mRNA transcription reaction was allowed to continue for 2hrs incubation at 37°C. Following incubation DNA was digested with 5µL RQ1 RNase-free DNase (Promega) for 30min, 37°C. mRNA was then purified by adding 70µL RNase-free dH_2O followed by 100µL acid phenol:chloroform ($CHCl_3$, Ambion), vortexed and centrifuged at 14 000 × g for 2min. The top aqueous phase was removed and step was repeated. ChromaSpin™ columns (Clontech, Mountain View, U.S.A) were then prepared by centrifuging twice at 700 × g, 2min after which mRNA volume was added into the column and centrifuged at 700 × g for 4min, 4°C. RNA was precipitated overnight at -30°C in $1/10^{th}$ volume (8µL) 3M sodium acetate ($NaOA_2$, pH4.2) and 2.5 volumes (400µL) 100% ethanol, followed by centrifugation at 14 000 × g for 30min, 4°C. The pellet was washed twice in 80% ethanol and air dried on ice for 15min and resuspended in 15µL nuclease free water. Purity and concentration of the sample was determined using the Nanodrop spectrophotometer and concentration was adjusted to 1mg/mL. mRNA integrity was confirmed by applying 0.5µL of sample in 6× loading buffer (Promega) to a 1% agarose gel that was stained with Gel Red Nucleic Acid stain (Biotium). The gel was run for 10min at 50V in 1×TBE buffer after which RNA bands were analysed using an ultraviolet (UV) transilluminator.

2.10.4 *in vitro* translation

The following reagents from the nuclease treated rabbit reticulocyte lysate *in vitro* translation kit (Promega) were added in an RNase-free tube:

- Rabbit reticulocyte lysate (35µL)
- Amino acid mixture minus leucine, 1mM (0.5µL)
- Amino acid mixture minus methionine, 1mM (0.5µL)
- RNasin® RNase inhibitor (1µL)
- Nuclease free dH_2O (6µL)

In duplicate samples HNP1, LHNP1 or W26A were added to individual tubes for a total sample volume of 50µL. Samples were incubated for 30min at 30°C on an Eppendorf thermo mixer (Hamburg, Germany) set at 300rpm. At 30min 2µL Luc-A0 mRNA (1µg/mL) and CSFV-Gal mRNA (1µg/mL) were added to each tube. 5µL of reaction mixture was immediately removed from each sample, snap frozen on dry ice and stored for pre-translation mRNA quantitation. Samples were incubated for 90min at 30°C, 300rpm after which 5µL was removed, snap frozen on dry ice and stored at -80°C for post-translation mRNA quantitation. Protein expression was then quantitated by luminescence for both Luciferase and β-gal reporters as follows:
For luciferase protein expression, two 5µL aliquots were removed from each sample and placed in separate FACS tubes. The Lumat LB 9507 luminometer (Berthold Technologies, Bad Wildbad, Germany) was primed twice with Luciferase Assay Reagent (Promega) before samples were read. For β-galactosidase expression the detection substrate Tropix® Galacton Plus (Applied Biosystems) was diluted 1:100 in Tropix® Galacto reaction buffer diluent (Applied Biosystems) before adding 5µL of sample (in duplicate) and incubating for 1hr in the dark at room temperature. The luminometer was primed twice with Tropix® Accelerator II (Applied Biosystems) before quantitation. The average of duplicate samples was taken for data analysis.

2.10.5 mRNA quantitation

To validate the integrity of mRNA pre- and post-translation, RNA extraction of frozen samples was performed using the Trizol method. mRNA was then assessed either by non-denaturing agarose electrophoresis and by qPCR.

For electrophoresis 1% agarose gel was made up by dissolving 1.5g agarose (Biogen Idec, Zug, Switzerland) powder in 130mL DEPC-dH_2O and microwave heated. 15mL 10x MOPS buffer [0.2M MOPS, 50mM Sodium Acetate, 10mM EDTA, pH7.0] was added once cooled together with 5mL formaldehyde solution and gel cast. For sample preparation, 13µL RNA was added to 2.6µL 5x RNA loading buffer [20% (v/v) glycerol, 30.9% (v/v) foramide, 40% (v/v) 10x MOPS buffer, 2.79% (v/v) formaldehyde, 4mM EDTA, pH8.0, trace amount Bromophenol Blue, Xylene Cyanol]. Samples were heated to 65°C for 10min followed by 5min on ice before being loaded onto the gel. The gel was run at 100V for 4hrs in 1x MOPS running buffer, after which the gel was stained using a 1:20 000 dilution of Gel Red Nucleic acid stain in 1x MOPS buffer for 1hr at room temperature. Gel images were captured using by FLA-5100 Fluorescent Image Analyser (FujiFilm, Tokyo, Japan), using the Image Reader FLA-5000 series V1.0 software, at laser wavelength 473nm.

For *Luc* gene quantitation by qPCR, 1µg purified RNA was reverse transcribed and 1µL from a 1 in 10 cDNA dilution was used for subsequent *Luc* gene quantitation by SYBR Green qPCR (as previously described in section 2.7.3). Gene targets were analyzed using custom made primers for Firefly Luciferase purchased from Integrated DNA Technologies (Coralville, U.S.A)
(Forward sequence (100µM):GGCGCGGTCGGTAAAGTT; Reverse (100µM): AGCGTTTTCCCGGTATCCA)

2.10.6 Immunoprecipitation (IP)

The experimental set for *in vitro* translation assays (as described in section 2.10.4) were utilized for IP studies. Rabbit reticulocyte lysate reaction mixtures were incubated with 25µg/mL HNP1, W26A or vehicle (0.01% acetic acid) 30min prior to 20ng Luc-A0 mRNA addition followed by 90min incubation at 30°C.
IP of HNP1 and analysis of rps20 expression was performed from an adapted protocol detailed in Park *et al.* (1998)[124]. Reaction mixtures were divided into two equal volumes and added to separate tubes containing 1mL NET-2 buffer [150mM NaCl; 50mM Tris-HCl, pH7.5; 0.05% (v/v) NP40; EDTA-free 1× protease inhibitor

cocktail, and 40U RNasin in DEPC-dH_2O]. Duplicate samples were then incubated with either 500ng monoclonal mouse anti-human HNP1-3 antibody or 500ng $IgG_{1,\kappa}$ isotype control antibody (BD Biosciences, Franklin Lakes, U.S.A) for 2hrs at 4°C on a head-over-end eppendorf rotator.

Protein G Sepharose beads (GE Healthcare) to be used (10µL per sample) were washed in 1mL NET-2 buffer, vortexed briefly and pelleted by centrifugation prior to being added to IP mixtures. Samples were returned to rotator for overnight incubation at 4°C. Beads were then washed five times in 1mL NET-2 buffer and pelleted, keeping supernatant from first wash for protein precipitation. From the first supernatant wash a volume was removed for TCA protein precipitation, equivalent to 0.5µL of rabbit reticulocyte lysate. Pelleted beads and precipitated proteins from supernatants were resuspended in 1× Laemmli buffer boiled at 95°C for 10min, centrifuged and electrophoresed by 12% SDS-PAGE as previously described (section 2.5) using home-made gels. As a positive control for rps20 detection, samples of 0.5µL pure rabbit reticulocyte lysate were included. Membranes were immunoblotted using polyclonal rabbit anti-rps20 (1:2000 dilution) followed by incubation with Clean-Blot IP detection reagent (Thermo Fisher Scientific, dilution 1:500). Protein bands were detected by chemiluminescence using West FEMTO Supersignal kit and BioMax Light X-ray film on the Konica SRX-101A X-ray developer.

2.11 Electrophoretic Mobility Shift Assays (EMSAs)

Oligonucleotides consisting of 25bp Adenine (Poly A), Cytosine (Poly C) and Uracil (Poly U) labelled with a Cy5 flourophore at the 5' end were purchased from Eurogentec (Seraing, Belgium). 10pmol (picomole) of oligo was incubated with titrated pmol ratios of HNP1 or W26A in 10µL binding buffer adapted from Sladic *et al.*(2004)[125] [20mM Tris-HCl, pH8.0, 20% (v/v) glycerol, 0.1% (v/v) IgePal CA-630, 2mM DTT, 140mM KCl (potassium chloride), 200ng/mL BSA, 3mM $MgCl_2$ (magnesium chloride)]. Samples were incubated on ice for 30min after which 5× loading buffer [10% [v/v] Glycerol, 5% DMSO, 0.1% Bromophenol Blue] was added for a 1× dilution. Binding reactions were electrophoresed in a non-denaturing 7% (v/v) polyacrylamide gel [60:1, 1×Tris/borate/EDTA, 0.07% (v/v) ammonium

persulphate, 0.1% TEMED] for 5hrs at 150V, 4°C (gel were pre-run overnight at 150V). Gels images were obtained using the FLA-5100 image reader using a 635nm laser to detect Cy5 and free, migrated oligonucleotide was quantitated using AIDA Image Analyser software (Raytest, Straubenhardt, Germany). Note that early binding buffer optimisations involved comparing above used buffer (termed buffer 'SL') to binding buffer used for EMSA experiments below (termed buffer 'GT').

For EMSAs investigating peptide interactions with HMDM RNA, total RNA was extracted using the NucleoSpin RNAII kit (Thermo Fisher Scientific). 1µg RNA was incubated with titrated amounts (µg) of HNP1, LHNP1 or W26A in 20µL binding buffer 'GT' adapted from Park *et al.* (1998)[124] [10mM Tris-HCl, pH8.0, 5% (v/v) glycerol, 1mM EDTA, 1mM DTT, 20mM KCl, 50µg/mL BSA, 1µL (20U) Rnasin®] and incubated for 1hr at room temperature. Note that at this point for supershift EMSA experiments, monoclonal mouse anti-HNP1-3 antibody was added to samples (1ng/µL) and incubated for a further 30min at room temperature. 6× blue/orange loading dye (Promega) was added for a 1× dilution and electrophoresed on a 1% agarose gel [1xTBE, GelRed nucleic acid stain (Biotium), 1:10 000 dilution] for 1hr at 125V. Gels images were obtained on a transilluminator (UVP) or the FLA-5000. 18S and 28S rRNA band volumes were semi-quantitated using the AIDA Image Analyser software. In initial experiments, 28S and 18S rRNA mean grey values were semi-quantitated using ImageJ.

2.12 Calcium flux

HMDMs were seeded in Teflon pots and treated overnight with 25µg/mL HNP 1-3 or left untreated. After washing the cells in cation-free 1× PBS the Ca^{2+} fluorescent probe Fura 2-AM was added at 2µM and cells were incubated at 37°C for 30min in cation-free 1× Hanks Balanced Salt Solution (HBSS, PAA Laboratories GmbH). Cells were washed, incubated at 37°C for a further 10min and seeded in calcium-containing 1× HBSS. Real time cytoplasmic calcium mobilisation was quantitated using the LS50B Fluorescence Spectrometer (Perkin Elmer) using dual wavelength excitation (340nm and 380nm) and emission at 510nm. To quantitate calcium mobilisation within the cell cytoplasm, 1µM Plate-Activating Factor (PAF) was

added to cells 30sec after real time recording began. To calibrate fluorescence values, maximal (R_{max}) and minimal (R_{min}) values were determined by adding 10% Triton X-100 and 0.1M EGTA respectively. $[Ca^{2+}]i$ was calculated from the relationship $[Ca^{2+}]i = Kd.(R- R_{min})/ (R_{max}-R).b$, where:

$[Ca^{2+}]i$ is the cytoplasmic calcium concentration,

R is the ratio of fluorescence obtained at 340nm and 380nm in the cuvette before calibration,

R_{max} is the fluorescence ratio under saturating $[Ca^{2+}]i$,

R_{min} is the fluorescence ratio in the absence of Ca^{2+},

Kd is the dissociation constant for Fura 2-AM, taken as 224nm at 37°C and,

b is the fluorescence ratio at 340nm of cells in the absence and presence of Ca^{2+}.

Cytoplasmic calcium values were assessed by measuring the approximate area under the curve after mean basal calcium levels had been subtracted for each curve. Time point intervals were then divided into parallelogram segments and calculated, followed by the addition of all the segments to obtain total area under the curve.

2.13 Endoplasmic Reticulum stress

2.13.1 BiP, CHOP and spliced XBP-1 gene expression

HMDMs in culture were stimulated with R848 either alone or in the presence of 25% NN, 12.5μg/mL HNP1 or LHNP1. ER stress inducer thapsigargin was included in experiments as a positive control. Cells were incubated at time intervals over 24hrs after which cells were lysed and RNA extracted using the ISOLATE RNA mini kit (Bioline) and cDNA synthesised using the High Capacity cDNA RT kit (Applied Biosystems) as per manufacturer's instructions. cDNA samples were then sent to collaborators Professor Pieter Hiemstra and Emily van't Wout (Department of Pulmonology, Leiden University Medical Centre, Albinusdreef 2, The Netherlands) for gene expression by qPCR. From cDNA samples gene expression was quantitated by SYBR Green qPCR for the molecular chaperone BiP (immunoglobulin binding protein), spliced XBP-1 (X-box binding protein-1) and CHOP (C/EBP-homologous protein) according to previously published methods[126]. For spliced XBP-1 quantitation, primers spanned the 26 base pair intron that is removed by IRE1 to

obtain the spliced XBP-1 mRNA (XBP-1spl) (forward: 5′-TGCTGAGTCCGCAGC AGGTG-3′; reverse: ′GCTGGCAGGCTCTGGGGAAG-3′).

Primers used for CHOP (forward: 5′-GCACCTCCCAGAGCCCTCACTCTCC-3′; reverse: 5′-GTCTACTCCAAGCCTTCCCCCTGCG-3′) and BiP (forward: 5'-CGAGGAGGAGGACAAGAAGG-3'; reverse 5'-CACCTGAACGGCAAGAA CT-3') mRNA expression were used.

Quantitative PCR was carried out at the following conditions: 95°C for 3 min followed by 40 cycles of denaturation at 95°C for 10s, annealing at 62°C for 15s and extension at 72°C for 30s using IQ SYBRGreen supermix (Bio-Rad, Hercules, CA, USA). Each assay was run on a Bio-Rad CFX Real-time PCR system in triplicate and arbitrary mRNA concentrations were calculated by the Bio-Rad software, using the relative standard curve method. Stable housekeeping genes were selected using the Genorm software[127]. Relative mRNA concentrations of ATP5B and RPL13A (GeNorm, Primerdesign, Southampton, UK) were used as reference genes to calculate the normalized expression of the XBP-1spl mRNA. The identity of the PCR products obtained with the XBP-1 spliced primers was verified by DNA sequencing.

2.13.2 Eukaryotic Initiation Factor (eIF) 2α phosphorylation

HMDMs seeded in 24 well plates at 1.8×10^5 cells/well were (in triplicate wells) stimulated with R848 alone together with 12.5μg/mL or 1μM thapsigargin and incubated time intervals over 24hrs. After time points, cells were lysed on ice for 10min in 50μL lysis buffer [20mM Tris-HCl (pH7.5), 150mM NaCl, 1% (v/v) Triton X-100, 10% (v/v) glycerol, 1mM Na_3VO_4, 100mM NaF and Complete™ protease inhibitor cocktail with EDTA (Roche)].

Samples were centrifuged at 10 000 × g for 10min, 4°C and protein concentrations were determined in supernatants by Bio-Rad protein assay. 20μg protein was electrophoresed by 10% SDS-PAGE followed by Western blotting. Membranes were blocked and immunoblotted against phosphorylated eIF2α using monoclonal rabbit anti-eIF2 (phospho S51) (Abcam, dilution 1:250). Membranes were then incubated with polyclonal goat anti-rabbit Ig/HRP secondary antibody (Dako, dilution 1:2000) and protein bands were visualised by chemiluminescence using the VersaDoc imaging system.

Membranes were then stripped of bound antibody by a 20min incubation with Restore Western Blot stripping buffer (Thermo Fisher Scientific), followed by a 1hr wash in 1× TBS/0.1% Tween-20. Complete antibody absence was confirmed by chemiluminescent detection. The membranes were immunoblotted against β-actin as previously described.

2.14 Polysome analysis

HMDMs were seeded in 60mm culture dishes (Corning) and stimulated with R848 alone or with HNP1 alongside untreated controls. At time points specified after incubation, spent media was removed for TNF-α ELISA quantitation while cells were incubated with 150μg/mL cycloheximide for 30min.

After washing in 1× PBS (with 150μg/mL cycloheximide), cells were lysed in 200μL 1× lysis buffer containing:

- 20mM Hepes buffer (pH7.6)
- 2mM $MgCl_2$
- 150mM KCl
- 2mM DTT
- 0.5% IgePal CA-630 (NP-40)
- 7μL RNase inhibitor (100U/mL)
- 150μg/mL cycloheximide
- 1x Complete protease inhibitor cocktail (with EDTA)
- 1mM Na_3VO_4
- 25mM NaF

After 10min incubation on ice, cells were scraped and collected in 0.6mL eppendorf tubes and centrifuged at 10 000 x g for 10min, 4°C. Supernatant were collected into new tubes and KCl concentration adjusted to 0.25M.

Sucrose gradients were prepared by dissolving sucrose powder in dH_2O and adding to 2× gradient buffer for a 1× dilution. Sucrose gradient range was from 50, 42, 34, 26, 18 to 10 (% w/v). 1× gradient buffer consisted of:

- 40mM Hepes buffer (pH7.6)
- 4mM $MgCl_2$

- 500mM KCl
- 5mM DTT
- 1µg/mL heparin

Gradients were layered from 50% to 10% with 650µL per gradient in a 4.4mL Sorvall 3P thin walled polyallomer tube (Thermo Fisher Scientific), freezing each gradient at -80°C for 20min before adding the next gradient. Gradients were stored at -80°C until used.

Lysates were layered onto thawed gradients and centrifuged using a Sorval Ultra Pro 80 ultracentrifuge at 274 823.9 × g (45 000rpm) in a Sorval TH-660 rotor for 80min, 4°C. Tubes were then set up to fractionating equipment (Foxy Jr, Teledyne ISCO, Lincoln, U.S.A) and a UA-6 UV/Vis detector (Teledyne ISCO) to measure the absorbance of samples passing through the detector at 254nm. Peak profiles were plotted on graph paper attached to the detector and digitally recorded using the PeakTrak software, v1.10.

Collected eluent fractions were divided into two fresh eppendorf tubes for TRIzol RNA extraction and protein purification using the ProteoExtract RNA was electrophoresed in a 1% non-denaturing agarose gel. Protein samples were electrophoresed by 10% SDS-PAGE followed by Western blotting. Membranes were immunoblotted using antibodies to rps20 (dilution 1:1000) or rabbit anti-Poly(A)-binding protein (PABP1, 1:100 000 dilution, produced in house). Membranes were then incubated with polyclonal goat anti-rabbit Ig/HRP secondary antibody (Dako, dilution 1:100 0000) and protein bands were visualised by chemiluminescence using the VersaDoc imaging system.

Where appropriate, amounts of TNF-α mRNA were quantified within each collected fraction by SYBR Green qPCR (as previously described in section 2.7.3). For normalisation of quantitated TNF-α, 2µL of 10ng/µL Luc-A0 mRNA was added to each fraction (obtained from section 2.10.3). 250ng of purified RNA was reverse transcribed followed by the addition of 1µL cDNA (diluted 1 in 10) added in wells containing 9µL SYBR Green mastermix. The mastermix contained custom made

forward and reverse TNF-α primers purchased from Eurogentec (Forward sequence (100μM): CCATGTTGTACGAAACC;
Reverse sequence (100μM): TCTCAGCTCCACGCCTT). In a separate qPCR reaction, quantitation of Luc-A0 mRNA was performed as previously described (section 2.10.5).

2.15 Sucrose density gradient centrifugation

Sucrose density ultracentrifugation was performed on samples derived from the *in vitro* translation assay described above using Luc-A0 reporter mRNA.
The reaction mixtures were incubated with HNP1 or W26A at 25μg/mL in duplicate incubate for 30min at 30°C, after which 40ng Luc-A0 mRNA was added to each reaction mixture and incubated for a further 90min at 30°C. 5μL sample was removed post incubation for luciferase quantitation using the Lumat luminometer. To the remaining lysate, two volumes of translation stop buffer was added (in DEPC-dH_2O):

- 20mM DTT
- 150μg/mL cycloheximide
- 665μg/mL heparin
- 1x Complete protease inhibitor cocktail (with EDTA)
- 1.5μL RNase inhibitor (100U/mL, Applied Biosystems)

Lysates were layered onto a 1.2mL 15-40% (15, 24, 32, 40) sucrose gradient as described for polysome analysis (section 2.14). Tubes were centrifuged at 215 000 × g for 80min at 4°C using the Sorvall RC M150 GX (fixed rotor S100 AT6). Ten, 120μL fractions were removed, placed into fresh eppendorf tubes and RNA was extracted the Trizol extraction method, keeping the phenol-ethanol portion containing proteins. RNA fractions were electrophoresed in a 1% non-denaturing agarose gel for the confirmation of rRNA in each fraction as assessed from resulting gel images. Fractions containing rRNA had their corresponding phenol-ethanol fractions pooled together for protein extraction as per TRIzol protocol guidelines. DNA was first removed by adding 30% (v/v) ethanol (100%), incubating for 3min at room temperature and centrifuging at 2000 × g for 5min, 4°C to pellet DNA.

Supernatant was removed to which 1.5 volumes isopropanol was added to Trizol volume followed by incubation at room temperature for 10min and centrifuged at 12 000 × g for 10min at 4°C. Protein pellet was washed and incubated twice with 0.3M Guanidine Hydrochloride in 95% ethanol for 20min at room temperature. Tubes were centrifuged at 7500 × g for 5min, 4°C to remove supernatant. 100% ethanol was then added and incubated for 20min at room temperature followed by centrifugation at 7500 × g for 5min, 4°C. After air drying the pellet, proteins were solubilised in 1× Laemmli buffer and electrophoresed on a 12% SDS-PAGE gel. A Western Blot was performed for the detection of HNP1/W26A using monoclonal mouse anti-HNP1-3 antibody as previously described.

2.16 Wound healing

Eight week old female CD1 mice were anaesthetised and a full-thickness 10mm × 2mm excision was made aseptically on the shaved dorsal skin. BMDMs to be injected into the wound were prepared from CD1 female mice as described in 2.2.3. Day 6 BMDMs were incubated in Teflon pots for 24hrs in serum free DMEM F12 Glutamax™ media only or containing 25% human NN supernatant. 100µL saline containing 3×10^6 BMDMs were injected subcutaneously at four points around the wound. Control mice received 100µL of saline. Wounds were photographed daily over a nine day period. From obtained images the area of the wound sizes were measured according to scale using a ruler placed within the image in the same plain as the wound. These measurements were plotted on a percentage graph relative to the area of the original wound size. This experiment was performed in accordance with project licence number (PPL) 60/3948.

2.17 Statistical methods

Statistical analysis was performed under the guidance of a course provided by the Institute for Academic Development, University of Edinburgh. The course was presented by Professor Amanda Lee (Medical Statistics Team, Division of Applied Health Sciences, University of Aberdeen) and Gillian McHugh (Centre for Population Health Sciences, University of Edinburgh). All statistical analysis was performed using GraphPad Prism 4 for Windows.

Where appropriate, results from single experiments are reported as mean ± Standard Deviation (SD) with triplicate repeats. For n distinct observations results are reported as mean ± Standard Error of the Mean (SEM). Parametric statistics was used for assessments of normally distributed data. Comparisons between two groups was determined with the Student's *t*-test while data containing more than two groups was analysed by Analysis of Variance (ANOVA) showing similar variance between samples using Barlett's test where appropriate. *Post hoc* analysis between groups was assessed using the Dunnett's or Bonferroni test as appropriate for the group comparison. For non-parametric statistical analysis where normal distribution of data was not assumed, comparisons of more than two groups was performed using the Kruskal-Wallis ANOVA, using Dunn's multiple comparison test for *post hoc* analysis. P-values below 0.05 were considered significant to reject the null hypothesis. In the figures, P-values smaller than 0.05, 0.01, and 0.001 are presented as *, ** and ***, respectively.

Chapter 3

3 The anti-inflammatory properties of α-defensins

3.1 Introduction

The immunomodulatory functions of α-defensin have been extensively studied and date back to the early 1980's from pioneers in the field, notably Professors R. I. Lehrer, T. Ganz, W. Lu and Dr A.K. Lichtenstein. Their early work not only began examining the antimicrobial properties of defensins and other antimicrobial peptides but also their effects on various mammalian cells. It is their research that has paved the way for a large collection of publications on α-defensins over the last 30 years which is still growing. The published functions of α-defensins vary greatly between the different cell types studied. This introduction summarises the collective immunomodulatory findings of α-defensins with an emphasis on leukocyte activity.

α-Defensins have been found to be released not only from dying human neutrophils[87] but also when activated[128]. Released HNP1 and 2 (but not HNP3) were demonstrated to act as chemotactic factors for monocytes in nanomolar concentrations[129], suggesting that released α-defensins not only fulfil immediate antimicrobial actions but most likely further recruit leukocytes to combat invading pathogens.

Not only do they act as chemokines but they also stimulate the release of chemokines and cytokines from cells. α-Defensin concentrations between 5-10μg/mL stimulated the release of IL-8 and MCP-1 (monocyte chemoattractant protein -1) in human bronchial (BEAS-2B) and alveolar (A549) epithelial cells[130]. In moderate to high concentrations (10-20μg/mL), α-defensins elicited caspase-3 activation in these cells resulting in apoptosis 24hrs after exposure. α-Defensin concentrations below 10μg/mL not only stimulated a host of inflammatory mediators in monocyte derived immature dendritic cells (IL-8, TNF-α, IL-1β, IL-12p40, IL-10), but also lead to their maturation *in vitro* by way of increased cell surface expression CD86, CD83 and HLA-DR[131]. Conversely higher concentrations of α-defensins lead to a decrease in all mature DC cell surface markers as well as attenuation of all cytokines but IL-8.

Shi *et al.* (2007) suggested that HNP1 (20-100μg/mL) blocked IL-1β secretion specifically but not TNF-α in LPS stimulated monocytes[115].

The cytotoxicity of α-defensins has also been studied at great length. HNP1-3 at concentrations of 25-100μg/mL effectively induced cytolysis in a variety of human lymphoma cells and non-malignant target cells[132]. Interestingly cytolysis was induced in cell lines made resistant to TNF and NK-cytolytic factor killing. In a comparative cytotoxic study of PMN granule constituents, defensin-containing fractions were the most lethal against human leukaemia, carcinoma and lung fibroblasts[44]. In the same study defensin cytotoxicity appeared to be synergistic with released hydrogen peroxide, suggesting that these two components released from neutrophils work in tandem to sacrifice cells in the general vicinity of infection.

In a mechanistic study using erythroleukemia cells (K562) and 50μg/mL HNP1-3, data showed that defensin-mediated cytolysis occurs as a result of initial membrane binding, internalisation and critically interference with cellular metabolism by way of glycolysis and ion transport[133]. Cytolysis could not be reversed by the blocking actions of serum on HNP1-3 if serum was administered more than 30min after of HNP exposure. This gave an indication of the rapid cytotoxic actions of α-defensins on cells which require more than simply membrane binding to exert their effect, as was demonstrated by defensin-resistant murine cell line L929 which still showed comparable binding to that of K562 cells.

From what it appears, α-defensin cytotoxicity is more harmful than microbial infection itself. The consolation is in the limitations of peptide function beyond the immediate extracellular spaces. In a review on this topic by Ganz (1987)[128], suggestions are that half of released defensins become incorporated into the PMN membrane and of the remaining half, functionality will be limited to intercellular spaces that exclude macromolecules which inhibit their function, for example through lectin-like binding to glycosylated proteins in serum. Thus it would appear that only in areas of severe inflammation with high numbers of activated and/or

dying neutrophils, do α-defensins facilitate this function of perhaps required collateral damage.

With regard to their inhibitory effect on macrophages, the actions of α-defensins appear to be specific to peptide concentration. Miles *et al.* (2009)[87] showed all inflammatory mediators tested to be inhibited by α-defensin in the range 12-25μg/mL (TNF-α, IL-1β, IL-6, IL-8, IL-10 and nitric oxide). Other research groups showed the presence of HNP1-3 (<1μg/mL) boosted macrophage phagocytosis of IgG-opsonized *Staphylococcus aureus* through increased expression of the Fcγ receptors CD32 and CD64 while releasing TNF-α and IFN-γ[134].
This chapter sets out to recapitulate the inhibitory findings of α-defensins on human macrophages and to begin unravelling the mechanism responsible.

3.2 Results

3.2.1 Optimization assays of buffy coat-derived HMDM stimulants

Previously, HMDMs were obtained from whole blood donations taken on the same day from healthy volunteers within the Centre for Inflammation Research. Blood from unused buffy coats also became a readily available source of HMDMs. Initial cell culture assays were focussed on optimising the appropriate agonist for downstream studies involving necrotic neutrophil supernatants and human neutrophil peptide (HNP). These optimisation experiments were performed since buffy-coat derived HMDMs did not become activated with CD40L and IFN-γ stimulation, which was the conventional stimulation method used in Miles *et al.* (2009). Details on the results of these optimisation experiments can be found in Appendix A.

Levels of secreted cytokines in culture supernatants were quantitated by ELISA in a series of experiments assessing the inhibitory effect of α-defensins on macrophages. Initial experiments investigated the inhibitory effect of Necrotic Neutrophil supernatants (NN), which consist of a milieu including α-defensins, cathelicidin and pro-inflammatory stimulants such as proteases and elastase. These NN supernatants were made from freeze/thawed neutrophils, purified by ultracentrifugation to pellet membrane material. NN was able to effectively inhibit TNF-α production in buffy coat-derived HMDMs when added together with LPS, with the amount of added NN expressed as a percentage of total cell culture volume (Figure 3.1). Inhibition was observed with 5% NN (equivalent to $2.5x10^6$ neutrophils), 15% NN ($7.5x10^6$ neutrophils) and 25% NN ($12.5x10^6$ neutrophils).

With TNF-α reproducibly attenuated in R848-stimulated buffy coat HMDMs with NN treatment (see Appendix A), further experiments continued to assess this effect on other cytokines. Results from Figure 3.2 showed the inhibitory effect of 25% NN together with R848 at concentrations 2.5μg/mL and 1μg/mL. This was assessed in secreted levels of IL-6, IL-8 and IL-10 at 4hrs and 24hrs incubation. Levels of IL-6 were strongly attenuated by 25% NN at both time points, in excess of 100 fold inhibition at 24hrs. While there was a declining trend of IL-8 at 4hrs, a clear

inhibition was noticeable at 24hrs. A similar pattern was observed with IL-10 expression even though basal IL-10 levels were moderately high at around 100pg/mL seen with untreated control cells. R848 stimulation at 2.5μg/mL clearly elevated levels of IL-10 in comparison to untreated controls. Since stimulation with 2.5μg/mL R848 sufficiently upregulated all cytokines tested, the decision was made to proceed using these parameters to assess α-defensin mechanisms in buffy coat macrophages.

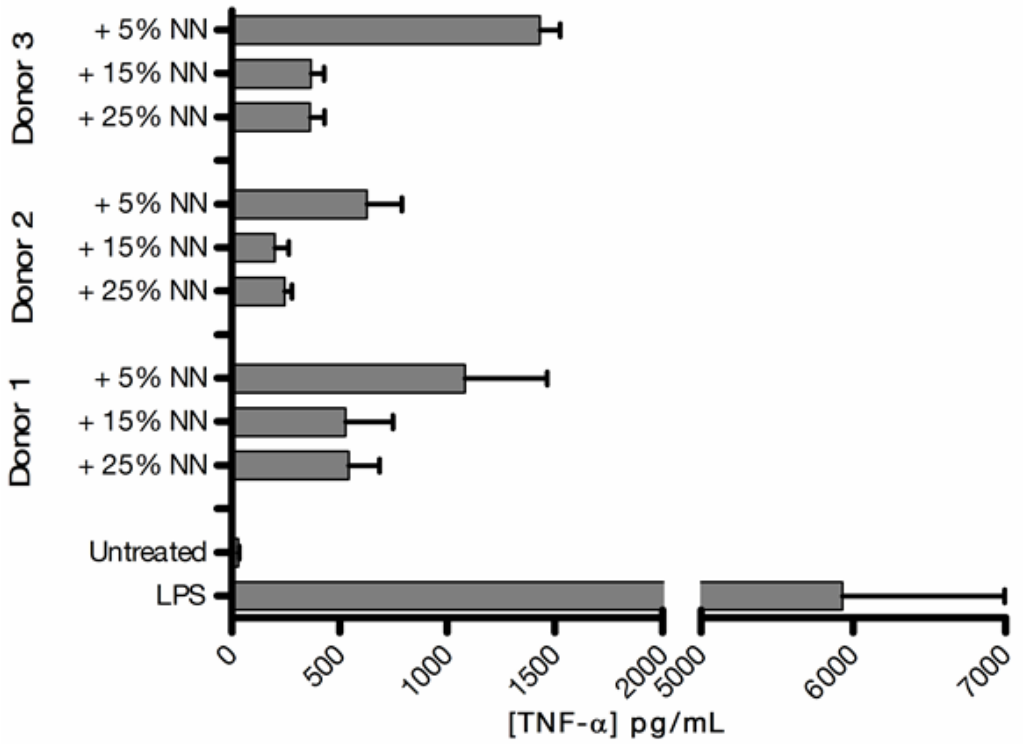

Figure 3.1: The effect of Necrotic Neutrophil supernatants in LPS stimulated HMDMs

Secreted TNF-α quantitated by ELISA of buffy coat HMDMs stimulated with 1ng/mL LPS alone or in the presence of titrated necrotic neutrophils supernatants (NN) from three neutrophil donors, expressed as the final volume percentage in culture wells (% v/v). Graph represents the mean ±SD of a single experiment with three experimental replicates, tested on a single HMDM donor.

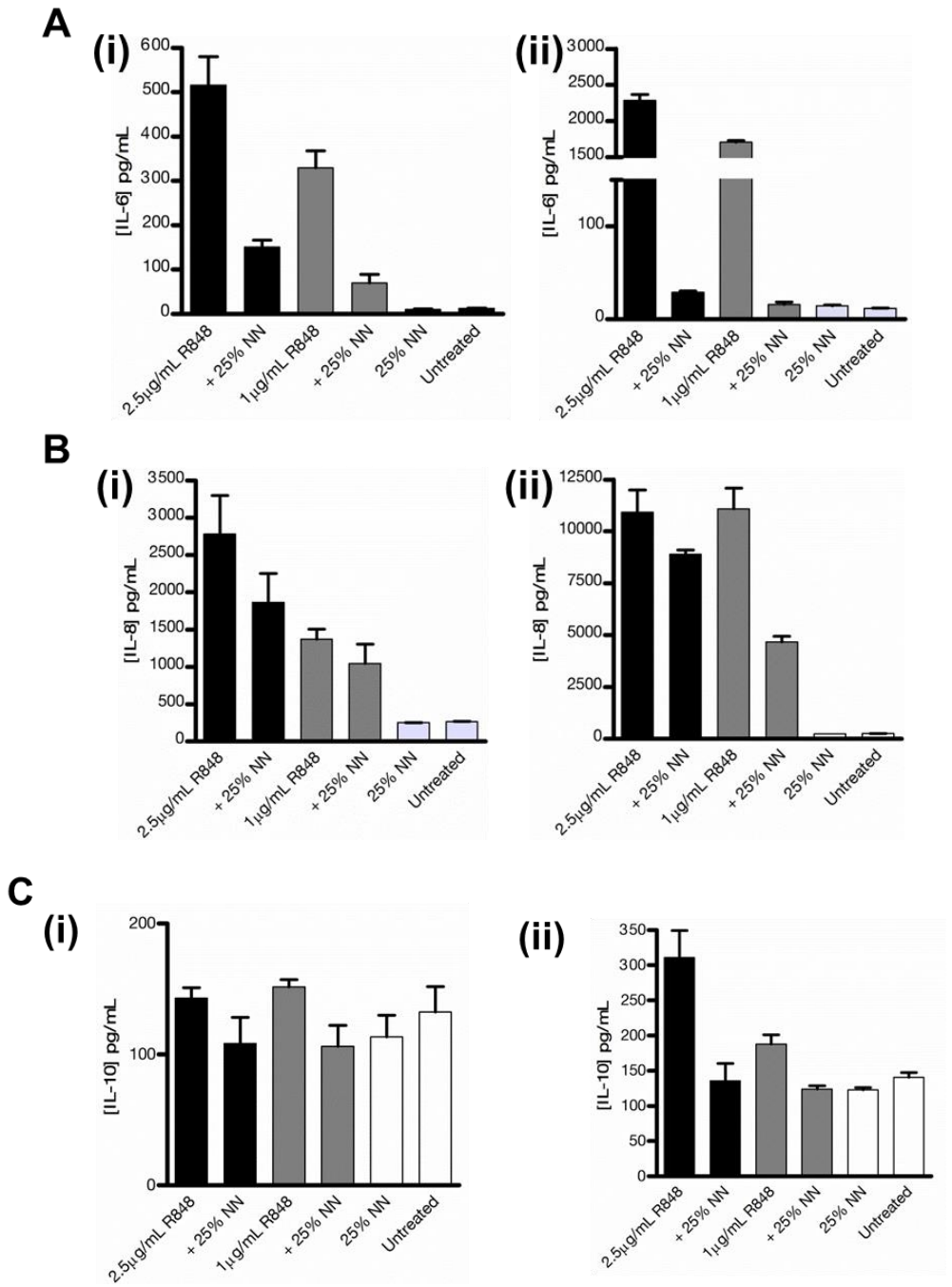

Figure 3.2: Quantitated IL-6, IL-8 and IL-10 secretion in R848-stimulated buffy coat HMDMs with NN

ELISA results of quantitated IL-6 (**A**), IL-8 (**B**) and IL-10 (**C**) in supernatants at 4hrs (**i**) and 24hrs (**ii**) after stimulation with 2.5 and 1µg/mL R848 with 25% NN. Error bars represent the mean ±SD from n=1 donor with 3 experimental replicates.

3.2.2 HNP amino acid composition is essential to inhibitory function

Assessments of the inhibitory properties of NN were established in R848-stimulated HMDMs. Further experiments were performed to confirm the inhibitory properties of HNP on TNF-α as previously published[87], adapting the agonist to effectively stimulate buffy coat HMDMs.

Stimulation using R848 (5μg/mL), SAC (*Staphylococcus aureus* Cowan strain; 0.1%) and Poly I:C (5μg/mL) were tested together with 25μg/mL HNP1-3 for 18hrs (Figure 3.3). HNP1-3 attenuated quantitated TNF-α in R848 stimulated cells but not in SAC, while Poly I:C showed no stimulation compared to untreated controls. It is thought that SAC most likely neutralised α-defensins at this concentration through binding, thus explaining the lack of inhibitory actions on stimulated HMDMs. In a separate experiment R848 concentrations were reduced to 2.5 and 0.5μg/mL while SAC concentrations were reduced to 0.01% and 0.001% (Figure 3.4). HNP1-3 at 25μg/mL was again effective at reducing secreted TNF-α at all concentrations tested and this time in both R848 and SAC stimulated HMDMs.

In more extensive experiments in the second half of the research period, access to a second chemically synthesized HNP1 mutant became available courtesy of our collaborator, Professor Wuyuan Lu. This was in addition to previous use of linear HNP1 (LHNP1) published in Miles *et al.* (2009) showing no inhibitory effect. This mutant peptide, W26A, was a single amino acid substitute of tryptophan at residue position 26 with alanine (W26A) which was previously found to be the most deleterious mutation in its ability to kill *Staphylococcus aureus*, inhibit anthrax lethal factor, and bind to HIV-1 gp120 protein[58]. This was attributed to the peptide's altered hydrophobicity and ability to dimerise and possibly form higher order oligomers with itself.

Figure 3.5*A* represents the results (n=3) of R848-stimulated HMDMs together with 12.5 or 7.5μg/mL HNP1, LHNP1 and W26A. HNP1 at 7.5μg/mL and 12.5μg/mL showed a trend towards inhibited TNF-α levels compared to R848-stimulated alone

controls in the three HMDM donors tested, while W26A and LHNP1 showed no inhibitory effect on secreted TNF-α.

When available, frozen PBMCs obtained from clinically diagnosed Rheumatoid Arthritis (RA) patients were thawed and processed as normal following PMBC isolation from blood preparations to obtain HMDMs, as described in Chapter 2, section 2.2.1. In three attempts to differentiate PBMCs into mature HMDMs of sufficient cell number for experiments involving HNP1, only a single donor was successful. Mature HMDMs from the RA patient were subsequently stimulated with 1μg/mL R848 together with 12.5μg/mL HNP1, which showed effective inhibition of secreted TNF-α (Figure 3.6*A*). Frozen PBMCs from healthy donors thawed and matured into HMDMs as performed for RA donor cells showed a similar trend of TNF-α attenuation with HNP1 (Figure 3.6*B* and *C*).

In a series of experiments to ascertain the minimal inhibitory threshold of HNP1, R848 stimulated HMDMs were treated together with HNP1 concentrations 1, 5, 10 and 12.5μg/mL, alongside LHNP1 and W26A. HNP1 showed no inhibitory effect at 1 and 5μg/mL as TNF-α values remained similar to R848-stimulated alone controls (Figure 3.7). HNP1 remained inhibitory at a concentration of 10μg/mL.

As the actions of α-defensins are sensitive to the presence of serum proteins, the concept of incorporating HNP1 into liposomes for treatment in serum-containing media was briefly addressed. POPC liposomes were formulated with the incorporation of 2% mol HNP1 as described in Chapter 2, section 2.2.7 (alongside empty liposome controls). From this formulation, titrated liposome concentrations were tested in R848-stimulated HMDMs in culture media containing 10% human serum or without. No effect on TNF-α was observed on cells treated with liposomes added at 300 and 600μg/mL in both culture media conditions (Figure 3.8*A*). No significant effect was observed using 1.2mg/mL liposomes in a single experiment using serum-free culture media (Figure 3.8*B*).

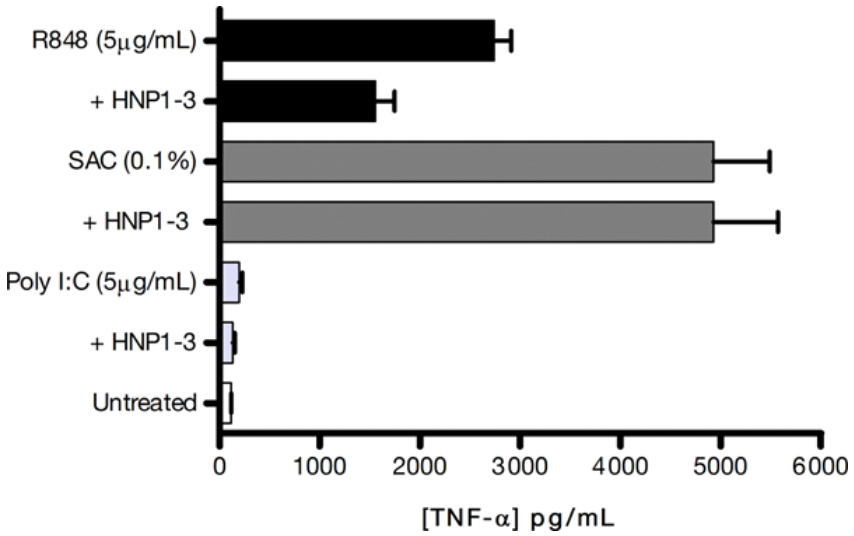

Figure 3.3: The effect of HNP1-3 on buffy coat HMDMs stimulated with R848, SAC and Poly I:C

Secreted TNF-α values obtained after 18hrs incubation in agonist-stimulated HMDMs alone or together with 25μg/mL HNP1-3. Results represent the mean ±SD for treatments from a single experiment (n=1) with three experimental replicates.

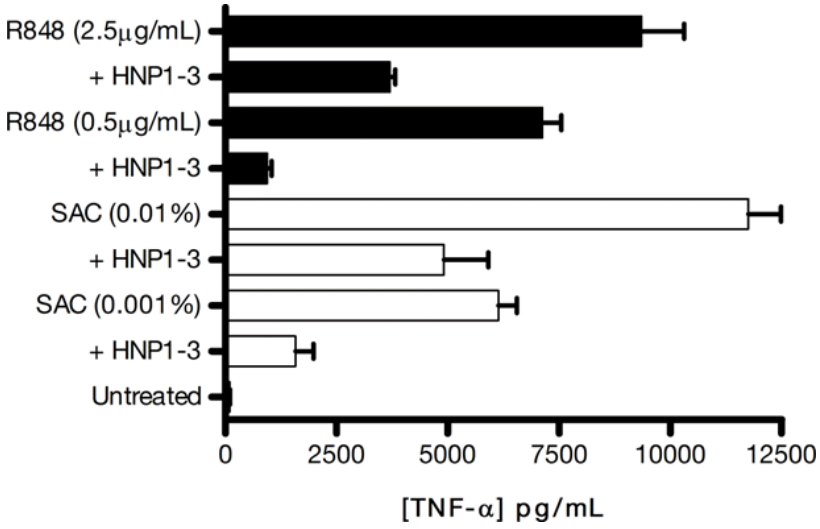

Figure 3.4: The effect of HNP1-3 in fresh HMDMs stimulated with R848 and SAC

Quantitated TNF-α by ELISA at 18hrs incubation post treatment. HMDMs obtained from a fresh blood donation were R848-stimulated alone or together with 25μg/mL HNP1-3 and graphs represent the mean ±SD of a single experiment (n=1) with three experimental replicates.

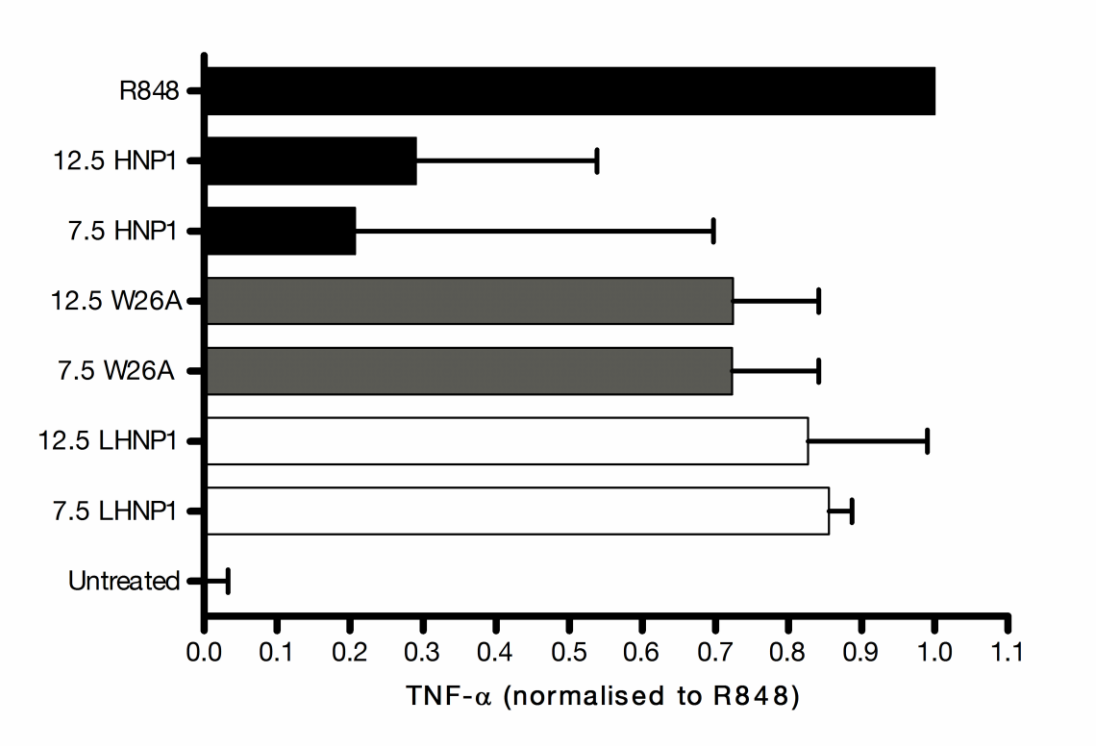

Figure 3.5: The effect of HNP1 and mutant derivatives on R848-stimulated HMDMs

Secreted TNF-α quantitation of fresh HMDMs stimulated with 1μg/mL R848 in culture with HNP1, LHNP1 or W26A after 18hrs incubation. Peptide concentrations of 12.5μg/mL and 7.5μg/mL were used. (**A**) Secreted TNF-α values were normalised to cells stimulated with R848 alone obtained from three independent experiments (n=3) with each sample performed in triplicate. Values are of the median with error bars representing the interquartile range. Nonparametric statistical analysis was performed between peptide groups of the same concentrations using the Kruskal-Wallis test, with no significance obtained (P values).

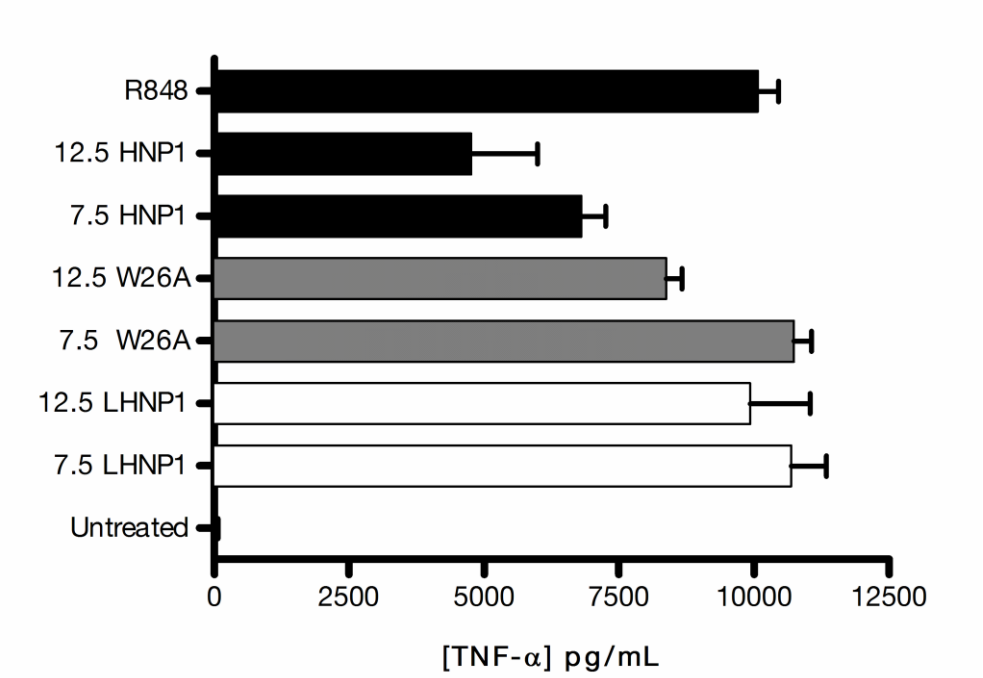

Figure 3.5 (continued): The effect of HNP1 and mutant derivatives on R848-stimulated HMDMs

(**B**) Representative graph indicating quantified TNF-α amounts (in pg/mL) from one of the three repeat experiments. Error bars represent the mean ±SD for samples with three experimental replicates.

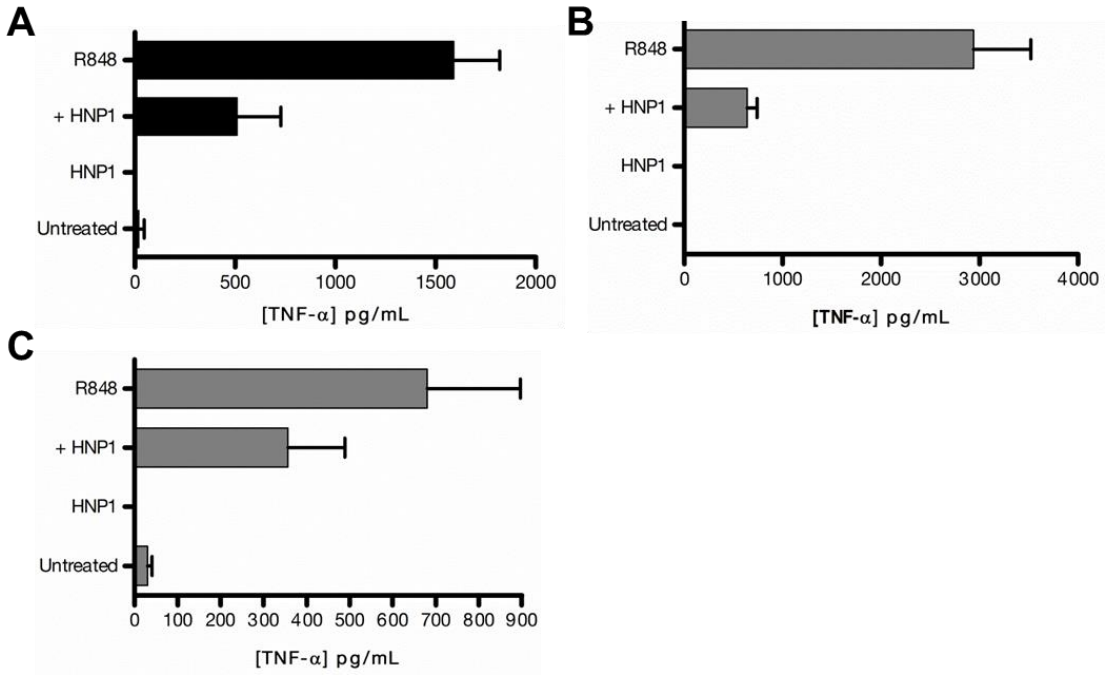

Figure 3.6: The effect of HNP1 in Rheumatoid Arthritis HMDMs

Secreted TNF-α from rheumatoid arthritis HMDMs (**A**) or healthy donors (**B** and **C**) taken from fresh blood donations and stimulated with 1µg/mL R848 alone with 12.5µg/mL HNP1 at 24hrs. Error bars represent the mean ±SD of n=1 with three experimental replicates.

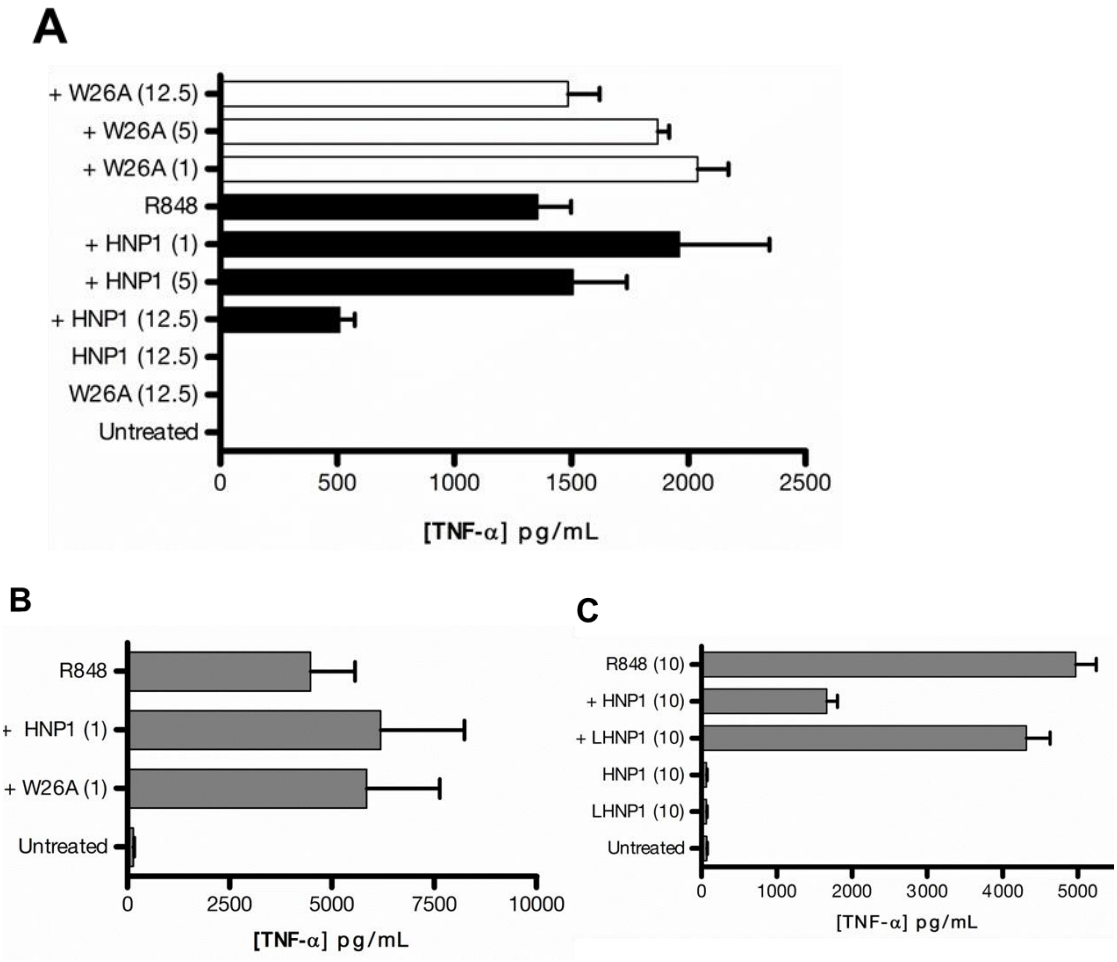

Figure 3.7: Minimum inhibitory HNP1 concentrations

(**A**) Secreted TNF-α from buffy coat HMDMs stimulated with 2.5μg/mL R848 alone or with 1, 5 or 12.5μg/mL HNP1 or W26A alongside unstimulated controls (at 24hrs).

(**B**) Secreted TNF-α from buffy coat HMDMs stimulated with 2.5μg/mL R848 alone or in the presence of 1μg/mL HNP1 or W26A (18hrs).

(**C**) Secreted TNF-α in from buffy coat HMDMs stimulated with 2.5μg/mL R848 alone or the presence of 10μg/mL HNP1 or LHNP1 (24hrs).

All results are of the mean ±SD for and n=1 experiment with three experimental replicates.

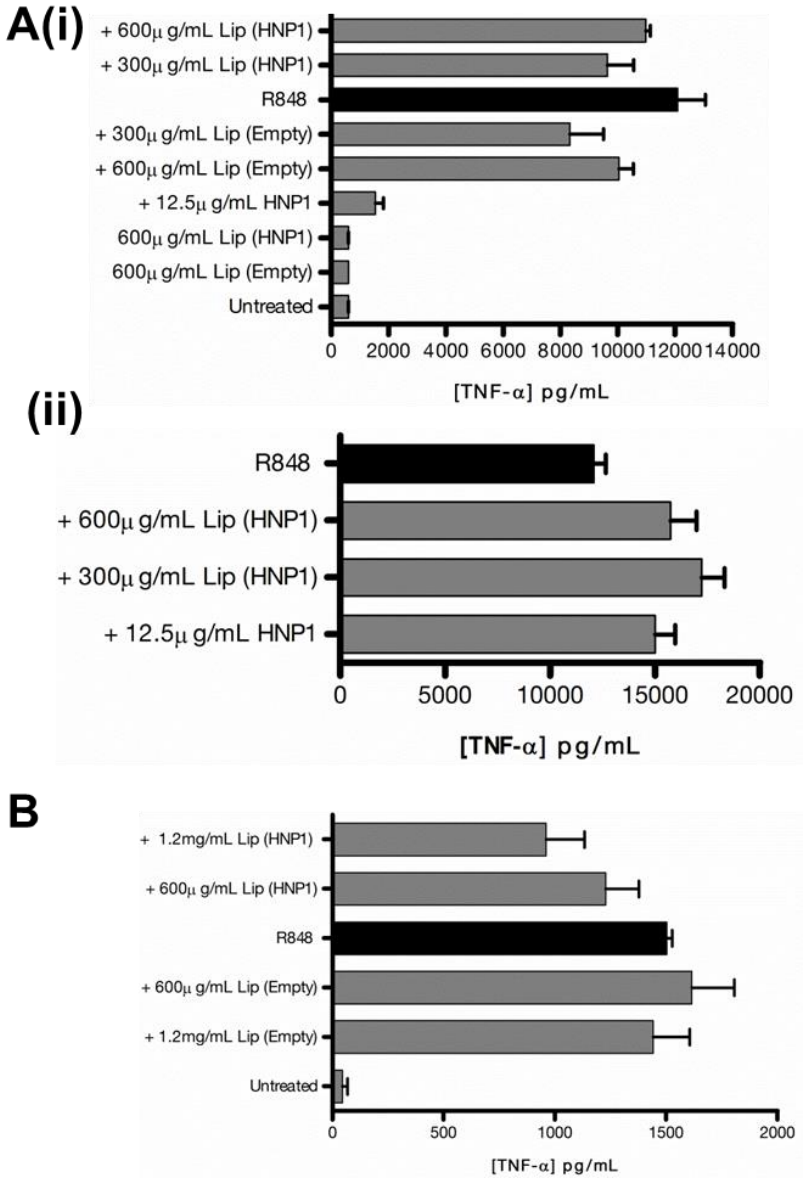

Figure 3.8: The addition of HNP1-treated liposomes in stimulated HMDMs

TNF-α ELISA results of HMDMs (fresh blood donations) stimulated with 1µg/mL R848 alone (black bar) or with titrated POPC liposome concentrations containing 2% mol HNP1 or empty liposomes after 24hrs. (**A - i**) Results from treatments performed in the absence of serum along with HNP1 alone, liposomes alone and an untreated control. (**ii**) Treatments in serum-containing media. (**B**) A repeat experiment with higher liposome concentrations in the absence of serum. Error bars represent the mean ± SD of single experiments (n=1) with three experimental replicates.

3.2.3 The effect of α-defensins on cytokine gene expression

The section above described the inhibitory actions of α-defensins on secreted cytokines which supports previously published results. The next section investigated the question concerning TNF-α mRNA expression over the critical time points (i.e. <24hrs). This was to establish whether the anti-inflammatory effect seen was due to the prevention of mRNA expression of key inflammatory cytokines.

Previous (unpublished) mRNA quantitation experiments were performed by Katherine Miles, from the Dr Mohini Gray research group, using freshly-prepared HMDMs stimulated with 3μg/mL CD40L + 5ng/mL IFN-γ (CI), with validated TNF-α secretion inhibition by HNP1 as represented in (Figure 3.9*B-ii*). CI stimulated HMDMs were treated with 25μg/mL HNP1 and cells were harvested over a 24hr period for RNA and subsequent qPCR for TNF-α and IL-10 mRNA expression (Figure 3.9*A*). Results show a similar gene expression of both cytokines over 24hrs compared with CI-stimulated alone controls. Expression of TNF-α mRNA was analysed in repeated experiments over 6hrs (Figure 3.9*B* – D) with varying degrees of expression between experiments. In (*B*), TNF-α mRNA declined sharply in HNP-treated cells between 1.5 and 2hrs and remained approximately 25% lower over 2hrs compared to CI-stimulated alone controls. In (*C*) mRNA values remained similar over 3hrs. While expression in controls remained steady over the time course, expression declined in HNP-treated samples by approximately half at 4hrs and 6hrs. In (*D*) TNF-α gene expression showed a similar trend between treatments although a sharper decline was observed between 2-3hrs in HNP-treated samples. In all experiments the initial upregulation of mRNA expression was similar in the presence of HNP1 compared to stimulated controls in all experiments. This suggests that signal transduction pathways leading to TNF-α and IL-10 mRNA transcription appear unaffected in the presence of HNP.

From the above results it was hypothesized that the rapid decline of TNF-α mRNA over short time periods might be attributed to a decrease in mRNA stability with HNP addition, possibly explaining the lack of secreted TNF-α. Within cells, Tristetraprolin (TTP) is a major constituent in the regulation of inflammatory

mRNAs by binding to adenine-uridine (AU)-rich regions resulting in deadenylation or removal of the poly-(A) tail[135]. p38 MAPK activation stabilizes inflammatory mRNAs (including TNF-α) by the phosphorylation of TTP by MK2, a downstream kinase of p38[136]. Thus it was hypothesized that HNP1 might prevent TTP phosphorylation in stimulated cells, resulting in increased TTP activity and explaining the reduction of secreted TNF-α. To test this hypothesis, $TTP^{-/-}$ knock out bone marrow derived macrophages (BMDMs) derived from C57 BL/6 mice were kindly donated by Dr Jonathan Dean (Department of Medicine, Imperial College London) and cultured as described in Chapter 2, section 2.2.3. TTP BMDMs were stimulated with FGK45 (the murine equivalent of CD40L) and murine IFN-γ alone or together with HNP1 or LHNP1. Wild type BMDMs from the same background were included as controls (Figure 3.10). After 18hrs incubation, quantitated TNF-α by ELISA from collected supernatants showed that HNP1 remained inhibitory in $TTP^{-/-}$ BMDMs, as shown in a representative result from three independent experiments (Figure 3.10*A*). Normalising TNF-α expression of HNP1 and FGK/IFN-γ-stimulated alone values to LHNP1 values from n=3 experiments (Figure 3.10*B*), results showed a significant reduction ($P<0.01$) of TNF-α in wild type and $TTP^{-/-}$ BMDMs. These results effectively ruled out the hypothesis that increased TTP activity was the cause of the decline in TNF-α mRNA expression with HNP1 treatment.

HMDM TNF-α mRNA expression studies were continued for further clarification using buffy coat HMDMs stimulated with R848 and treated with 5% NN over 24hrs (Figure 3.11). In addition to simultaneous treatments of NN and R848, test samples also included HMDMs pre-treated with NN for 1hr and 24hr prior to stimulation. This was in order assess if longer incubation with α-defensins would lead to the further manifestation of the slight differences initially observed.

qPCR results of TNF-α mRNA expression showed very similar patterns of gene expression in HMDMs which had 1hr NN pretreatment and HMDMs with NN added at the time of stimulation over 24hrs (Figure 3.11*A*-*i*). Interestingly, initial increases in TNF-α mRNA with α-defensins were about 1.3 fold higher in value than stimulated-alone controls, yet expression at 4hrs suggested a sharp attenuation of

TNF-α mRNA to levels similarly observed in stimulated-alone controls. Where the treatments differed was in secreted TNF-α protein. While R848 alone HMDMs showed unhindered TNF-α production, 1hr NN pretreatment showed a greater level of inhibition compared to NN added at the time of stimulation (Figure 3.11*A-ii*). This provided early suggestions that the inhibitory actions of NN occurred not at the level of transcription but at a later stage. It also suggested that the degree of inhibition became greater with longer exposure to NN.

A different trend was observed in 24hr NN pretreated HMDMs which questioned if longer NN exposure affected TNF-α mRNA inhibition differently to that observed at shorter time intervals. Cells pretreated with NN for 24hrs prior to stimulation showed a similar pattern of initial upregulation of TNF-α mRNA, but declined sharply to near basal levels after 4hrs. Secreted TNF-α in these 24hr pretreated samples was substantially lower in value to near baseline levels throughout the time course.

Contrary to the minor differences in TNF-α mRNA expression with NN treatment, the assessment of IL-10 mRNA over 24hrs showed similar expression across all treatments over 24hrs while secreted IL-10 values were markedly reduced in all NN-treated cells from 8hrs onwards (Figure 3.11*B*). This result agreed with the suggestion that α-defensins did not affect mRNA expression yet still inhibited secreted cytokines, proposing an inhibitory effect at a later stage, possibly during the translation process. Between the assessments of TNF-α and IL-10 in this single experiment, the only conflicting result was that of TNF-α mRNA expression in 24hr NN pretreated samples. This would, however, require further repeat testing to confirm these results. Based on these findings, this result brought into question if mRNA stability was a factor with prolonged NN exposure and required further assessment.

In order to specifically assess TNF-α mRNA stability with NN, mRNA decay rates were assessed using actinomycin D, an antineoplastic antibiotic which inhibits DNA-primed RNA synthesis by binding to deoxyguanosine residues on double-stranded DNA (information sourced from the Sigma-Aldrich reagent data sheet), blocking

transcription. Actinomycin D was added 1hr post R848 stimulation – at the peak of TNF-α mRNA expression - in HMDMs pretreated with 5% NN for 24hrs alongside stimulated-alone controls (Figure 3.12). The resulting data from time points collected over 2hrs after actinomycin D treatment suggested a similar pattern of mRNA decay in NN treated and R848-stimulated alone HMDMs. This result suggested that NN were not affecting the stability of transcribed mRNA, even in prolonged exposures, and that the inhibitory actions were perhaps mediated by other mechanisms.

This experiment analysing TNF-α decay rates over 2hrs was repeated in buffy coat HMDMs treated with 12.5μg/mL HNP1 or LHNP1 alongside R848-stimulated alone controls (Figure 3.13*A* and *B*). This was performed since earlier experiments assessing TNF-α mRNA expression in HNP-treated HMDMs might have suggested a sharper decline in expression compared to R848-stimulated alone controls (Figure 3.9). Decay rates between treatments appeared similar over 2hrs incubation with actinomycin D, with the slight exception of a short (20min) decline in decay in HNP1-treated HMDMs after 10mins of actinomycin D incubation (Figure 3.13*A*-*i*). Meanwhile, a more gradual TNF-α decay was observed in LHNP1 and stimulated-alone controls. For the validation of HNP1-mediated inhibition on secreted TNF-α, a parallel set of cells receiving treatments, with the exception of added actinomycin D, confirmed the inhibitory effect of HNP1 not observed in LHNP1 controls (Figure 3.13*A*-*ii*). Secreted TNF-α from stimulated controls containing actinomycin D treated were included in ELISA quantitation as a positive control for the effect of the antibiotic. This single experiment would suggest an increase in decay for a short interval, but it is uncertain if this apparent increased decay period had any bearings on the overall inhibition on secreted TNF-α. This is especially considering that TNF-α mRNA levels near-paralleled that of LHNP1 while secreted TNF-α between the two treatments showed a clear difference.

In a repeat experiment (Figure 3.13*B*), results appeared contradictory to the above findings. TNF-α decay rates in HNP1 and LHNP1 treated HMDMs showed similar patterns of decline following actinomycin D. This observed similarity was despite the fact that secreted TNF-α in HNP1 treated cells was clearly inhibited while

unaffected in LHNP1-treated cells compared to stimulated-alone controls. Quantitated TNF-α mRNA in R848-stimulated alone controls showed unusual decay patterns, which made it difficult to use as a comparative control.

Overall, the data in this section could not confidently conclude a link between the profound inhibitory effects of α-defensins on secreted cytokines with differences in mRNA expression or decreased stability. A more substantial hypothesis emerged during the same period of research with an alternative suggestion to the inhibitory mechanism. It was decided to pursue this hypothesis in more detail and will be covered in Chapter 4.

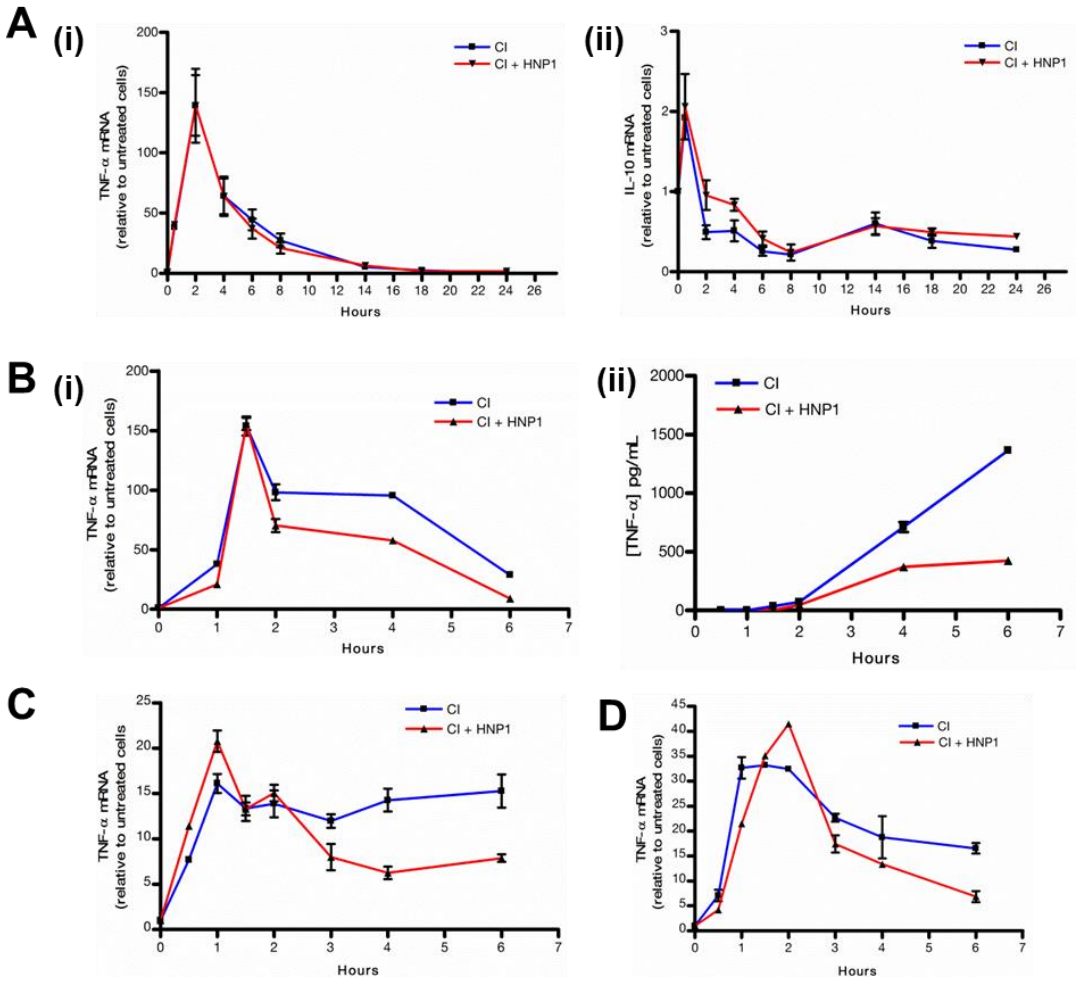

Figure 3.9: TNF-α and IL-10 mRNA expression in HNP1 treated HMDMs

qPCR of gene expression in HMDMs (fresh blood donations) stimulated with 3µg/mL CD40L + 5ng/mL IFN-γ alone or in the presence of 25µg/mL HNP1.

(**A**) TNF-α (**i**) and IL-10 (**ii**) mRNA expression over 24hrs.

(**B-i**) Quantitated TNF-α mRNA with secreted cytokine proteins (**ii**) over 6hrs.

(**C** and **D**) Repeat TNF-α mRNA expression experiments over 6hrs.

In all experiments mRNA expression was normalised to 18S rRNA and plotted relative to untreated control cells. Data represents the mean ±SD of single experiments (n=1) performed using triplicate repeats for each sample. Experiments performed by Katherine Miles.

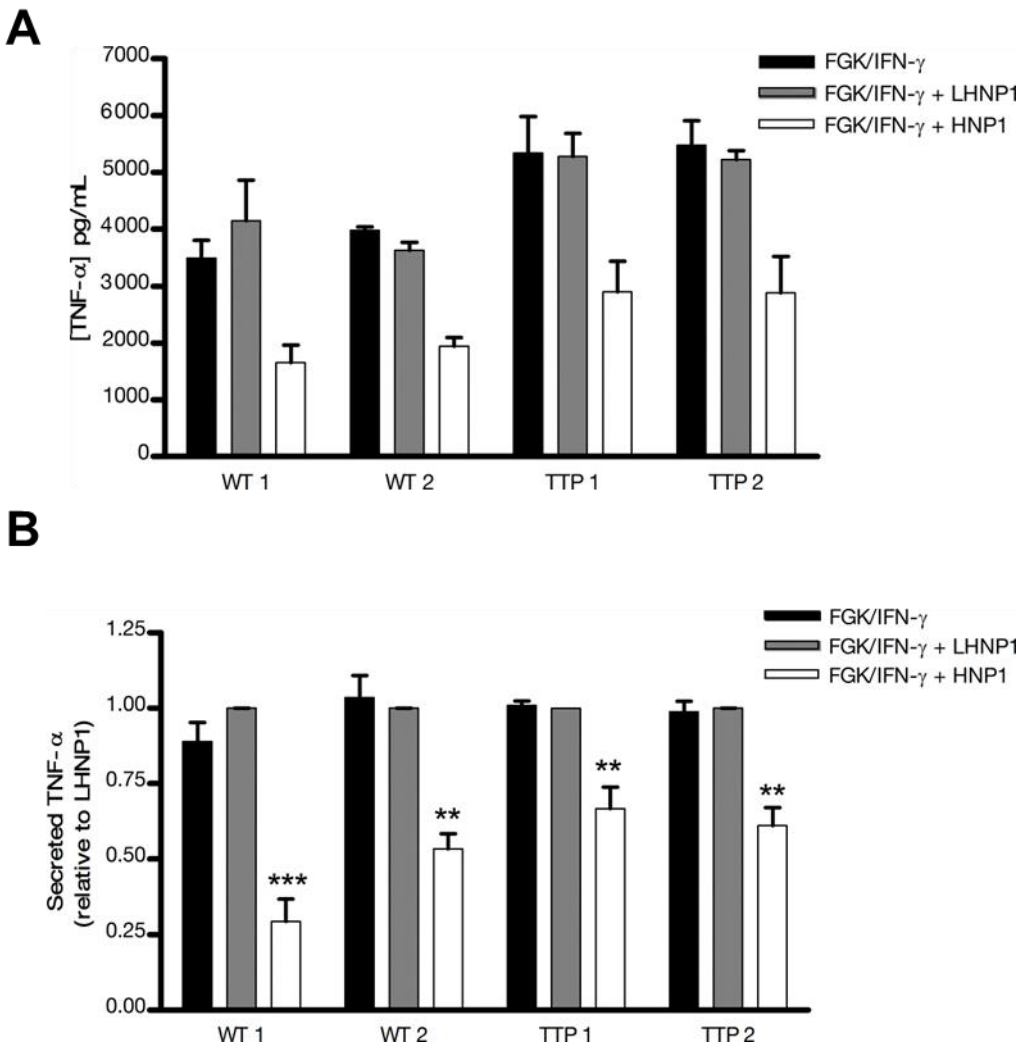

Figure 3.10: The effect of HNP1 in TTP$^{-/-}$ BMDMs

Secreted TNF-α quantitated at 18hrs incubation. Bone Marrow Derived Macrophages obtained from the femurs of C57 BL/6 female mice (2x WT, 2x TTP$^{-/-}$ KO) and stimulated using 50μg/mL FGK-45 + 5ng/mL IFN-γ alone or in the presence of 25μg/mL HNP1 or LHNP1. (**A**) One representative graph from three repeat experiments, with error bars showing the mean ±SD. (**B**) Secreted TNF-α plotted relative to LHNP1 controls with values of the mean ± SEM from three independent experiments, with triplicate samples for each treatment. Statistical analysis was performed using Tukey's *post hoc* analysis following one way ANOVA. **P<0.01, ***P<0.001.

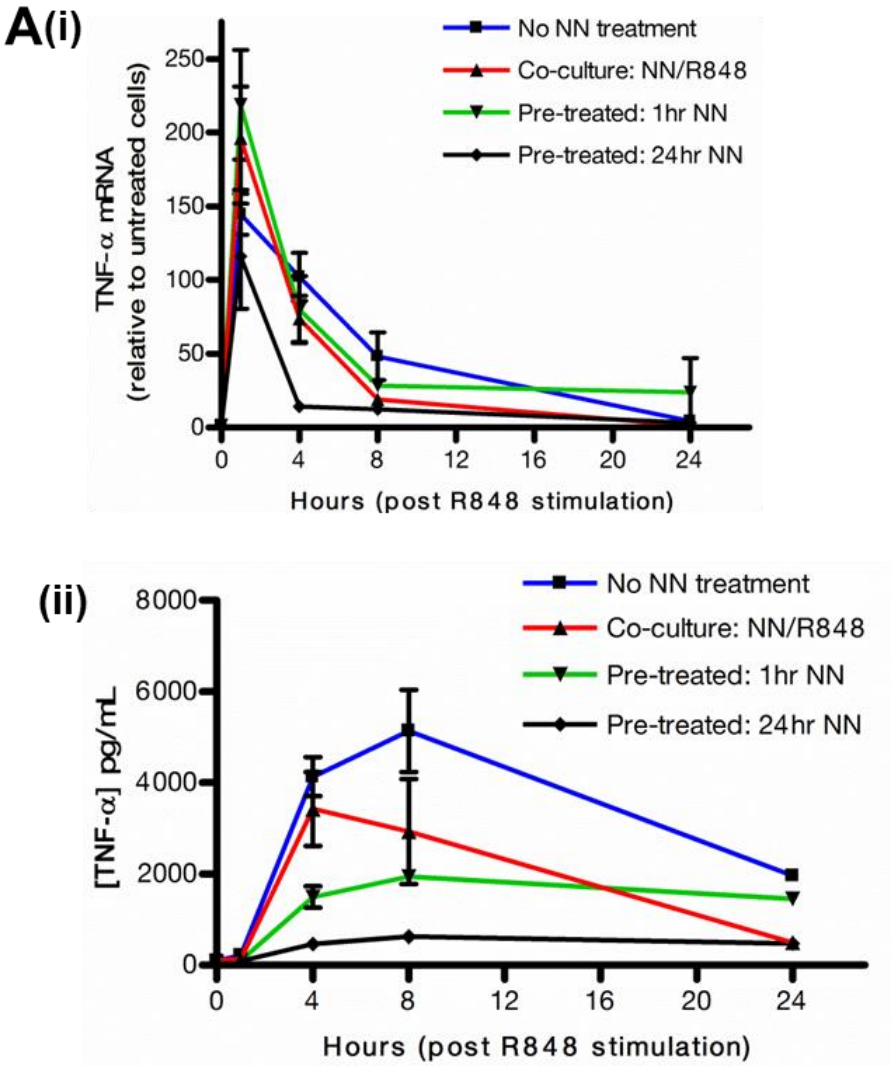

Figure 3.11: TNF-α mRNA expression in NN treated HMDMs

(**A**) TNF-α mRNA expression over 24hrs in R848 stimulated buffy coat HMDMs with 5% NN added in simultaneously or added 1 or 24hrs prior to stimulation (**i**). Results represent mRNA expression normalised to 18S rRNA and plotted relative to untreated control cells. (**ii**) Secreted TNF-α quantitated by ELISA. Data represents the mean ±SD of a single experiment (n=1) with three experimental replicates.

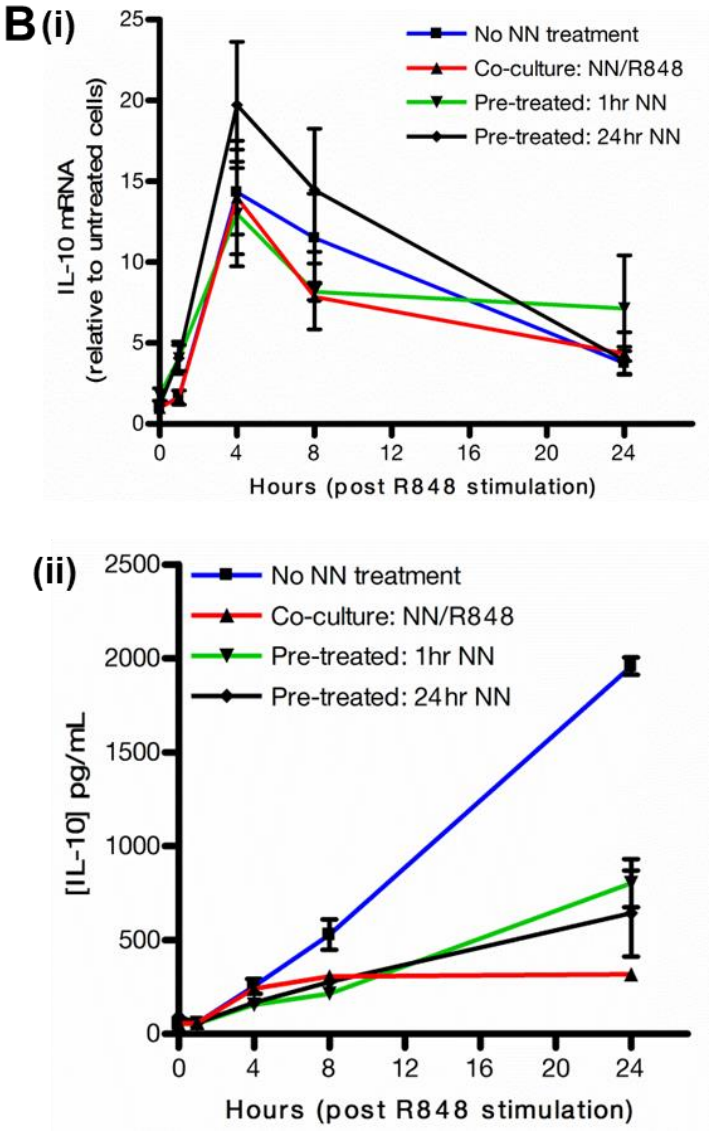

Figure 3.11 (continued): IL-10 mRNA expression in NN treated HMDMs

(**B**) IL-10 mRNA expression over 24hrs in R848 stimulated buffy coat HMDMs with 5% NN added in simultaneously or added 1 or 24hrs prior to stimulation (**i**). Results represent mRNA expression normalised to 18S rRNA and plotted relative to untreated control cells. (**ii**) Secreted IL-10 quantitated by ELISA. Data represents the mean ±SD of a single experiment (n=1) with three experimental replicates.

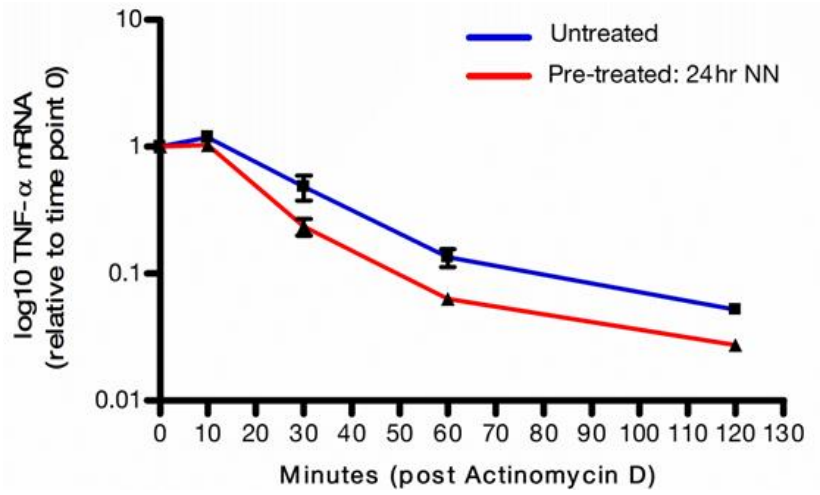

Figure 3.12: TNF-α mRNA decay rate in NN treated HMDMs

qPCR of buffy coat HMDMs pre-treated for 24hrs with 5% NN alongside untreated controls. After 1hr R848 stimulation, actinomycin D was added to cells and TNF-α mRNA decay rates were assessed. Results are from a single experiment (n=1) with values representing the mean ± SD from three experimental replicates.

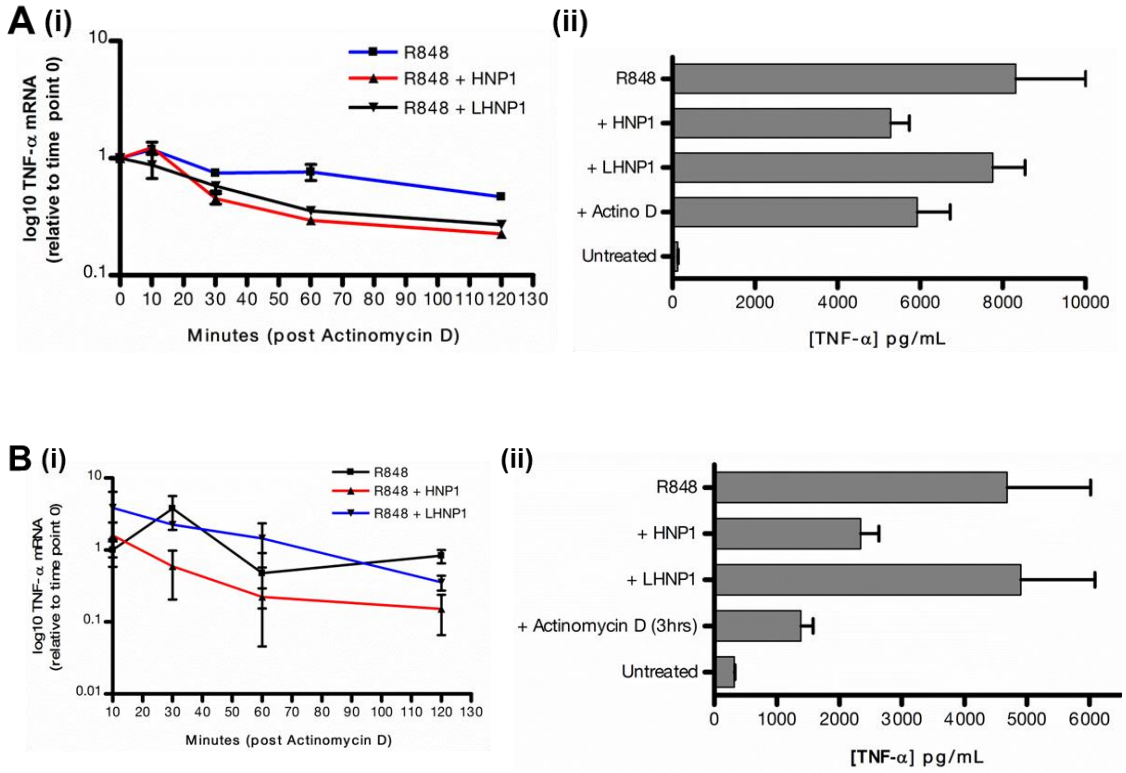

Figure 3.13: TNF-α mRNA decay in HNP1 treated HMDMs

Two independent experiments (**A** and **B**) of quantitated TNF-α mRNA in HMDMs (fresh blood donations) stimulated either alone with 12.5μg/mL HNP1 or LHNP1. (**i**) Actinomycin D was added 1hr after stimulation and TNF-α mRNA quantitated over 2hrs. (**ii**) Secreted TNF-α results taken from samples performed in parallel to (**A**) without actinomycin D treatment (at 4hrs). In addition, secreted TNF-α from actinomycin D treated controls were included for TNF-α ELISA analysis. Results are from single experiments (n=1) with error bars representing the mean ± SD from samples with three experimental replicates.

3.2.4 The effect of HNP1 on other cell types

While the main focus of research was in investigating the immunomodulatory effect of α-defensins on human macrophages, the diversity of the inhibitory effect was questioned in other cell types. In a limited number of studies, experiments were conducted in primary murine B cell and tumour cell lines.

Figure 3.14 illustrates the NN effect on $CD19^+$ B cells isolated from fresh blood donations in a single experiment. After 72hrs of stimulation with CpG, peptidoglycan (PGN), LPS or R848 alone together with 5% or 25% NN, IL-10 ELISAs showed an inhibition across agonists with both NN concentrations compared to controls groups.

HNP1 was further tested in B cell lymphomas (Mutu-1) and the effect was assessed by measuring metabolic activity as well as cell proliferation. Using the reduction of the added Alamar Blue reagent as a readout for metabolic activity, Mutu-1 cells were incubated over 72hrs with 12.5 or 50μg/mL HNP1 or LHNP1 alongside untreated controls. 5μg/mL actinomycin D was added as a positive control for arrested cell metabolism and apoptosis induction in tumour cells[137]. The results demonstrated that HNP1 was unable to inhibit Mutu-1 cell metabolism, as Alamar Blue reduction was near identical to untreated controls. Actinomycin D meanwhile showed almost complete prevention of Alamar Blue reduction as a positive control (Figure 3.15*A-i*). Simultaneously, cell proliferation and cell viability (by Trypan Blue exclusion) were assessed in Mutu-1 cells seeded at 20 000 cells/well and counted 72hrs after treatment with 50μg/mL HNP1 or LHNP1 alongside untreated controls (*A-ii*). Total cell number appeared less in HNP1 treated cells compared to controls with a suggestion of increased cell death. It was noticed, however, that Mutu-1 cells were failing to proliferate under the given culture conditions with the thought that starting cell numbers were exhausting cell culture growth nutrients. A repeat experiment was performed for proliferation assays with the number of seeded cells reduced to 11 000 cells/well (Figure 3.15*B*). After 72hrs treatment with 50μg/mL HNP1, LHNP1, untreated controls or actinomycin D, cell proliferation appeared to be stagnated in all treatments. Actinomycin D treatment resulted in near 100% cell death, as measured by the percentage of Trypan Blue positive cells. A validation experiment of Mutu-1

cells was tested for rates of proliferation in culture media containing titrated fetal bovine serum (Figure 3.15*C*). Cells seeded at 20 000 per well showed strong proliferation with 10% FBS, reaching approximately 140 000 cells after 72hrs. A 10 fold reduction in FBS immediately resulted in limited proliferation. As HNP1 activity is impeded in the presence of serum proteins, experiments were discontinued using Mutu-1 cells.

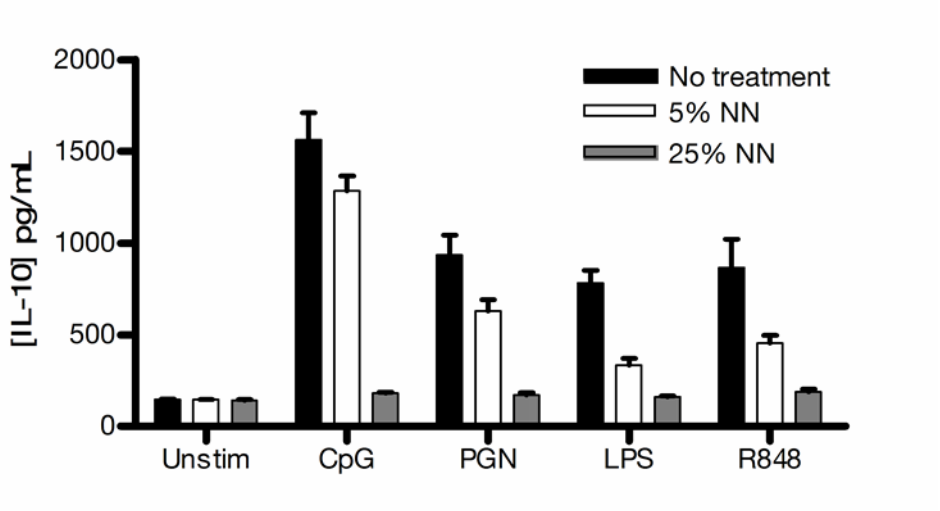

Figure 3.14: Secreted IL-10 in murine B cells treated with human NN

Splenic $CD19^+$ B cells from fresh blood donations isolated in culture and stimulated with CpG (1µg/mL), PGN (10µg/mL), LPS (2µg/mL) or R848 (0.1µg/mL) alone or with NN for 72hrs alongside untreated controls. Results of secreted IL-10 were quantitated by ELISA and represent the mean ±SD from a single experiment (n=1) with three experimental replicates.

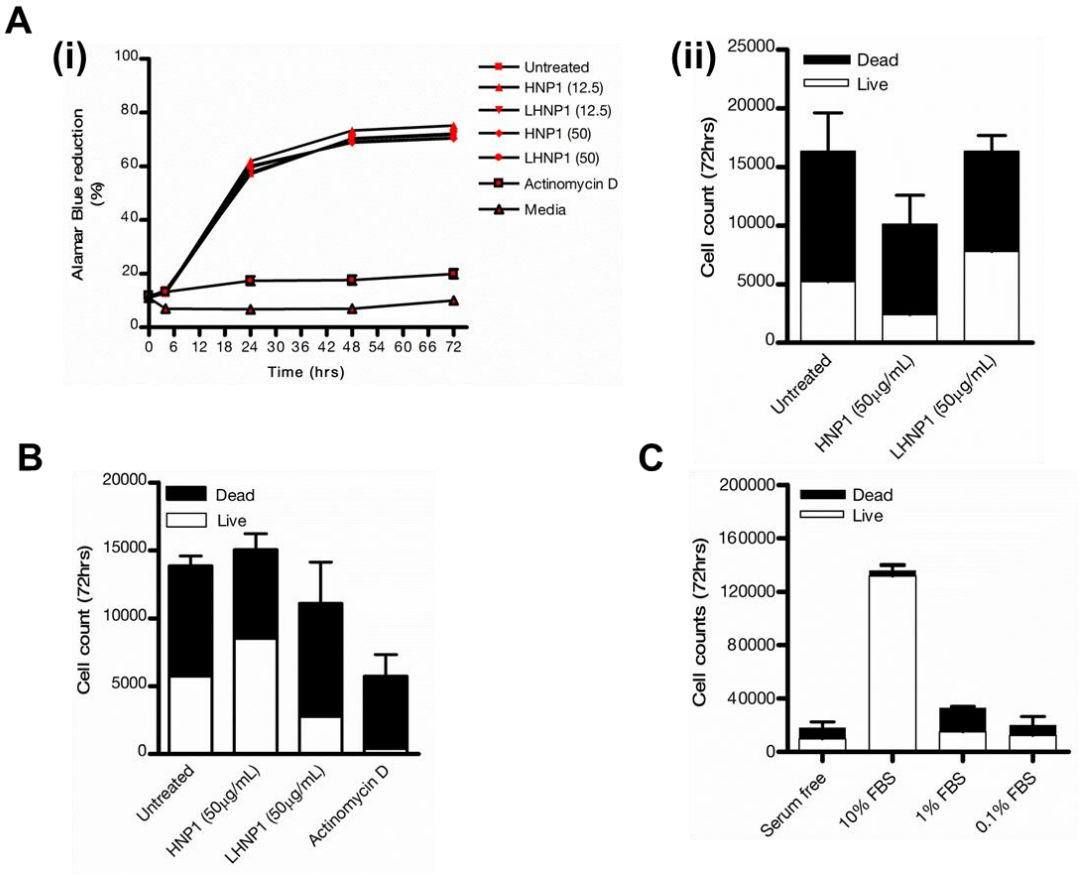

Figure 3.15: HNP1 effect on Mutu-1 metabolism and cell proliferation

(**A-i**) Reduction of Alamar Blue in Mutu-1 cells with HNP1 or LHNP1 treatment at 12.5 or 50µg/mL over 72hrs. Included controls were 5µg/mL actinomycin D treated cells and wells containing media alone. (**ii**) Live and dead cell counts at 72hrs with 50µg/mL HNP/LHNP alongside untreated controls with a starting cell number of 20 000 per well.

(**B**) Repeat of (**A**) with cells seeded at 11 000 per well. Actinomycin D treatment added as a proliferation control.

(**C**) Mutu-1 cell counts at 72hrs in FBS-containing media with a starting cell number of 20 000 per well. Results are of single experiments (n=1) with error bars representing the mean ±SD from three experimental repeats for all samples.

3.2.5 The effect of NN-treated BMDMs in wound healing *in vivo*

Since α-defensins rendered macrophages limited in their inflammatory potential *in vitro*, the question was asked if this new (although transient) macrophage phenotype had any influence under physiological conditions. More specifically it was questioned if these macrophages facilitated enhanced resolution and tissue regeneration in an *in vivo* murine wound healing experiment.

Pilot experiments were set up to compare the influence of injected BMDMs treated for 24hrs with 25% NN (human) compared to untreated BMDMs. For these experiments, BMDMs obtained from CD1 female mice were harvested from bone marrow as described in Chapter 2, section 2.2.3 with the experimental procedure detailed in section 2.16. With two mice per treatment group for each BMDM treatment (plus a single added saline control), rates of wound closure of a 10mm x 2mm excision made on the dorsum of each animal were assessed relative to original wound dimensions on Day 0.

Figure 3.16*A* shows captured images on rates of wound closure between the treatment groups. Day 7 images show near complete wound closures in NN treated groups compared to untreated controls. Day 9 wounds appeared closed in NN treated controls, with the underside tissue showing signs of angiogenesis with limited redness in the dermal layer. At the same point, control mice with untreated BMDMs displayed signs of unclosed wounds at Day 9 with the underside dermal tissue showing a reddish colour and scarring. The saline control group visually showed a similarity in wound healing rate compared to mice that received NN-treated BMDMs throughout the nine day period. Graphed wound closure rates re-emphasized this observation between the two groups with both showing a clear improvement compared to untreated BMDM control mice. The underside dermal tissue of the saline control mouse still showed a reddish colour with few signs of scarring.

The experiment was repeated with n=5 per group comparing BMDMs treated for 4hrs with 25% NN to untreated BMDM controls (Figure 3.17). Over an assessment of 10 days, no clear difference in wound closure rates were observed between the

two groups. This was confirmed in both the images taken (*A*) and the recorded wound dimensions (*B*).

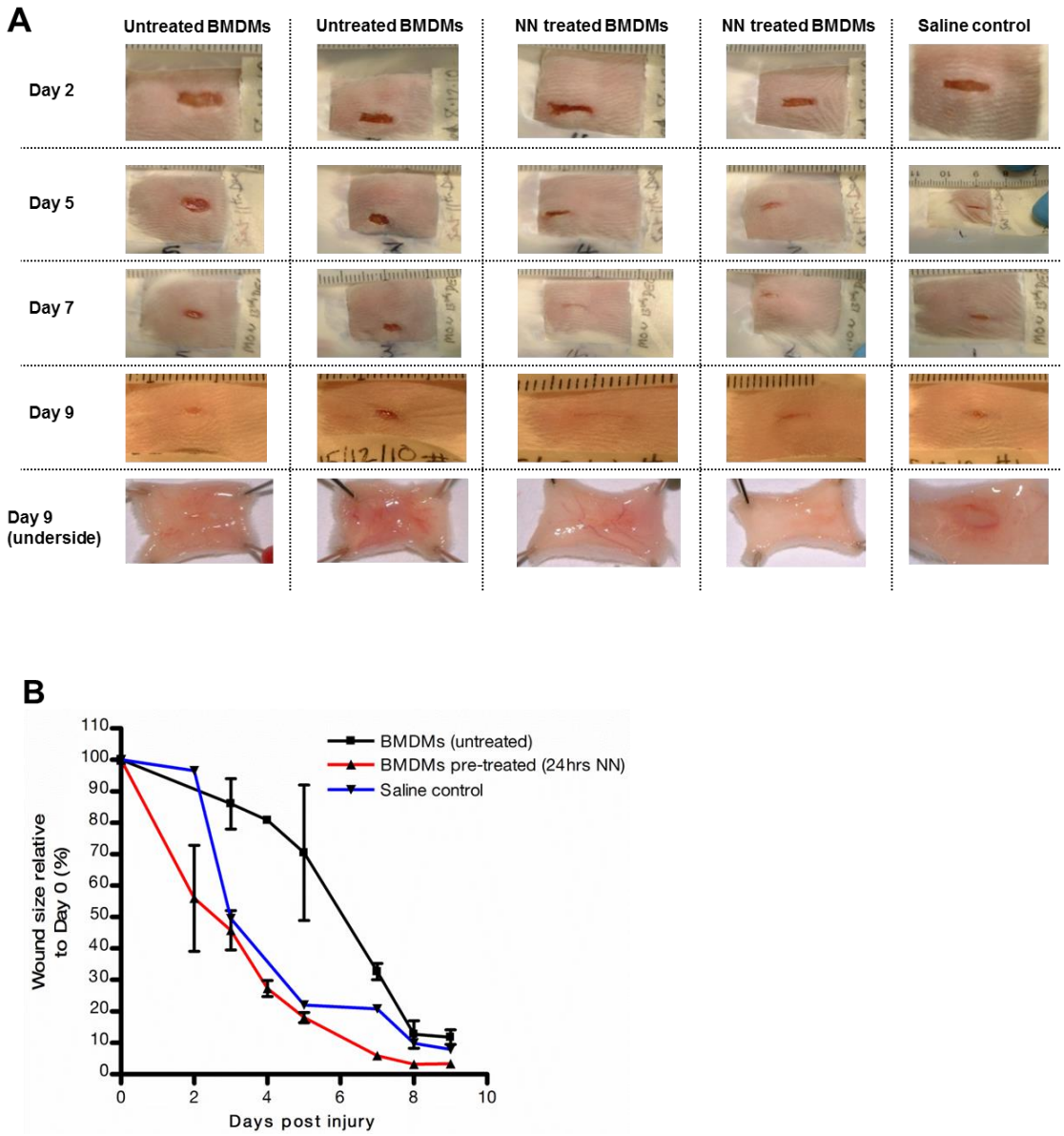

Figure 3.16: Influence of human NN treated BMDMs on wound healing in CD1 mice (Run 1)

(**A**) Mature BMDMs obtained from female CD1 mice treated for 24hrs with 25% NN and injected into 8 week old CD1 female mice alongside untreated BMDMs (two mice per treatment). 3x 10^6 BMDMs were injected around a dorsal 10mm x 2mm wound with dimensions recorded daily over 9 days. A single saline control was added for comparison. (**B**) Percentage graph plotted relative to the original wound size with error bars indicating the mean ± SD of a single experiment with two mice per group.

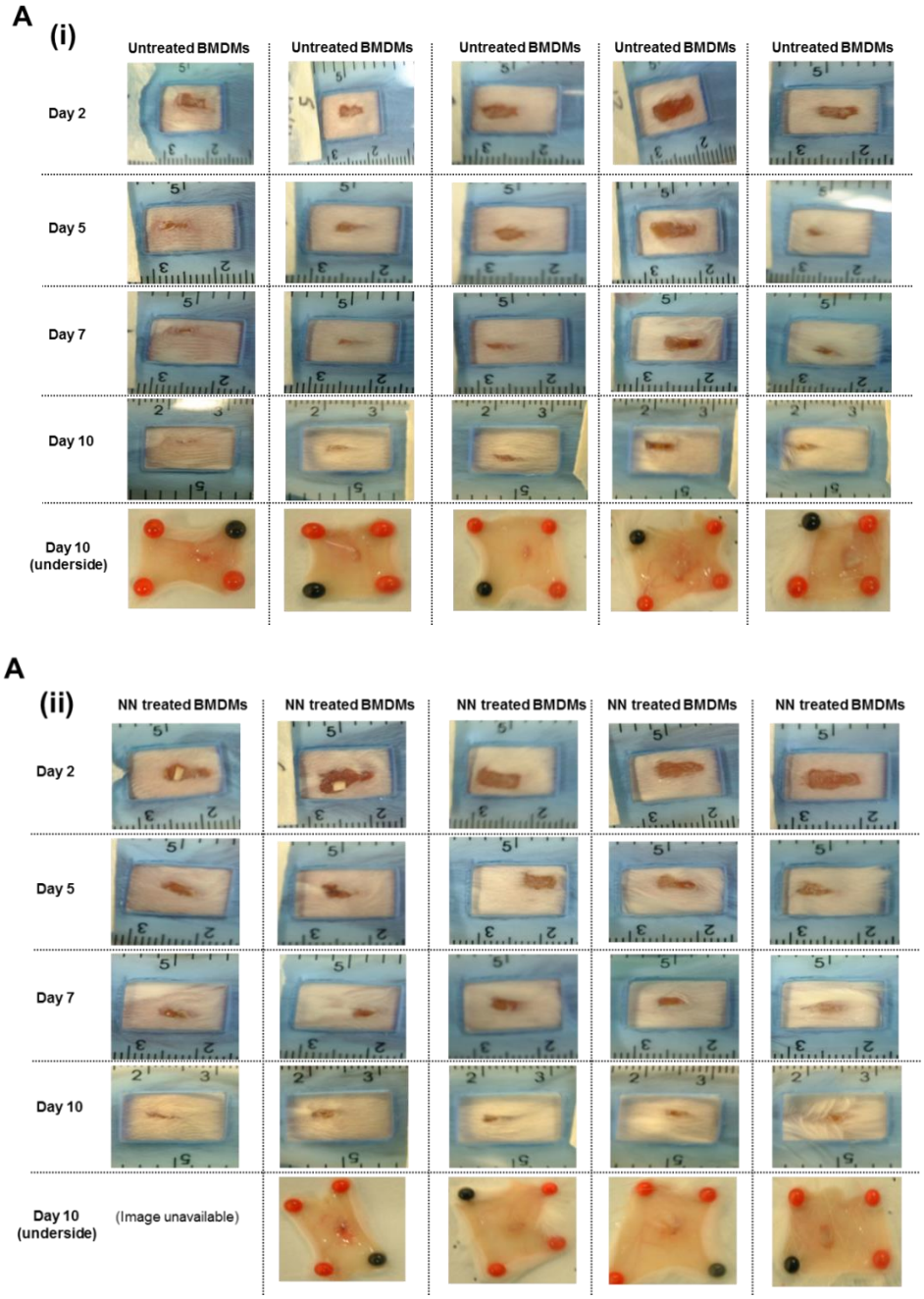

Figure 3.17: Influence of human NN treated BMDMs on wound healing in CD1 mice (Run 2)

A modified experiment of the experiment performed for Figure 3.16 with mature CD1 BMDMs treated for 4hrs with 25% NN (**ii**) alongside untreated BMDMs (**i**). 3x 10^6 BMDMs were injected around a dorsal 10mm x 2mm wound (5 mice per group) with images taken every two days (**A**). (continued overleaf)

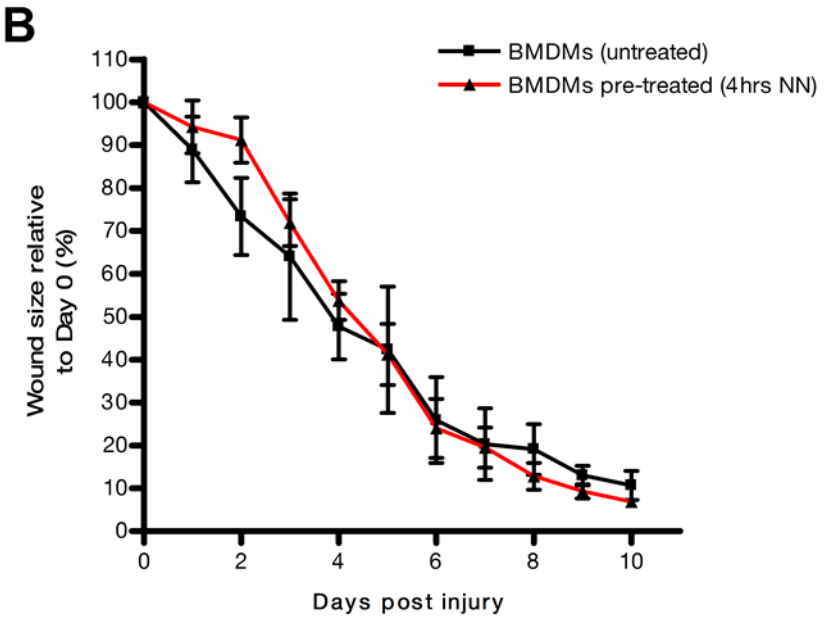

Figure 3.17 (continued): Influence of human NN treated BMDMs on wound healing in CD1 mice (Run 2)

Percentage graph was plotted relative to the original wound size with error bars of the mean ± SD (**B**, overleaf).

3.3 Discussion

Results from this chapter provided supporting evidence to previously published findings by our research group. It also provided initial insight into the anti-inflammatory mechanisms of necrotic neutrophil supernatants and purified HNP on macrophages.

Preliminary data demonstrated the potent inhibitory effect of human NN supernatants on the *E. coli*-derived LPS ability to stimulate HMDMs. This was assessed using three human neutrophil donors all showing similar inhibitory effects on TNF-α production. It is worth mentioning at this point that TNF-α was the chosen cytokine measured for most cell culture assays investigating the impact of α-defensins. This is because secreted TNF-α is regarded as the earliest inflammatory response signal which triggers numerous downstream inflammatory responses[113]. The anti-inflammatory effect of NN can be, in part, attested to the effect of α-defensins. This was previously shown by our group where NN depleted of hydrophobic proteins regained their inhibitory effect on stimulated HMDMs with purified α-defensin added into culture. This effect was further demonstrated to be specific for human neutrophils as murine neutrophils, lacking human α-defensin homologues, showed no similar property[87]. Still, it is appreciated that other immunomodulatory components do exist in human neutrophil supernatants (e.g. LL-37), which are likely to contribute to the observed inhibitory effect on secreted cytokines.

The inhibitory effects of α-defensin with necrotic neutrophil supernatants on LPS-stimulated macrophages, or any stimulation using bacterial cell wall components (e.g. *Staphylococcus aureus* Cowan Strain), are likely to be attributed to two modes of action: The first being neutralization of the agonist as α-defensins display strong lectin-like properties and bind in a multivalent fashion to carbohydrates and glycosylated proteins on bacterial cell walls[50]. The second mode being similar in function to the hypothesized inhibitory mechanism observed in T cell surrogate stimulation (CD40L/IFN-γ) and the anti-viral amidazoquinoline compound R848. Although the binding properties of α-defensins to these two agonists is untested and as yet unpublished, it is highly unlikely to be the cause for the inhibitory action as

qPCR data shows unhindered TNF-α mRNA expression similar to that of R848-stimulated alone controls (section 3.2.3).

As buffy coat-derived HMDMs were more readily available for utilization compared to fresh donations, continued used of CD40L/IFN-γ for stimulation was the preferred option. It soon became apparent that the physiological condition of buffy coat HMDMs were different to that of HMDMs from fresh blood donations, as CI stimulation of the former was inadequate. Extensive testing ensued to find an alternative agonist in the form of R848, SAC, PGN and CpG. Switching to THP-1 cells was considered but displayed slight physiological differences to HMDMs in regard to adequate R848 stimulation (see Appendix A, Figure A.4). In addition, the inhibitory properties of α-defensin on THP-1 cells had not been researched to date. Since stimulation using R848 was favoured, buffy coat HMDMs were selected to proceed with as they effectively expressed all cytokines tested (TNF-α, IL-6, IL-8 and IL-10). Also, it was deemed important to continue investigations into the inhibitory mechanisms on already published cell types.

The inhibitory findings of NN in this chapter differ from other published findings from similar studies. Fadok *et al.* (2001)[84] showed lysed neutrophil supernatants to be pro-inflammatory with increased TNF-α, IL-8 (and IL-10). The inflammatory effects of lysed neutrophil supernatants were directly attributed to the release of elastase and serine protease as assessed by the use of antibodies and chemical inhibitors (PMSF), respectively. Where the differences were likely to be between results in this chapter and those published by Fadok *et al.* (2001) was perhaps in the use of the bacterial cell wall component zymosan at 50μg/mL for stimulation. At such a high agonist concentration, zymosan more than likely neutralized α-defensins by direct binding, possibly explaining the lack of inhibition. This neutralisation could possibly be similar to the lack of HNP1 inhibition observed with 0.1% SAC (Figure 3.3). The cell equivalent of NN used might also explain the difference as the number neutrophils used to obtain supernatants was 10 fold less compared to experiments in this chapter. What is unclear (and untested to date) is the viability of HMDMs treated with varying NN concentrations. This would be essential in order to relate the anti-

inflammatory effect of NN as one that influences HMDM physiology as opposed to inducing cell death. Increased cell viability was previously ruled out for α-defensins (25μg/mL), with no changes to Alamar Blue reduction compared to untreated controls as well as no increase in Lactate Dehydrogenase within culture media over 24hrs[87].

α-Defensins have been shown to be resistant to proteolytic activity by way of a conserved salt-bridge between Arg5 and Glu15[138]. This coupled with the fact that it they constitute approximately 30-50% of the total protein in azurophil granules and 5-7% of the total protein content[48], it would seem reasonable to suggest that the inhibitory actions might serve to counterbalance the effects of inflammatory mediators in tissue containing large neutrophil numbers undergoing necrosis.

Focussing on the structural importance of HNP1 for inhibition, results clearly demonstrate that key amino acids within the 30aa residue are essential to the inhibitory effect on HMDMs (Figure 3.5). HNP1 was selected since it is the most abundantly expressed out of the four isoforms within neutrophils (~72.2%)[139]. Substitution of the six cysteines in LHNP1 with alanine results in altered conformation as cysteines are required for disulphide bond pairing which give defensins their structure and function[55]. The substitution of tryptophan at residue 26 (W26A) with alanine results in complete loss of inhibitory activity, owing to a change in peptide hydrophobicity as well as the ability to form dimers or even higher order oligomers[58]. Thus the data so far suggests that the hydrophobicity of HNP1 coupled with dimerization is an important component of inhibitory function.

Importantly the inhibitory effect of HNP1 was reproduced in HMDMs from Rheumatoid Arthritis patients (Figure 3.6). This provided very early stage indications of a new therapeutic potential in the treatment of this disease. From these data it is also suggested that the minimal inhibitory concentrations of HNP1 are about 7.5μg/mL on HMDMs under these experimental conditions. No pro-inflammatory effects could be seen at lower concentrations, contrary to findings in previous publications[134].

Analysis of the mRNA expression profiles suggests that NN might induce a higher than normal initial upregulation of TNF-α. This this may be in part due to a synergistic effect of R848 stimulation together with inflammatory mediators including serine protease and elastase in the supernatant. However, the resultant secreted TNF-α remains attenuated from as early as 4hrs with the indication that longer exposure to NN results in even greater inhibition. Even so, it is interesting that TNF-α mRNA levels in 1hr NN pre-treated HMDMs are nearly identical to that of NN added at the time of stimulation. This would suggest that the effects of HNP are taking place elsewhere, possibly affecting mRNA following transcription and possibly becoming more inhibitory over time. IL-10 mRNA appears similar in expression to R848-stimulated alone controls across the 24hr period. This is while secreted IL-10 is markedly reduced, providing further support to the suggestion that the inhibitory effect of NN appears to be post-transcriptional. It is appreciated that these findings using NN are based on evidence from a single HMDM donor and there are, therefore, limitations to the interpretation of these findings. Extensive repeated testing would be required to confirm the trends observed.

The rapid decline in TNF-α mRNA in 24hr NN-pretreated HMDMs could not be overlooked since TNF-α mRNA was attenuated by ~100 fold between the hours of 1hr and 4hrs post stimulation. To specifically determine if mRNA stability was affected, actinomycin D was used to block transcription in 24hr NN-pretreated HMDMs one hour after stimulation. Subsequent TNF-α mRNA decay rates over 2hrs paralleled that observed in R848-stimulated alone controls, suggesting that decay rates were similar to stimulated-alone controls.

There were inconclusive results in TNF-α mRNA expression observed in four repeats of CI stimulated HMDMs treated with HNP. Although initial levels of TNF-α mRNA appeared similar, expression appeared somewhat lower after 2-3hrs in two of the repeat experiments (Figure 3.9*B* and *C*). On the contrary, an experiment over 24hrs and a repeat over 6hrs (Figure 3.9*A* and *D*, respectively) showed little difference in TNF-α expression compared to controls.

To clarify if HNP affected TNF-α mRNA decay, actinomycin D treatment was applied to R848-stimulated buffy coat HMDMs with HNP1. Data from the first run showed a slight decline in mRNA with HNP between 10-30min post-actinomycin D treatment compared to controls (Figure 3.13*A*). It suggested that TNF-α decay was increased with HNP in a fairly tight time period followed by a levelling off similar to that of LHNP1 and R848-stimulated alone controls. It is uncertain at this stage whether this period of decay is critical to the overall TNF-α gene expression. In contrast a repeat experiment showed a steady TNF-α decay in HNP1 treated cells (and LHNP1) while R848-stimulated alone decay appeared more erratic (Figure 3.13*B*). Secreted TNF-α confirmed the typical inhibitory profile with HNP1 and actinomycin D treatments compared to controls. Thus assessing TNF-α mRNA decay profile in HNP treated HMDMs using actinomycin D did not definitively provide consistent results and would require further testing.

In the limited published literature, no evidence exists that suggests HNP1 has an inhibitory effect on inflammatory cytokine gene production. This has been addressed in human bronchial epithelial cells (HBECS) and Rheumatoid Arthritis fibroblast-like synoviocytes (FLS) using similar peptide concentrations[140,141]. Although an increase in IL-6, IL-8 and MMP1 mRNA expression was observed in RA FLS using 10μg/mL HNP1, no follow on experiments confirmed whether secreted cytokines levels were altered.

What was further established is that Tristetraprolin (TTP) activity is not implicated in the decreased expression of secreted TNF-α with HNP1. This effectively rejected the hypothesis of enhanced TTP-mediated mRNA decay brought on by HNP interference of TTP-mediated regulation. Although TNF-α mRNA stability cannot be ruled out based on these results alone, collective evidence from mRNA expression suggests that other factors must be involved that explain the overall inhibitory actions of HNP1. Indeed it would not be inconceivable to speculate at this point that the inhibitory effects of α-defensins may perhaps be multi-functional, possibly including mRNA stability.

Evidence suggested that the inhibitory effects of NN may be extended to other leukocytes, as suggested by the attenuation of IL-10 in CpG stimulated primary CD19+ B lymphocytes. This was, however, observed in a single experiment and would need to be repeated along with the effects on other cell types of interest e.g. neutrophils, T lymphocytes and dendritic cells.

At the HNP1 concentrations used, with the highest being 50μg/mL, HNP1 appeared unable to inhibit the metabolic activity in Mutu-1 lymphoma cells (Figure 3.15). It was unclear if HNP1 would have affected Mutu-1 proliferation without the experimental necessity of added serum to the culture media. It has been published that purified defensins are cytotoxic to human and murine tumour cells in the concentration range of 25 – 100μg/mL after 6hrs in culture, assessed using intracellular chromium release and dye exclusion assays[132]. As Mutu-1 cells showed resistance to HNP1 at concentrations tested, higher titration assays would be able to determine the concentration threshold needed to kill these lymphoma cells. Determining this would offer up the potential to apply HNP1 as an antitumourigenic therapy but for the limitations of serum inhibition[133]. The idea of packaged HNP1 for delivery, i.e. into liposome vesicles, would be one strategy to overcome this obstacle. This strategy was briefly tested on stimulated HMDMs in serum-containing culture media with no success (Figure 3.8). Given the pharmacological complexity in formulating this compound (HNP1 membrane binding interactions for one), extensive optimisation would be required to develop this further. A suggested strategy would be to use bioengineering techniques to develop HNP1 peptides chemically adjoined to an inhibitory pro-piece by an ester link incorporated within liposomes. This would inhibit HNP1 activity until inside the cell after which bond cleavage by cellular esterase would release a 'Trojan horse' effect.

Lastly, Miles *et al.* (2009) described a phenotypic defensin-treated macrophage unable to elicit a pro-inflammatory response whilst displaying enhanced phagocytic capability. On the basis of these results, it was asked if α-defensin-treated BMDMs could accelerate wound healing in mice (Figure 3.16). BMDMs treated with NN 24hrs prior to injection around a wound area showed accelerated wound closure

compared to untreated BMDM controls with fewer signs of inflammation after nine days. Limitations to this pilot study were numbers of test specimens. This study included only one saline injected control which showed a similar rate of wound closure to NN treated BMDMs. If the saline control result were to hold true in repeated experiments, it would infer the possible activation of the injected untreated BMDMs which contribute towards inflammation, as opposed to the pro-resolution properties of NN-treated BMDMs.

The limitations to this experiment using HNP (which was attempted without success) were the large number of cells required coupled with the amount of proportional HNP needed to culture cells in large volumes within Teflon pots. The experiment was repeated, however, using 4hr NN-treated BMDMs and compared to untreated control cells, this time using five mice per treatment in each group (Figure 3.17). Results suggested no difference in wound healing rates between the two groups. Thus it is yet to be determined if macrophages treated with α-defensins are able to shape inflammatory tissue and promote accelerated resolution *in vivo*.

Chapter 4

4 The impact of α-defensins on protein synthesis

4.1 Introduction

Based on the findings from the previous chapter, the observation was made that initial mRNA upregulation of inflammatory cytokines was unaffected by the presence of α-defensins. This signified that HMDM pattern recognition receptors remained functional, namely the external surface receptor CD40 for CD40L binding and internal TLR7/8 receptors for R848 stimulation. It also suggested that the signalling pathways involved and subsequent transcription activation remained unaffected.

How α-defensins inhibit the inflammatory functioning of human macrophages was unknown up until this point. For a modulatory agent to have such a profound effect on all secreted cytokines tested (and nitric oxide) as was published in Miles *et al.* (2009)[87], questions arose concerning the impact on not just secreted proteins but overall protein synthesis. Upon detection of cellular stresses such as heat and osmotic shock, UV treatment and nutrient deprivation, cells are rapidly able to halt global protein synthesis at the level of translation through several key regulatory pathways, whilst still facilitating the translation of a subset of mRNAs required for an appropriate response to the stimulus. Therefore, it was proposed to investigate whether α-defensins were disrupting global protein synthesis and if so, by what mechanism. Research into this question requires a brief overview into the regulatory mechanisms governing translation initiation.

Ribosomes are the cell's protein synthesis factories, rapidly translating mRNA that has been exported from the nucleus into the cytoplasm. The molecular process of translation initiation is highly complex and involves the binding of a number of proteins that mark the translational competency of an mRNA in order to license the binding of the pre-translation initiation complex[142]. The small ribosomal subunit

(40S) in association with initiator ternary complex, consisting of methionine (Met) bound to its cognate transfer RNA (tRNA) and guanosine triphosphate (GTP)-bound eukaryotic initiation factor (eIF) 2α (eIF2α-tRNAi^{Met}), is recruited to the 5' end of an mRNA and scans along the mRNA until it encounters an AUG start codon in an appropriate context (Figure 4.1, overleaf). Once aligned with AUG, the large 60S subunit completes full ribosome assembly (80S) and hydrolysis of GTP to GDP releases eIF2α and the tRNA for recycling. Subsequent tRNA-bound amino acids enter the ribosome sequentially to link amino acids together to begin polypeptide chain elongation.

Translating ribosomes remain within the cytosol where proteins are synthesised for transport to the nucleus, mitochondria or peroxisomes. Ribosomes translating polypeptides destined for secretion, lysosomes or the plasma membrane become associated with the endoplasmic reticulum (ER)[143]. It is within the ER lumen that these newly synthesised proteins undergo folding into their functional conformations, facilitated by molecular chaperones, after which they will be transported to the Golgi for subsequent relocation to membranes or lysosomes, or secretion in the case of externalized proteins.

The stage of translation initiation is the rate-limiting step of protein synthesis. Changes to homeostatic balances (e.g. ER stress, glucose deprivation, viral infections, heme deficiencies) result in the shutdown of all non-essential protein synthesis at the point of translation initiation. As the ER is an important organelle for protein synthesis, it also functions as a key sensory organelle to homeostatic imbalances. In addition, it is the major site of calcium storage within the cell and therefore undergoes rapid changes in Ca^{2+} levels, depending on the metabolic needs of the cell[144]. Calcium-dependent chaperone proteins within the ER, notably the abundantly expressed BiP (binding immunoglobular proteins) are functionally sensitive to unregulated calcium fluctuations[145,146]. Calcium irregularities impair BiP chaperone activity, leading to the accumulation of unfolded or misfolded proteins.

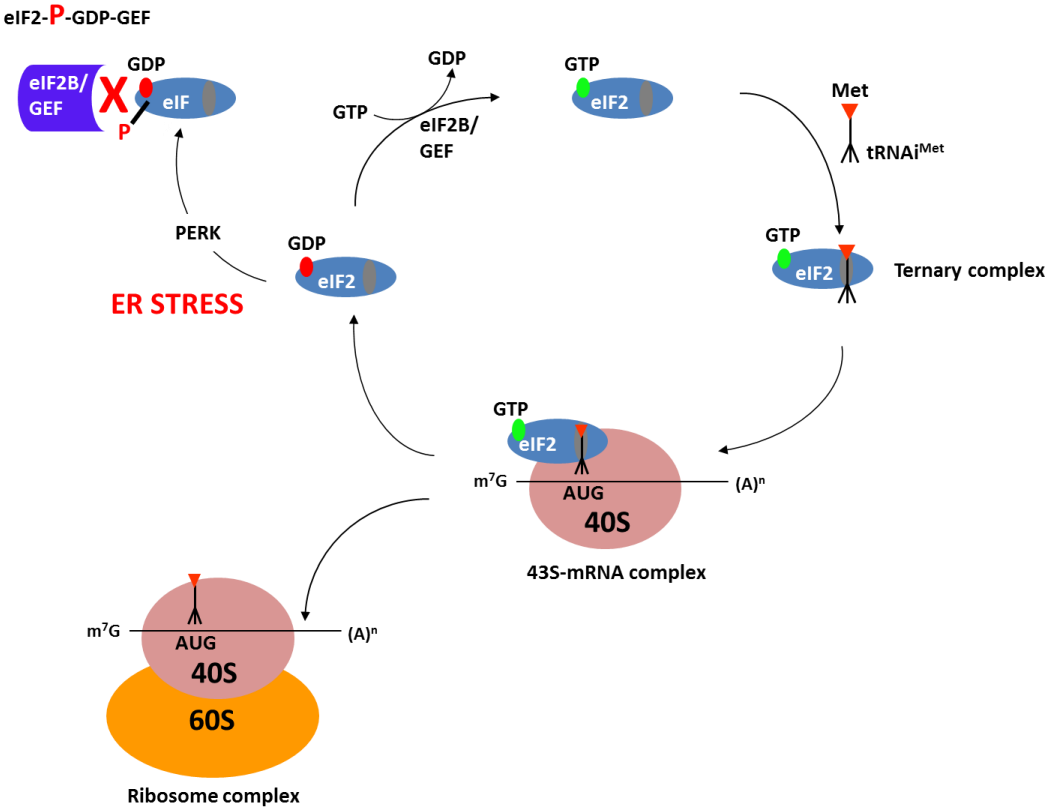

Figure 4.1: Translation initiation regulation by eIF2α phosphorylation

Eukaryotic initiation factor 2α (eIF2) is bound in a ternary complex by guanine triphosphate (GTP) to a methionine with cognate transfer RNA (tRNA). In complex with the small ribosomal subunit (40S), this complex is recruited to the 5'end of mRNA to align with the AUG start codon. Codon pairing with the tRNA anti-codon will initiate full ribosome assembly, with eIF2α mediating the binding of $tRNAi^{Met}$ to the ribosome by GTP→GDP hydrolysis. Cellular stresses (e.g. ER stress) activate stress response kinases to phosphorylate the α-subunit of eIF2. This prevents the eIF2β-subunit (eIF2B), acting as guanine nucleotide exchange factor GTPase (GEF), from exchanging GDP for GTP, thus blocking functional ternary complex formation.

An accumulation of mis-folded protein triggers an ER stress event that is recognised by three ER-resident transmembrane sensory proteins: the kinase and endoribonuclease IRE1 (inositol-requiring protein-1), PERK (protein kinase RNA-like kinase) and the activating transcription factor ATF6[147].

These sensors are associated tightly with BiP and their dissociation triggers a series of events, collectively known as the Unfolded Protein Response (UPR) that effectively shuts off global translation while coping with the backlog of unfolded proteins. Notably autophosphorylation of PERK phosphorylates eIF2α which prevents the eIF2B-mediated exchange of GDP to GTP on the ternary complex required for translation initiation (Figure 4.1). Thus increasing eIF2α phosphorylation leads to translational inhibition and, as such, is a commonly assayed measure of ER stress[148].

Dissociated ATF6 translocates to the Golgi where it undergoes protease cleavage-mediated activation before it enters the nucleus to induce transcription of genes containing an ER stress response element (ERSE) in their promoter. These include the ER-chaperone protein BiP to regain protein folding homeostasis, transcription of the proapoptotic activator CHOP (C/EBP homologous protein), and XBP-1 (X-Box binding protein-1). Transcribed XBP-1 mRNA undergoes modification by splicing of a 26-nucleotide intron by activated kinase IRE1. Spliced XBP-1 is a potent transcription factor which regulates a subset of UPR genes that promote ER-associated degradation of misfolded proteins and ER biogenesis[149,150]. Thus quantitation of BiP, CHOP and XBP-1 gene expression are also commonly used to assess ER stress in cells[126].

It therefore seemed reasonable to question if α-defensins had elicited a global reduction in protein synthesis, given the prior knowledge of its inhibition of the biosynthesis of multiple cytokines. If so, it was necessary to assess whether this was due to HNP1-induced ER stress, possibly resulting from calcium modulation given that HNP1-treated membranes become rapidly permeable to calcium flow[151]. If intracellular calcium mobilisation was affected, it was essential to establish if this triggered UPR pathway activation, specifically phosphorylation of eIF2α and gene upregulation of BiP, CHOP and spliced XBP-1.

4.2 Results

4.2.1 HNP1 inhibits protein synthesis

An experiment was performed to quantitate *de novo* incorporation of ^{35}S radiolabelled methionine (^{35}S-Met) in HNP-treated HMDMs (method detailed in Chapter 2, section 2.9). After incubating HMDMs in methionine depleted culture media for 2hrs, 100μCi/mL ^{35}S-Met was added to cells that were either left untreated, treated with 25μg/mL HNP1 or were stimulated with CD40L and IFN-γ in the presence and absence of 25μg/mL HNP1. Incorporation of radiolabelled methionine into secreted proteins (within the supernatant) and intracellular proteins (within the cell lysate) was assessed after 4hrs and following overnight incubations in three independent experiments. Protein electrophoresis was performed of all samples and radioactive protein bands were imaged by phosphorimaging. Total volumes of all protein bands were semi-quantitated and normalised to radiolabelled methionine incorporation in untreated HMDMs.

Figure 4.2*A* shows the ^{35}S-Met incorporation from two independent experiments at 4hrs. Varying results showed no or minor decreases in levels of protein synthesis in intracellular proteins. Assessing the secreted proteins, there is a trend towards an attenuation of synthesis in HNP1 alone controls and to a lesser extent in stimulated cells treated with HNP1 as early as 4hrs. This result suggests a gradual reduction of *de novo* protein synthesis by HNP1. Overnight HNP1 treatment alone showed a significant drop in ^{35}S–Met incorporation in intracellular proteins compared to incorporation in untreated HMDMs ($P<0.05$) (Figure 4.2*B*). This inhibition of intracellular protein synthesis by HNP1 was also seen in stimulated HMDMs, although it did not achieve statistical significance. The inhibitory impact of HNP1 was maximally demonstrated in secreted proteins after overnight incubations. Here, there was a clear and significant inhibition in both stimulated and unstimulated cells, supporting the concept that HNP1 inhibits macrophages regardless of the phenotypes tested to date. There remains a clear difference between the inhibitory actions of HNP1 in cellular protein synthesis and that of secreted proteins which requires further investigation.

Figure 4.3 is a representative depiction of gel images showing both total proteins and radiolabelled proteins from all experimental repeats. Images obtained from repeat experiments can be found in Appendix B, Figure B.1 and B.2. Total proteins, stained with Gelcode Blue showed visible patterns where protein bands became either feint with HNP1 treatment or even missing in some instances (depicted within green highlighted boxes). The absence of bands was particularly noticeable in secreted proteins after overnight incubations. Attempts to excise and identify proteins visually affected by HNP1 by mass spectrometry were unsuccessful, with outsourcing options limited given the radioactive nature of the samples. The gel images of ^{35}S-Met incorporated proteins showed a profound drop in band intensity in both secreted and cellular proteins in all three experiments after overnight culture, visually confirming the results in Figure 4.2. Panel *B* in all repeats validated the anti-inflammatory effect of HNP1 on secreted TNF-α, quantitated by ELISA.

Key investigative experiments using HNP1 were performed throughout the project at concentrations 25μg/mL and 12.5μg/mL. The inhibitory effect of HNP1 at the latter concentration was tested in ^{35}S-Met incorporation experiments in a single experiment (Figure 4.4). Results show a similar inhibitory profile after 18hrs incubation, with HNP1 having a profound effect on synthesis of secreted proteins. No significant differences were observed in *de novo* synthesis of intracellular proteins, giving preliminary suggestions that higher HNP1 concentrations are required for an effect on cellular proteins.

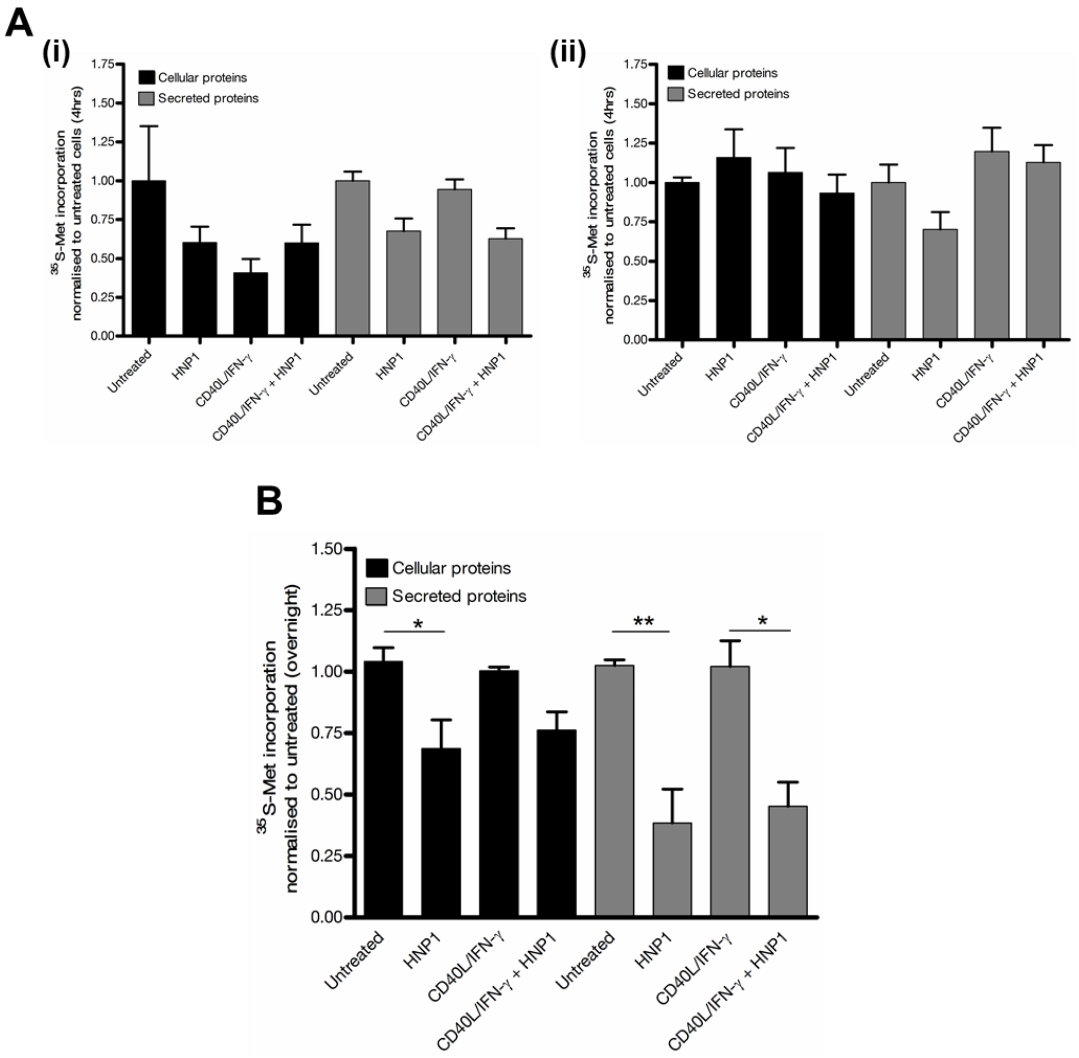

Figure 4.2: ^{35}S-methionine incorporation in HNP1-treated HMDMs

Quantitation of incorporated ^{35}S-Met in HMDMs (fresh blood donations) from all three experiments performed (Figure 4.3 and Appendix B, Figure B.1 and B.2). Incorporation is expressed normalised to untreated controls at 4hrs from two independent repeats experiments (**A-i**, **ii**), and after overnight incubation (**B**) from n=3 experiments. Error bars are the mean ± SD (**A**) and mean ± SEM (**B**). Statistical analysis was performed for (**B**) using Tukey's *post hoc* analysis following one way ANOVA. This was performed after sample data within each replicate was normalised to a single control replicate (Untreated). The mean values along with respective standard deviations from all three replicates were then combined to determine the statistical significance from the resulting SEM.

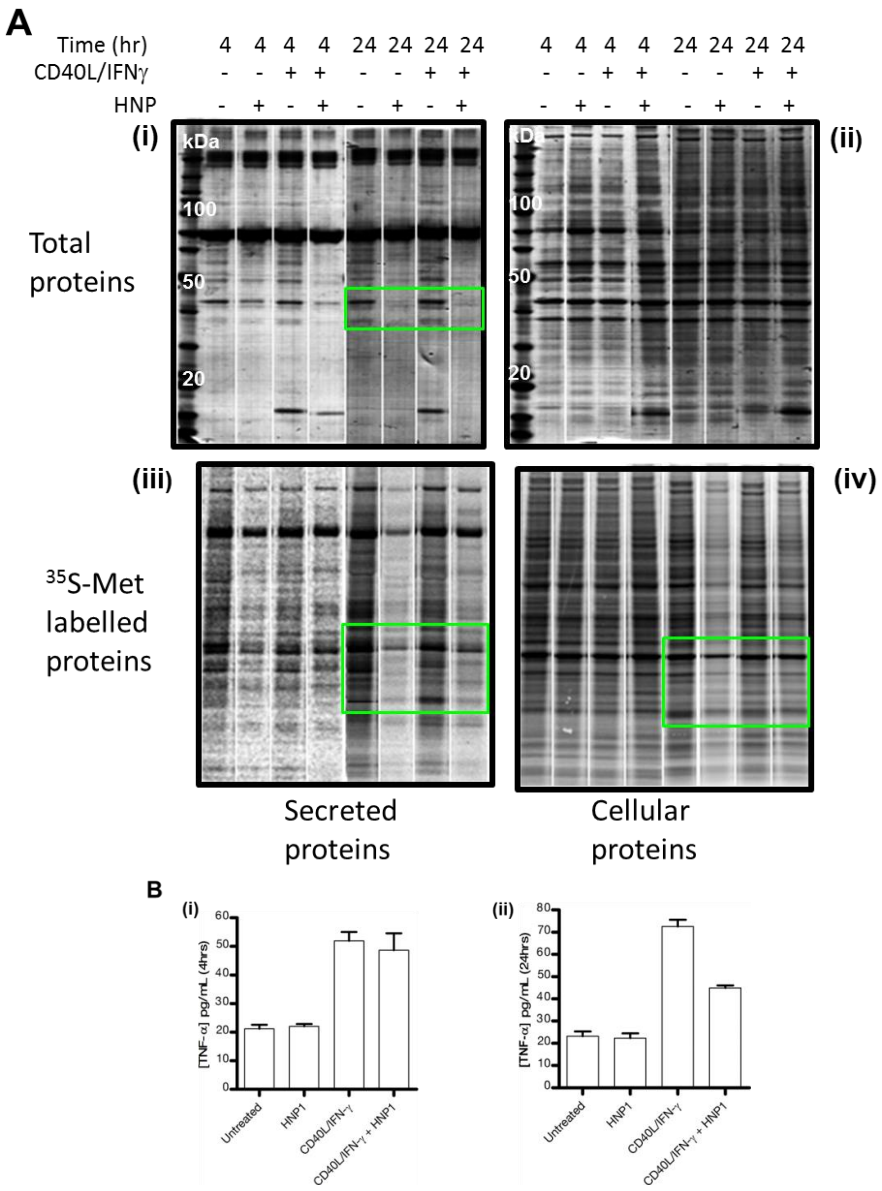

Figure 4.3: HNP1 effect on secreted and intracellular HMDM protein synthesis (Run1)

(**A**) Protein gel images of HMDMs (fresh blood donations) treated with 25μg/mL HNP1 alone or simultaneously stimulated with 3μg/ml CD40L and 5ng/mL IFN-γ in culture at 4hrs and 24hrs (alongside untreated controls). Gelcode Blue stained gels showing total secreted (**i**) and intracellular (**ii**) proteins. Radiolabelled protein images of *de novo* secreted (**iii**) and intracellular (**iv**) protein synthesis, with green boxes indicating areas of reduced or absent proteins. (**B**) TNF-α ELISAs of secreted cytokine at 4hrs (**i**) and 24hrs (**ii**) with error bars of the mean ±SD of triplicate repeats. Experiment performed by Dr Matthew Brook.

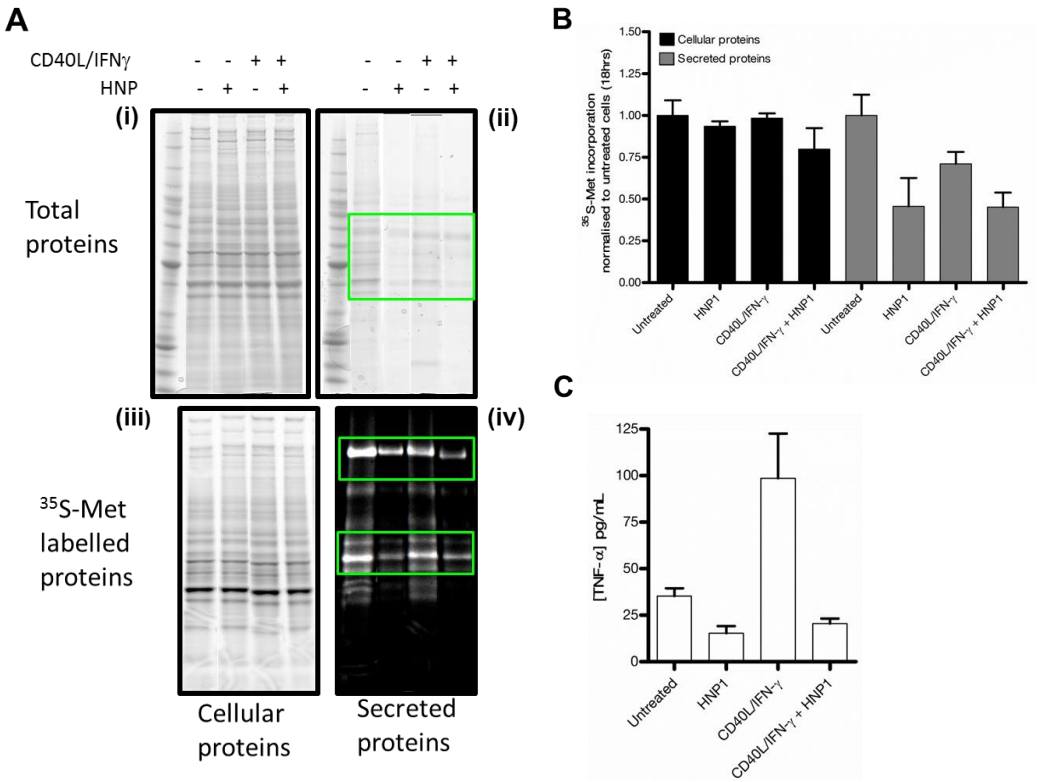

Figure 4.4: Secreted and intracellular HMDM protein synthesis using 12.5µg/mL HNP1

Repeat experiment of Figure 4.3 using 12.5µg/mL HNP1. (**A**) Gelcode Blue stained gels showing total intracellular (**i**) and secreted (**ii**) proteins at 18hrs incubation. Radiolabelled protein images of *de novo* intracellular (**iii**) and secreted (**iv**) protein synthesis, with green boxes indicating areas of reduced or absent proteins. (**B**) Quantitation of incorporated ^{35}S-Met in HMDMs (fresh blood donations), normalised to untreated controls. (**C**) TNF-α ELISAs of secreted proteins at 18hrs. Error bars represent the mean ±SD from a single experiment (n=1). Experiment co-performed with Dr Matthew Brook.

4.2.2 Inhibitory effects of HNP1 on HMDM intracellular calcium mobilization

From the data described in the previous section it was apparent that HNP1 affected secreted protein synthesis in HMDMs within 24hrs of treatment, as well as intracellular protein synthesis to a lesser extent. Research questions subsequently addressed whether this was an ER stress-mediated halt on translation initiation. As addressed in the introduction, cell physiology requires tightly regulated calcium homeostasis for optimal ER function. BiP chaperone protein function is impaired if cellular calcium imbalances occur, causing an ER stress event with the onset of accumulated mis- or unfolded proteins. Given the evidence of an attenuation of protein synthesis, it was hypothesised that intracellular calcium homeostasis, a key effector in the induction of ER stress, may be impacted by α-defensins.

The impact of HNP on cytoplasmic calcium mobilisation was tested by measuring real-time changes in fluorescence of a calcium sensitive probe, Fura-2/AM (detailed in Chapter 2, section 2.12). This probe, when incubated in cells, is cleaved by intracellular esterase enzymes to permit the binding of calcium to the active Fura-2 component causing an excitation of the probe. The resulting emission wavelength can then be measured in real-time using a spectrofluorometer. Furthermore α-defensins have not been shown to affect uptake of fluorophores in previously published findings[152]. To observe detectable differences in calcium mobilisation between untreated and HNP-treated HMDMs, two known inducers of macrophage calcium flux were used; C5a from complement component C5 and Platelet-Activating Factor (PAF). These agonists were first used to confirm a calcium flux in untreated HMDMs as shown in Figure 4.5. Calcium flux, measured in nanomolar concentrations showed a positive initial flux in calcium using both PAF and C5a with a gradual tapering off to near basal levels. PAF was used for the induction of calcium mobilisation in further experiments.

Buffy coat HMDMs were then treated overnight with 25μg/mL HNP1-3 alongside untreated controls followed by incubation with Fura-2/AM. Changes in calcium mobilisation between the two test groups were first analysed in cation-containing buffer (Hank's Balanced Buffer Salt Solution – HBSS), as shown in Figure 4.6.

Using PAF to stimulate HMDMs, three independent experiments showed a sizeable reduction in calcium mobilisation in HNP-treated HMDMs. The graph is representative of two out of the three independent repeat experiments performed, and the remaining graphs can be found in Appendix B (Figure B.3*B* and *C*). Not only were initial PAF-induced fluxes attenuated but there was a clear lack of subsequent oscillations, characteristic of calcium upregulation within activated cells. By calculating the area under each curve from the point of PAF induction, the difference in calcium mobilisation highlights the effect of HNP (Table 4.2.1). Combining these differences in calcium mobilisation values from the three independent experiment repeats performed and plotting graphically resulted in no statistical significance achieved (Figure 4.7).

Table 4.2.1: Comparisons of calcium mobilisation in HNP-treated HMDMs to untreated controls (with external cations)

Figure	*Untreated*	*HNP treated*	*Difference (with HNP)*
A	31703.87	3066.33	- 28637.54
B	39952.14	9936.42	- 30015.71
C	5236.38	3069.15	- 2167.23

In two of the experiments (Figure 3*B* and *C*, Appendix B) the observation was made that basal calcium levels were approximately 100nM and 200nM, respectively, higher in HNP1-3 treated HMDMs prior to calcium induction with PAF. Although further tests would need to confirm this trend and its significance, it suggests that HNP treatment causes elevated basal levels of calcium, possibly derived from the influx of calcium within the HBSS buffer ($CaCl_2$ concentration of 1.26mM). Initial tests into this suggested that there was no detectable change to calcium levels upon HNP1-3 treatment i.e. within 5 minutes of treatment (Figure 4.8).

The effects of HNP on calcium mobilisation were repeated in the absence of external cations. This way an assessment could be made as to whether the calcium signalling pathway (illustrated in Figure 4.15), which triggers calcium release from ER stores, was affected in HNP-treated HMDMs (Figure 4.9). In three independent experiments, no distinct differences were observed in the amplitudes of initial

calcium fluxes induced by PAF. In addition, negligible differences were observed in total calcium levels in HNP1 treated HMDMs compared to controls (values not shown). This suggested that calcium signalling pathways and the subsequent release of stored calcium remained unchanged. A representative graph of the results is depicted (*A*), with the graphs of the two repeat experiments located in Appendix B, Figure B4 (*B* and *C*). In addition, calcium oscillations were comparable to untreated controls in two of the three experiments (*A* and *C*) while non-existent in (*B*).

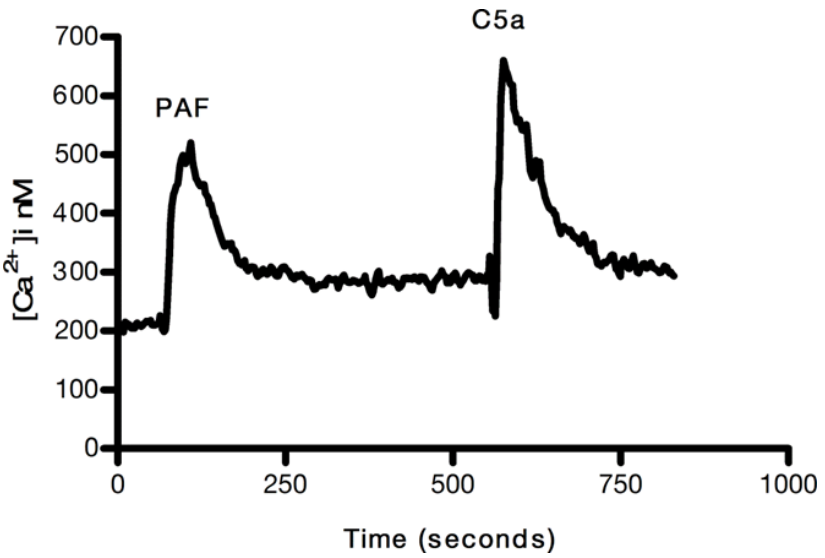

Figure 4.5: Validation of PAF- and C5a-induced calcium flux in HMDMs

Measurement of intracellular calcium flux in buffy coat HMDMs induced with 1μM Platelet-Activating Factor (PAF) followed by 0.1μM complement factor C5a (n=1). Flux was measured in real-time by the excitation of the fluorescent calcium indicator Fura-2 using a spectrofluorometer.

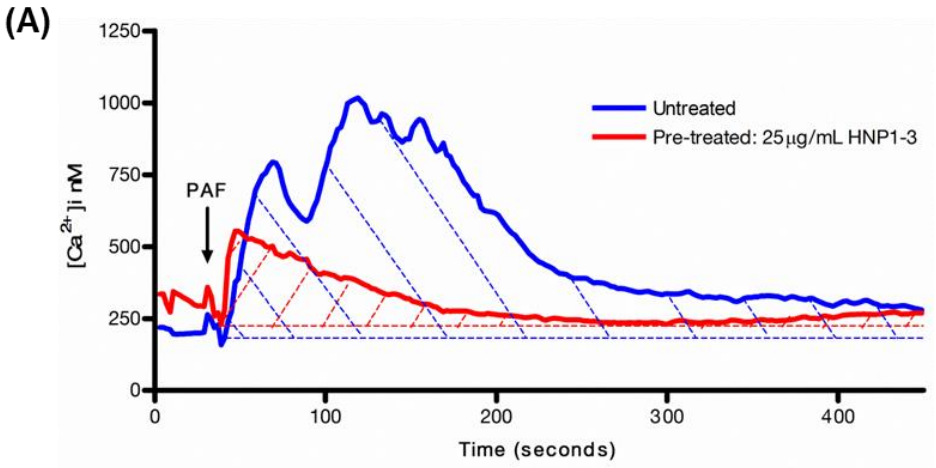

Figure 4.6: Calcium mobilisation in HNP treated HMDMs (with external Ca^{2+} ions)

Calcium flux was induced using 1µM Platelet-Activating Factor (PAF) on buffy coat HMDMs treated overnight with HNP in Ca^{2+}-containing HBSS buffer. Cytoplasmic calcium was measured in real-time and total amounts were calculated using the area under each curve (See Table 4.2.1). Result is a representative of two out of three independent experiments performed.

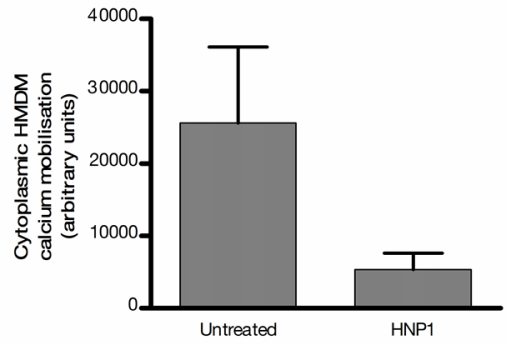

Figure 4.7: Semi-quantitated calcium mobilisation in untreated HMDMs or treated with HNP1

Combined results of three independent HMDM donors measuring the total amount of calcium mobilisation in HMDMs treated with 25µg/mL HNP1 or left untreated. The obtained values were of calculated areas under the curves from Figure 4.6, Figure B 3 (**B** and **C**), and represented in Table 4.2.1. Error bars represent the mean ± SEM and statistical analysis was performed using of the student's t-test, resulting in no statistical significance.

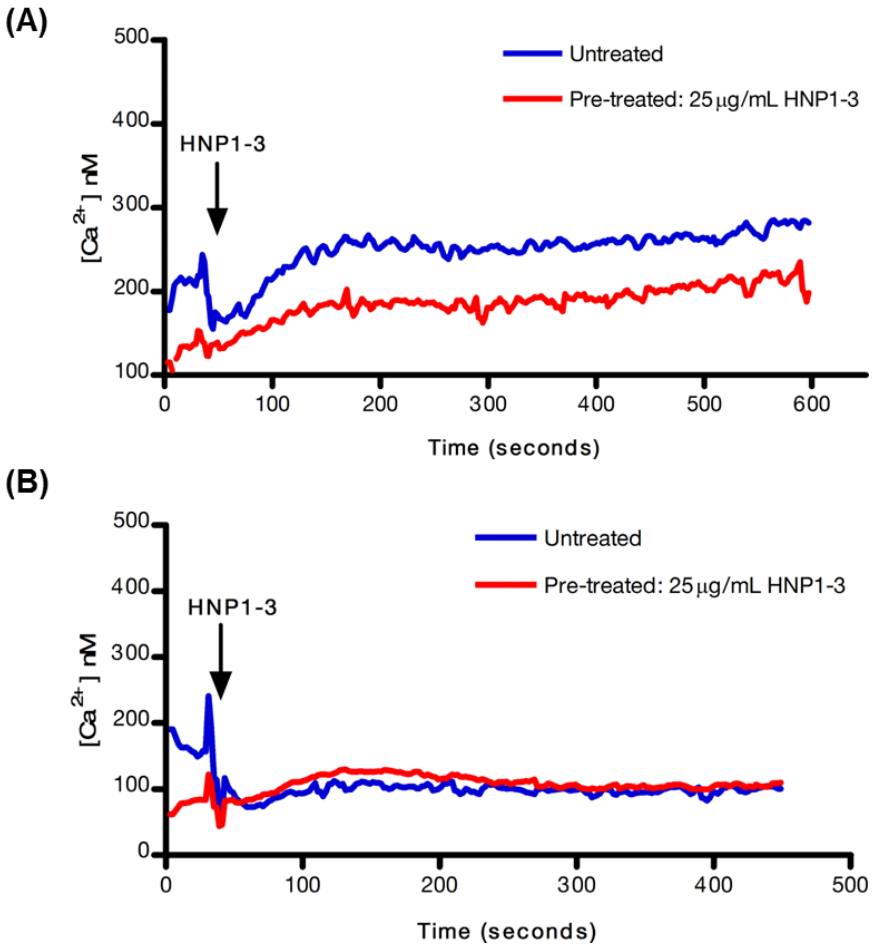

Figure 4.8: Intracellular calcium mobilisation in HNP pre-treated HMDMs in response to HNP1-3

(**A** and **B**) Independent repeat experiments of buffy coat HMDMs pre-treated for 24hrs with 25μg/mL HNP1-3 alongside untreated controls. Intracellular calcium mobilisation was quantified in real-time following the addition of 25μg/mL HNP1-3.

(A)

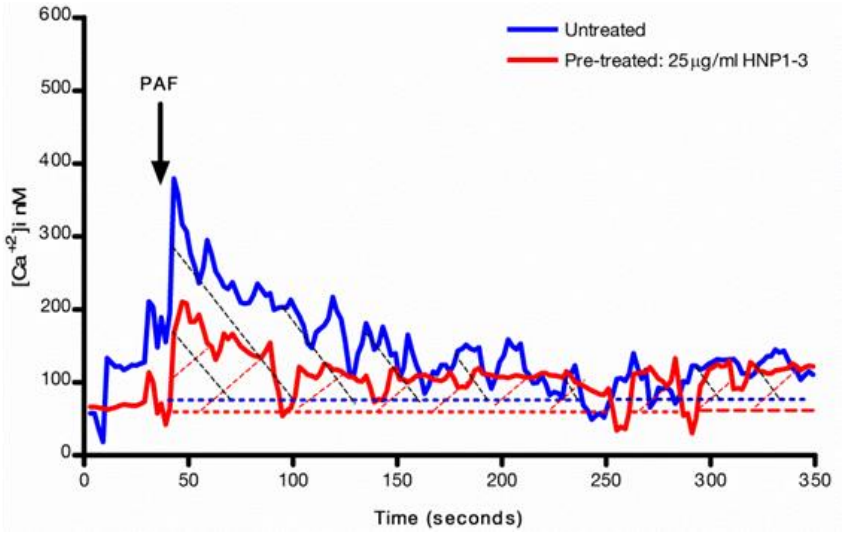

Figure 4.9: Calcium mobilisation in HNP treated HMDMs (without external Ca^{2+} ions)

Calcium flux was induced using 1μM Platelet-Activating Factor (PAF) on buffy coat HMDMs treated overnight with HNP in HBSS buffer free of Ca^{2+} ions. Cytoplasmic calcium was measured in real-time and total amounts were calculated using the area under each curve for all three independent experiments (**A** – **C**).

4.2.3 Inhibitory actions of α-defensins on protein synthesis is not attributed to endoplasmic reticulum stress

4.2.3.1 Expression of phosphorylated eukaryotic Initiation Factor 2α

So far data pertaining to the effects of HNP displayed a reduced level of HMDM calcium mobilisation together with a reduction in protein synthesis. It was wondered if these two results indicated the onset of an ER stress event. ER stress, together with deficiencies in heme or amino acids and viral infections, triggers upstream kinase enzymes to phosphorylate the α-subunit of eIF2, thereby preventing the hydrolysis of GDP to GTP catalysed by eIF2B (a guanine nucleotide exchange factor)[147,153]. Thus experiments were performed in HMDMs to assess whether HNP1, which altered intracellular calcium homeostasis, triggered eIF2α phosphorylation and a subsequent inhibition of translation initiation.

For these experiments western blotting was used to determine the expression of phosphorylated eIF2α (at amino acid serine 51), as described in Chapter 2, section 2.13.2. The first experiments assessed the expression of phosphorylated eIF2α over 2hrs in HMDMs stimulated with CD40L and IFN-γ (CI) alone or together with 25μg/mL HNP1 as well as HNP1 in unstimulated cells (Figure 4.10). eIF2α phosphorylation levels showed no change over 2hrs across treatments (Figure 4.10 *A-i*), although notably expression of protein bands were feint in this run.

To observe eIF2α phosphorylation levels over a wider time period, the experiment was extended to include time points for 4, 8 and 24hrs (Figure 4.11). Protein bands in this run allowed for the comparison between all treatments across all time points, which did not show any increased levels of eIF2α phosphorylation (Figure 4.11 *A-i*), apart from a slightly enhanced level at 24hrs with CI stimulation alone. β-actin loading controls appeared consistent amongst samples (Figure 4.11 *A-ii*).

A repeat experiment was performed over 24hrs again using CI stimulated cells (Figure 4.12). In this sample eIF2α phosphorylation (Figure 4.12*A-i*) appeared upregulated in HNP1 alone treated cells at 4hrs but in contrast remained unchanged in stimulated cells with HNP1 treatment at the same time point. At 8 and 24hrs, eIF2α phosphorylation appeared increased in cells stimulated with CI alone as well

as in stimulated cells with HNP1 treatment, but not in HNP1 alone. β-Actin loading controls were consistent amongst samples (Figure 4.12*A-ii*). This would suggest that the enhanced eIF2α phosphorylation was caused by CI stimulation and not HNP1 itself.

In keeping with the conversion to using R848 stimulated buffy coat HMDMs, eIF2α phosphorylation was also assessed in these stimulated cells treated with 12.5μg/mL HNP1 (Figure 4.13). As an added positive control for eIF2α phosphorylation, HMDMs were treated with 1μM thapsigargin (TG), a plant-derived compound which impairs Ca^{2+} transport across the endoplasmic reticulum and induces ER stress. At 1hr, 2hrs and 24hrs incubation following stimulation, no difference was observed between R848-stimulated alone controls and HNP1 treated HMDMs, while transient eIF2α phosphorylation was observed with thapsigargin treatment at 2hrs and to a lesser extent at 24hrs. By the assessment of eIF2α phosphorylation, there were no strong indications of any ER stress-induced effects caused by α-defensins. This was examined further using gene expression markers of the Unfolded Protein Response (UPR) pathway: BiP, CHOP and XBP-1.

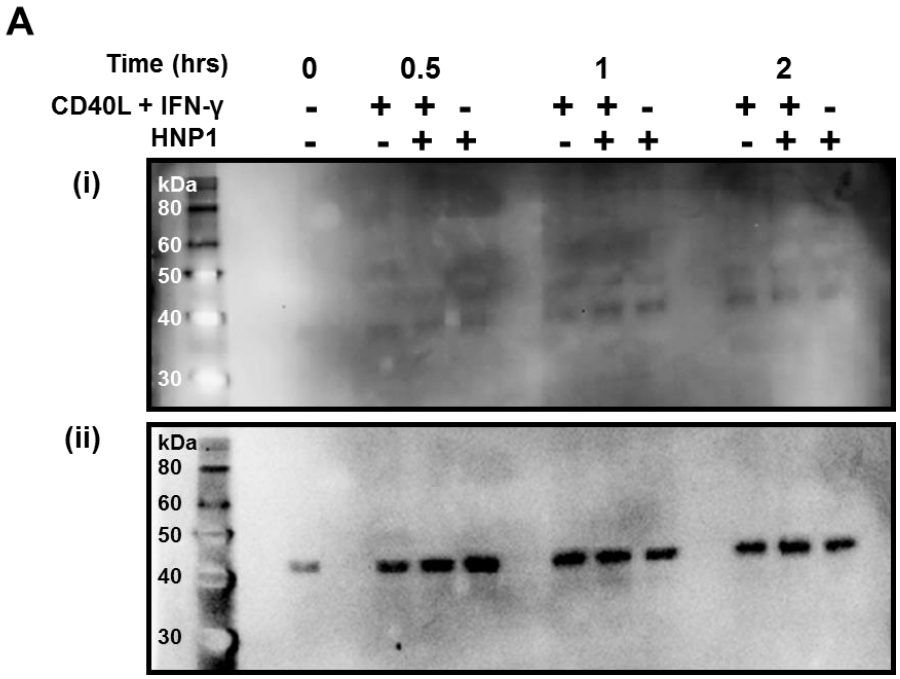

Figure 4.10: Expression of phosphorylated eIF2α in HNP1 treated HMDMs over 2hrs

HMDMs from fresh blood donations were treated with 25μg/mL HNP1 alone or stimulated with 3ug/mL CD40L + 5ng/mL IFN-γ over 2hrs prior to lysis and SDS-PAGE. Western blot was performed for the detection of phosphorylated (S51) eIF2 (~36kDa, **i**) and for β-Actin (~42kDa, **ii**) as a loading control.

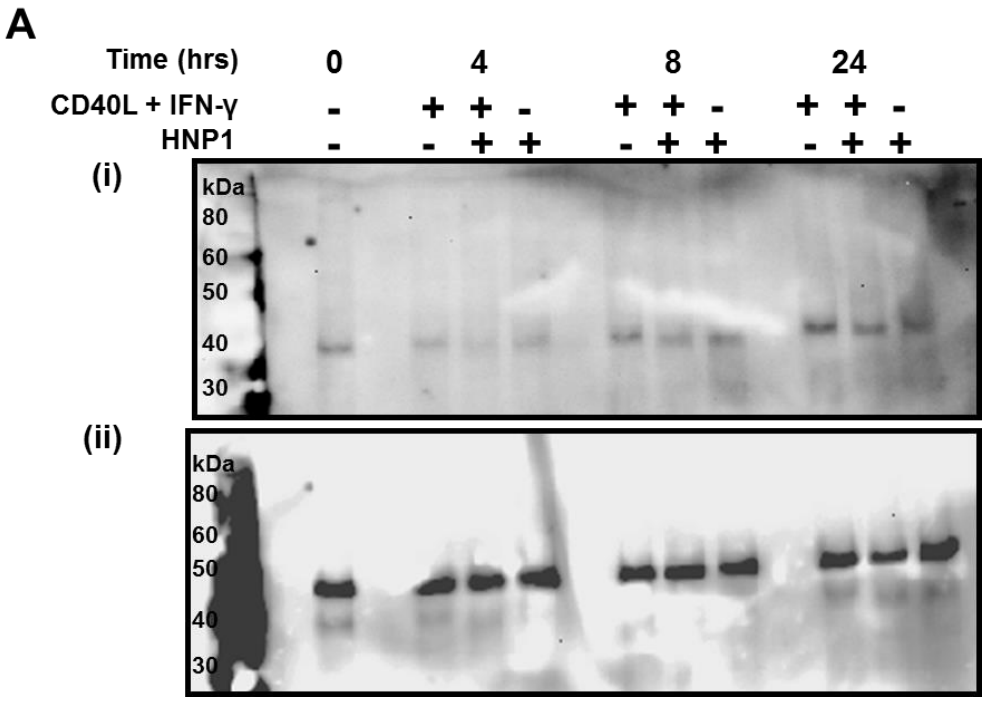

Figure 4.11: Expression of phosphorylated eIF2α in HNP1 treated HMDMs over 24hrs (Run1)

HMDMs from fresh blood donations were treated with 25μg/mL HNP1 alone or stimulated with 3ug/mL CD40L + 5ng/mL IFN-γ over 24hrs prior to lysis and SDS-PAGE. Western blot was performed for the detection of phosphorylated (S51) eIF2 (~36kDa, **i**) and β-Actin (~42kDa, **ii**).

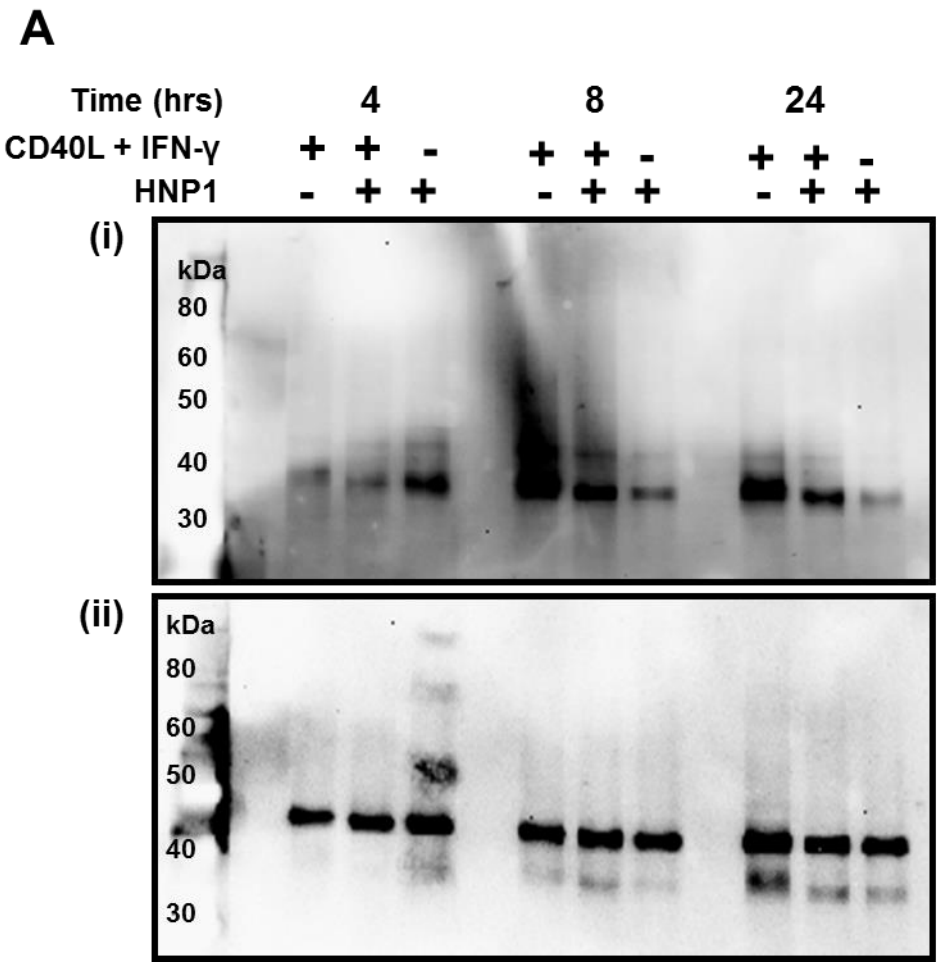

Figure 4.12: Expression of phosphorylated eIF2α in HNP1 treated HMDMs over 24hrs (Run 2)

Repeat experiment of Figure 4.11. Western blot was performed for the detection of phosphorylated (S51) eIF2 (~36kDa) depicted in (**i**). Detection for β-Actin (~42kDa), was also performed, as depicted in (**ii**). HMDMs were obtained from fresh blood donations.

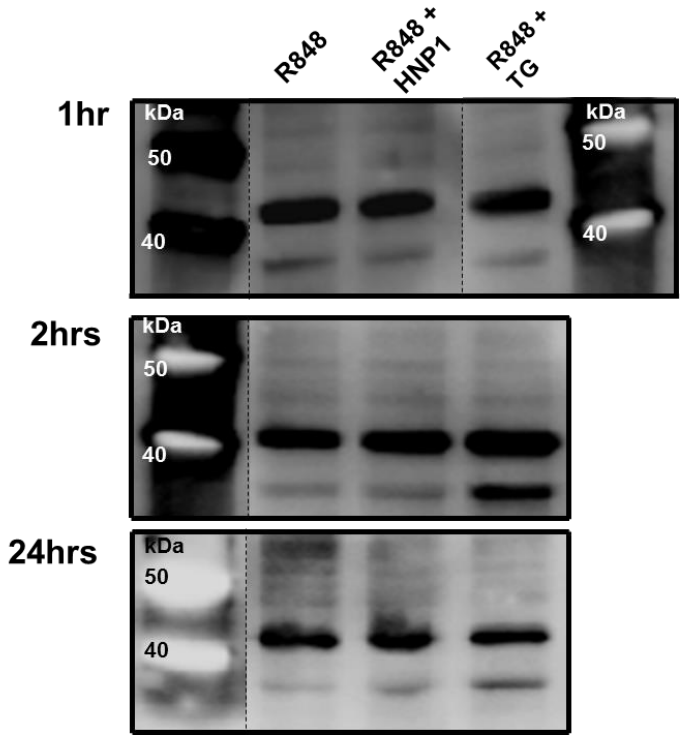

Figure 4.13: Expression of phosphorylated eIF2α in R848 stimulated HMDMs treated with HNP1

Western blot analysis of buffy coat HMDMs stimulated with 2.5μg/mL R848 and treated with 12.5μg/mL HNP1. Thapsigargin was added at 1μM as a positive control for ER stress. Western blotting was performed for phosphorylated (S51) eIF2 (~36kDa) and β-actin (~42kDa). Non-contiguous lanes from the same gel but spliced together have been indicated by dashed lines (n=1).

4.2.3.2 Upregulation of ER stress-associated gene expression

In order to reaffirm the results on eIF2α phosphorylation which gave no clear indication of an ER stress event caused by HNP1, the gene expression of key UPR modulators were assessed. As described in the introduction, upregulated expression of BiP, CHOP and spliced XBP-1 mRNA follow the activation of sensory proteins involved in early ER stress responses[147]. Thus the gene expression of these three ER stress markers were looked at in HMDMs treated with α-defensins.

R848-stimulated HMDMs from three buffy coat donors were treated together with 25% NN or 12.5μg/mL HNP1 or LHNP1 over a 24hr period. For the positive induction of ER stress, stimulated control HMDMs were treated with thapsigargin. RNA was extracted from the cells and resulting cDNA was sent to Professor Pieter Hiemstra and Emily van't Wout (Department of Pulmonology, Leiden University Medical Centre, The Netherlands) who kindly performed qPCR for quantitation of BiP, spliced XBP-1, and CHOP (detailed in Chapter 2, section 2.13.1).

Results from all three donors are shown, with a representative result shown in Figure 4.14 and the remaining two repeat experiments included as Figure B.5 and B.6, Appendix B. Expression of BiP, spliced XBP-1 and CHOP (Figures *A*, *B*, and *C* in each figure, respectively) showed similar levels of expression in α-defensin treated HMDMs compared to R848 alone controls over the 24hr incubation period. Functionally though, α-defensin was still having an inhibitory effect on secreted TNF-α in all three donors (Figure *D*), strongly suggesting that the inhibitory actions of α-defensins on protein synthesis was not attributed to an ER stress-mediated event. Thapsigargin, however, rapidly enhanced the expression of all three ER stress markers in all three of the donors tested, confirming the positive induction of ER stress in HMDMs.

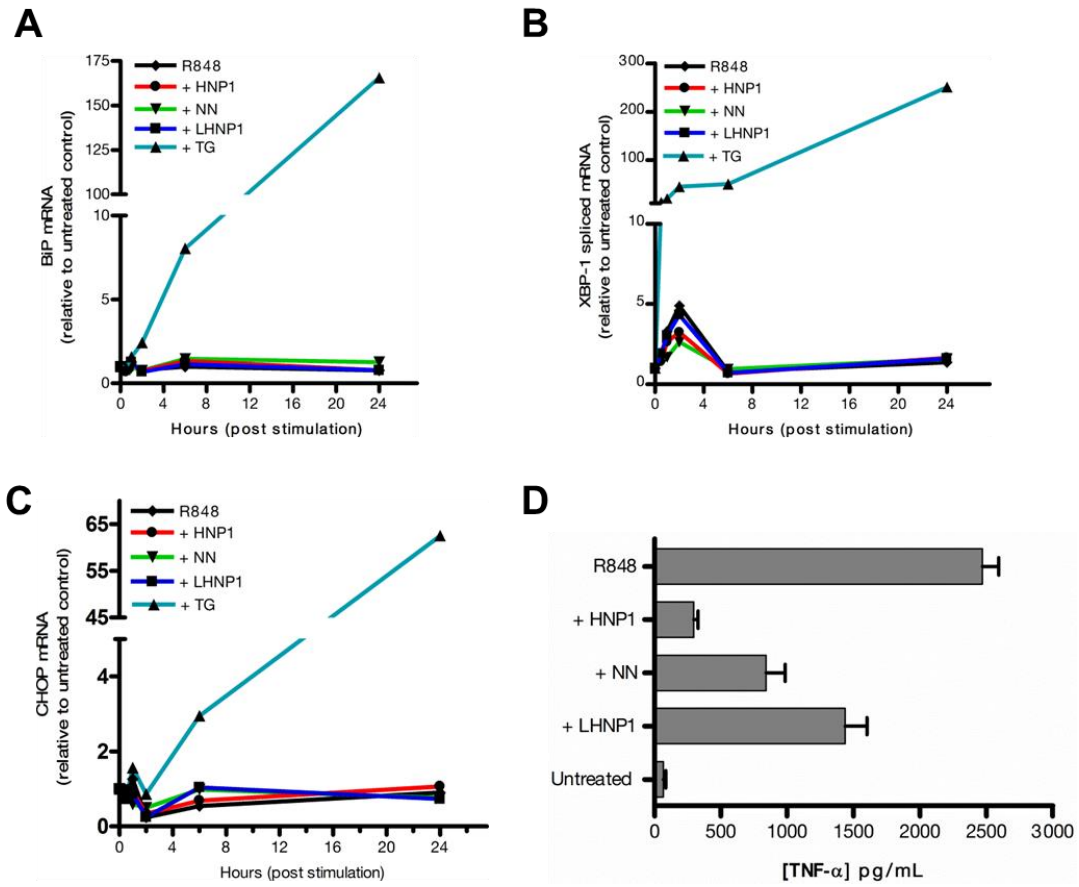

Figure 4.14: Gene expression of ER stress markers BiP, spliced XBP-1 and CHOP with α-defensins (Run1)

qPCR quantitation over 24hrs of ER stress markers BiP (**A**), spliced XBP-1 (**B**) and (**C**) CHOP normalised to basal levels in untreated cells. Buffy coat HMDMs were stimulated with R848 alone or in co-culture with 25% NN, 12.5µg/mL HNP1, LHNP1, or 1uM thapsigargin as a positive control. (**D**) Quantitated secreted TNF-α by ELISA at 24hrs. Values obtained are from triplicate repeats for all samples with mean ± SD for error bars. Results co-performed in conjunction with the Professor Pieter Hiemstra research lab (Leiden University, The Netherlands).

4.3 Discussion

From an early point in the investigations of α-defensins, evidence alluded to a non-discriminatory underlying mechanism. This was attributed to the inhibition of a range of secreted cytokines – both pro- and anti-inflammatory – as well as nitric oxide. Thus it was important to decipher if the role of α-defensins transcended from being just an immunomodulatory agent to one that has an even larger influence in overall cell metabolism.

By temporarily depleting HMDMs of methionine and re-introducing radiolabelled methionine at the time of HNP1 treatment, it became possible assess the difference in the amount *de novo* synthesised proteins, for both cellular and secreted proteins. By quantitation of the radiolabelled protein bands separated by SDS-PAGE, results were able to show HNP1 was beginning to have an inhibitory effect on secreted proteins as early as 4hrs, since there was a slight attenuation observed with HNP1 treatment compared to untreated controls. This result is supported by the fact that secreted TNF-α was already attenuated at 4hrs (Figure 3.13), suggesting that HNP1 is rapidly efficacious. Within 18 – 24hrs the inhibitory impact of protein synthesis by HNP1 is evident; secreted protein synthesis was significantly impaired and so were intracellular proteins but to a lesser extent. It is unclear at present as to reason for the difference between intracellular and secreted protein synthesis which would require further investigation. A suggestion is that there might be a preferential inhibition of endoplasmic reticulum-associated ribosomes which could enhance the level of inhibition of secreted proteins versus non-secreted proteins. Alternatively HNP1 could be directly implicated for this difference. Of the potentially multiple effects of HNP1, it is plausible that its effects may extend to impeding the translocation of ribosomes to the ER containing polypeptides destined for folding within the ER lumen. Final destinations for proteins folded within the ER are either for the secretory pathway, incorporation in the plasma membrane or lysosomes. If this scenario of impaired ribosome translocation to the ER were correct, then decreased plasma membrane and lysosome proteins could also be contributing toward the observed decrease in intracellular protein synthesis.

In a single experiment using 12.5μg/mL HNP1 (Figure 4.4), a similar trend showed the inhibitory effect on protein synthesis inhibition albeit with secreted proteins only. Only a slight inhibition of intracellular protein synthesis was detected in stimulated cells with HNP1 treatment. This would suggest that higher HNP1 concentrations are required to impair intracellular protein synthesis, although repeat experiments would be needed to confirm this observation. In addition, no distinct differences in HNP1-mediated translation inhibition could be made between untreated or stimulated HMDMs, implying that the function of HNP was independent of phenotype.

Comparing these new findings of attenuated protein synthesis by HNP1 to current literature, only two papers published in the 1980s have so far reported similar findings. Using 40μg/mL HNP1-3 on the human erythromyeloblastoid leukemia cell line K562, Lichtenstein *et al.* (1988)[133] found no inhibition of protein synthesis prior to cell lysis by assessing inhibition of [^{3}H] leucine incorporation simultaneously with cell lysis (chromium dye release). In a study using *E.coli*, Lehrer *et al.* (1989)[46] attributed cytotoxicity caused by HNP1 and -2 (50μg/mL) to inner membrane permeabilization and loss of intracellular contents for the cessation of DNA, RNA and protein synthesis. Granted, HNP cytotoxicity at these concentrations has not been ascertained in HMDMs and may very well cause irreversible cell membrane permeabilization. Thus the findings using 12.5 and 25μg/mL HNP, which correlate with concentrations determined in rheumatoid arthritis synovial fluid[87], suggest an intermediate modulatory effect on the inflammatory macrophage. In the concluding chapter to this thesis, I will elaborate on the regulatory effects of α-defensins at low/medium/high concentrations, something which I have termed 'the three tiers of α-defensin modulation' which are governed by the severity of inflammation.

Since HNP1 treatment had no effect on multiple markers of ER stress, it is appropriate to reject the hypothesis that induced ER stress is the mechanism of HNP-mediated translation inhibition. Although it was observed that intracellular calcium mobilisation is notably impaired, it is uncertain at this stage as to what the implication of this is on cell physiology and more to the point, inflammatory potential.

Assessing intracellular calcium storage release (i.e. in the absence of external Ca^{2+}), it would appear that the calcium signalling pathway was unaffected by HNP1 (Figure 4.15). More specifically, cleavage of phosphatidylinositol 4,5-bisphosphate (PIP_2) by phospholipase C (PLC) to yield diacylglycerol (DAG) and the secondary messenger inositol 1,4,5-triphosphate (IP_3). Soluble IP_3 migrates through the cytoplasm, activating IP_3 receptors located on intracellular calcium stores, such as the ER, triggering the release of calcium into the cytoplasm. The impaired inhibition appears to take place when the cell requires a calcium boost from the extracellular matrix through the plasma membrane-situated calcium channels SOC (Store Operated Channels) and CRAC (Calcium Release Activated Channel)[154].

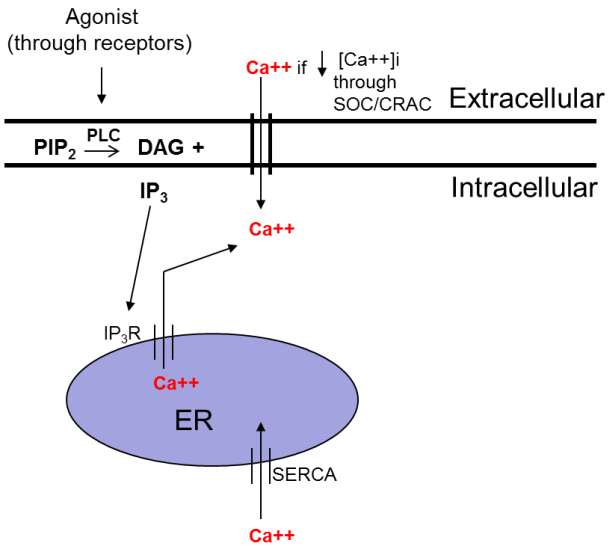

Figure 4.15: Schematic diagram of intracellular calcium signalling

This diagram depicts a common mechanism triggering the release of intracellular calcium in eukaryotic cells. Agonist binding to its cognate plasma membrane receptor activates a receptor-associated guanine nucleotide exchange factor (or GEF, not shown) to activate phospholipase C (PLC). PLC-mediated hydrolysis of phosphatidylinositol 4,5-bisphosphate (PIP_2) produces diacylglycerol (DAG) and the secondary messenger inositol 1,4,5-triphosphate (IP_3). Soluble IP_3 binds to IP_3 receptors (IP_3R) on ER membranes which open channels and release stored calcium. SOC (Store Operated Channels) and CRAC (Calcium Release Activated Channel) channels facilitate extracellular calcium influx when cytoplasmic calcium levels remain low.

Studies have previously shown that α-defensins rapidly form voltage gated channels within the lipid bilayer membranes, assessed by Kagan *et al*. (1990)[151]. In this study voltages were applied across membranes which were impervious to the flow of electric current prior to HNP1 treatment. In as little as 20 seconds, 50μg/mL HNP1 was able to generate a sustained transmembrane current. Membrane conductance is a direct reflection of the permeability to ions including Ca^{2+}, K^{+} and Na^{+}. Spectrofluorimetry studies were unable to show this rapid translocation of calcium in HMDMs treated with 25μg/mL HNP1 in the absence of PAF (Figure 4.8). While these studies were at half the HNP1 concentration used by Kagan *et al.*, the lack of observed effect is most likely attributed to equipment sensitivity and would require further testing using the patch clamp technique. Interpreting the biophysical data of Kagan and colleagues, it is not inconceivable to suggest that HNP1 rapidly forms ion permeable pores within the HMDM plasma membrane. Therefore depolarisation of the membrane potential with the likelihood of intracellular calcium desensitization may explain the impaired calcium flux and lack of subsequent oscillations observed. This scenario would appear more feasible than the direct impairment of L-type calcium channels by α-defensins as briefly tested (supplementary data; Chapter 7). Here, attempts to chemically induce calcium channel opening in order to restore TNF-α production proved unsuccessful. In addition, attempts to chemically induce calcium influx by way of calcium ionophores as well as calcium-dependent Protein Kinase C activation also proved unsuccessful (supplementary data, Appendix B).

Interestingly, the inhibitory effect of α-defensins on HMDMs is a transient one, shown previously in Dr Gray's research. Here, observations showed the full restoration of TNF-α production 72hrs after a 24hr incubation with HNP1[87]. It would be interesting to determine if calcium flux is also restored 72hrs post HNP treatment, as this could provide further clues into the relevance the calcium data. If there is a correlation, only a single calcium-influenced event has been ruled out thus far (ER stress). Further research into other calcium-dependant pathways would need to be addressed if this observed calcium mobilisation impairment has any bearings on other biochemical pathways.

The final points in this chapter return to the impact on global translation inhibition. Since cytokine exocytosis is not implicated in α-defensin-mediated inhibition, and impaired cellular and secreted protein synthesis is not ER stress-mediated, it implies that the actions of α-defensins are likely upstream of these processing stages. These results, coupled with the as yet unconvincing data on pro-inflammatory mRNA expression and stability, effectively narrow down the mechanism to a pivotal stage in the process of protein synthesis: translation initiation.

Chapter 5

5 Elucidating the inhibitory mechanisms of α-defensins on translation

5.1 Introduction

The results from Chapter 4 showed that HNP was an inhibitor of translation in HMDMs, thereby providing new mechanistic insight into how inflammatory cytokine expression is attenuated by α-defensins. While these results provided a clearer understanding of the overall inhibitory action, the molecular mechanistic actions of the peptide remained unclear. The inhibitory mechanism was not caused by a regulatory shut down of translation in response to an α-defensin-mediated cellular stress. Thus it was hypothesised that HNP1 may directly inhibit eukaryotic mRNA translation.

In this chapter, this hypothesis was tested by comparing two functionally different modes of translation initiation using a cell-free translation system; cap-dependent versus cap-independent, internal ribosome entry site (IRES)-mediated translation. It was also examined if the extent of mRNA incorporation into translating polyribosomes (polysomes) might be altered in HNP1-treated HMDMs. Finally, the possibility that HNP1 may bind RNA to inhibit mRNA translation was assessed. The HNP1:RNA binding stoichiometry was assessed using Electrophoretic Mobility Shift Assays (EMSAs), as previously used in published literature to investigate the binding interactions of other antimicrobial peptides to RNA and DNA[124,155].

In eukaryotic cells, with the exception of histone-encoding mRNAs which lack a poly(A) (poly-adenylated) tail, mRNAs are capped and poly-adenylated and are translated via a canonical cap- and poly(A)-dependent mechanism of translation. mRNA capping is the co-transcriptional 5’ attachment of 7-methylguanylate (m7G(5’)ppp(5’)G) – abbreviated to m7G, and this ‘cap’ structure facilitates mRNA nuclear export, stability and translation initiation. Similarly, the mRNA is modified at the 3’ end via co-transcriptional addition of a poly(A) tail of approximately 250

nucleotides in length. The cap and poly(A) tail are the major determinants of mRNA half-life and efficiency of translation. In the cytoplasm the 5' cap is bound by the cap-binding protein eIF4E and the poly(A) tail is bound by Poly(A) binding protein (PABP). Both of these factors then associate with eIF4G which serves to bring the 5' and 3' ends of the mRNA into close proximity to one another and pseudo-circularise the mRNA into a structure termed the closed-loop. Furthermore, eIF4G binding simultaneously enhances both the interaction of eIF4E with the cap and the binding of PABP to poly(A)[123], so stabilising the complex. These interactions result in the recruitment of the RNA helicase eIF4A, and this multi-protein complex is termed eIF4F (Figure 5.1). eIF4F facilitates 5' end unwinding and recruits the key factor eIF3, which is required for recruitment of the 43S pre-initiation complex, consisting of the 40S subunit, the eIF2-GTP-Met-tRNA^{Met}i, eIF1A, eIF1 and possibly eIF5. The eIF4F-eIF3-43S complex then scans the mRNA until it reaches an AUG initiation codon in the correct sequence context. Following initiator codon recognition and 48S complex formation, eIF5 and eIF5B promote the hydrolysis of the eIF2-bound GTP, causing subsequent eIF2-GDP to be released from the 48S complex. It also results in the release of initiator factors and the joining of the 60S subunit. Complete 80S ribosome formation then allows for polypeptide chain elongation to commence. This occurs by the entry of the cognate aminoacyl-tRNA into the entry site (referred to as the A-site, or acceptor site) within the 40S subunit, which binds to the corresponding codon. This binding is catalysed by eEF-1 (eukaryotic elongation factor) through the hydrolysis of a GTP. Once this aminoacyl-tRNA is bound the polypeptide chain is transferred from the aminoacyl-tRNA occupied in the P-site to the amino acid attached the tRNA in the A-site. This peptide bond formation between the polypeptide chain and the aminoacyl-tRNA in the A-site is catalysed by peptidyl transferase. eEF-2 and GTP hydrolysis facilitate the unlocking of the current ribosome formation, allowing for translocation of the tRNAs and mRNA within the ribosome. This shifts the empty tRNA molecule into the E-site for exiting the ribosome, while moving the polypeptide chain-containing tRNA into the P-site so that incoming aminoacyl-tRNAs can bind in the A-site containing the next sequential codon[156]. This completes once cycle of chain elongation. Chain termination commences when the ribosome reaches a stop codon on an mRNA strand (UAG,

UUA or UGA), which has no corresponding amino acid. Release factors will bind in the A-site causing the polypeptide chain to be cleaved from the tRNA. This releases the polypeptide to undergo folding, while the ribosome will dissociate into its subunits for translation initiation of the next available mRNA strand.

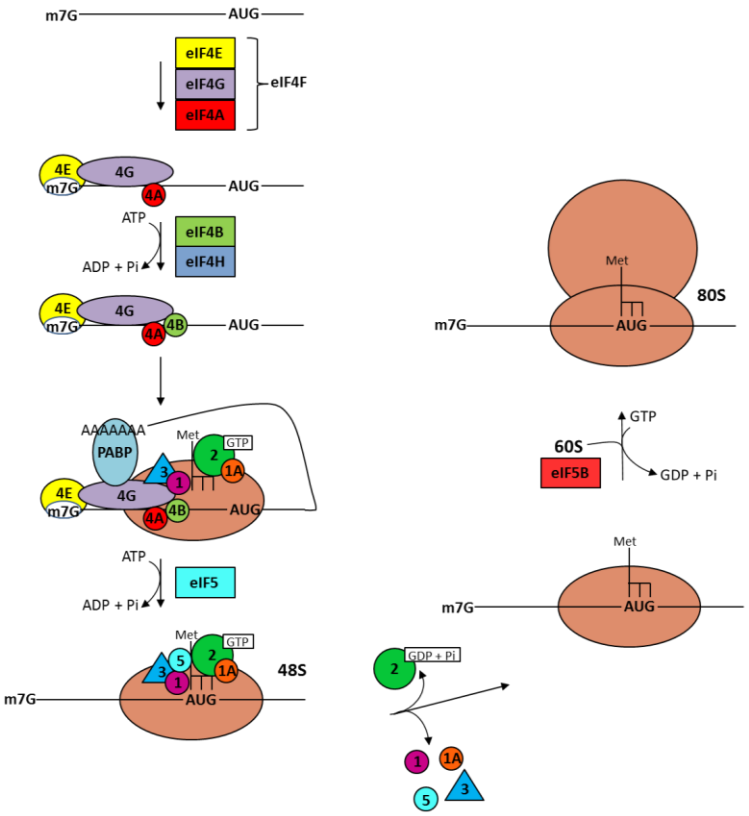

Figure 5.1: Cap-dependent mRNA translation

mRNA preparation for ribosome attachment is initiated by eIF4E binding to the 5' m7G-cap structure and enhanced by Poly(A) binding protein (PABP) attachment to the poly-adenylated 3' end. eIF4G binds eIF4E and PABP in close proximity to form an mRNA loop structure for stability. eIF4A completes the multicomplex eIF4F structure, which unwinds the 5' cap-proximal region assisted by eIF4B. eIF3 binds to eIF4G, 40S, eIF1 and eIF5 and recruits the eIF2-GTP-$tRNA^{Met}i$ ternary complex for 40S binding. This complex then scans downstream to the initiator codon. Translation commences with codon-anticodon pairing, induced by eIF5-mediated hydrolysis of GTP bound to eIF2α- $tRNA^{Met}i$. eIF2 along with the remaining factors are dissociated from the complex by eIF5B, which through GTP hydrolysis permits the binding of the 60S subunit. Figure adapted from Kieft (2008)[157].

The effect of HNP1 on cap-dependent translation was compared with that of cap-independent translation. This cap-independent mode of translation initiation is most commonly utilized by viruses to 'hijack' infected-cell translation machinery in order to synthesise proteins required for its replication. The virus blocks cap-dependent translation and then encodes its own mRNAs that contain secondary structures, known as IRES (Internal Ribosome Entry Sites), which recruit ribosomes directly to an internal position on the mRNA and are therefore cap-independent (Figure 5.2). Although IRES structures from some viruses can facilitate translation initiation independently of eukaryotic factors, some viral species utilise differing sub-sets of host initiation factors[142].

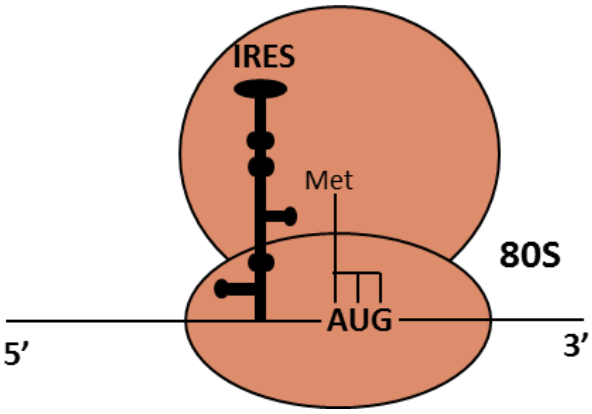

Figure 5.2: Cap-independent, IRES-mediated translation initiation
RNA structural elements, known as IRES (internal ribosome entry site), recruit ribosomes to internal locations in mRNA strands. This is independent of 5' capping and, in this example of IRES-mediated translation initiation, independent of host initiation factors.

Given the complexities surrounding eukaryotic cap-dependent translation, it was proposed that α-defensins could be affecting one or more of the molecular events required during translation. These effects were studied using a cell-free *in vitro* translation system in rabbit reticulocyte lysates. This commonly used molecular research tool is a highly efficient *in vitro* eukaryotic protein synthesis system used for the translation of exogenous mRNAs. It is a useful way to study the molecular

mechanisms of translation independent of transcription regulation, pre-mRNA processing (e.g. splicing), transcript stability and turnover. *In vitro* translation systems are typically derived from cells that are engaged in high rates of protein synthesis, such as rabbit reticulocytes, wheat germ and *E.coli*. They are prepared as crude extracts containing all the macromolecular components required for translation of exogenous mRNA including: ribosomal subunits, amino acids, tRNAs, aminoacyl-tRNA synthetases, initiation, elongation and termination factors. In addition they are supplemented with energy sources in the form of ATP and GTP and also contain energy regenerating systems, for example creatine phosphate and creatine phosphokinase for eukaryotic systems. More specifically, rabbit reticulocytes are immature red blood cells responsible for the synthesis of haemoglobin. These cells are nuclease-treated to remove all endogenous RNA and are thus a widely used as the RNA-dependent cell-free system for the application of exogenous mRNA. They subsequently possess low nuclease activity which allows for the detailed study of molecular mechanisms on translation.

5.2 Results

5.2.1 HNP1 inhibits both cap-dependent and cap-independent translation

The impact of HNP1 on cap-dependent and cap-independent mRNA translation was assessed in the rabbit reticulocyte lysate (RRL) system (described in section 5.1) using two reporter mRNAs. To assess cap-dependent translation, a capped but not polyadenylated firefly luciferase-encoding mRNA was used (referred to as Luc-A0) (see Chapter 2, section 2.10 for mRNA synthesis methodology). Cap-independent translation was assessed using a non-adenylated β-galactosidase-encoding mRNA, which contained a classical swine fever virus (CSFV) IRES mRNA (referred to as CSFV-Gal). m7G capping of this mRNA was replaced with a non-physiological cap analogue (ApE (G'(5)ppp(5')A). As a functional readout for the effect of HNP1 on both forms of translation initiation, the activity of synthesised luciferase and β-galactosidase protein was quantitated by luminometry. For each experiment, a fresh batch of reporter mRNAs were synthesised by *in vitro* transcription from freshly digested plasmid DNA. Reaction mixtures were incubated with 25μg/mL HNP1, LHNP1, or W26A alongside a vehicle control (0.01% acetic acid) for 30min at 30°C prior to the addition of both reporter mRNAs, each at a final concentration of 100ng/μL. After 90min of further incubation, protein expression from both reporter mRNAs was quantitated.

Results from these findings uncovered an astounding and unambiguous impact on translation by HNP1. Cap-dependent translation of Luc-A0 mRNA was significantly inhibited in the presence of HNP1 and exhibited only ~9% of the luciferase expression of the control reaction (Figure 5.3*A*). Astonishingly this inhibition on cap-dependent translation was completely absent in the presence of the mutant forms LHNP1 and W26A. This result convincingly demonstrated that HNP1 was in fact having a direct inhibitory effect on eukaryotic mRNA translation in agreement with the formulated hypothesis. It also suggested that this inhibitory mechanism must be due to a direct molecular interaction with the machinery that drives translation. Importantly, the data showed that tertiary conformation (LHNP1) as well as the

hydrophobic and dimerization (W26A) properties of HNP1 are essential for this activity.

Conventionally, the CSFV-Gal cap-independent reporter mRNA serves as an internal reference control to detect any changes to global translation and to normalise for variation between technical replicates. Rather surprisingly, results showed a significant translation inhibition of β-galactosidase by HNP1 compared with the LHNP1 sample, with only ~33% of protein expressed compared to vehicle control. This is while LHNP1 and W26A showed no effect on translation. This result further supports the suggestion the most simplest of mechanisms required for translation are inhibited by HNP1, since even fundamental IRES-mediated translation is attenuated. The differences in levels of inhibition between cap-dependent (~9% versus control) and IRES-mediated (~33% versus control) suggests that HNP1 inhibition may extend to interference with m7G cap-structure recruitment of initiation factors which bind ribosomes. This may explain the difference in inhibitory levels between the two modes of translation initiation but requires further testing.

For the inhibitory actions of HNP1 on translation to be valid, it was important to negate any suggestions of mRNA degradation. For this, small volumes (5μL) of reaction mixture were removed and snap frozen on dry ice immediately after the addition of mRNA as well as after the 90min incubation period (termed ‘pre-‘ and ‘post-translation’). Following RNA extraction, samples were electrophoresed on a denaturing agarose gel and stained for RNA. Images were developed for the semi-quantitative comparison of mRNA pre- and post-translation with Figure 5.4 being a representative image from all three repeat experiments. Comparing the RNA band expression of samples to control lanes consisting of either reticulocyte lysate alone (lane 1, from left) or starting amounts of Luc-A0 and CSFV-Gal (lane 2 and 3, respectively), it became difficult to accurately identify the reporter mRNA bands. As a result it was not possible to compare mRNA pre- and post-translation using this method. However, quantitation of Luc-A0 was performed in follow-on experiments by qPCR analysis, described in the next paragraph. In addition to this, a parallel experiment was performed mimicking the incubation conditions of peptides with

both mRNAs (Figure 5.5). In the vehicle solution used to reconstitute lyophilised peptide (0.01% acetic acid), both Luc-A0 and CSFV-Gal mRNA were incubated with 25μg/mL HNP1, LHNP1 or W26A alongside a vehicle control for 90min at 30°C. Subsequent non-denaturing agarose gel electrophoresis of the samples and migrated band semi-quantitation suggested no nuclease-type degradative effects by HNP1 that could account for the lack of luciferase and β-galactosidase synthesis.

Since 25μg/mL HNP1 caused a considerable reduction on cap-dependent translation, it was beneficial to determine the inhibitory concentration range to assess if it correlated with the concentration limitations of HNP1 seen with secreted TNF-α in HMDMs (Chapter 3, Figure 3.7). In essence the half maximal inhibitory concentration (IC50) of HNP1 on cap-dependent translation was determined. Figure 5.6-*i* shows the result from three independent experiments determining the IC50 of HNP1 on cap-dependent translation. HNP1 concentrations were titrated down by two fold serial dilutions ranging from 14μM (45.3μg/mL) to 0.875μM (3.93μg/mL). Plotting the log10 luciferase expression of HNP1-containing samples relative to an untreated control showed a gradual decline in HNP1 efficacy. The mean IC50 was determined to be 2.5 ± 0.87μM (8.62 ± 3.0 μg/mL) which were similar in value to the minimum inhibitory concentrations used to inhibit TNF-α in HMDMs, which was between 5-10μg/mL (determined in Chapter 3). The phenomenal inhibitory actions of HNP1 were demonstrated at the maximum HNP1 concentration used (14μM/45.3μg/mL). Translation of Luc-A0 was virtually non-existent at this concentration compared to untreated, LHNP1 and W26A controls, further proving the potency of this peptide to inhibit eukaryotic translation (Figure 5.6*B*).

In addition to IC50 determination, small volumes of reaction mixture were collected pre- and post-translation (as described above) from 14μM and 7μM (22.65μg/mL) HNP1-treated samples. This was also performed alongside untreated and vehicle control samples, after which RNA was extracted for qPCR analysis. Using custom-made primers for the luciferase (*luc*) gene (kindly donated by Dr Richard Smith, Centre for Reproductive Health, Edinburgh University), qPCR was performed to quantitate the amount of transcribed gene present in samples pre- and post-

translation, as an indication of mRNA stability (Figure 5.6-*ii*; n=3). Plotting expression relative to untreated control samples, no statistical changes to Luc-A0 mRNA quantitation pre- and post-translation could account for the significant reduction in luciferase translation, which suggested sustained mRNA integrity throughout the duration of the experiments.

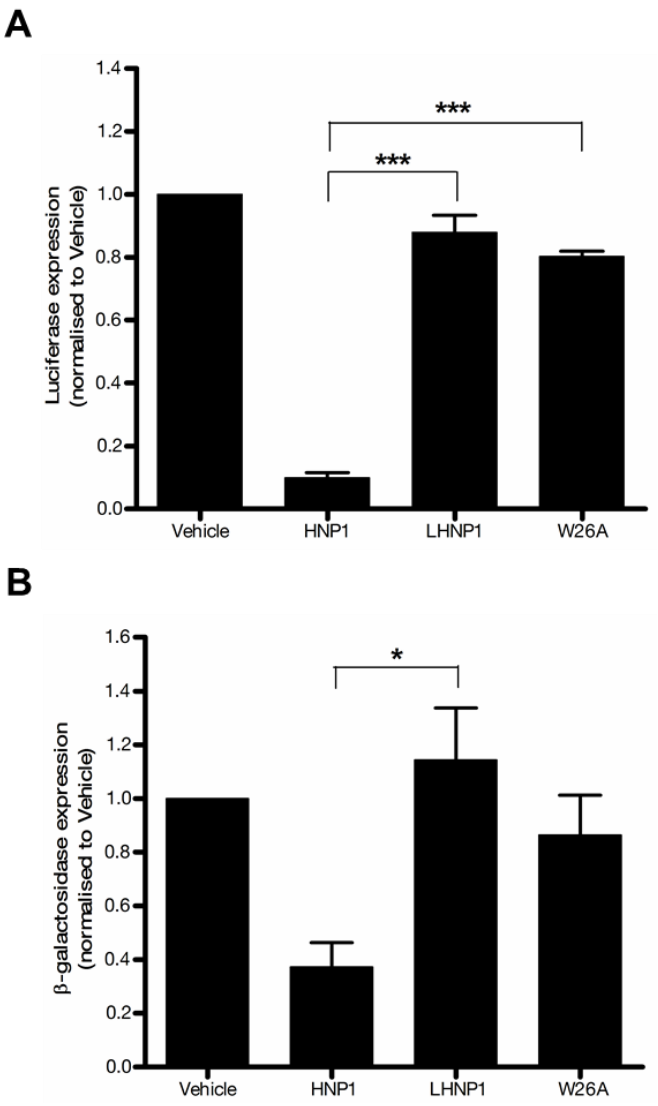

Figure 5.3: The impact of HNP1 on cap-dependent and cap-independent translation

(**A**) Luciferase protein expression following cap-dependent Luc-A0 reporter mRNA translation.

(**B**) β-galactosidase protein expression following cap-independent, IRES-mediated translation of β-Gal reporter mRNA.

Translation reaction mixtures were treated with HNP1, LHNP1 or W26A added at 25μg/mL alongside a vehicle control (0.01% acetic acid). Protein expression was quantitated by luminometry and plotted relative to Vehicle control samples. Error bars represent the mean ±SEM of three independent experiments. ***P<0.001, *P<0.05 (Tukey's multiple comparison *post hoc* test following one-way ANOVA).

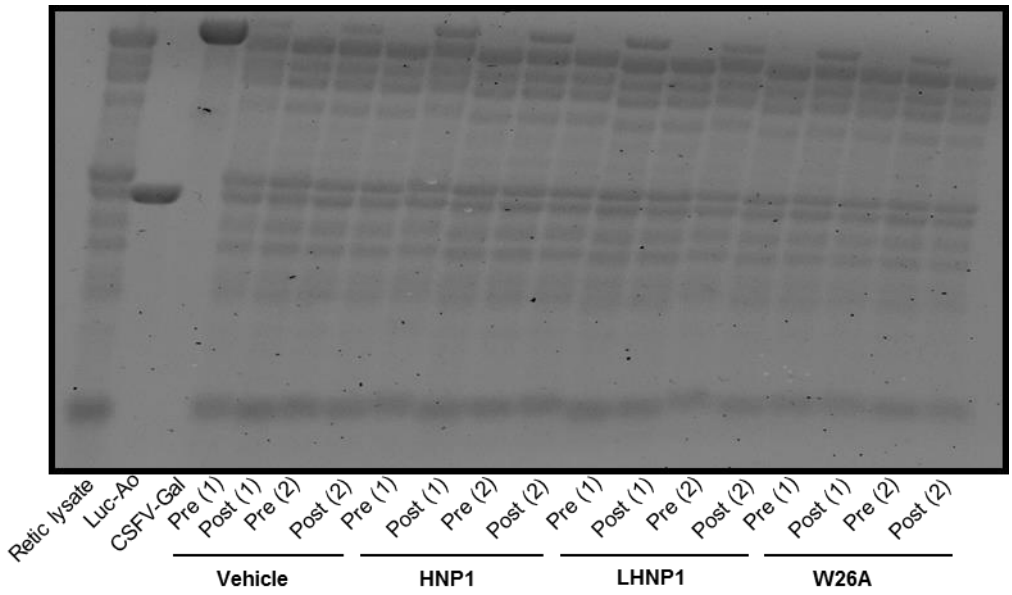

Figure 5.4: Denaturing gel electrophoresis of rabbit reticulocyte RNA samples pre and post *in vitro* translation

Representative image from Figure 5.3 of samples taken pre- and post-translation in the presence of HNP1, LHNP1, W26A and vehicle control (performed in duplicate). Agarose gels were run for the purpose of semi-quantitation of Luc-A0 and CSFV-Gal mRNA pre- and post-incubation with HNP1. Included were lanes containing reticulocyte lysate alone (first lane, from left) as well as starting amounts (2μg) of both mRNAs (second and third lane).

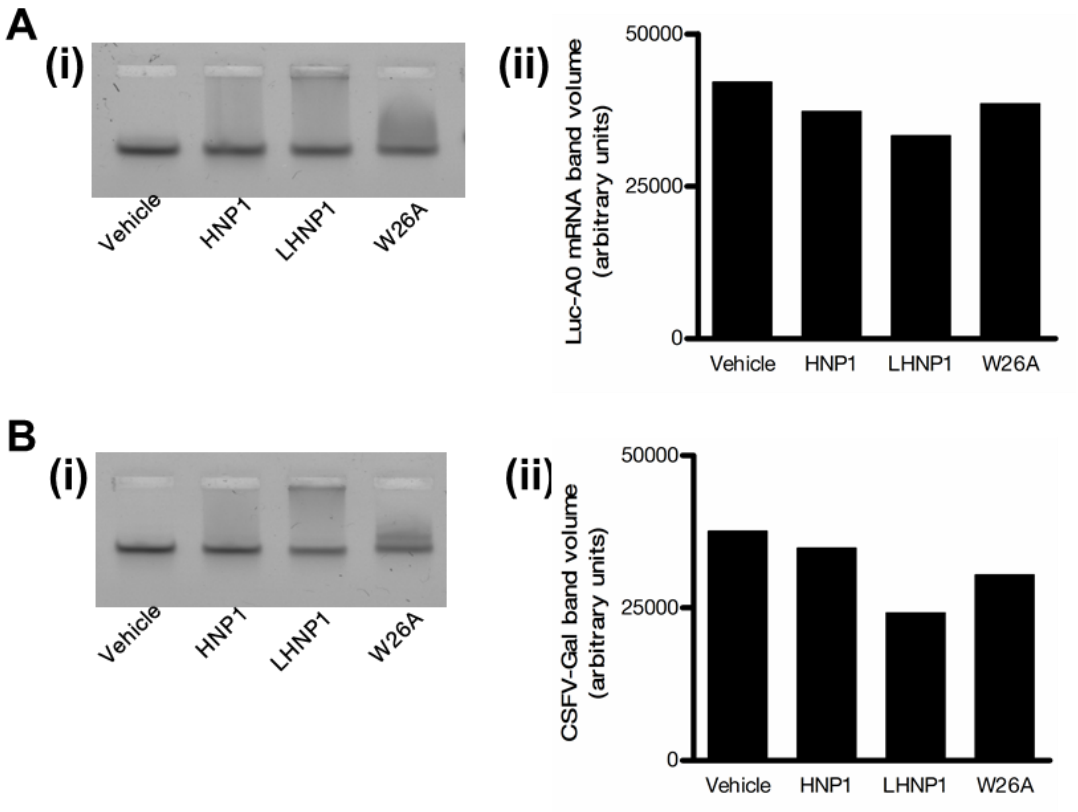

Figure 5.5: Validation of reporter mRNA integrity with HNP1 treatment

Non-denaturing agarose gel electrophoresis results of Luc-A0 (**A**) and CSFV-Gal (**B**) mRNA post incubation with 25μg/mL HNP1, LHNP1 or W26A in 0.01% acetic acid (vehicle solution) under the same incubation conditions as in Figure 5.3. (**i**) Gel images were acquired followed by band volume determination (**ii**) expressed in arbitrary measurement units. Results are of an n=1 validation experiment performed.

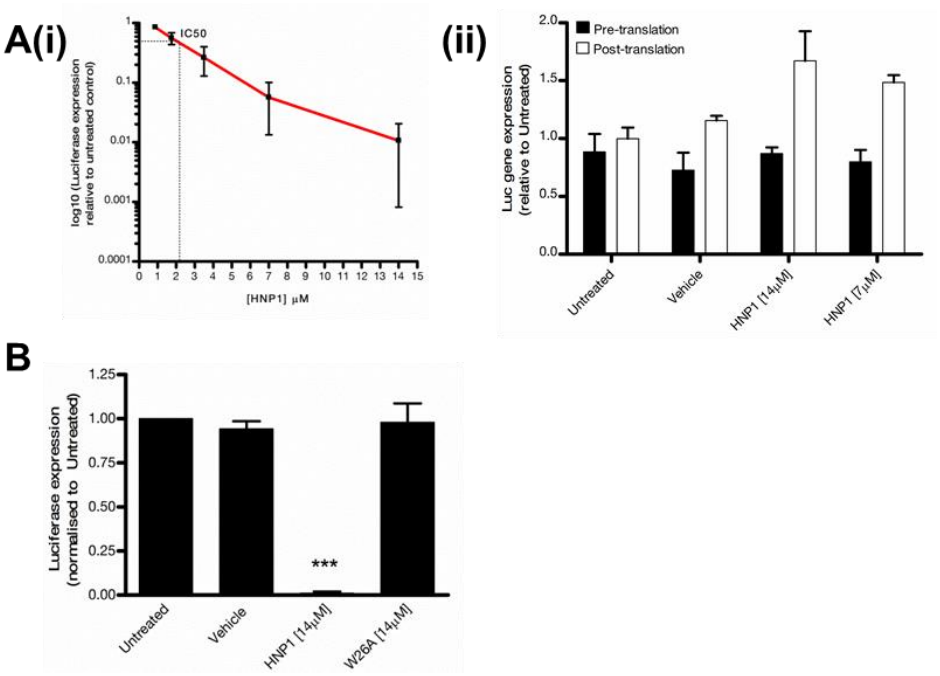

Figure 5.6: Half maximal inhibitory concentration (IC50) of HNP1 in cap-dependent translation

(**A**) Result of luciferase protein expression following cap-dependent Luc-A0 mRNA translation following incubation with titrated HNP1 at micromolar concentrations. (**i**) Quantitated luciferase protein expression relative to untreated control samples with the IC50 of HNP1 inhibition indicated (calculated to be ~2.5 ± 0.87µM or 8.62 ± 3.0µg/mL). (**ii**) Luc-A0 mRNA expression in samples pre- and post-translation incubation quantitated by qPCR and normalised to untreated control group. Error bars represent the mean ±SEM from three independent experiments (duplicate experimental replicates) with no statistical significance between post-translation HNP1 treated samples compared with post translation Vehicle control (one-way ANOVA).

(**B**) Quantitation of luciferase protein expression following Luc-A0 mRNA translation in samples incubated with 14µM HNP1 (45.3µg/mL) and W26A (46.6µg/mL). A vehicle (0.01% acetic acid) and untreated control were included for comparison and luciferase expression was normalised to untreated control samples. Error bars represent the mean ±SEM from three independent experiments. ***P<0.001 (Tukey's multiple comparison *post hoc* test following one-way ANOVA).

5.2.2 Polysome analysis of HNP1 treated HMDMs

In vitro translation data strongly indicated that HNP1 had a direct inhibitory effect on both cap-dependent and cap-independent translation. It was yet to be determined how mRNA translation was inhibited by HNP1. For over forty years the principle of mRNA sedimentation being affected by its incorporation within ribosomes within sucrose gradients has allowed researchers to study effects on translation in detail[158]. By *in vitro* assessment of attached ribosomes to strands of mRNA (collectively referred to as polysomes), polysome analysis has made it possible to decipher the *de novo* state of translation in cells. This method can make visual comparisons between ribosomes active at the point of translation initiation, polypeptide chain elongation and termination. Thus assessing the differences of polysomes distribution can reflect changes to translation efficiency and provide a global 'snapshot' of the overall ribosome distribution within a cell at a given moment.

It was decided to utilise polysome analysis in HNP1-treated HMDMs with the methodology detailed in Chapter 2, section 2.14. The general principle was to HMDMs after a period of incubation with HNP1 in a lysis buffer which preserves polysome-mRNA interactions, notably by the addition of cycloheximide which acts as a stabilising agent preventing ribosome run-off. Lysed HMDMs were layered onto a sucrose gradient buffer of increasing sucrose density (10, 18, 26, 34, 42, 50% (w/v)). Following ultracentrifugation, samples were collected by fractionation across ten fractions while measuring RNA absorbance at 254nm in real-time. Thus it was possible to visualise the differences in ribosomal peaks ranging from: low density ribonuclear fractions containing unincorporated RNA material, increasingly dense ribosomal subunit material (40/43S and 60S), followed by monosomes as 80S assembled ribosomes, and dense fractions of translating polysomes.

Preliminary optimisation experiments determined that 10^6 HMDMs per sample contained sufficient biological material for detection by the UA-6 UV/Vis detector to measure RNA absorbance within samples. Further optimisation experiments assessed the inhibitory effect of cycloheximide to prevent ribosome run-off. This antibiotic was used throughout the assay added 30min prior to cell lysis. The effect of

translation inhibitor puromycin dihydrochloride was also tested, which disrupts peptide transfer on ribosomes causing premature chain termination and used as a positive indication for arrested translation. Polysome analysis confirmed the contrasting effects of these antibiotics on HMDM translation. Incubation with cycloheximide (Figure 5.7*A*) showed the presence of polysomes in the latter fractions (fractions 6-10). As a result, this positively indicated the effective use of cycloheximide in preventing ribosome run-off. However, diminutive polysome traces did suggest the requirement for either increased amounts of biological material or an adjustment of machine sensitivity, with the risk of creating distorted readings due to unacceptable levels of machine background 'noise'. Incubation with puromycin showed the cessation of translation, indicated by the absence of polysomes with only a subtle peak visible of the trace, possibly indicating the presence of mRNA associated with fewer ribosomes. Translation inhibition was also signified by a single 80S peak, suggesting stalled ribosomes. Dividing the collected fractions for RNA extraction and protein precipitation, non-denaturing agarose gel electrophoresis of RNA was unable to convincingly show differences in translation profiles by visualisation of 28S and 18S rRNA (within 60S and 40S subunits, respectively) in each fraction. Western blotting was used to assess the distribution of rps20 - a ribosome protein on the 40S subunit - across the fractions. Rps20 showed a more even distribution of 40S that spanned into polysome fractions (fractions 6-10) in cycloheximide-treated HMDMs. This indicated that ongoing translation within cells prior to cycloheximide treatment. The inhibitory effects of puromycin were seen with rps20 as this protein was largely accumulated in the pre-translation initiation stages (fractions 3 and 4) and in the 80S ribosome-containing fraction (fraction 5).

Subsequent experiments assessing the effect of HNP1 on polysome analysis were less definitive. Figure 5.8*A* is representative of three experimental attempts where no visual presence of polysomes could be identified in R848-stimulated HMDMs alone or treated with 12.5μg/mL HNP1 or W26A for 6hrs. This was while the inhibitory effect of HNP1 on secreted TNF-α was still apparent (Figure 5.8*B*). The increase in machine sensitivity to detect subtle changes in polysomes meant that differences in 40S, 60S and 80S peaks could not be compared as recordings of these went beyond

chart and absorbency limitations. However, the primary objective of this assay was to gauge any differences in polysome distributions with added HNP1, so this was deemed a satisfactory trade-off. It was thought that differences in extracted RNA and translation-associated proteins within fractions could still harbour useful information into the inhibitory effect of HNP1. Inconsistent RNA quality meant it was difficult to effectively compare distributions of 28S and 18S between treatments. In addition, quality of precipitated proteins did not permit accurate distribution assessments of rps20 (not shown) or PABP1, which is attached to both stored and polysomal mRNAs[159].

In a final attempt at polysome analysis with the RNA absorbance sensitivity settings finalised using 10^6 HMDMs, cells were stimulated with R848 either alone or together with 12.5μg/mL HNP1 for 4hrs alongside untreated controls (Figure 5.9). RNA traces revealed similar patterns of polysomes and 60S/80S peaks. Comparing R848-stimulated HMDMs with R848 and HNP1-treated samples, there was a noticeable absence of RNA material in the translation-inactive regions with HNP1 (fractions 1 - 4). Untreated HMDMs showed a similar pattern of expression to HNP1 treated HMDMs, while the inhibitory effects of HNP1 on secreted TNF-α was confirmed. Given that this observation was made once after three previously unsuccessful attempts, it is currently uncertain if this result has any bearings on the early stage effects of HNP1 and would require further testing to confirm its relevance.

Since previous attempts to analyse the distribution of rRNA across the fractions proved fruitless, extracted RNA from fractions was reverse transcribed by RT-PCR and subsequent qPCR was performed for TNF-α. This was in an attempt address the distribution of TNF-α mRNA incorporated within ribosomes with HNP1 treatment. As a normalisation control to compare the resulting TNF-α gene expression across the ten fractions in each treatment, fractions were spiked with 20ng of Luc-A0 mRNA for subsequent *luc* gene quantitation by qPCR, as previously described previously for *in vitro* translation assays. qPCR for TNF-α mRNA was performed using custom-designed forward and reverse primers kindly donated by Professor Ken Donaldson (Centre for Inflammation Research, University of Edinburgh).

Quantitation by qPCR was unable to detect TNF-α mRNA across all fractions in all treatments. Simultaneous validation experiments of TNF-α primers used were able to quantitate baseline levels of TNF-α mRNA samples of primary human skeletal muscle satellite cells, kindly donated by Jennifer McLeish, Centre for Inflammation Research (data not shown). Going forward, a repeat of the qPCR experiment could be performed on these samples optimising the amount of starting cDNA in an attempt to successfully quantitate TNF-α mRNA.

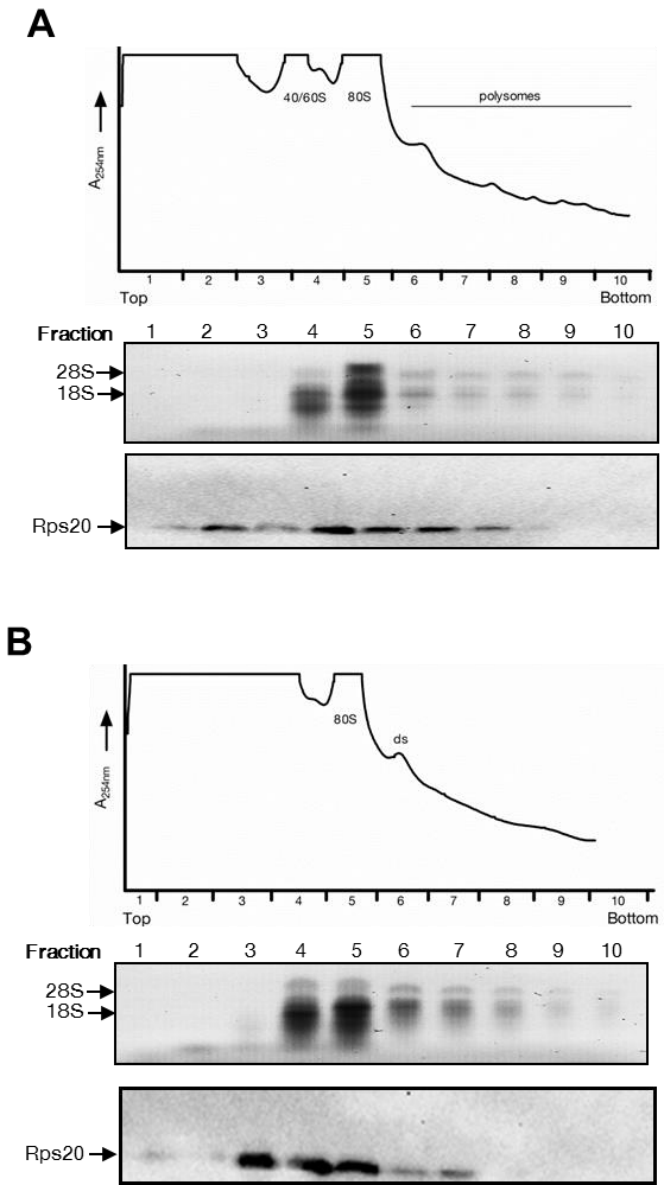

Figure 5.7: Polysome analysis of R848-stimulated HMDMs with cycloheximide and puromycin treatment

Results obtained of R848 stimulated HMDMs (4hrs) followed by 30min incubation with 150µg/mL cycloheximide (**A**) or 500µg/mL puromycin (**B**) prior to lysis and polysome analysis (n=1). Ribosome peaks are labelled for the indication of 40S, 60S, 80S and disomes ('ds'). Collected fractions were processed for downstream expression of 28S and 18S rRNA by non-denaturing agarose gel electrophoresis as well as by western blotting for ribosomal protein S20.

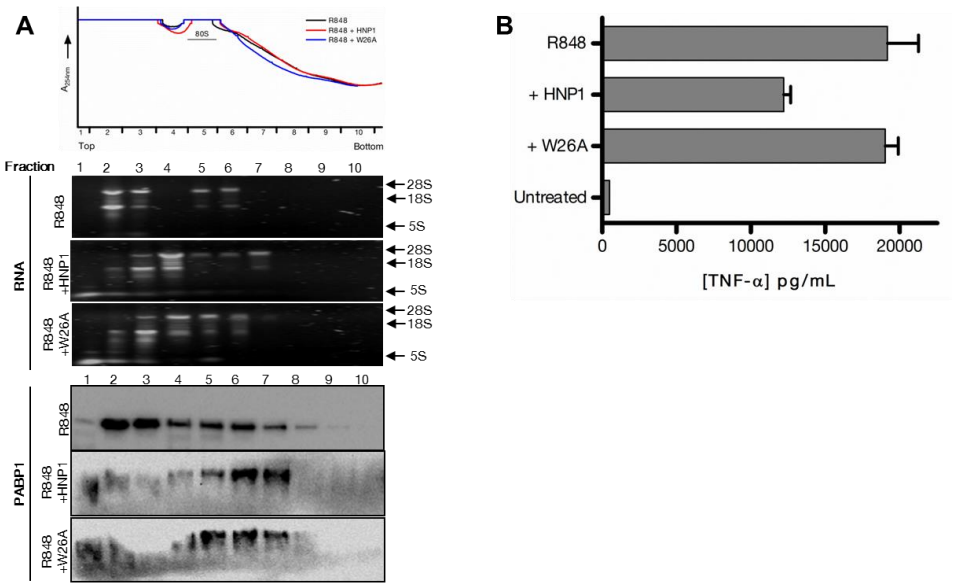

Figure 5.8: Polysome analysis of R848 stimulated HMDMs with HNP1 and W26A treatment

(**A**) Results of HMDMs stimulated with 1µg/mL R848 alone or with 12.5µg/mL HNP1 or W26A for 6hrs prior to lysis and polysome analysis (n=1). Collected fractions were processed for RNA gel electrophoresis and Western blotting for PABP1.

(**B**) TNF-α ELISAs were performed from supernatants (performed in triplicate) with mean ± SD for error bars.

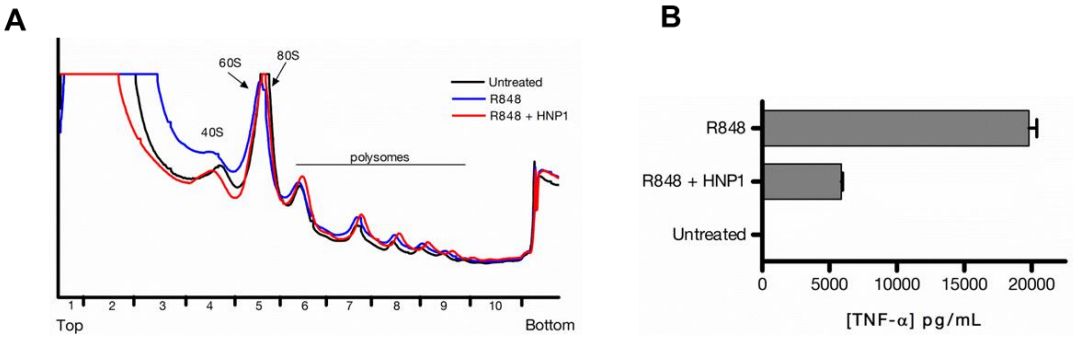

Figure 5.9: Polysome analysis of HMDMs with HNP1 treatment

(**A**) Polysome analysis of HMDMs stimulated with 1µg/mL R848 alone or in culture with 12.5µg/mL HNP1 alongside untreated control after 4hrs incubation. (**B**) TNF-α ELISAs from collected supernatants (performed in triplicate) with mean ± SD for error bars (n=1).

5.2.3 The binding affinity of HNP1 in Electrophoretic Migration Shift Assays (EMSAs)

The technique of polysome analysis was utilized ideally to find clues into how α-defensins might alter the distribution of translating ribosomes during mRNA translation. If the assay was successful in identifying an inhibition of translating polysomes, complementary assays would still need to pinpoint the underlying inhibitory mechanism to determine which part of the translation machinery is impaired within the cell.

It is now widely accepted that the pathogen killing mechanisms of antimicrobial peptides include not only transmembrane pore formation or cell-wall synthesis prevention, but are also mediated through intracellular targets including inhibition of nucleic acid and protein synthesis as well as interference with enzyme activity[160]. In addition, studies by Park *et al.* (1998)[124] studied the killing mechanisms of a 21 amino acid antimicrobial peptide Buforin II obtained from the Asian toad *Bufo bufo garagrizans*. Results described a peptide mechanism independent of pore-formation which showed a strong affinity for binding to RNA and DNA. Given this prior knowledge and since HMDMs remained viable when treated with 25μg/mL HNP while inhibiting translation in both cells and cell-free systems, it became reasonable to hypothesise that HNP1 could bind to RNA-containing components involved in translation.

Electrophoretic Mobility Shift Assays (EMSAs) were used to test the affinity and furthermore the stoichiometry of HNP1 for RNA. EMSAs, also known as gel shift/retardation assays, are a commonly used tool to visualise protein-RNA and protein-DNA interactions. It relies on the property that nucleic acids will move through an agarose or polyacrylamide gel matrix towards the anode in an electric field. Migration of nucleic acids are governed by three properties: the molecular weight and charge, its three-dimensional shape, and the physical properties of the gel matrix[161]. A protein or peptide with an affinity for nucleic acids will either modulate the conformational structure of the RNA/DNA or substantially increase the molecular weight which can alter the mobility through the gel. Affinity of HNP1 for HMDM RNA was studied, which will be covered in detail in Chapter 6. This section

set out to assess the HNP1 binding affinity for three of the four nucleobases within RNA: adenine (A), cytosine (C) and uracil (U). This study involved the use of three 25bp oligonucleotide sequences consisting of either A, C, or U, referred to as Poly A, Poly C and Poly U, respectively. These oligonucleotides were kindly donated by Dr Matthew Brook (Centre for Reproductive Health, Edinburgh University).

5.2.3.1 Optimisation experiments

Initial experiments began with optimising the migration of Poly A and C in two differing binding buffer conditions adapted from sources in literature. This was in an attempt to obtain the most gradual of oligonucleotide 'shifts' in the gel with increasing HNP1 concentrations (detailed in Chapter 2, section 2.11). The migration in these two sets of buffers were electrophoresed in two differing percentages of non-denaturing acrylamide gels (5% and 7% [60:1] acrylamide/bisacrylamide), again to obtain the most gradual shift of oligonucleotide for subtle changes in migration patterns with titrated HNP1 (Figure 5.10). Initial assessments of the differences were made by incubating fixed amounts of Poly A or Poly C (10pmol) with 75pmol HNP1 (oligo:HNP1 ratio of 1:7.5) for 30min followed by electrophoresis. The migration of unbound oligonucleotide was visually compared to that of untreated controls, fluorescently detected by the Cy5 fluorophore label at the 5' end of each oligonucleotide.

By visual comparison, HNP1-bound Poly A and C within buffer 'GT' resulted in a streak of impeded oligonucleotide noticeable throughout the entire gel lane, as opposed a more favoured shift in the whole oligonucleotide band as seen in the majority of protein-nucleic acid interactions using EMSAs. This streak was less severe in buffer 'SL' in both 5% and 7% acrylamide gels (Figure 5.10*A* and *B*, respectively). This suggests that the reagents in buffer SL supported a more stable HNP1-oligonucleotide complex during migration, resulting in a more definitive shift compared to buffer GT. In both acrylamide gel percentages, no shift pattern of bands occurred within the gel. Results showed that oligonucleotides either migrated freely within the gel (visible at the migration front), migrated to variable degrees (visible as a streak within the lane), or was prevented from entering the gel matrix completely

(visible as a complex situated within the loading wells). This lead to early suggestions that HNP1 formed a complex with Poly A and C that was too complex to migrate through the gel to form a shifted band. It was anticipated that the use of a 5% acrylamide gel would allow for a matrix pore size large enough to accommodate this complex. The difference in gel integrity was visibly noticeable between 5% and 7% gels without showing much difference in migrated oligonucleotide. As further reductions in acrylamide percentages would only compromise gel stability, it was decided to perform subsequent experiments using 7% acrylamide gels, abandoning the desired band shift concept.

Further optimisation experiments compared the HNP1 binding association with Poly A and Poly C in buffer GT and SL containing 3mM magnesium chloride, included to simulate the physiological requirement of magnesium for optimal protein-RNA binding as a result of Mg^{2+}-stabilised RNA conformations (Figure 5.11)[162,163]. HNP1 was tested at ratios to oligonucleotide of 7.5 and 15 and the samples containing $MgCl_2$ displayed fewer streaks of oligonucleotide compared to samples without $MgCl_2$, suggesting an enhanced complex stability. As a result, EMSA binding buffers would include $MgCl_2$. Assessment of migrated oligonucleotide comparisons between buffers showed that buffer SL displayed a more gradual decline in migrated (unbound) Poly A and C in the presence of HNP1, which was favoured in order to effectively compare differences in the stoichiometric binding ratios of HNP1 with Poly A, C and U. Evidence from optimisation experiments was beginning to suggest that buffer SL containing $MgCl_2$ was the preferred incubation conditions for binding assessments.

The final optimisation procedure was to compare the differences in HNP1 and W26A affinity for oligonucleotides using both binding buffer systems (Figure 5.12). In two repeat experiments (Figure 5.12*A* and *B*) using HNP1 and W26A at ratios of 7.5 and 15 to Poly A and Poly C, a clear contrast was observed between the evident binding capability of HNP1 and lack thereof with W26A. Semi-quantification of free oligonucleotide was performed for Figure 5.12*A*, defined by the total band volume within each lane excluding the complex within the loading well and plotted relative

to the nil peptide control lane. Results confirmed the strong binding affinity of HNP1 for both oligonucleotides, again with buffer SL displaying the more gradual binding affinity between the 7.5 and 15 ratios. In the case of W26A, unbound oligonucleotide migration was comparable to untreated controls with a slight streaking observed for ratios at 15. Visual inspection on the second repeat suggested a similar binding trend (Figure 5.12*B*).

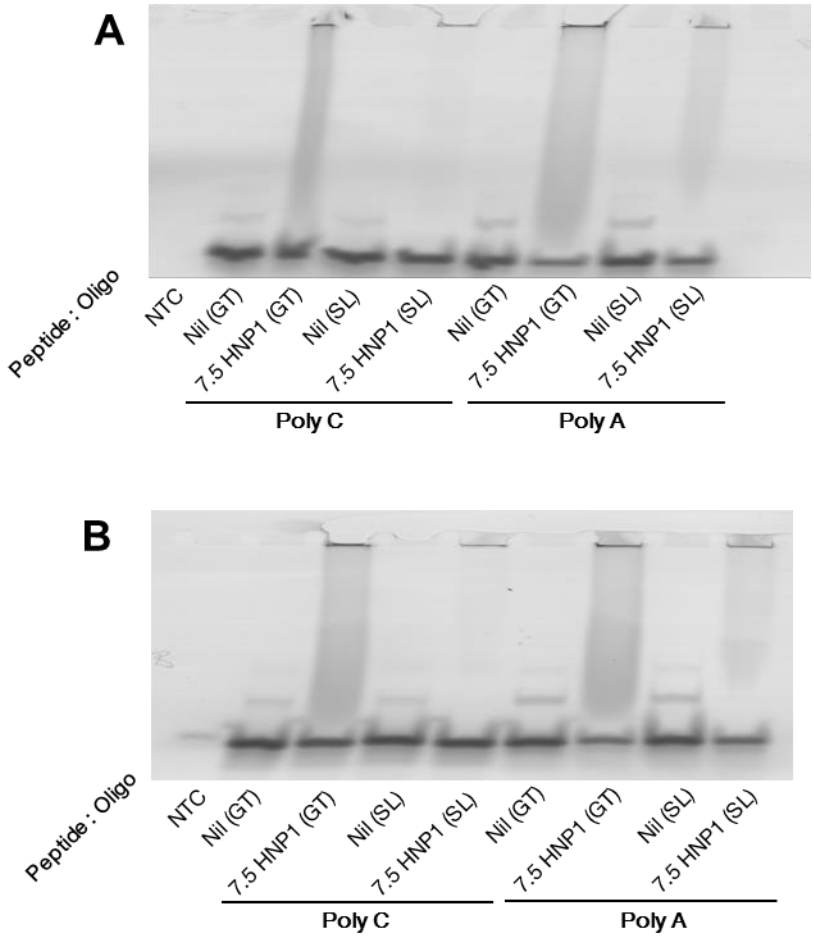

Figure 5.10: Comparative migration of Poly A and Poly C in differing binding buffer conditions and acrylamide concentrations

Electrophoretic migration of 10pmol Poly A and Poly C after incubation with 75pmol HNP1 (ratio of 1:7.5) in either buffer 'GT' or 'SL' compared to Nil peptide control. A non-template control (NTC) with no oligonucleotide was included. Samples were electrophoresed in either a 5% (**A**) or 7% (**B**) [60:1] acrylamide/bisacrylamide non-denaturing gel (n=1).

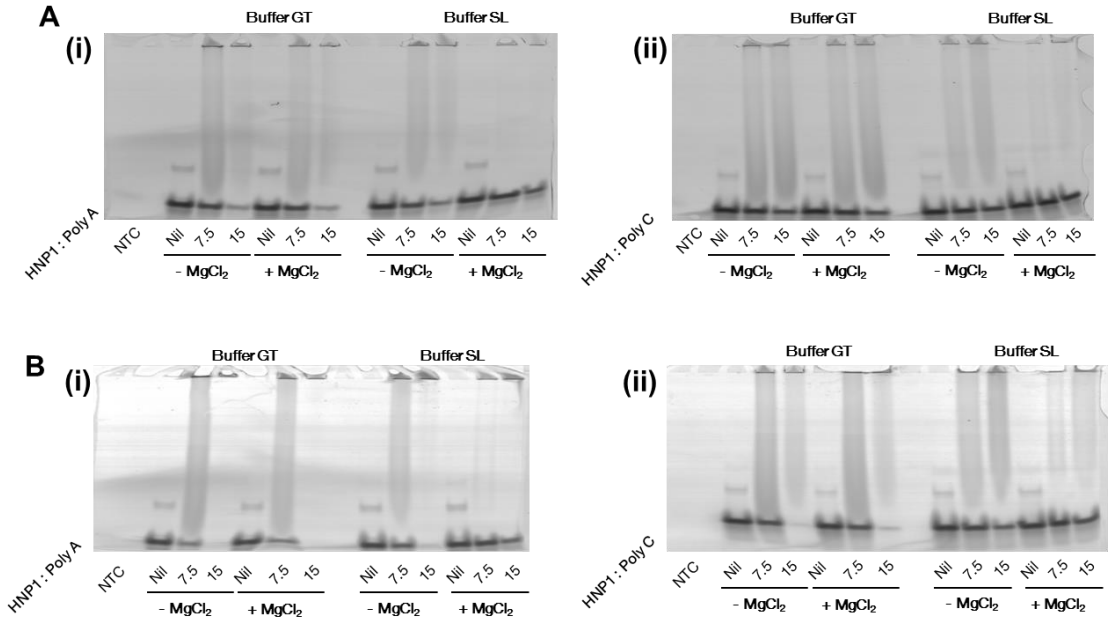

Figure 5.11: Comparative EMSA gels of differing binding buffer conditions and $MgCl_2$ inclusion

Electrophoretic migration after Poly A (**i**) and Poly C (**ii**) incubation with HNP1 (pmol) in either buffer 'GT' or 'SL' with or without the addition of 3mM $MgCl_2$ added to the buffer. Migration of free oligonucleotide was compared to nil peptide control while a non-template control (NTC) was included. Results are of two independent experiments (**A**) and (**B**).

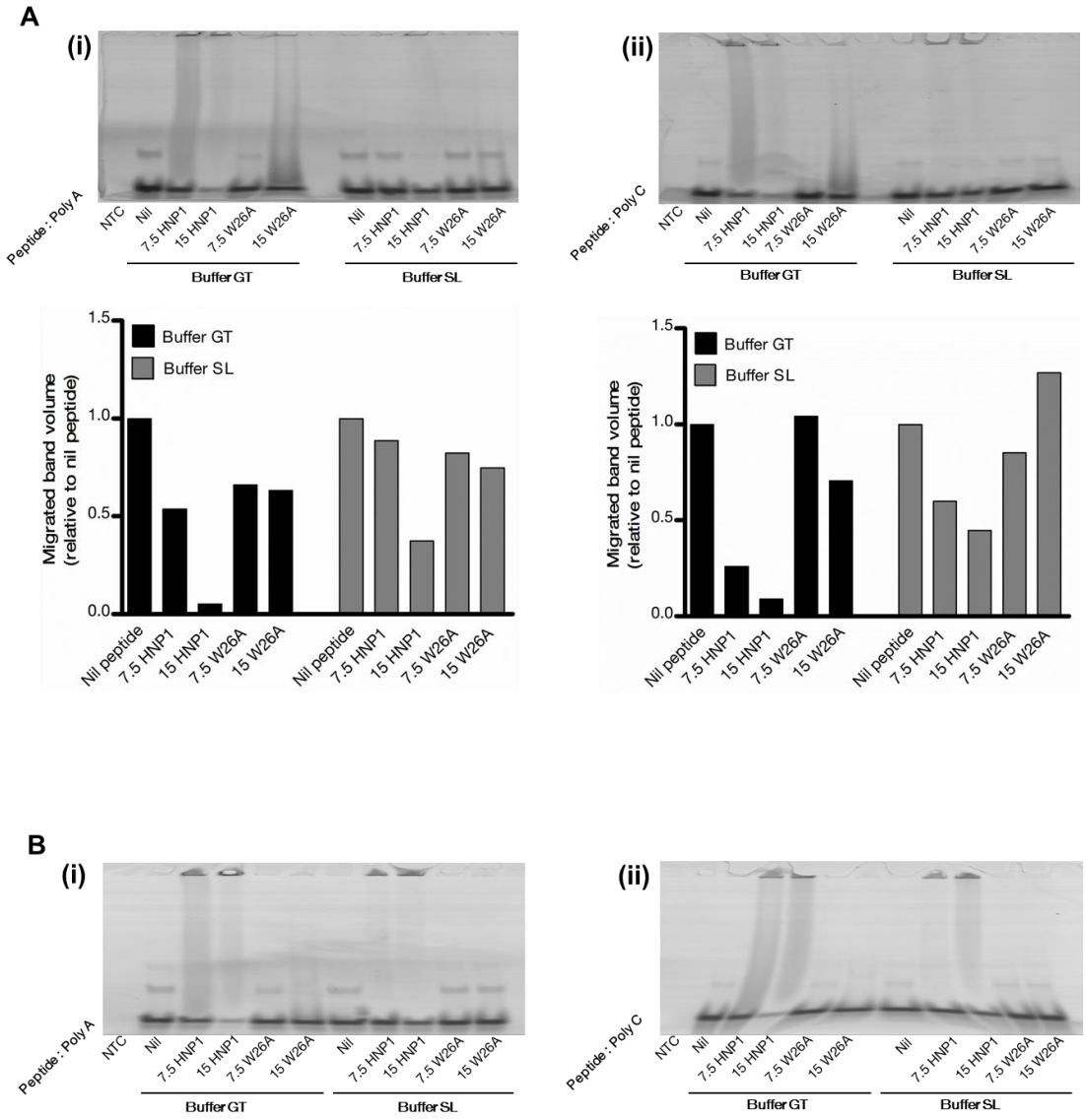

Figure 5.12: Comparative EMSA gels of differing binding buffer conditions containing $MgCl_2$

(**A**) Electrophoretic migration after Poly A (**i**) and Poly C (**ii**) incubation with HNP1 or W26A (pmol) in either buffer 'GT' or 'SL' containing 3mM $MgCl_2$. Migration of free oligonucleotide was compared to nil peptide control while a non-template control (NTC) was included. Resulting gel images were compared and migration of free oligo was semi-quantitated using Quant1 TL software analysis.

(**B**) Repeat experiment of (**A**) for visual comparison of electrophoretic migration of Poly A (**i**) and Poly C (**ii**).

5.2.3.2 HNP1 binds non-selectively to oligonucleotides in EMSAs

Following optimisation experiments, it was possible to employ a stoichiometric assessment of HNP1 binding Poly A, C and U, using equivalent molar ratios of HNP to oligonucleotide (Figure 5.13 – 15, respectively). It was also possible to determine if dimerization and hydrophobicity (altered in W26A) were critical to binding. In each experiment, the fixed amount of oligonucleotide (10pmol) was incubated with titrated molar equivalent ratios of HNP1 or W26A, using a two-fold serial dilution to result in a range of ratios: 28, 14, 7.5, 3.5, 1.25 and 0.875. In three repeats for each oligonucleotide, results showed a statistically significant decrease in the amount of unbound oligonucleotide with increasing ratios of HNP1 relative to W26A. In Poly A and C, significance is reached in HNP1-oligonucleotide ratio of 14:1 onwards. Interestingly, the amount of unbound Poly U compared to W26A is significantly attenuated at an HNP1-Poly U ratio of 7:1. This preliminary finding suggests a stronger interaction with the RNA nucleobase uracil, as half the amount of HNP1 is required to impede its migration compared to adenine and cytosine. By plotting a graph from the calculated fraction of unbound (migrated) oligonucleotide, the increased affinity of HNP1 for Poly U could be visualised to that of Poly A and C, which appear similar (Figure 5.16). Thus the hypothesis was concluded that HNP1 is able to bind to oligonucleotides sequences in a manner that suggests independence of sequence specificity, given that all nucleobases bound within a small stoichiometric range. An early indication suggests an increased binding affinity for uracil; however this increased affinity remains to be demonstrated in more complex binding systems in order to remain a valid observation (covered in the discussion).

What was clearly evident was the tendency of HNP1 to transition from having minimal association with oligonucleotide to forming complexes unable to apparently transition into the gel matrix within a very tight stoichiometric range. This is in contrast to conventional protein-RNA binding interactions which show a more sigmoidal binding pattern over several magnitudes of protein concentration[161]. This could be attributed to the role of dimerization to form complex oligomers once bound to oligonucleotides, which will be addressed in the discussion section. What was also noticed was that HNP1 at approximately 3.5μM (12.04μg/mL) began inhibiting Poly

U migration. This was in agreement with the inhibitory concentrations observed for TNF-α production as well as *in vitro* translation of reporter mRNAs, and begins to suggest a common threshold concentration required for this inhibitory mechanism.

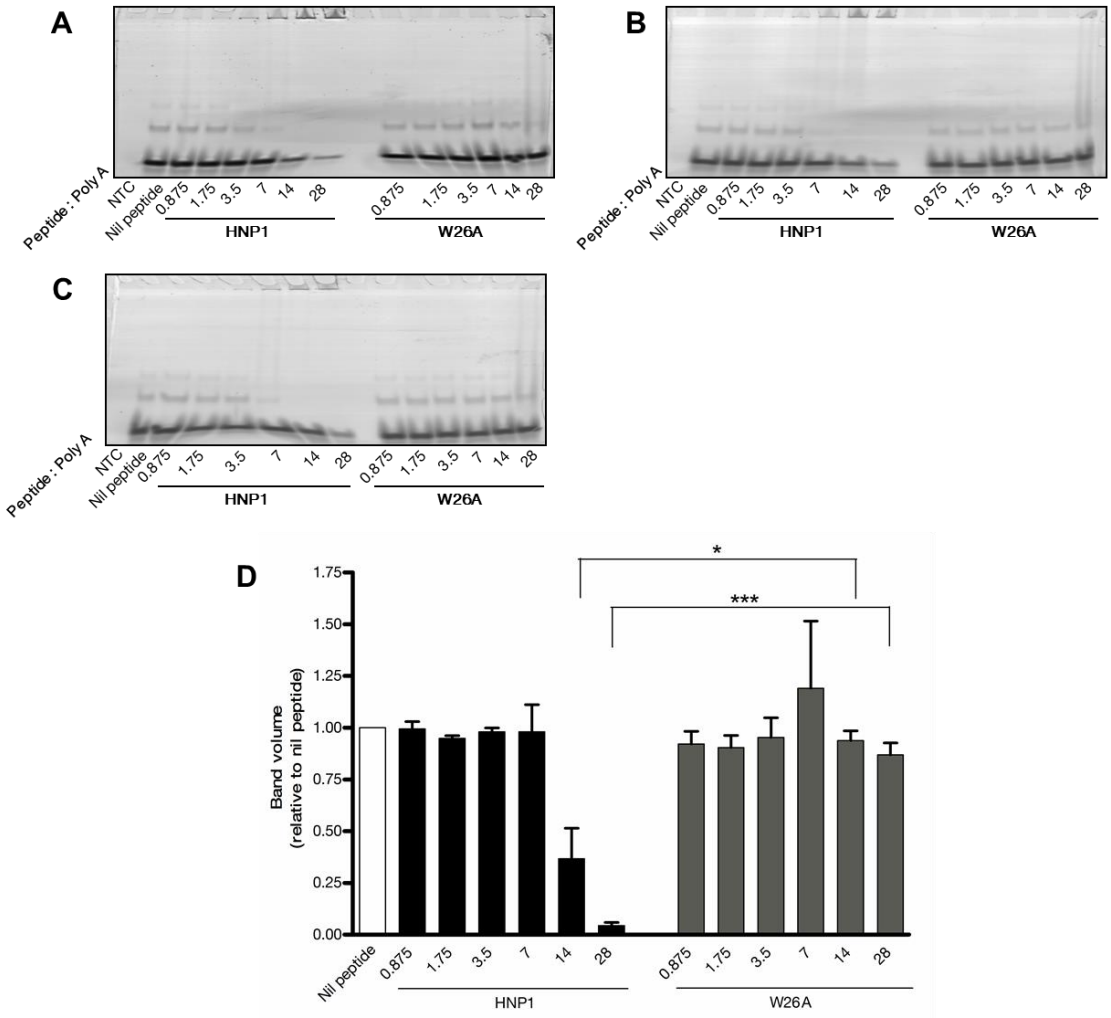

Figure 5.13: EMSA of Poly A following incubation with titrated HNP1 or W26A

Migration of Poly A (10 picomole) after incubation with increasing picomole ratios of HNP1 or W26A, resolved by non-denaturing electrophoresis. (**A** – **C**) EMSA gel images of Poly A compared to nil peptide control sample with NTC control included. (**D**) Semi-quantitation of unbound Poly A from n=3 experiments with error bars representing the mean ±SEM relative to untreated controls. ***P<0.001, * P<0.05 (Student's t-test).

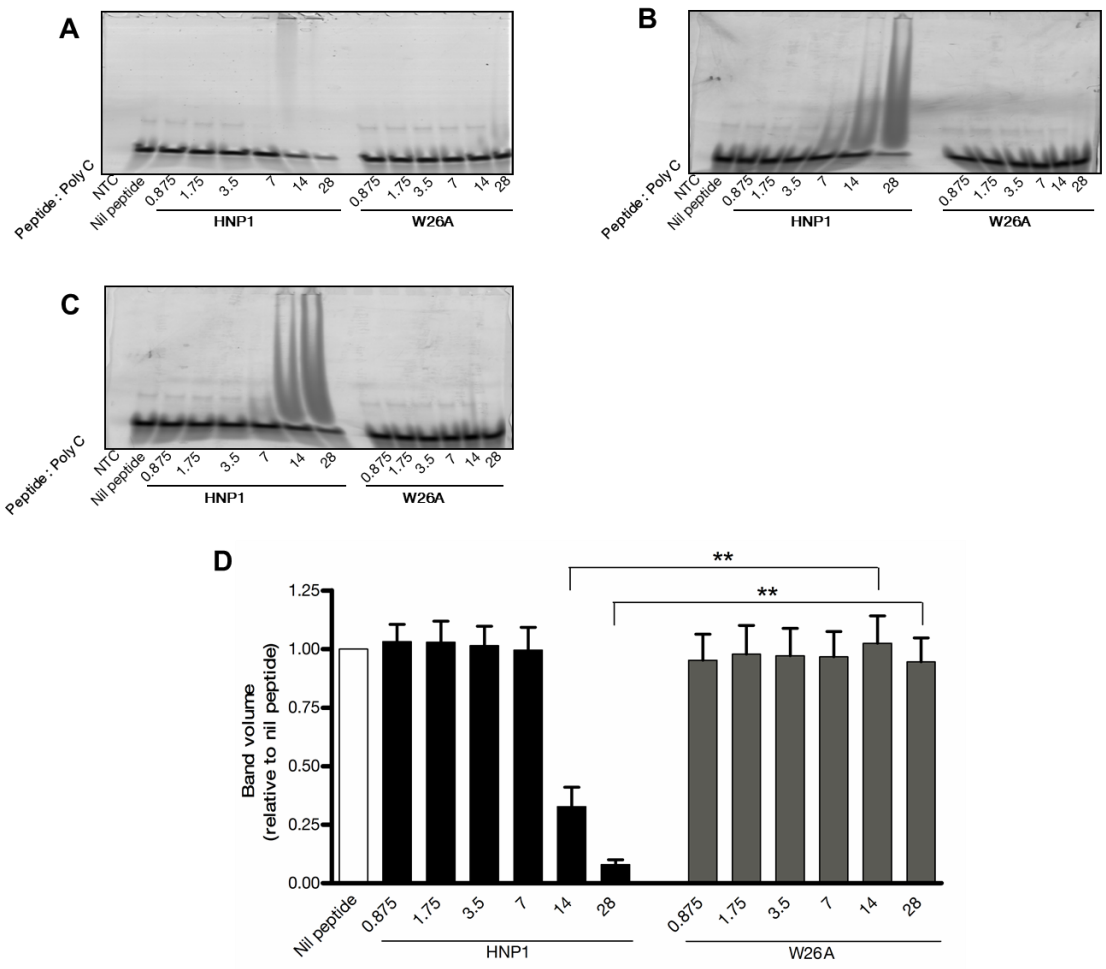

Figure 5.14: EMSA of Poly C following incubation with titrated HNP1 or W26A

Migration of Poly C (10pmol) after incubation with increasing pmol ratios of HNP1 or W26A, resolved by non-denaturing electrophoresis. (**A** – **C**) EMSA gel images of Poly C compared to nil peptide control sample with NTC control included. (**D**) Semi-quantitation of unbound Poly C from n=3 experiments with error bars representing the mean ±SEM relative to untreated controls. **P<0.01 (Student's t-test).

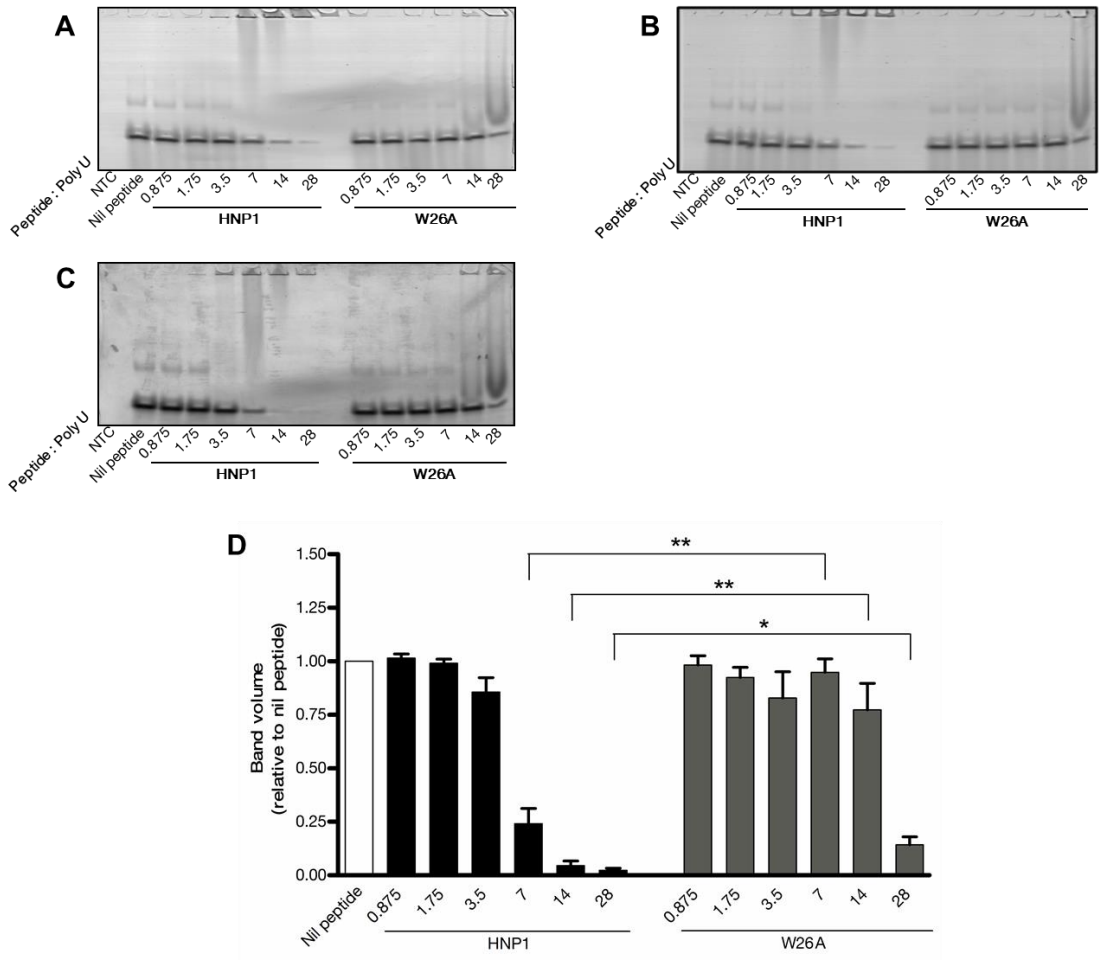

Figure 5.15: EMSA of Poly U following incubation with titrated HNP1 or W26A

Migration of Poly U (10pmol) after incubation with increasing pmol ratios of HNP1 or W26A resolved by non-denaturing electrophoresis. (**A** – **C**) EMSA gel images of Poly U compared to nil peptide control sample with NTC control included. (**D**) Semi-quantitation of unbound Poly U from n=3 experiments with error bars representing the mean ±SEM relative to untreated controls. **P<0.01, *P<0.05 (Student's t-test).

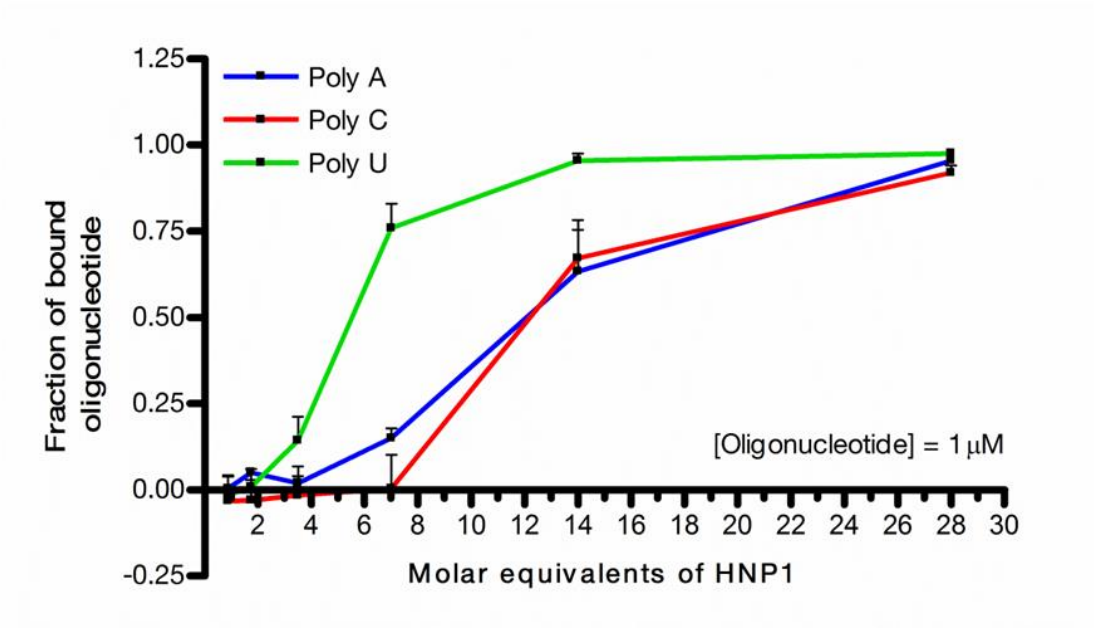

Figure 5.16: Stoichiometric interactions of HNP1 with Poly A, C, and U

Fractions of bound Poly A, C and U (y-axis) were calculated from quantitated unbound oligonucleotide and plotted against increasing molar equivalents of HNP1 (x-axis).

5.3 Discussion

The main rationale behind the experiments in this chapter was to begin investigating the molecular mechanisms behind the inhibitory observations of HNP1 on protein synthesis in HMDMs. This was in light of the fact that no apparent cellular stress event involved in translation regulation could account for the inhibition of protein synthesis observed. Studying the mechanistic actions of HNP1 in an *in vitro* translation system allowed for a more detailed understanding of the fundamental inhibitory mechanism. This system was useful as translation of reporter mRNAs with two very different modes of translation initiation could be assessed.

Using this system, it was evidently clear that HNP1 unambiguously inhibited cap-dependent translation and to a lesser extent cap-independent (IRES-mediated) translation. This suggests HNP1 was able to block the activity of fundamental translation components in some way which resulted in a loss of translation capability. Inhibition of cap-independent translation was an unexpected result, as protein expression of this translated mRNA is often relied upon as an internal reference control to normalise against experimental variations. Provided with this evidence of cap-independent translation inhibition, emerging suggestions are that HNP1 might impede the most fundamental of mRNA-ribosome associations required for translation initiation. This inhibitory action may be further hindered in cap-dependent translation initiation by the complexity of eIF4E binding to m7G and subsequent initiation factor recruitment which is required for assembly of the pre-translation initiation complex. This was suggested by the even greater reduction in luciferase protein compared to untreated controls. Going forward from this, the implication of HNP1-affected translation initiation could be elucidated; An *in vitro* translation experiment could be performed identical to the IC50 experiment comparing the inhibitory rates of translation inhibition between a cap-dependent and cap-independent reporter mRNA. This would require two identical reporter mRNAs, differing only in the addition of an m7G cap or non-physiological cap analogue. If the rate of translation inhibition is similar in the two reporters with titrated HNP1, this would imply that translation inhibition is likely to be due to other mechanisms not relating to translation initiation. Should the rate of translation inhibition differ,

this would provide evidence that the HNP1 inhibitory mechanism includes the impediment of translation initiation, contributing to the underlying inhibitory mechanism.

What is untested at this stage is if HNP1 affects translation at multiple stages, inhibiting not only initiation, but polypeptide chain elongation or termination. It was anticipated that analysis of polysome distribution could provide an answer to this question. For example a build-up of 43S/60S ribosome complex and lack of polysomes could imply inhibition at the point of translation initiation, while an accumulation of dense polysomes in latter fractions could imply stalled ribosomes unable to dissociate from mRNAs. Unfortunately after multiple optimisation attempts, a result from a single experiment showed no difference in polysome distribution with HNP1 treatment compared to controls at 4hrs. Without repeating the experiment in Figure 5.9, it is difficult to interpret the observation of decreased translation-inactive RNA material in HNP1-treated cells. The fact that a difference was observed provides justification into the continuation of these experiments, encompassing multiple time points over 24hrs to map the differences in ribosome distribution with HNP1. In addition to the analysis of polysome distribution, qPCR of a gene of interest such as the single attempt at quantitating TNF-α mRNA could provide further information into how HNP1 affects translation of such a key inflammatory mRNA.

The results from the EMSA experiments began to define the mechanistic actions of HNP1 from a biochemical perspective. EMSA assays have long been used as an analytical tool that serves as valuable control model in defining the binding interactions for any biological system. These introductory EMSA experiments set out to address if there was any sequence selectivity in HNP1 binding, assessed by comparing the stoichiometric interactions between the nucleobases that make up three quarters of RNA (adenine, cytosine and uracil). Through fixed amounts of an oligonucleotide sequence and titrating in molar-equivalent amounts of HNP1, these preliminary studies showed a sequence-independent binding affinity for Poly A, C and U, suggesting non-selective binding interactions with RNA. This shows that, in

principle, there is the propensity for HNP1 to bind to all RNA once inside a cell, whereas W26A would most likely not. This strongly suggests the importance of HNP1 hydrophobicity and dimerization potential to interact with RNA. What was noticed in these direct titration experiments (i.e. in non-competitive binding interactions) is that there was a significantly increased binding affinity for uridine in this system. This affinity was observed at a HNP1:Poly U ratio of approximately 3.5:1 compared with Poly A and C (approximately 7:1). Interpretation of this observation would infer that there may be an affiliation for uridine within RNA. However this increased affinity should be scrutinised further in order to confirm this observation. By assessing the HNP1-oligoncleotide binding in a competitive binding experiment, competitor RNA (unlabelled) could be titrated in with the labelled Poly U-HNP1 complex, and the efficiency of the competitor RNA to disrupt the complex can be determined by native gel electrophoresis. Plotting the fraction of bound (labelled) oligonucleotide could assess if the stronger interaction for uridine still remained valid compared with results performed with Poly A and Poly C.

Conventionally, analysis of protein-mediated 'shifts' of RNA within native gels make it theoretically possible to determine the protein-to-RNA stoichiometry by virtue of the degree of shift within the gel[161]. This implies that one is able to assess whether proteins bind to RNA in a homodimer (2:1) complex, or 3:1, or 4:1 etc. While HNP1 binding with oligonucleotide was observed at a peptide:oligo ratio of 3.5:1 in Poly U, the apparent accumulation of labelled oligonucleotide at the top of the loading well as opposed to a conventional shift pattern suggests that a large, multimeric complex formation is the general binding characteristic of HNP1. Using examples as defined by Ryder *et al.* (2008)[161], protein-RNA binding interactions are normally gradual spanning over at least two orders of magnitude (100 fold) between the binding minimum (unbound RNA) and maximum (completely bound RNA). From this rule-of-thumb, it is evident that the binding property of HNP1 was quite unusual and very rapid once binding was initiated. This was apparent in Figure 5.16 as the fraction of completely unbound Poly U became almost completely bound to HNP1 within an approximate 7 fold increase in HNP1 concentration.

Collectively these results support the newly established hypothesis that the inhibitory actions HNP1 could be attributed to a structurally complex binding with RNA-containing components involved in protein synthesis, such as ribosomal RNA or mRNA. It is suggestive in these initial EMSA experiments that, if an RNA binding event is indeed implicated in the inhibitory mechanistic action of HNP1, the magnitude and rapid complexity of binding would surely be detrimental to cellular functions, most notably protein synthesis.

Chapter 6

6 α-defensin interactions with ribosomes

6.1 Introduction

Electrophoretic mobility shift assays in Chapter 5 demonstrated the strong association of HNP1 for oligonucleotide sequences of adenine, cytosine and uracil. In conjunction with the inhibitory observations on *de novo* protein synthesis in HMDMs and within *in vitro* translation systems, the hypothesis was formulated that the HNP1 inhibitory mechanism on translation could be mediated by binding to, and interference with, nucleic acids within translation machinery. This hypothesis could infer that upon entry into cells, HNP1 could migrate to areas of active translation and bind to rRNA, preventing ribosome complex formation with mRNAs. The hypothesis could also include the potential to bind to mRNA itself, possibly impeding shuttling to the ribosomes and attachment to eukaryotic initiation factors and 43S pre-initiation complexes. In addition, binding activity may well impede tRNA delivery of amino acids to ribosomes. The implications of this hypothesis are potentially considerable to the cell's translation capabilities and could establish a new therapeutic target for inflammation regulation. If binding under physiological conditions replicates the binding affinity observed in representative analytical methods such as EMSAs, the potential effects on cell function could be far-reaching.

Thus, the final set of results in this thesis expands on the binding interactions of HNP1 with nucleic acids. It would seem reasonable to suggest that ribosomes could be one of the main targets of HNP1 within a cell given the size, abundance and RNA composition. Eukaryotic ribosomes are very large macromolecules situated within the cytoplasm, with approximately $10^6 – 10^7$ units per cell and a molar mass of about 4.3 million Daltons, of which ~60% is attributed to rRNA content[164,165]. As briefly touched on in the previous chapter, ribosomes are comprised of two subunits: The large 60S subunit which consists of three rRNA molecules (28S, 5.8S, and 5S) together with 46 proteins, while the 40S subunit includes one 18S rRNA chain and about 33 proteins.

Thus with this background knowledge into ribosomes together with the newly discovered properties of HNP1, the focus of research going forward was to determine whether ribosomes were a potential target for HNP1 binding. Since the EMSA data using oligonucleotides provided good evidence for RNA binding, it was extended using total HMDM RNA to assess whether 28S and 18S rRNA shifts could be observed. Furthermore, immunofluorescence experiments were performed identifying the location of HNP1 within HMDMs in relation to ribosomes. If this emerging data agreed with the growing body of evidence provided in previous chapters, it could further substantiate the hypothesis that HNP1-mediated translation inhibition could include the binding of peptides to RNA.

6.2 Results

6.2.1 HNP1 causes an electrophoretic shift in HMDM rRNA

Building on the EMSA results from Chapter 5, the binding affinity of HNP1 for nucleic acids was tested on total RNA extracted from HMDMs. This method was derived from assays described in two previous publications, which linked the binding of antimicrobial peptides to nucleic acids as the proposed target for bacterial killing[124,155]. The methodology involved incubating 1μg of RNA with titrated amounts of HNP1, LHNP1 and W26A added into binding buffer 'GT', adapted from Park *et al.* (1998)[124]. Details on the method are described in Chapter 2, section 2.11. After 1hr incubation, samples were electrophoresed by non-denaturing gel electrophoresis. The visible shifting effects between HNP1 and LHNP1 on 28S and 18S rRNA were compared from the resulting gel image obtained (Figure 6.1*i*). The influence on 18S rRNA migration was observed by its impaired migration (or shift) relative to the untreated control migration front with each increasing HNP1, represented by the horizontal dashed line across the gel image. This visually apparent shift suggested that minimal HNP1 in ratio with RNA was required in order to induce a shift, beginning at an HNP1:RNA ratio of 0.2:1 (200ng:1μg). It was also suggested that the shift steadily increased with added ratios of HNP1. In contrast, no distinct shift in migrated 18S rRNA was noticeable in LHNP1 treated samples. In addition to a shift, HNP1 treatment also resulted in a gradual reduction on the band intensity of 18S rRNA from a peptide/RNA ratio of 0.1 onwards, culminating in an approximate 25% loss of unbound, migrated 18S rRNA at a ratio of 1:1, confirmed by semi-quantitative band analysis (Figure 6.1*ii*). In contrast, the band intensity of unbound, migrated 18S rRNA with LHNP1 treatment remained above 90% compared to untreated controls. This affinity of HNP1 for RNA was comparable to two antimicrobial peptides known to bind RNA tightly; both bovine neutrophil-derived Indolicidin[155] and Buforin II, a derived form of Buforin I obtained from stomachs of Asian toads[124], also elicited a shift at peptide/RNA 0.2. In contrast Magainin 2, a membrane-active antimicrobial peptide obtained from frog skin showed binding affinity for RNA at a much higher petide/RNA ratio of 5:1[124].

While the shift on 18S rRNA was clearly evident, effects of HNP1 on 28S rRNA were more subtle. Shifts in 28S rRNA migration were visibly apparent compared to untreated controls with minor changes to semi-quantitated band intensities (Figure 6.1-*iii*). In comparison, LHNP1 had no effect on 28S rRNA in both the migration of and band intensities quantitated. The reason for the reduced shift of 28S rRNA could be explained by the fact that 28S rRNA is almost three times the length of 18S rRNA (5025nt and 1869nt, respectively)[166,167]. Thus the impact of the added weight of bound HNP1 is suggested to be almost negligible when assessing the migration of 28S rRNA given its size.

In light of this, a slight modification was made to these experiments in an attempt to create a more substantial shift in 28S and 18S rRNA with bound HNP1. In this process, peptide/RNA incubations were followed by a further 30min incubation with 1ng/μL monoclonal mouse anti-HNP1-3 antibody prior to electrophoresis (termed a supershift EMSA). The proposed idea was that the migration of rRNA, which was bound to HNP1, would be further retarded with HNP1 subsequently linked to an immunoglobulin G with an approximate monomeric weight of 150kDa. Initial experiments using the supershift EMSA were performed for HMDM RNA with titrated HNP1 and LHNP1 (Figure 6.2*A*). Although antibody addition did not lead to increased band shifts, it did result in greater reductions of unbound 18S rRNA at the migration front compared to the untreated sample (which also contained antibody). This was suggested by semi-quantitation of the unbound 18S rRNA, which showed an approximate 70% reduction at a peptide/RNA ratio of 1:1 (Figure 6.2*A*-*ii*). Migration of 18S rRNA in the presence of LHNP1 closely resembled that of the untreated control sample although band semi-quantitation did show a moderate reduction with increasing LHNP1 amounts, albeit over half as inhibitory compared to HNP1.

A peculiarity occurred in the 28S rRNA band expression with HNP1 treatment in the form of uneven band distribution across the width of the lane. This made it difficult to accurately ascertain the true migration difference in this experiment. It also meant that 28S rRNA band semi-quantitation was skewed somewhat with HNP1 treatment, showing a slight reduction in band density compared to LHNP1 and untreated

controls (Figure 6.2*A*-*iii*). In a validation experiment of the anti-HNP1-3 affinity to both HNP1 and LHNP1, Western blot analysis confirmed specificity for the wild type peptide but not LHNP1 (Figure 6.2*B*). This created a bias in shift with HNP1 over LHNP1, meaning that comparisons between the two in a supershift assay could not be made.

Supershift assays were then employed to compare the inhibitory effects of HNP1 with structurally similar W26A, confirmed by NMR spectroscopy[58], and since shift comparisons between the two peptide forms were performed using oligonucleotide sequences (Figure 6.3). The use of W26A in these supershift assays was validated since mouse anti-HNP1-3 antibody was able to detect the mutant form as confirmed by Western blotting (Figure 6.2.3*C*). In two independent RNA shift experiments comparing HNP1 and W26A at ratios 0.2 and 0.4, gel images showed clear shifts in 28S rRNA with HNP1 not observed with W26A (Figure 6.3*A*). Combined semi-quantitative analysis of the migrated 28S rRNA bands from both runs showed contrasting results as to whether HNP1 decreased the amount of unbound RNA (Figure 6.3*B*-*i*). Despite this, both experiments did suggest positive HNP1 binding to 28S rRNA as was evident by a visual shift in migration, an effect which was not observed in W26A-treated 28S rRNA.
Comparing the effects on 18S rRNA, HNP1 caused shifts in migrated bands as well as an approximate 50% decrease in the amount of unbound RNA at a ratio of 0.4 (Figure 6.3*B*-*ii*). This was in contrast to W26A which showed no visible shift with a slight reduction in unbound rRNA compared to untreated controls.

One final assessment of HNP1 binding interactions with RNA using EMSAs addressed the effects on mRNA. Using mRNA previously utilized during *in vitro* translation assays, Luc-A0 and CSFV-Gal mRNA were individually incubated with HNP1 or W26A at peptide/RNA ratios of 0.2 and 0.4 in a supershift EMSA (Figure 6.4). At both ratios tested HNP1 was clearly able to shift both forms of mRNA, indicating strong binding interactions that were not observed with W26A. On the basis of this finding, it showed that HNP1 was able to bind to all RNA forms tested so far using EMSAs. Together with the EMSA experiments on oligonucleotides

(Chapter 5), it added further evidence that supported the hypothesis of HNP1 binding to RNA as a mechanism of translation inhibition. Currently untested was the binding potential of HNP1 in a cellular environment, on ribonucleoproteins (RNPs) such as ribosomes or mRNA (mRNPs), which are assembled immediately after transcription[168].

Overall the EMSA results in this Chapter present a less rigorous assessment of HNP1 binding interactions to rRNA compared to that of Chapter 5, but still show a superior binding potential over both LHNP1 and W26A. These experiments formed the preliminary assays which helped establish the hypothesis of HNP1 interactions with RNA-containing translation machinery. In order to further this hypothesis, it was important to find supportive evidence in cell-based assays, starting off by identifying the interactions of HNP1 with ribosomes.

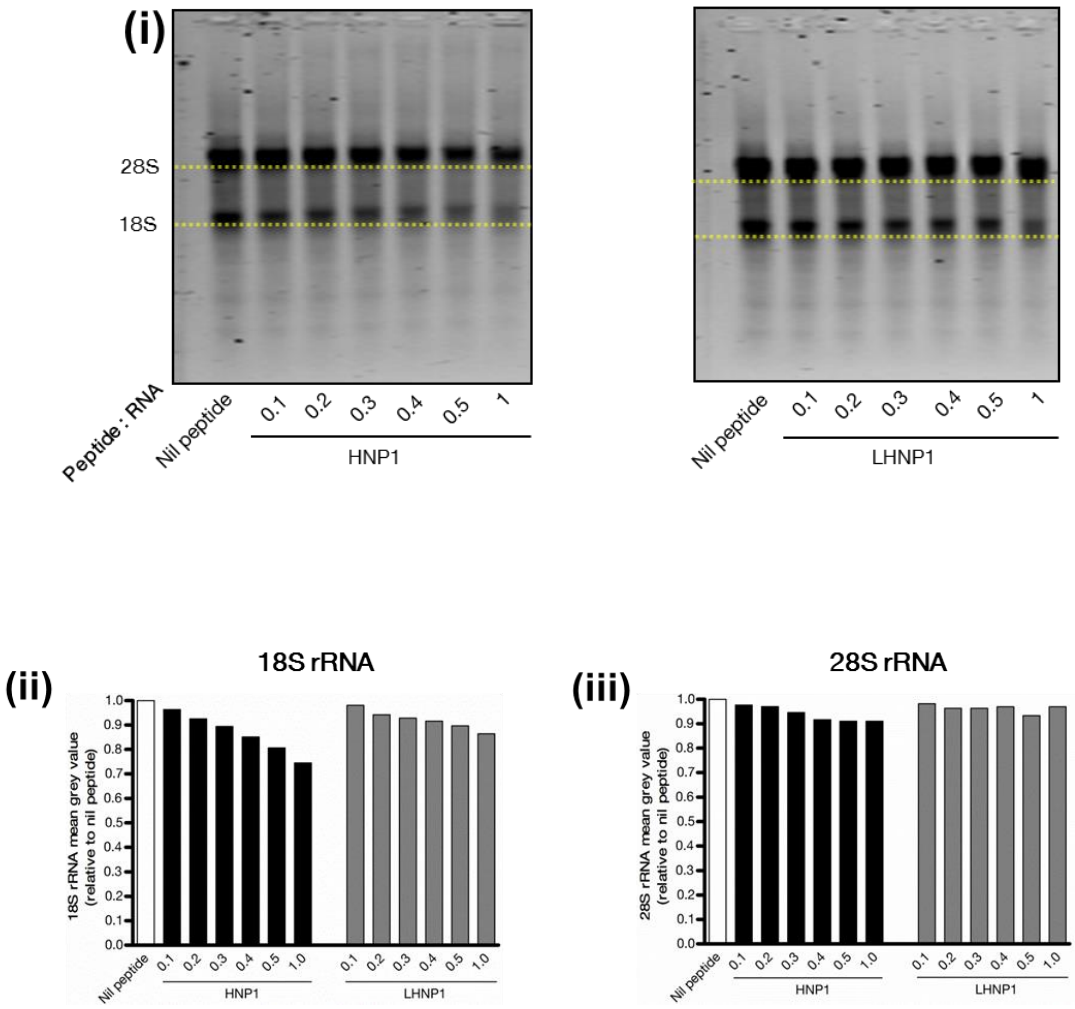

Figure 6.1: Electrophoretic Mobility Shift Assay (EMSA) of HMDM RNA in the presence of HNP1 and LHNP1

Non-denaturing agarose gel electrophoresis of migrated HMDM RNA (1µg) with increasing HNP1 or LHNP1 ratios (in µg) between 0.1 and 1.

(**i**) Gel images of migrated RNA with peptide ratios between 0.1 and 1. Horizontal dotted lines (yellow) represent the migration front of 28S and 18S rRNA of nil peptide control for shift comparisons with peptide inclusion. Mean grey values of migrated 18S (**ii**) and 28S (**iii**) rRNA bands normalised to nil peptide control (white bar). Results are of a single experiment performed.

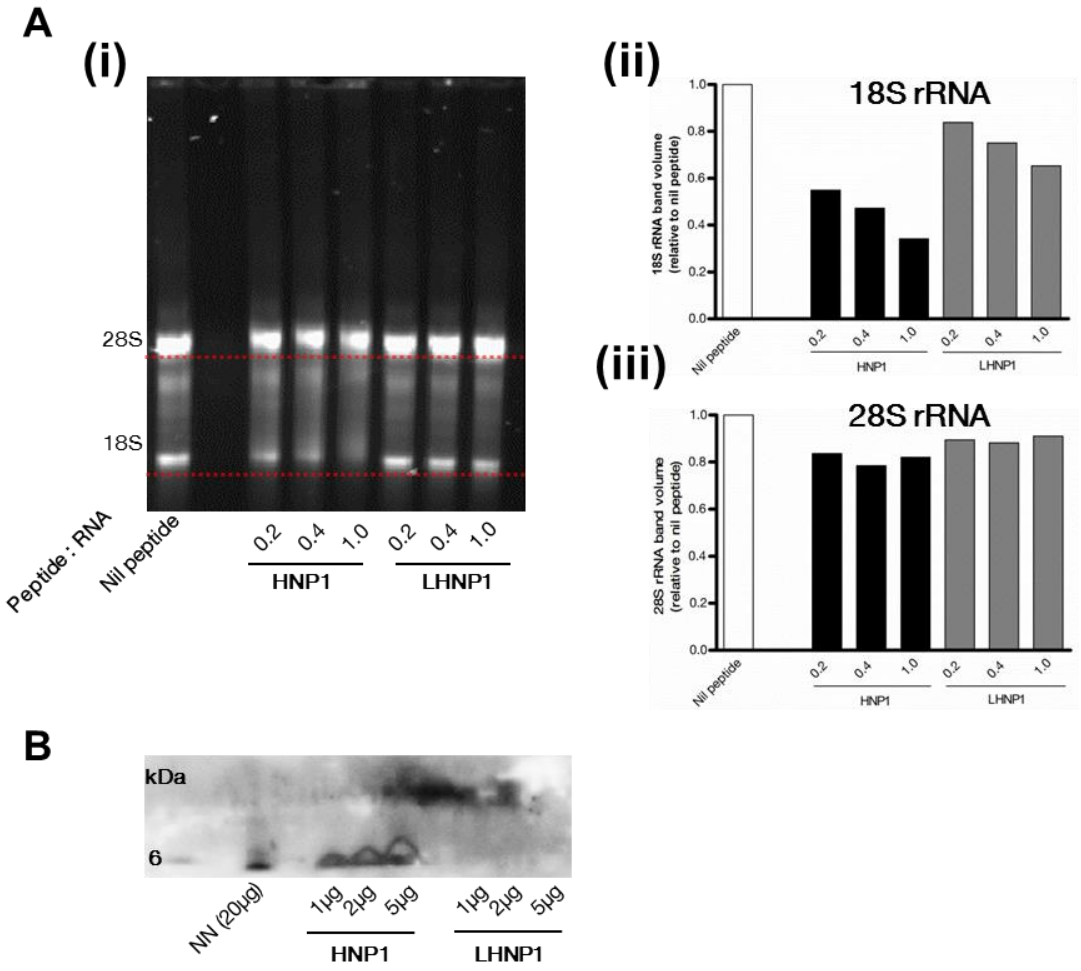

Figure 6.2: The migration of HMDM RNA following HNP1 and LHNP1 incubation in a supershift EMSA

(**A**) The electrophoretic migration of HMDM RNA following incubation with titrated HNP1 or LHNP1. Monoclonal mouse anti-HNP1-3 antibody was added to all samples 30min prior to electrophoresis in 1% non-denaturing agarose (**i**). Semi-quantitation of migrated 18S (**ii**) and 28S (**iii**) rRNA relative to nil peptide control sample (n=1). Horizontal dotted lines (red) represent the migration front of 28S and 18S rRNA of nil peptide control for shift comparisons with peptide inclusion. (**B**) Antibody detection of HNP1 as well as HNP1-3 within 20µg of necrotic neutrophil protein ('NN') by Western blotting. The antibody used was unable to detect the presence of LHNP1.

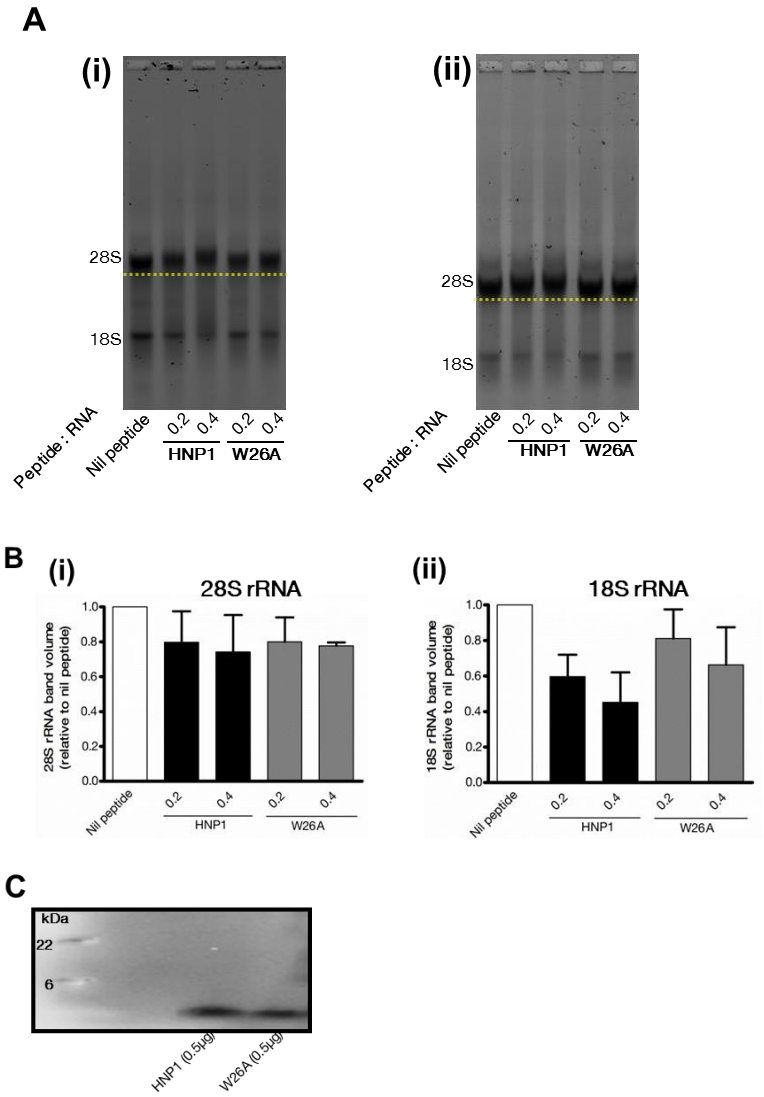

Figure 6.3: The migration of HMDM RNA following HNP1 and W26A incubation in a supershift EMSA

(**A**) Two independent EMSA experiments (**i** and **ii**) of HMDM RNA migration following incubation with titrated HNP1 or W26A. Monoclonal anti-HNP1-3 antibody was added to samples 30min prior to 1% non-denaturing agarose gel electrophoresis. Horizontal dotted lines (yellow) represent the migration front of 28S rRNA of nil peptide control for shift comparisons with peptide inclusion. (**B**) Semi-quantitation of migrated 28S (**i**) and 18S rRNA (**ii**) relative to nil peptide control sample with error bars representing the mean ± SD of band volumes (n=2). (**C**) Immunoblotting of HNP1 and W26A using a monoclonal mouse anti-HNP1-3 antibody.

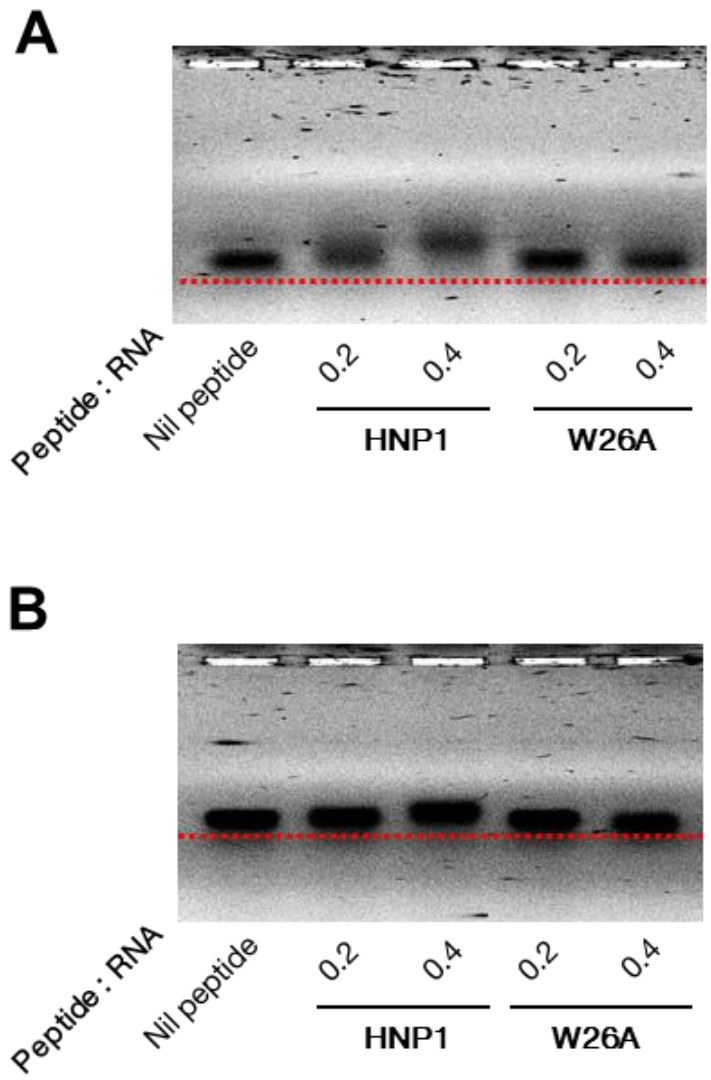

Figure 6.4: Supershift EMSA of mRNA with HNP1 and W26A treatment

Electrophoretic migration of 1µg Luc-Ao (**A**) and CSFV-Gal (**B**) mRNA incubated with titrated µg amounts of HNP1 and W26A. Monoclonal anti-HNP1-3 antibody was added to all samples 30min prior to electrophoresis in 1% non-denaturing agarose (n=1).

6.2.2 HNP1 association with ribosome proteins

With binding assays demonstrating the affinity of HNP1 to bind to RNA, the research progressed to provide supporting evidence of this effect in HMDMs *in vitro*. The most insightful assay to take the research forward was determined to be the localisation of HNP1 relative to ribosomes using immunocytochemistry by confocal microscopy. Using the monoclonal mouse anti-HNP1-3 antibody used for Western blotting in the previous section, HMDMs were stained for HNP1 after 4hr and 24hr treatments following incubation with either 12.5μg/mL or 25μg/mL HNP1 or W26A. Simultaneously, ribosomal protein S20 (rps20), which forms part of the 40S subunit, was detected using rabbit polyclonal anti-rps20 antibody. Details on the methodology are listed in Chapter 2, section 2.8. Using highly cross adsorbed Alexa Fluor secondary antibodies against mouse (HNP1) and rabbit (rps20), images of staining were obtained for HMDMs at 4hrs (Figure 6.5) and 24hrs (Figure 6.6) following treatment.

Rps20 staining was characteristically condensed around the perinuclear region, forming a 'halo'-like pattern around the DAPI-stained nucleus for reference and indicative of ribosomes associated with endoplasmic reticulum (rough ER). Results at 4hrs show that HNP1 was abundantly present within cells. Typically, HNP1 displayed a characteristic condensed accumulation in and around the perinuclear region. F-actin filament staining of the whole the cell using Phalloidin confirmed this condensed HNP1 accumulation around the perinuclear region (Figure 6.6*B*). Supposed co-localisation of HNP1 and rps20 was indicated by the green HNP1 staining and red rps20 staining merging to form yellow in the images. There existed patterns of minimal yellow staining, forming a halo-like association surrounding the nucleus (indicated by purple arrows). This staining could suggest that there may be evidence of HNP1 accumulation within regions of active translation. However, the patterns of overlap are minimal in comparison to the overall expression of HNP1 relative to rps20, and remains uncertain at present as to whether this is genuine co-localisation or areas of random signal overlap. There was weak evidence of areas of condensed, yellow staining (indicated by yellow arrows). It is currently uncertain if this suggested areas of bound ribosomes with HNP1. This was exampled in Figure

6.5*A* (third row). In this example there is an indication of a HNP1/rps20 association that is found on the periphery of the perinuclear region. This might well be an early indication of possible HNP1/rps20 aggregate formation caused by HNP1/rRNA binding. It is unclear at present as to the reason for this apparent dissociation away from the immediate perinuclear region, but initial interpretation is that perhaps these complexes were destined for cell-mediated clearance in an attempt to rid the cell of defective ribosomes bound by HNP1. The data, however, remains unconvincing and would require substantial further investigations to confirm or deny the preliminary findings.

Further observations for HNP1/rps20 co-localisation were performed at 24hrs incubation with HNP1 (Figure 6.6). Weak HNP1/rps20 associations were indicated by yellow arrows away from the immediate perinuclear region. Purple arrows indicated that there still existed areas of HNP1 surrounding the perinuclear region, which was also observed for cells treated with W26A. While W26A staining showed the peptide's capability to accumulate similar to that of HNP1, no evidence of condensed W26A/rps20 accumulation away from the perinuclear region existed at 24hrs.

Furthermore, an attempt was made to obtain quantitative analysis on the degree of co-localisation of HNP1/rps20 compared to that of W26A. Normally in immunofluorescence where co-localisation exists, it is possible to statistically assess the linearity or correlation between the two stains by quantitating the amount of overlapping pixels relative to pixels where no overlap exists. This method of analysis, known as the Pearson's correlation coefficient, calculates correlation relationships ranging from a high degree of correlation (value of around 1) to having low or no correlation (value around 0), as detailed in Chapter 2, section 2.8.1.2. Using image analysis software (ImageJ), the Pearson's correlation was performed in ten random field samples for both HNP1 and W26A treated HMDMs at 4hrs and 24hrs (Figure 6.7). Analysis using this method found low correlation values between HNP1 as well as W26A staining relative to rps20, with no statistical significant between the two peptides. This correlation data suggests that there is weak

correlation between HNP1 and W26A relative to rps20, visually evidential using observations of the staining patterns. Thus, if there were areas of subtle co-localisation (if any), this quantitative method of analysis would be too insensitive to detect subtle peptide/rps20 association. This is due to the widespread peptide dispersion throughout the cell.

Concerning the hypothesis of HNP1 binding to nucleic acids, EMSA results from Chapter 5 demonstrated that HNP1 bound to oligonucleotides consisting of uracil sequences as well as the DNA-containing adenine and cytosine oligonucleotides. This would imply that it is hypothetically possible for HNP1 to bind to DNA within cells. In all images of HNP1 staining within HMDMs, no evidence suggested that HNP1 accumulated within the nucleus and bound to DNA. In fact in the majority of images, HNP1 staining was minimal in the areas of DAPI-stained nuclei. Studies measuring the sizes of nuclear pore complex (NPC) were shown to be phylogenetically conserved at ~45Å (4.5nm)[169], and demonstrated that macromolecules under 40kDa are able to passively diffuse into the nucleus[170]. Thus diffusion of the ~5kDa HNP though the NPC within HMDMs was theoretically plausible if unhindered by interactions with other organelles. In addition, the Triton X-100 detergent used in this assay to permeabilize cellular membranes was previously shown to permit the diffusion of anti-DNA immunoglobulins (IgG) binding to DNA in HeLa cells[171], suggesting that it was possible to immunostain for HNP1 if it were present in the nucleus. In light of this information, this could indicate that HNP1 migrates no further than the endoplasmic reticulum surrounding the nucleus, and as result is more likely to interfere with translation machinery containing RNA and less likely to bind to DNA and prevent transcription. This is supported by the evidence in Chapter 3 that initial gene upregulation of TNF-α mRNA appears unaffected, even in HMDMs pretreated with α-defensins 1hr and 24hrs prior to stimulation.

The confocal data gave a weak initial suggestion of HNP1/rps20 aggregate formation in HMDMs, particularly after 24hrs treatment. This result suggested an indication and did not conclusively prove HNP1 binding to ribosomes. With limited time

restrictions on the remaining research period, considerations turned to performing validation experiments in order to provide greater evidence of a confirmed binding event. Two approaches were taken to address this question: immunoprecipitation of the complex and secondly sucrose density ultracentrifugation to isolate ribosomes in an attempt to detect HNP1 by Western Blotting. Both assays were unable to successfully contribute towards the hypothesis, the details of which can be found in Appendix C.

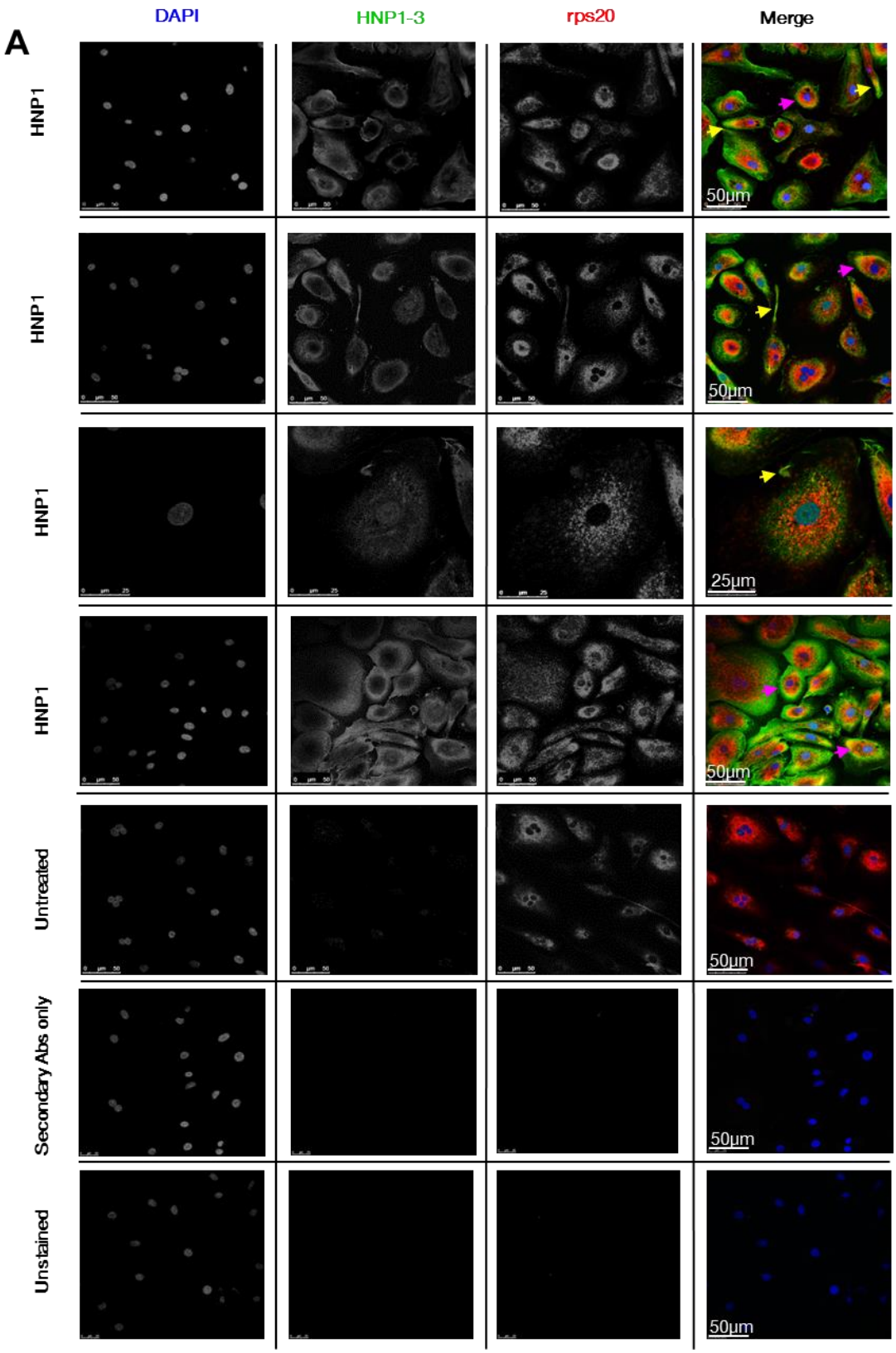

Figure 6.5: HNP1 and rps20 immunostaining in HMDMs (4hrs)

(Continued overleaf)

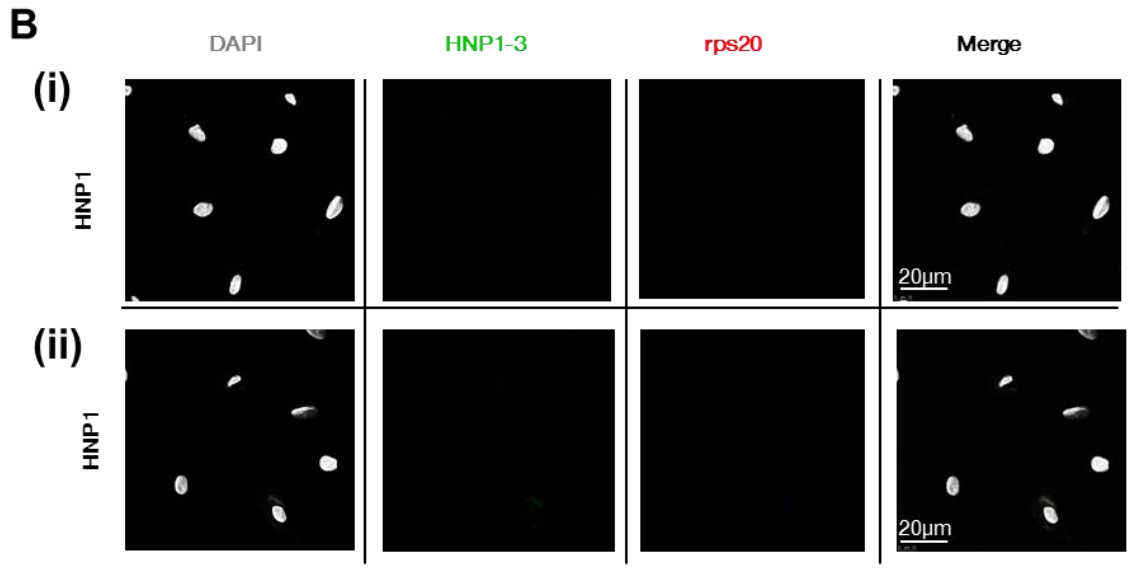

Figure 6.5 (continued)

(**A**) Confocal microscopy images of HMDMs immunostained for DAPI, HNP1-3 and rps20 (in columns). Results are of HMDMs treated with 12.5µg/mL HNP1 for 4hrs along with untreated cells (n=3). Treatments are labelled left of the images in rows. Yellow and purple arrows indicate areas of suggested co-localisation with yellow arrows indicating suggested areas of aggregate formation. Controls were included for: HNP1-3 staining in untreated cells, non-specific fluorescence of both secondary antibodies in cells not stained with primary antibodies, and non-specific autofluorescence in unstained cells (with DAPI).

(B) In the dual-antibody incubation system employed, an added validation control was included in HNP1-treated HMDMs for both secondary antibodies to control for specific binding to primary antibody targets (n=1). (**i**) Cells incubated with monoclonal mouse anti-HNP1-3 primary antibody followed by incubation with goat anti-rabbit Alexa Fluor 647 secondary antibody. (**ii**) Cells incubated with polyclonal rabbit anti-rps20 primary antibody followed by incubation with goat anti-mouse Alexa Fluor 488 secondary antibody.

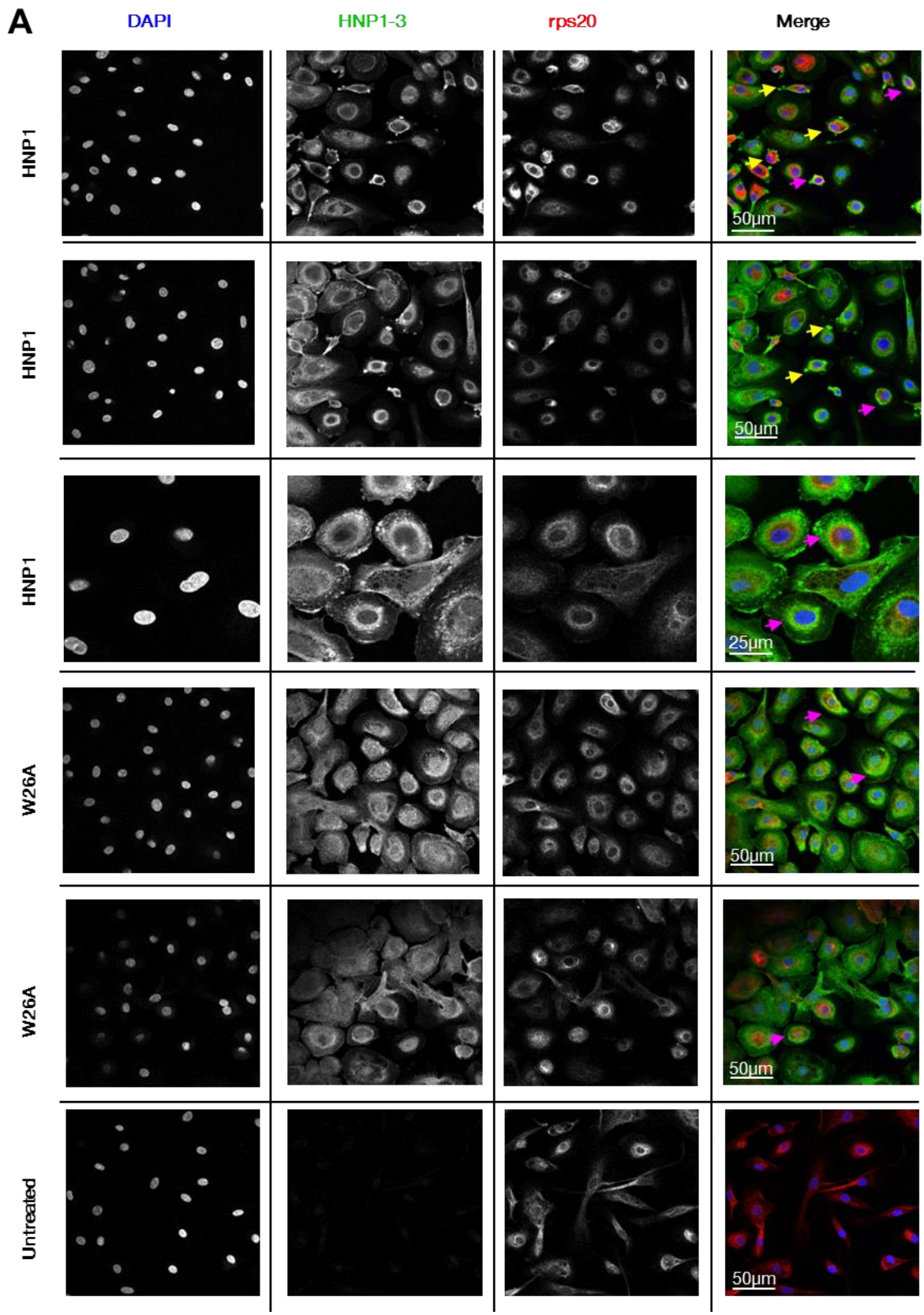

Figure 6.6: HNP1 and rps20 immunostaining in HMDMs (24hrs)

(Continued overleaf)

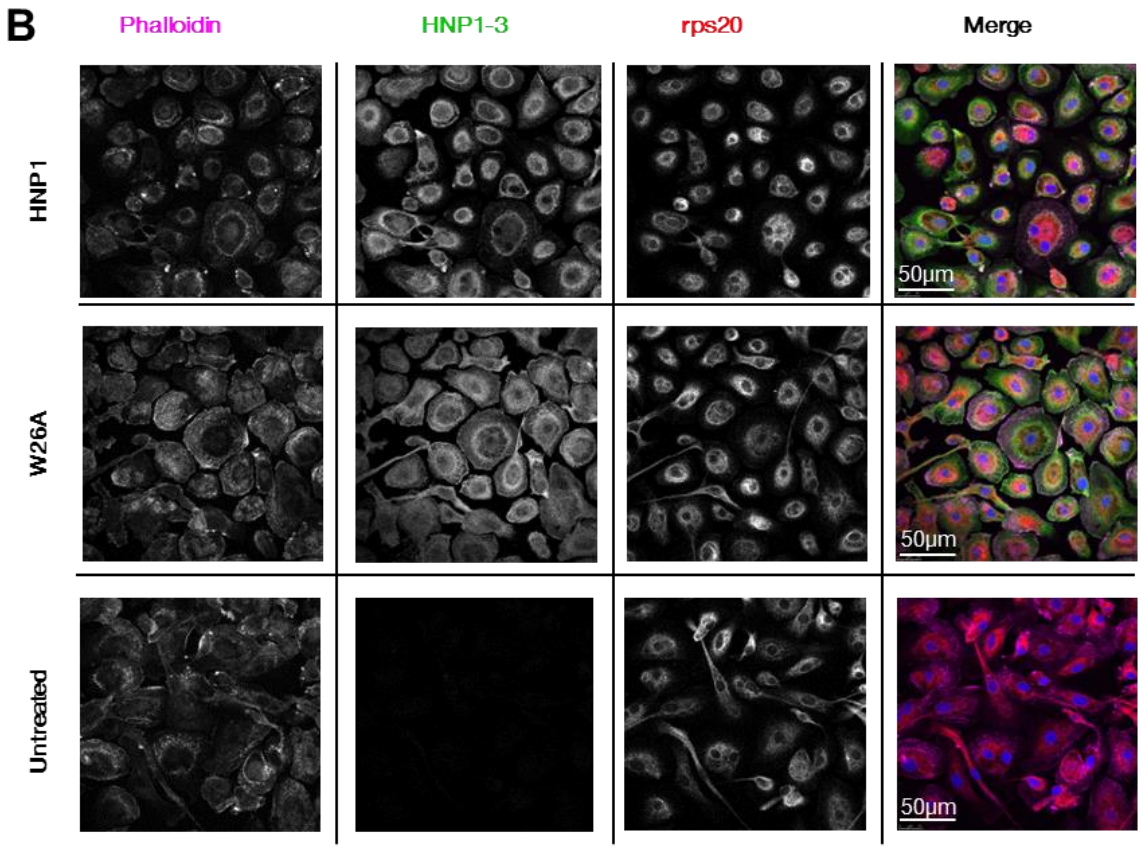

Figure 6.6 (continued)

(**A**) Confocal microscopy images of HMDMs immunostained for DAPI, HNP1-3 and rps20. Results are of HMDMs treated with 25µg/mL HNP1 or W26A for 24hrs alongside untreated controls (n=2). Yellow and purple arrows indicate areas of suggested co-localisation with yellow indicating possible areas of aggregates formation.

(**B**) F-actin staining in HMDMs using rhodamine phalloidin alongside HNP1-3 and rps20 immunostaining (n=1).

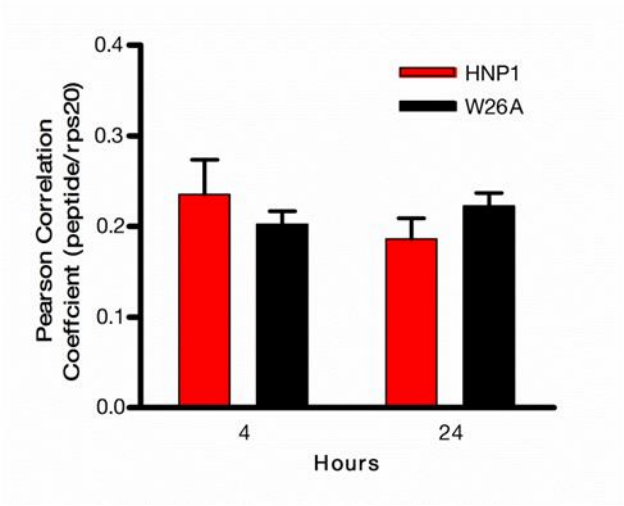

Figure 6.7: Quantitative image analysis of HNP1 and rps20 in HMDMs

Pearson correlation coefficient calculated from confocal microscopy images of HNP1 or W26A co-localisation to rsp20 in HMDMs treated with 12.5µg/mL peptide. Correlation was calculated from images obtained from 4hr and 24hr treatments. Results are of the mean ± SD from a single experiment, with a student's t-test statistical analysis performed for each time point showing no significant differences.

6.2.3 Assessing the fate of HNP1-associated ribosomes

Although weakly identified to date, the decision was to pursue with the suggestion of HNP1/ribosomes associations within the cytoplasm. These complexes tended to be located on periphery of the immediate condensed regions of ribosome expression, suggesting complexes that were possibly being removed from the immediate rps20-rich area. The fate of these complexes was questioned and whether they were either being degraded within the cell or even possibly destined for extrusion. By determining a possible loss of functioning ribosomes, this could be contributing to the decrease in translation rates due to less numbers of functioning ribosomes available. The possibility of a degradation of the rps20-containing complex was addressed, examining the most common form of macromolecule degradation within a cell, autophagy.

6.2.3.1 Autophagy-mediated ribosome clearance was undetermined in HNP1 treated HMDMs

As introduced in Chapter 1, expression of microtubule-associated protein light chain 3, homolog B (LC3B) is one of the most common parameters measured for autophagy induction in mammalian cells. LC3B induction is routinely qualitatively assessed by immunofluorescence, characterised by distinct puncta within the cytoplasm. Alternatively LC3B-I to –II conversion is analysed by Western blotting, with autophagy induction characterised by the increased expression of the ~14kDa LC3B-II relative to the ~16kDa LC3B-I[172]. It is thought that although PE-conjugated LC3B-II is heavier, it migrates faster during SDS-PAGE due to its extreme hydrophobicity. Both forms of assays characterising LC3B expression were attempted in HNP1 treated HMDMs.

Immunofluorescent analysis of LC3B

Confocal microscopy assays attempted to detect the expression of LC3B relative to suggested HNP1 and rps20 complexes over a 72hr period. However, erroneous selection and application of mouse anti-LC3B antibody meant it was not possible to co-represent this expression with that of HNP1 (alongside rps20), since HNP1 primary antibody was also derived from mice. Of the immunofluorescence results that could be used to assess LC3B expression relative to rps20, results suggested

minimal existence of co-localisation between the two stains (Figure 6.8). It is worth mentioning at this point that all HMDMs were treated with bafilomycin A1 (Baf) 4hrs prior to fixation and immunofluorescence staining. This compound was included to prevent the completion of the autophagic flux pathway, specifically at the point of autophagosome fusion with lysosomes. This was required to accumulate autophagosomes in order to make visual comparisons between expressions in test treatments compared to basal level expression seen in untreated cells. Yellow arrows within the images showed the suggestion of LC3B-rps20 associations in HNP1 treated cells, but without the ability to assess the relative expression of HNP1, this observation could be attributed to normal ribosome turnover (termed ribophagy). In addition, using the second row as an overall representation the experimental results, the occurrence of LC3B-rsp20 proximity in a single cell of five in total suggested that this was an uncommon phenomenon. W26A treated HMDMs were compared which showed no signs of LC3B-rps20 accumulation.

As a positive control for autophagy induction, control cells were treated with rapamycin, an inhibitor of the protein kinase mTOR (mammalian target of rapamycin) and mTORC1-mediated pathway which blocks autophagy whilst also mediating protein synthesis and cell metabolism amongst other responses[173]. Positive results saw rapamycin with bafilomycin-treated HMDMs display distinctive puncta associated with autophagy induction, which was not seen in either HNP1 or W26A treated cells. In order to gain more conclusive results, completion of these experiments would need to be repeated with validated antibodies used at various time intervals over 72hrs in order to confidently address whether suggested HNP1/rps20 complexes are cleared by autophagy induction.

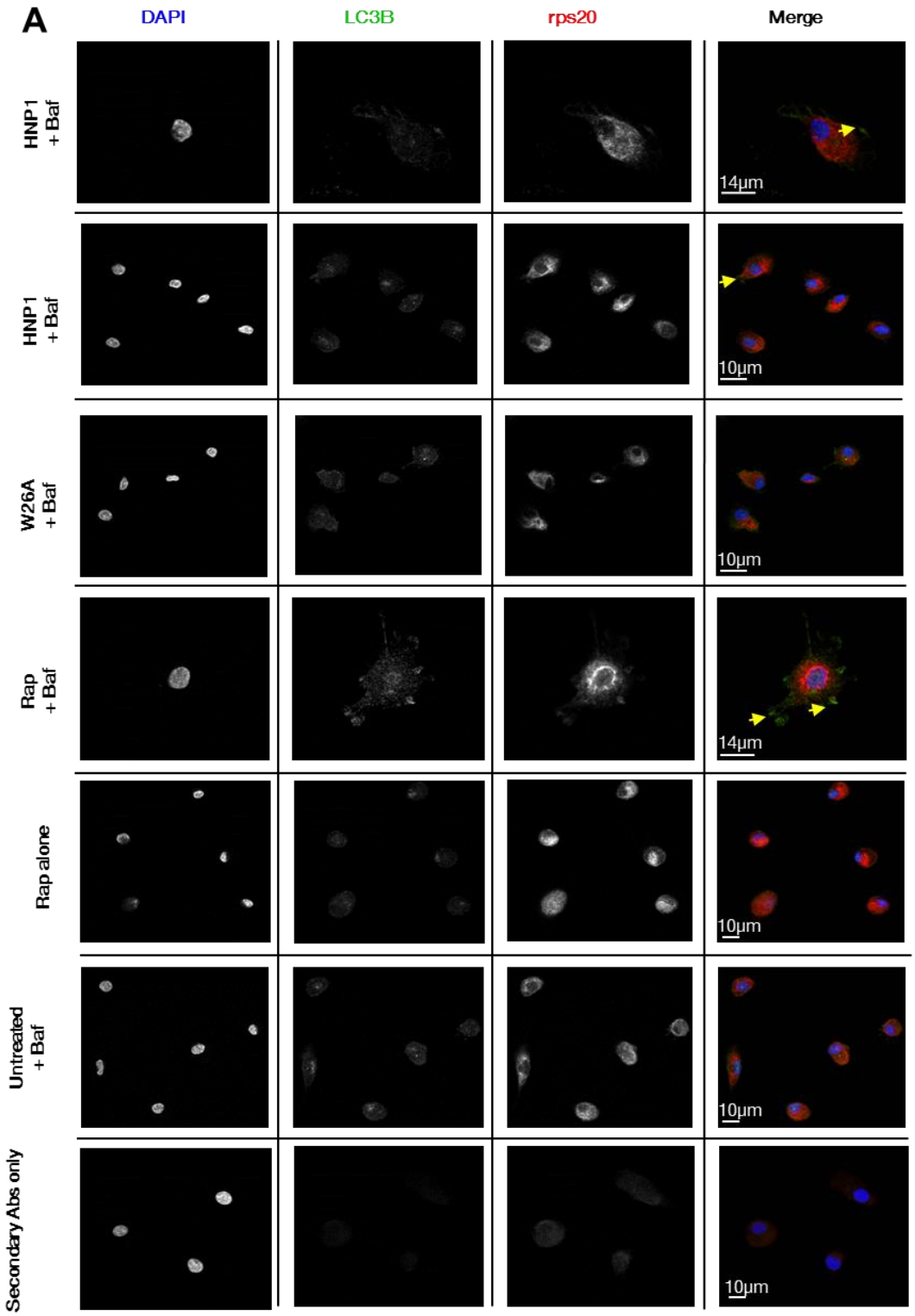

Figure 6.8: Immunocytochemistry of rps20 and LC3B in HNP1-treated HMDMs (4hrs)

(Continued overleaf)

Confocal microscopy images of HMDMs immunostained for ribosomal protein S20 (red), LC3B (green) and DAPI (blue).

Results are of HMDMs treated with 12.5µg/mL HNP1, W26A or 25µg/mL rapamycin (Rap) in the presence of 50nM bafilomycin A1 (Baf). Yellow arrows indicate areas of suggested co-localisation (n=1). Experiment performed by Jana Ovciarikova.

LC3B-I and –II expression by Western blotting

Analysis of LC3B conversion by Western blotting is considered a more stringent assay to measure autophagy. As a result of the unsuccessful attempts using immunocytochemistry, analysis of autophagy induction in HMDMs was further tested by Western blotting.

Most cell culture experiments to date were performed in culture media without serum to avoid the neutralisation of HNP1. Conscious of the fact that serum starvation is known to contribute to autophagy induction; it was decided to keep HMDM serum starvation to a minimum while still allowing for HNP1 to exert its inhibitory effect. To circumvent this dilemma, a single validation experiment was performed where R848-stimulated HMDMs were incubated with HNP1 for 2hrs prior to the addition of donor serum (Figure 6.9). After 18hrs incubation, TNF-α ELISA was performed on the supernatants which confirmed that 2hrs was an adequate incubation period in order for HNP1 to establish its inhibitory actions. Subsequent treatments in autophagy-related experiments were set up in this manner.

Experiments were set up to treat HMDMs with 12.5μg/mL HNP1 and W26A for 4hr and 24hr incubations alongside untreated controls, as well as rapamycin (Rap) treatment as a positive control for autophagy induction. Each experiment contained two sets of treatments: one set for the addition of bafilomycin 4hrs prior to cell lysis and another set without bafilomycin addition. According to Mizushima and Yoshimori (2007)[172], a positive indication for increased autophagy degradation is measured by the LC3B-I to –II conversion within each sample, indicated by an increased LC3B-II expression relative to LC3B-I. In addition, increased LC3B-II protein band expression in bafilomycin-treated cells should be more pronounced relative to LC3B-II expression in bafilomycin-untreated equivalent samples. This is considered to be a robust distinction between positive autophagy degradation over a mere treatment-induced accumulation of autophagosomes due to a defect in autophagic flux completion.

Using this assessment criterion, the induction of autophagy was firstly assessed at 4hrs in three independent experiments (Figure 6.10 *A*-*C*). In Figure *A*, the inadequate

separation of the two LC3B forms made it difficult to confidently interpret the autophagy expression profiles. Judging by the partial LC3B-II band expression in untreated cells without bafilomycin, already there was an indication of converted LC3B-II expression relative to LC3B-I. Both HNP1 and W26A treated with bafilomycin showed an increase in L3CB-II expression relative to their bafilomycin-untreated equivalents. This was in addition to showing larger LC3B-II expression over LC3B-I. This meant that both HNP1 and W26A were indicating early signs of autophagy degradation. This expression appeared similar to that of rapamycin (with bafilomycin) treated control samples as well as serum starved N2A cell lysates, which were included by the LC3B antibody supplier as a positive control for autophagy induction. β-Actin loading controls remained similar during all treatments, thus validating the differences in LC3B expression observed.

Of the three repeat experiments, Figure 6.10*B* was possibly the clearest result, albeit with limited information regarding the rapamycin-bafilomycin positive induction of autophagy. Results showed that LC3B-II expression was profoundly expressed in untreated, HNP1 and W26A samples treated with bafilomycin relative to their bafilomycin-untreated controls. Since untreated controls indicated autophagy degradation, this suggested that HMDMs were at the time undergoing autophagy under these given experimental conditions. Speculation was that the 2hr serum starvation might have induced this induction which was still ongoing at the time of treatments, thus obscuring the effect of HNP1 (if any) relative to W26A. The third repeat experiment in Figure 6.10*C* confirmed this trend, with LC3B-II notably increased in all treatments containing bafilomycin relative to treatments without bafilomycin. Assessment of autophagy at 4hrs was possibly too soon following the period of serum starvation.

At 24hrs and in two repeat experiments, the substantial expression of LC3B-II in all treatments regardless of bafilomycin addition supported the evidence that HMDMs prepared in this manner were inadequate for the studies on hypothesised HNP1-induced autophagy (Figure 6.11). In these cells, it could not be assessed if the actions of HNP1 caused ribosome degradation via the autophagy pathway. Going forward, these experiments should alternatively be conducted in stable cell lines preferably

with minimal baseline levels of autophagy and where the inhibitory actions of HNP1 on translation have been validated.

One final assessment was performed on these samples to qualitatively analyse if there was a noticeable change in the expression of ribosomes by Western blotting for rps20 at 4hrs, 24hrs and 48hrs (Figure 6.12). Results from two repeats showed no apparent decrease in rps20 expression with HNP1 compared to untreated and W26A control samples. There was also no difference in rps20 expression compared to bafilomycin-treated HNP1 samples, where autophagic flux (and hence ribosome degradation) was supposedly prevented.

This apparent lack of ribosome clearance was confirmed in semi-quantitative fluorescent analysis of rps20 by confocal microscopy (Figure 6.13). The images obtained from confocal microscopy, which were used previously to measure the degree of Pearson correlation between HNP1 and rps20 (section 6.2.2, above), were used to quantitate the expression of rps20 in HNP1, W26A and untreated cells after 24hrs incubation. Ten random field images were taken of each treatment with no adjustments made to the settings of the microscope between slides. Areas of rps20 were defined within cells and the integrated pixel density was determined and corrected for the background intensity of the image (termed the Corrected Total Cell Fluorescence, detailed in Chapter 2, section 2.8.1.1) as previously published[121]. No statistical difference existed for the fluorescence of rps20 in HNP1 treated HMDMs after 24hrs compared to W26A and untreated controls.

Thus in using two standard laboratory techniques available, no evidence could show a decrease in the amount of ribosomes over 24hrs with HNP1 treatment. Currently it remains unclear what the fate is of the possible HNP1/rps20 complexes and is a point to consider going forward (see Discussion).

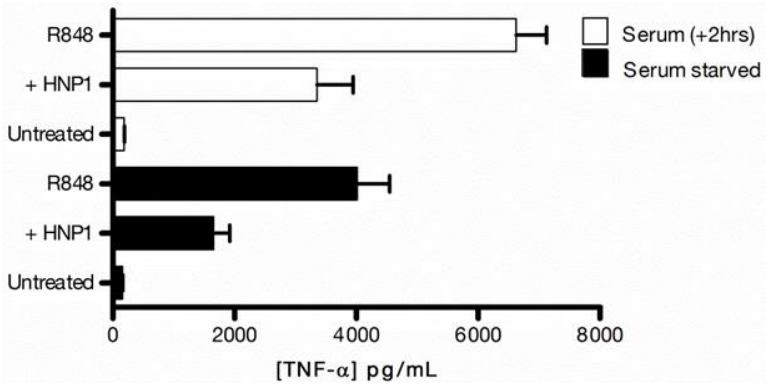

Figure 6.9: TNF-α ELISA of HNP1 treated HMDMs with serum addition

Quantitated TNF-α at 18hrs following R848-stimulated HMDMs alone or with 12.5µg/mL HNP1. White bars depict samples where 10% (final volume) donor serum was added to culture after 2hrs following treatment, while black bars represent samples that were serum-starved throughout the 18hr incubation period. Treatments were performed in triplicate and represent the mean ± SD from a single validation experiment.

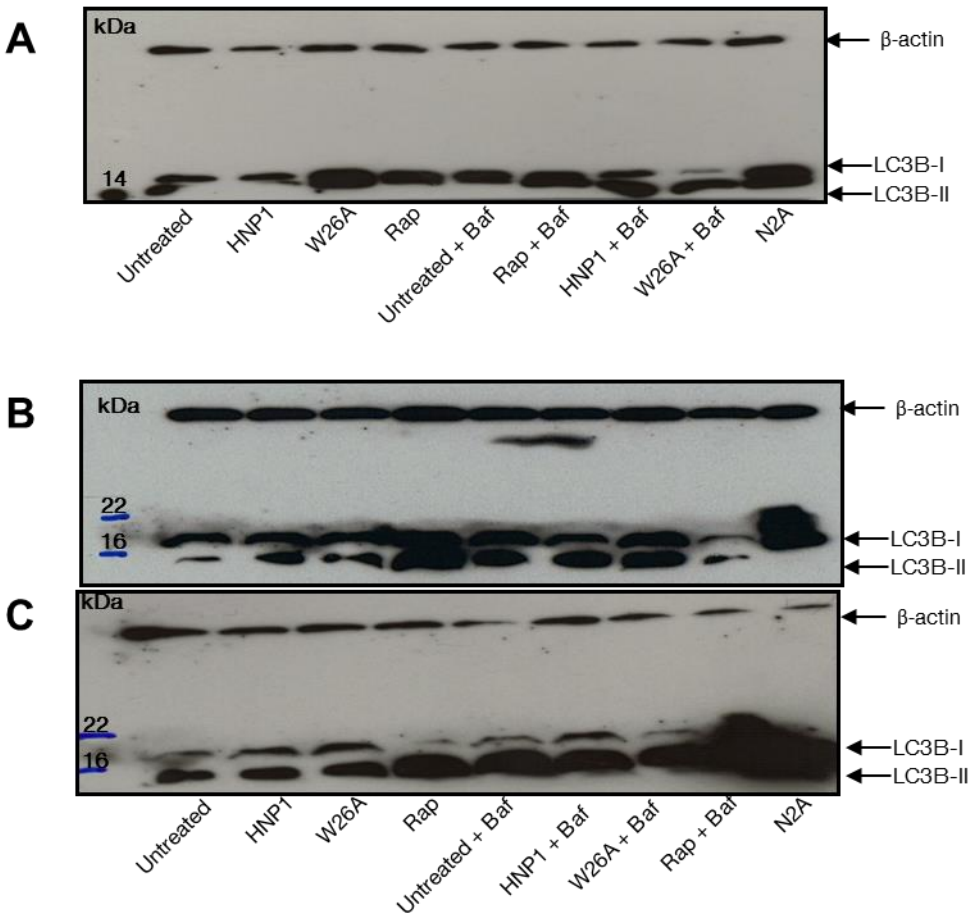

Figure 6.10: LC3B expression in HNP1-treated HMDMs at 4hrs

Western blot results for LC3B-I and –II expression in HMDMs treated with 12.5µg/mL HNP1, W26A or 20µg/mL rapamycin (Rap) alone or with 50nM bafilomycin A1 (Baf). Untreated controls were included as a negative control while serum-starved N2A cell line lysates were included as a positive induction of autophagy. Samples from first repeat (**A**) were electrophoresed by 12% SDS-PAGE while second and third repeat (**B** and **C**) were resolved by 15% SDS-PAGE (all home-made). β-actin detection was included as a sample loading control. Experiment performed by Jana Ovciarikova.

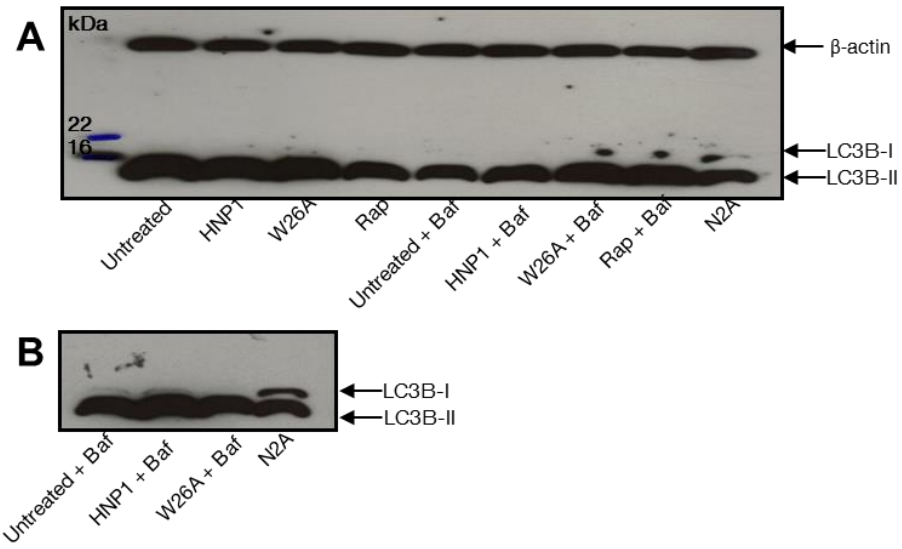

Figure 6.11: LC3B expression in HNP1-treated HMDMs at 24hrs

Western blot results for LC3B-I and –II expression in HMDMs treated with 12.5µg/mL HNP1, W26A or 20µg/mL rapamycin (Rap) alone or with 50nM bafilomycin A1 (Baf). Untreated controls were included as a negative control while serum-starved N2A cell line lysates were included as a positive control for autophagy induction. Electrophoresis was performed by 15% SDS-PAGE using home-made gels from two independent experiments (**A** and **B**). β-actin detection was included as a sample loading control. Experiments performed by Jana Ovciarikova.

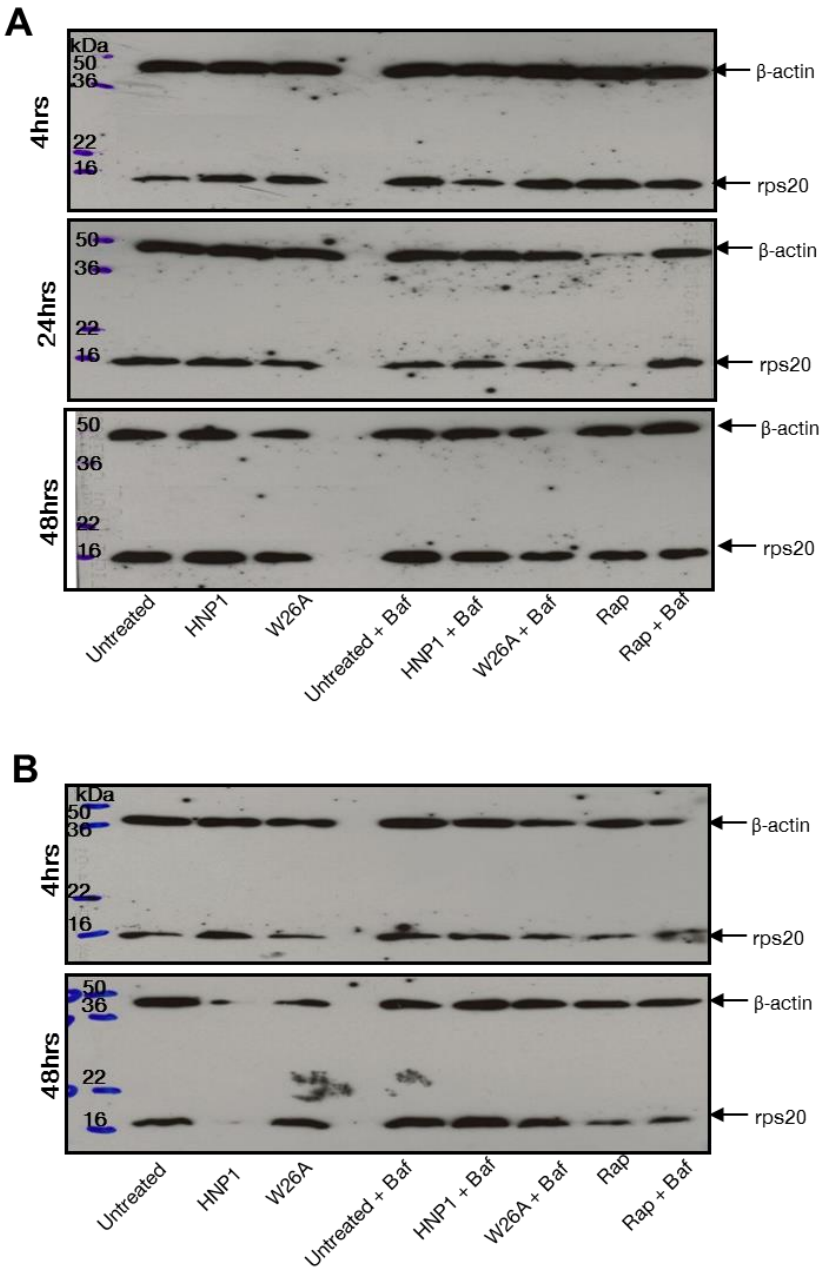

Figure 6.12: Rps20 expression in HNP1-treated HMDMs over 48hrs

Western blot results for ribosomal protein S20 in HMDMs treated with 12.5µg/mL HNP1, W26A or 20µg/mL rapamycin (Rap) alone or with 50nM bafilomycin A1 (Baf). Untreated controls were included as a negative control. Electrophoresis was performed by 15% SDS-PAGE using home-made gels from two independent experiments (**A** and **B**). β-actin detection was included as a sample loading control. Experiments performed by Jana Ovciarikova.

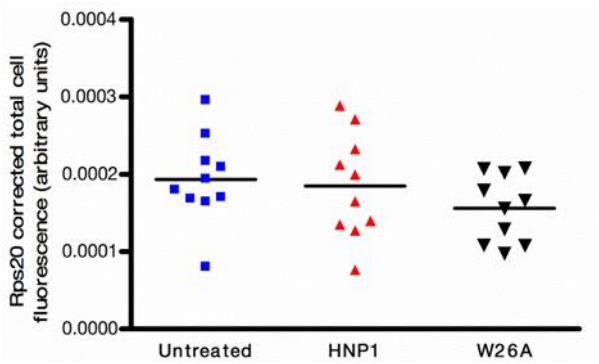

Figure 6.13: Quantitative image analysis of rps20 in HMDMs

Rsp20 corrected total cell fluorescence (CTCF) in HNP1 and W26A treated HMDMs at 24hrs compared to untreated controls, as described in Chapter 2 (2.8.1.1). Results are the mean ± SEM from 10 images per treatment from a single experiment. Statistical analysis was performed using Tukey's *post hoc* analysis following one-way ANOVA.

6.2.3.2 Evidence that ribosomes in HNP1 treated HMDMs may exist as heavy complexes in pelleted fractions

The last set of data attempting to determine the fate of ribosomes in HNP1-treated HMDMs was based again on the weakly identified rps20 aggregate formation within confocal microscopy images. These aggregates tended to be unusually large in size, using the stained nucleus as a reference organelle. It was questioned that these aggregates were large enough to be pelleted out along with other large organelles conventionally removed by bench-top centrifugation prior to subsequent applications such as for Western blotting or polysome analysis. General protocols describe performing centrifugation below speeds of 15 000 × g following cell lysis in order to pellet nuclei, cellular membranes, mitochondria, lysosomes and peroxisomes. This is normally performed to minimize complications with sample loading and migration during electrophoresis, for example. Since these suggested rps20-containing aggregates were approximately a quarter the size of DAPI-stained nuclei, it was wondered if these aggregates would pellet out using bench-top centrifugation speeds and if it was possible to quantitate this.

Using an adaptation of the method as performed for polysome analysis; HMDMs were treated for 6hrs with 25μg/mL HNP1 and compared to untreated samples. Cells were then incubated with 150μg/mL cycloheximide for 30min prior to lysis in the same polysome lysis buffer used before, which acts to stabilise translating complexes including preventing polysome run-off. Samples were then centrifuged for 10 000 × g for 10min after which supernatant and pellets were separated followed by RNA extraction. Samples were then resolved by non-denaturing gel electrophoresis and stained for RNA (Figure 6.14). Although only performed once, semi-quantitative analysis of both 28S and 18S rRNA (quantitated area highlighted in blue and red bars, respectively) revealed an increase in the amount of rRNA material in the pelleted fractions relative to rRNA in supernatants in HNP1-treated HMDMs. Comparisons in the percentage difference between HNP1-treated and untreated HMDMs showed a +8.4% increase in quantitated 28S rRNA and +16.2% increase in quantitated 18S rRNA with HNP1 treatment. It is appreciated that this was a single observation, which requires repeating in order to make a more convincing argument. Although this was an unrefined method to suggest ribosome aggregates, it provides

somewhat of a positive indication for the overall hypothesis which can be addressed in future using more rigorous testing methods.

A slight modification was made to this experiment, this time treating HMDMs with 12.5μg/mL HNP1 or W26A alongside untreated controls for 2hrs and 24hrs prior to incubation with cycloheximide and subsequent cell lysis. A two-tier centrifugation process was performed; firstly centrifuging lysates at 700 × g (10min) to pellet and collect the heaviest cellular organelles e.g. nuclei (labelled 'pellet A'), followed by remaining supernatant centrifugation at 15 000 × g (5min) to pellet medium-sized cellular organelles e.g. mitochondria and lysosomes ('pellet B'). Supernatants ('supe') were removed from Pellet B and all three fractions underwent RNA extraction and subsequent non-denaturing gel electrophoresis (Figure 6.15).

Semi-quantitation of the 28S and 18S rRNA bands at 2hrs revealed no difference in the rRNA expression in HNP1 treated HMDMs compared to W26A and untreated cells (Figure 6.15*A*). Expression of rRNA confirmed that most rRNA (hence ribosomes) was still retained within the supernatants ('supe'), with relative rRNA expression reduced by ~70% in 'pellet B' fractions, and by ~85% in 'pellet A'.

The change in this trend occurred in HNP1-treated HMDMs at 24hrs (Figure 6.15*B*). These fractions showed that there was an apparent reversal in the semi-quantitated amount of both 28S and 18S in the heavier 'pellet A' compared to 'pellet B'. Again appreciating the limitations of this experiment; it at least agreed with the trend observed in the previous result which suggests that rRNA, possibly implying ribosomes, form heavy aggregates in the presence of HNP1, which are fractionated out using low-speed centrifugation. This was an early indication of this phenomenon which does require thorough testing since it could be useful in building towards the overall hypothesis. If future experiments could confirm these preliminary findings, it could modify the hypothesis to suggest that: through the mechanism of binding with rRNA within ribosomes and possibly resulting in aggregate formation, HNP1 reduces global translation in inflammatory macrophages, contributing towards the inhibitory effects observed in secreted cytokines.

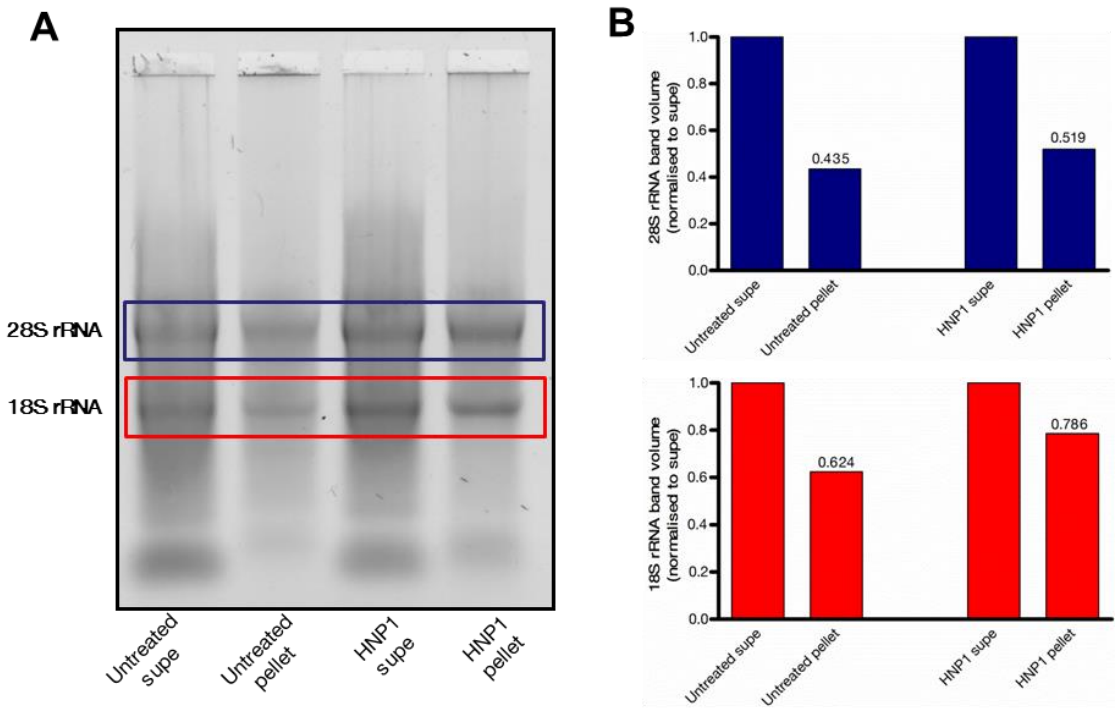

Figure 6.14: rRNA semi-quantitation of HNP1-treated HMDMs

Results of 28S and 18S rRNA band semi-quantitation for experiment performed as if for polysome analysis, where HMDMs were treated for 6hrs with either 25µg/mL HNP1 or left untreated prior to cycloheximide treatment and lysis. Samples were centrifuged (10 000 × g, 10min) followed by the separation of supernatant and pellet fractions after which RNA extraction was performed (n=1).

(**A**) Extracted RNA from fractions were electrophoresed in a non-denaturing agarose gel.

(**B**) Band semi-quantitation of rRNA from pelleted fractions normalised to rRNA from supernatant fractions.

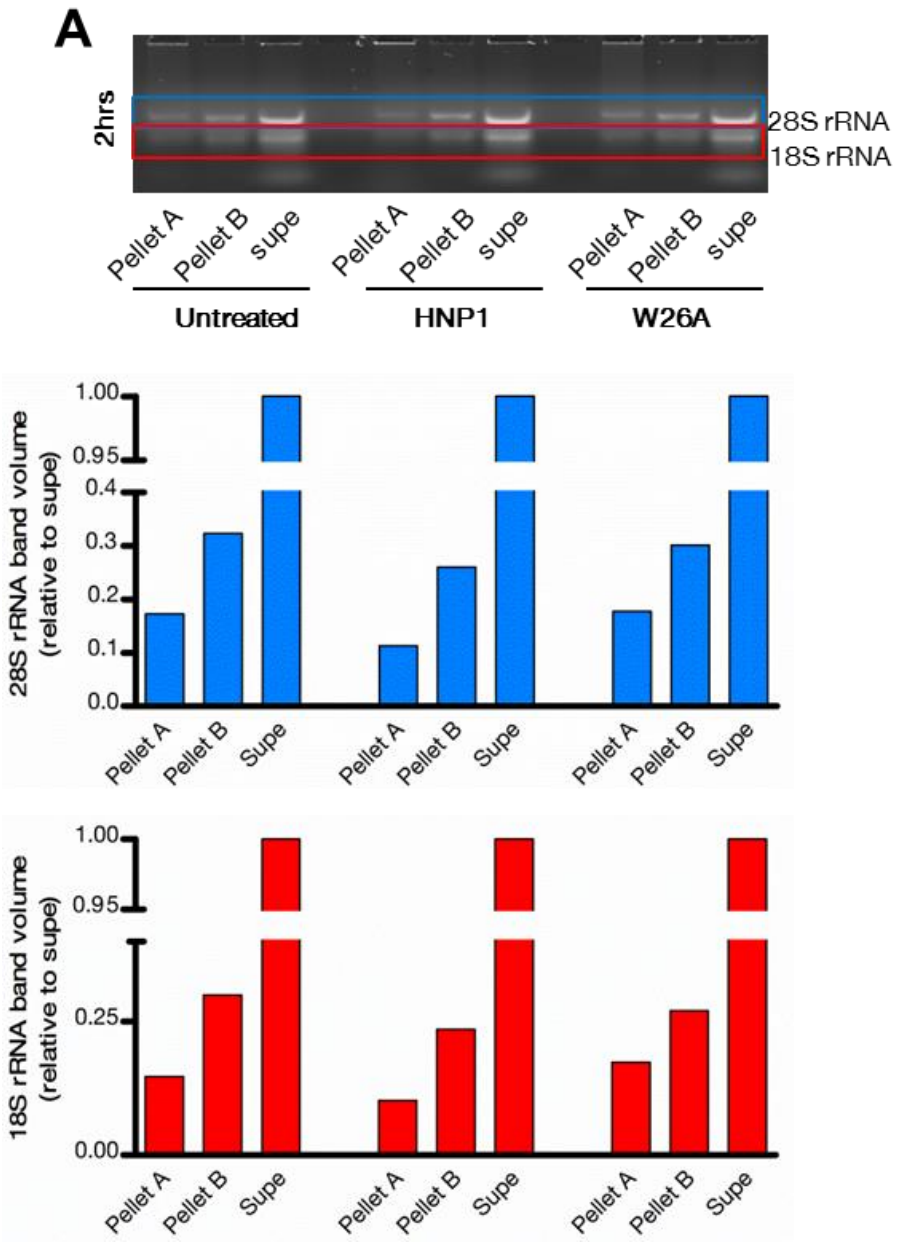

Figure 6.15: HMDM rRNA semi-quantitation of lysate fractions separated by centrifugation

Results of 28S and 18S rRNA band semi-quantitation for experiment performed as if for polysome analysis, where HMDMs were treated with 12.5µg/mL HNP1 or W26A alongside untreated control for 2hrs (**A**) or 24hrs (**B**, overleaf). RNA was extracted from collected fractions following cell lysate centrifugation at 700 × g, 10min ('Pellet A') and after 15 000 × g, 5min ('Pellet B'). rRNA in pelleted fractions were compared to rRNA amounts in remaining supernatants ('supe').

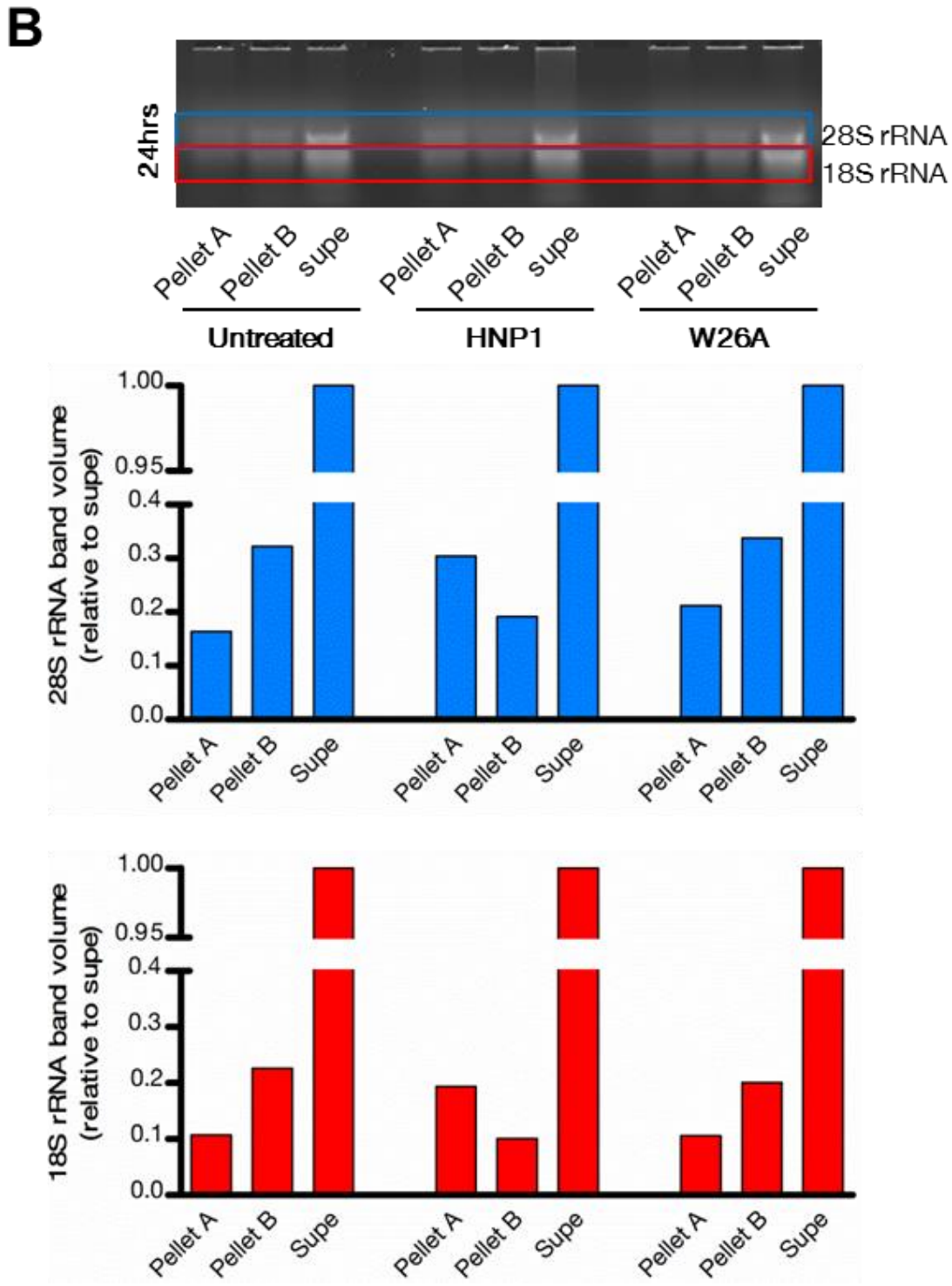

Figure 6.15 (continued)

(**B**) 28S and 18S rRNA band semi-quantitation of HMDMs treated with 12.5µg/mL HNP1 or W26A alongside untreated control at 24hrs. Results are of a single experiment performed.

6.3 Discussion

Evidence has been presented in this thesis which proposes a binding interaction between HNP1 and nucleic acids. Not only was this binding effect evident in short oligonucleotide sequences, but also on larger RNA complexes such as 28S and 18S rRNA, and also mRNA. Since all forms of RNA material tested so far have displayed an electrophoretic shift with HNP1 treatment, it implies that sequence selectivity is not required to facilitate HNP1 binding. While the wild-type peptide has repeatedly confirmed this binding interaction, mutant forms thereof (W26A and LHNP1) have demonstrated a much diminished binding affinity towards RNA.

Just how the binding interactions initiate and develop remains unknown and would require more advanced methods of computational biology and bioinformatics to decipher. Given the cationicity of HNP1 in the form of four arginine amino acids, it could be suggested that early electrostatic interactions initiate this attraction for RNA. However, this relatively weak force is most likely insufficient to sustain interaction since arginine amino acids are conserved in the mutant peptide forms. In support of this, Zou *et al*. (2007)[174] showed a deleterious effect on HNP1's ability to kill *Staphylococcus aureus* and *E.coli* by merely substituting arginine amino acids for similarly positively charged lysines. Furthermore, having a positive net charge does not directly infer good RNA binding. This is demonstrated by comparing the net charge of HNP1 (+3) to Buforin II (+6) which binds RNA tightly versus Magainin 2 which does not (+4)[124]. It is interesting to note that nucleic acid binding peptides do not share structural homology either. α-Defensins fall under the β-sheet peptide category, while Buforin II is characterised by α-helices. A DNA binding peptide Indolicidin, which has similar binding affinities to that of α-defensins and Buforin II, fall under the category as having extended peptide structures dominated by a proline and tryptophan amino acids[175]. This is possibly where the amphipathicity of a peptide is critical for association with nucleic acids.

There is evidence in Indolicidin interactions with DNA that suggest that the proximity of polarised nucleic acids brings about conformational changes to tryptophan amino acids[155]. It suggests that the altered polarity around non-polar tryptophan might mediate a structural change within the peptide which enhances

peptide/nucleic acid interactions. This is further supported by data within this thesis that HNP1 lacking its tryptophan amino acid (W26A) showed a severely diminished RNA binding potential. Furthermore, all three nucleic acid-binding peptides contain arginine amino acids while Magainin 2 does not. Since arginine has previously been shown to be important in mediating HIV-Tat protein binding to RNA[176], these collective publications suggests that altered tryptophan conformation brought about by polar RNA might increase the capacity for arginine residues to mediate RNA binding. This evidence provides preliminary insight into HNP1 interactions with RNA and could be further addressed using similar methods to those employed for Indolicidin-DNA binding interactions.

Based on the evidence presented to date, it is conceivable to suggest a binding mechanism in which strands of RNA in this system are laced with HNP1 peptides. This could possibly have led to an increased molecular weight which impeded electrophoretic migration suggested in both 28S and 18S rRNA. Also, it could account for the strong inhibition of migrated oligonucleotides, suggested by the accumulation of complexes at the top of the loading well apparently too large to transition into the gel. Not only could free monomers be contributing to the expanding complex, but also by RNA-bound HNP1 perhaps forming links with HNP1 bound to neighbouring RNA strands.

It is this biochemical binding property which formed the basis for the hypothesis of binding with ribosomes, contributing to the inhibition of translation. The keyword in the preceding statement is *contributing*, as it is appreciated (but as yet untested) that translation could also be inhibited by HNP1 binding to mRNA, or even tRNA-containing amino acids. Binding interactions would clearly need to be examined on a more detailed level in all of these RNA-containing components under physiological conditions in order to support this property of HNP1. Confocal microscopic data provided as-yet unconvincing suggestions of HNP1 interaction with ribosomes. Evidence at 4hrs suggested that HNP1 tended to concentrate in areas of translation activity, signified by the presence of rps20 within the perinuclear region where the endoplasmic reticulum is situated. This implies that HNP1 rapidly enters cells and

centralises around the endoplasmic reticulum. HNP1 has a well described affinity for membranes. Since the endoplasmic reticulum is an intracellular membranous structure; the ER could serve as a 'docking station', which could account for the high peptide concentration observed. It is in this area of concentrated ribosomes and HNP1 where hypothetical associations between the two could be allowed to interact. The weakly apparent HNP1/rps20 accumulations formed at 24hrs are however similar to the aggregates located at the top of the wells in the EMSA experiments, but this remains to be determined. If this hypothesis of ribosome binding is supported by further data, it is clear that this phenomenon could impair large amounts of ribosomes, decreasing the amount of free ribosomes available for translation. Already preliminary data has suggested an increase in the amount of sedimented rRNA with HNP1 at low centrifugation speeds. This result does support evidence of aggregated ribosomes, but more reliable experiments could be used in future to confirm this finding. An example of a more robust co-localisation techniques that could be utilized include FRET (Fluorescence Resonance Energy Transfer)[177]. In this method, interactions between two suspected protein partners are labelled with fluorescent molecules (donor and acceptor fluorophores). FRET can be quantitated within live cells *in vivo* by stimulating the acceptor fluorophore at an appropriate excitation wavelength. The emitted fluorescence intensities are measured at the wavelengths corresponding to the emission peaks of the donor compared to that of the acceptor. When the donor and acceptor fluorophores are within close proximity- due to the interaction of the two proteins (1-10nm) - emission spectra of the acceptor is predominantly observed, which is due to the intermolecular energy transfer (FRET) from the donor to the acceptor.

What the fate is of these suggested HNP1/rps20 structures is currently unknown. They did appear to be located on the outer periphery of the perinuclear region. Future experiments could assess whether these accumulations are cleared by 72hrs; for this would tie in with the published data that showed that TNF-α production was regained in stimulated HMDMs after 72hrs following HNP1 treatment[87]. Experiments were conducted to determine if autophagy was induced in order to clear these proposed complexes. Unfortunately limitations with the experimental protocol as well as the

HMDMs used meant it was not possible to answer this question at present. This valid question does require further testing, possibly in alternative cell types which do not display pre-existing elevated levels of LC3B-II expression. Interestingly, LC3B expression by Western blotting indicated that the HMDMs prepared for experimentation were naturally undergoing autophagy. This was evident even in HMDMs that were serum-starved for 2hrs to facilitate the effects of HNP1. This implied that the inhibitory effects of α-defensin were functionally independent of the activated autophagic pathways within the cell. This finding has possible implications *in vivo*, especially in nutrient-depleted cells that are undergoing autophagy. Not only then are concentrated areas of neutrophil death at sites of tissue injury impervious to the presence of macromolecules within serum which could bind α-defensins (e.g. albumin)[50], but α-defensins are able to mediate their inhibitory functions on these nutrient-starved cells.

Interestingly, autophagy is implicated in the clearance of polyubiquitinated protein aggregates which accumulate either in situations of routine protein clearance or under circumstances of stress, aging, and disease owing to damaged or misfolded proteins. This form of macroautophagy, known as aggrephagy, might well be a mechanism employed by the HMDMs and ubiquitin tagging of these HNP1/rps20 complexes could provide further clues into how this complex is removed[178].

Lastly, it was surprising to find no evidence of decreased rsp20 by either quantitative confocal image analysis or reduced rps20 protein expression by Western blotting. If there is future evidence supporting HNP1/ribosome aggregate formation, it would suggest that this did not lead to the clearance of HNP1-bound ribosomes to the extent that ribosome numbers were noticeably reduced within the given timeframe of HNP1-mediated inhibition (i.e. within 24hrs). Given that *de novo* protein synthesis (Chapter 4) resulted in an attenuation of intracellular proteins within 24hrs, it is currently unknown if ribosome biogenesis was affected and, if it was, at what point biogenesis was restored.

Chapter 7

7 Conclusions and future work

The work described in this thesis set out to extend the current understanding of the inhibitory actions of α-defensins on pro-inflammatory macrophages. Previously published data showed for the first time that α-defensins are released from dying human neutrophils and inhibit the secretion of cytokines from inflammatory macrophages[87]. The inhibitory mechanism by which cytokines were attenuated remained largely unknown and this thesis provides the first definitive insight into how this inhibition is achieved. The focus areas of research within the cell and the techniques used are summarised in Figure 7.1.

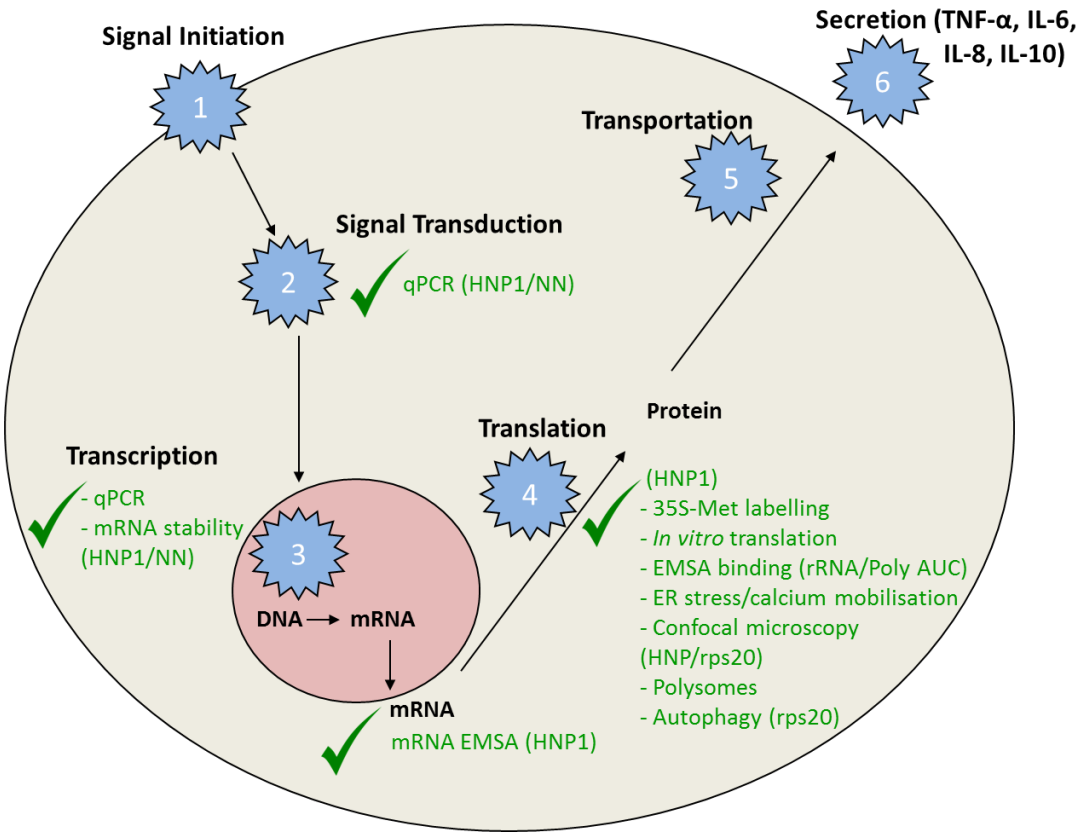

Figure 7.1: Summary of the intracellular research conducted that was potentially affected by α-defensins

The figure presents an overview of the main areas of cell biology that were researched in this thesis and potentially affected by α-defensins. The figure illustrates

the cellular recognition of PAMPs and DAMPs by PRR receptors (**1**) that activate signalling pathways and transcription factors (**2**), subsequent mRNA expression of inflammatory factors (e.g. TNF-α) (**3**), protein synthesis (**4**), protein folding and translocation (**5**) and finally cytokine secretion (**6**). Areas of research interest along the cellular pathway are indicated by green ticks where appropriate, along with the technique performed and the anti-inflammatory agent used (HNP1 or NN).

The inhibitory effect of membrane-free necrotic human neutrophil supernatants (NN) on secreted cytokines TNF-α, IL-6, IL-8 and IL-10 recapitulated the observations made in Miles *et al.* (2009) using TLR7/8 stimulated HMDMs (Chapter 3). Since the inhibitory effects of α-defensins were observed in HMDMs stimulated with either a TLR7/8 agonist or CD40L and IFN-γ, it so far suggests an inhibitory mechanism that is independent of the pattern recognition receptor (PRR) activated, subsequent signal transduction and transcription factor activation. α-Defensins were also shown to inhibit LPS and SAC activation of HMDMs, but this is more likely attributed to the known lectin-like properties of α-defensins which has been shown to block binding of LPS to LPS binding protein (LBP) required for CD14 receptor activation[50,179]. TNF-α and IL-10 mRNA expression in α-defensin treated HMDMs supported the evidence that signalling pathways remained unaffected, since initial upregulation of gene transcription of both cytokines were similar in magnitude to agonist-stimulated alone control cells. Beyond initial expression IL-10 mRNA was unaffected in two experiments using both NN and HNP1 while secreted protein was noticeably attenuated within 24hrs of treatment. For TNF-α mRNA expression, minor variations in expression between HMDM donors tested with α-defensins could not account for the consistent inhibition of secreted TNF-α observed. The same could be said for the mRNA decay rates of TNF-α in the two experiments performed. Arguments that another inhibitory factor was driving cytokine attenuation were more convincing. Notably, the unaffected mRNA levels of IL-10 while secreted IL-10 was notably reduced, together with the inhibition of *de novo* secreted proteins regardless of HMDM stimulation. This affect caused by HNP1 suggested that a more extensive

inhibitory mechanism within the cell was the major contributing factor as opposed to individual effects on selected cytokines.

Incorporation of ^{35}S-methionine during protein synthesis in HNP1-treated HMDMs was the first experiment linking the inhibitory mechanism of HNP1 to effects on translation (Chapter 4). This inhibitory effect, independent of cell stimulation, demonstrated that both secreted and intracellular protein synthesis was affected with the former showing a greater degree of inhibition within 24hrs. It is unclear at present as to how secreted proteins would be further inhibited over intracellular proteins and requires further testing. Confocal images of HNP1 localisation within HMDMs suggested concentrated areas where ribosomes were situated, which is in close proximity to the endoplasmic reticulum. It may be that the inhibitory action of HNP1 includes preventing ribosome attachment to the ER, thus reducing the number of polypeptides being assembled within the ER lumen destined for secretion. Based on ER stress data, the hypothesis was ruled out suggesting that HNP1 within cells caused a regulatory shutdown of translation due to misfolded proteins brought on by an imbalance of cytoplasmic calcium. Although HNP1 greatly impacted calcium mobilisation within the cell within 24hrs, this imbalance did not result in an ER stress event, with no apparent activation of the Unfolded Protein Response (UPR) pathway. Since the ER stress data implied no impairment at the stage of protein folding, it did lead to the thought that the mechanism was possibly occurring prior to this stage in translation, and is further supported in literature showing no halt in exocytosis of synthesised TNF-α [87].

The most powerful and unambiguous evidence presented within this thesis was the inhibitory impact of HNP1 on *in vitro* translation (Chapter 5). In a pure translation system, this assay was able to show the significant inhibition of both cap-dependent and cap-independent (IRES-mediated) mRNA translation. With this information, it became more evident that the inhibitory actions were mediated by a direct impairment of the translation machinery. Since the comparatively simpler form of cap-independent mRNA translation was also affected (but to a lesser extent), it raises the possibility that HNP1 could mechanistically inhibit at the level of mRNA

assembly with ribosomes. This mechanical interference with mRNA-ribosome assembly may be further hindered in cap-dependent translation, given the added complexity of the requirement for initiation factor recruitment to form the translation initiation complex. This could explain the differences in percentages of inhibition between cap-dependent and cap-independent reduction observed. This proposed model of mechanistic interaction would require extensive investigation, but it is also appreciated that this result does not give any insight into the effects of HNP1 on polypeptide chain elongation and chain termination. With that said, the process of initiation is by far the most complex stage in translation. It is the stage where absolute fidelity of message to be translated is required. It thus serves as pivotal point in translation regulation and also acts as the rate-limiting step. It is difficult not to concede that, if there was a point where HNP1 would likely impact the process of translation, it would be within the intricacies of initiation. The technique of polysome analysis was employed in HNP1-treated HMDMs in an attempt to uncover such details of translation inhibition. It was anticipated that polysome analysis could provide this detailed level of information into the impact effect of HNP1 on translating ribosomes. Polysome analysis was able to offer limited insight using HMDMs with a decrease in translation-inactive RNA material observed in a single observation. Since this assay became fully optimised at the latter stages of the research period, further experiments on polysome distribution are worthwhile continuing and may provide key answers into the mechanisms involved.

The hypothesis of HNP1 binding to RNA was formulated on the basis that published literature provided evidence of antimicrobial peptide binding to RNA/DNA. Exploring this concept using HNP1 binding to HMDM RNA in EMSAs showed an affinity similar to that of Buforin II and Indolicidin. Both these antimicrobial peptides are known to bind nucleic acids tightly, which is implicated in their mechanistic killing of bacteria independent of membrane permeabilisation leading to cell death. These cationic peptides share no similarities in charge or structure, but all possess arginine residues. Since arginine residues are implicated in mediating the binding with nucleic acids[176], this provides the first clue along with the observation that non-polar tryptophan amino acid conformations are altered with close proximity

to polarised nucleic acids, seen with Indolicidin[155]. Since evidence within this thesis showed RNA binding with W26A (lacking tryptophan) was lacking, it would be interesting to determine if the presence of RNA alters tryptophan conformation within HNP1, thus exposing arginine amino acids to mediate RNA binding.

More extensive studies using EMSAs revealed that HNP1 binding was not dependent on sequence specificity as it non-selectively bound with similar affinity to oligonucleotide sequences of adenine, cytosine and uracil. It remains to be shown if the apparent increased affinity of HNP1 for uracil would be demonstrated in a competitive binding environment. What is apparent is that the mechanism of binding to these oligonucleotides was complex to the point that these complexes remained within the loading wells, evidently too large to migrate into acrylamide gels. These observations provided the first evidence in the literature for suggested HNP1-RNA aggregation, potentially mediated by the property of HNP1 dimerization.

Together with evidence of retarded migration of HMDM 28S and 18S rRNA retardation with HNP1 during EMSAs, a hypothesis was formulated that the inhibitory mechanism of HNP1 is mediated through direct association with RNA-containing components involved in translation. So far, evidence suggests that it could potentially not only bind to rRNA within ribosomes but also mRNA, although binding to the latter remains to be tested within cells (Chapter 6). Immunofluorescence within HMDMs was able to indicate the concentrated localisation of HNP1 around the perinuclear region, which are the sites of active ribosome activity as indicated by rps20 protein that forms part of the 40S ribosomal subunit. This further supported the hypothesis of RNA binding interactions given the densely populated localisation of both rps20 and HNP1. Within 4hrs of HNP1 treatment, confocal microscopy suggested few yet so far unconvincing areas of HNP1-rps20 accumulation. By 24hrs confocal images began to show emerging evidence of possible HNP1-rps20 accumulation, but it remains unclear as to whether this is true co-localisation or areas of fluorescent signal overlap. With further supporting evidence, it is thought that these suggested complexes could contain impaired ribosomes which are undergoing removal for degradation or extrusion.

Although extrusion of these suggested complexes was not addressed, degradation by autophagy was performed with limited success in obtaining a clear indication of this process. It remains a valid proposition should the formation of an HNP1-ribosome complex be tangible and could be a study to address in future.

An interesting link was made in three key assays performed regarding the concentration range of HNP1 and the inhibitory potential. Where titration of HNP1 was performed, a trend was observed in the minimum HNP1 concentration threshold, below which inhibitory activity was noticeably limited. Using EMSAs, it was observed that migration of the uridine oligonucleotide became impeded at a peptide/RNA ratio of 3.5:1. This was also the concentration at which HNP1 was calculated to be 11.3μg/mL. Assessment of the half maximal inhibitory concentration (IC50) of HNP1 on cap-dependent translation determined the mean IC50 value to be ~8.62 ± 3.0μg/mL (n=3). These threshold concentrations were compared to the minimum inhibitory concentration affecting TNF-α production in HMDMs. HNP1 at 12.5μg/mL achieved a trend towards TNF-α inhibition, below which TNF-α remained largely unaffected (Chapter 3, section 3.2.2). Thus it brings into question if these minimum inhibitory ranges observed in three independent assays are more than simply coincidental. It perhaps identified a correlation between the binding to RNA, which can account for the inhibition observed in *in vitro* translation systems as well as in *de novo* protein synthesis in HMDMs, which showed attenuation at 12.5μg/mL HNP1. This link may ultimately account for the inhibitory effects of HNP1 observed on secreted TNF-α in HMDMs - the action which defines the ultimate purpose of this thesis. If this link in concentration can be pinpointed to RNA-binding identified in cell-based systems, it proposes an intriguing immunomodulatory role for α-defensins at this concentration range.

In the discussion section of Chapter 4 (section 4.3), I introduced an observation made on the activity of α-defensins depending on the peptide concentration, which is concluded from observations within this thesis as well from previous literature. I refer to it as the ‘three tiers of α-defensin modulation’ which proposes that the function of α-defensins is defined by the concentration of released α-defensins from

dying neutrophils, depending on the severity of inflammation. This suggests that early inflammation brings with it an appropriate number of infiltrating neutrophils which assume their conventional antimicrobial, phagocytic and immunoregulatory functions. Should the number of invading microbes and severity of inflammation overwhelm the capabilities of the leukocytes presently within the tissue, in death, neutrophils elicit a rescue response, which includes the release of α-defensins. Since lower concentrations of α-defensin have been shown to be pro-inflammatory and chemotactic for monocytes and dendritic cells[130,131] the function of α-defensin at lower concentrations, roughly below 1μg/mL, appears to be that of a chemokine and cell activator, supporting further leukocyte infiltration and inflammation.

In states of exacerbated inflammation (e.g. rheumatoid arthritis), the death of elevated neutrophil numbers is likely to bring with it the release of an intermediate concentration of α-defensins, as previously determined in the synovial fluid of twelve rheumatoid arthritis patients where the average HNP1-3 concentration was 12.4μg/mL[87]. It would appear that the peptide adopts a function of an inflammation suppressor by entering macrophages (and possibly other leukocytes) and preventing translation of inflammatory mediators, thus limiting their tissue destruction potential. The effect at this concentration was first proposed in Miles *et al.* (2009)[87] and is now supported by new evidence within this thesis.

Higher concentrations of α-defensin, above 40μg/mL, have been shown to possess cytotoxic effects on cells *in vitro*. These include lung epithelial cells (A549)[180], human erythroleukaemia cells (K562)[133], keratinocytes[181], as well as eight lymphoma cell lines tested by Lichtenstein *et al.* (1986)[132]. Indeed elevated concentrations of HNP1-3 have been reported in the serum of patients with sepsis and bacterial meningitis (up to 170μg/mL)[182], and in the sputum of cystic fibrosis patients (300-1600μg/mL)[183]. Thus it may be that in cases of severe inflammation the purpose of released α-defensins caused by extensive neutrophil death is in the containment of opportunistic infections at all costs to the detriment local host tissue. This collateral tissue damage by α-defensins may be considered a necessary trade-off as a last resort for the sake of host survival.

The impact of the primary discoveries within this thesis offers an extrapolation to the current knowledge regarding the role of α-defensins in an inflammatory environment. Using the chronic inflammatory disorder of rheumatoid arthritis as a tangible platform, this research suggests an added factor in the complexity of this debilitating disease. It is widely acknowledged that cytokines and chemokines secreted by synoviocytes are key contributors to disease progression and exacerbation[113,184]. Indeed overexpression of cytokines is present within rheumatoid synovium[107], with TNF-α key in inflammation regulation and a contributor to synovial pannus formation and bone and cartilage erosion[114]. Indeed, biological inhibitors of TNF-α in combination with Methotrexate have been a first-approach anti-inflammatory therapeutic strategy against rheumatoid arthritis disease progression[185]. In addition, secreted IL-1β potently amplifies and sustains neutrophil recruitment and inflammation[184]. Thus it would appear that α-defensins released from tissue areas of large-scale neutrophil death might serve to ameliorate an over heightened cycle of synoviocyte activation, cytokine and chemokine secretion, leukocyte infiltration, and joint destruction. By potentially blocking protein synthesis within synoviocytes, internalized α-defensins may well contribute to the immunosuppressive factors limiting a chronic inflammatory event, which is certain to result in irreparable cartilage damage if uncontrolled.

Future work

The central hypothesis proposed in this thesis suggested that the underlying mechanistic inhibitory property of α-defensins, which accounts for the anti-inflammatory effect on HMDMs, is mediated during translation by binding to RNA. This may include binding to rRNA within ribosomes but could also include binding to other RNA forms, such as mRNA. Data from immunofluorescence analysis has unconvincingly (to date) proposed an interaction between HNP and ribosomes within HMDMs. Thus in order to further the hypothesis, future work would need to show definitive evidence of HNP-ribosome binding, and if possible HNP binding to the rRNA portions of ribosomes. Attempts to provide further evidence of this were attempted using immunoprecipitation assays as well as immunoblotting for HNP1 in sucrose fractions containing ribosomes separated by ultracentrifugation (Appendix

C). Although these experiments were unsuccessful, similar approaches could be employed to confirm this binding effect (e.g. FRET). If this were proven, it could present a novel approach to targeting inflammation regulation.

Importantly, the inhibitory effects of α-defensins were briefly demonstrated on HMDMs obtained from clinically diagnosed rheumatoid arthritis patients as well as primary B cells (Chapter 3). Not only does this work support a future therapeutic role for α-defensins in the treatment of this chronic inflammatory disease but could be expanded upon to assess the inhibitory effect on a multitude of cells involved in the inflammatory cascade. Notably, it would be interesting to determine if dying neutrophils prevent activated neutrophils from releasing pro-inflammatory mediators, forming a negative feedback system.

Ultimately the immunomodulatory actions of α-defensins, or synthesised mimetics thereof, could go on to be trialled in the treatment of diseases relating to inflammation *in vivo*. Prior mention has been made that delivery of these serum-sensitive peptides would need to be addressed. Future work could include the bioengineering of inactive forms of the encapsulated peptide, perhaps utilizing current delivery systems such as liposomes. Upon liposome ingestion by phagocytes, the active form of α-defensin would be released to inhibit the activated cell by mechanisms suggested within this thesis. It is thought that this could efficaciously alleviate localised inflammation, bringing with it a chance for accelerated tissue regeneration and regained homeostasis.

Appendix A

Optimization assays of buffy coat-derived HMDM stimulants

Continuation of the inhibitory actions of NN on buffy coat HMDMs was performed using the agonist CD40L and IFN-γ. HMDMs were treated with titrated NN from a single donor together with 3μg/mL CD40L and 5ng/mL IFN- γ (CI) in two independent experiments. Observations did show a partial reduction in TNF-α with increasing NN percentages, although maximal stimulation remained low in CI stimulated cells after 18hrs incubation (Figure A.1*A*). CI was unable to stimulate HMDMs in Figure A.1*B* as quantitated TNF-α was similar to untreated negative control values.

Attempts were made to optimise CI stimulation in buffy coat HMDMs starting with increasing the concentration of human IFN-γ in culture with 3μg/mL CD40L (Figure A.2*A*). IFN-γ concentrations ranging from 5, 10, 20 or 50ng/mL did not enhance TNF-α values compared to controls where no IFN-γ was added. The addition of 100ng/mL IFN-γ doubled the amount of quantitated TNF-α to 100pg/mL, but remained low compared to previously published amounts using HMDMs obtained from fresh blood donations (>500pg/mL). Further experiments were conducted to test if the current batch of IFN-γ had expired. The original IFN-γ batch (labelled 'IFN-γ batch1') was compared to a second batch of human IFN-γ ('IFN-γ batch2') donated by Dr David Kluth (Centre for Inflammation Research, Edinburgh University). Using HMDMs from a single buffy coat donor, titrated IFN-γ concentrations from either batch were unable to effectively stimulate HMDMs in combination with 3μg/mL CD40L to published TNF-α levels (Figure A.2*B*).

An experiment was performed with increased CD40L concentration (5 and 10μg/mL) in an attempt to stimulate buffy coat HMDMs. As a comparison, the same stimulant was added to mature THP-1 cells as a potential alternative human macrophage source (Figure A.3*A* and *B*). Both cell types demonstrated low levels of produced TNF-α after 18hrs incubation.

Experiments were conducted to test alternative agonists for buffy coat HMDMs and THP-1 activation. *Staphylococcus aureus* Cowan Strain (SAC), the amidazoquinoline compound R848 and Peptidoglycan (PGN) were effective at stimulating HMDMs at stipulated concentrations (Figure A.4*A*), with secreted TNF-α values >3000pg/mL. Stimulation with 5μM CpG ODN 2006 was not able to induce TNF-α production. In THP-1 cells SAC and PGN stimulation effectively resulted in increased TNF-α production while LPS (1ng/mL), R848 (5μg/mL) and CpG ODN 2006 (5μM) showed no effect (Figure A.4*B*).

The effect of titrated NN was re-introduced into experiments and the inhibitory properties of NN were strongly demonstrated in buffy coat HMDMs stimulated with 5μg/mL R848, with TNF-α values close to near basal control levels (Figure A.5*A*). Although NN concentrations increasingly inhibited TNF-α in THP-1s stimulated with R848, TNF-α levels remained relatively low (Figure A.5*B*). The same experiment was applied to 0.1% SAC stimulated cells and the inhibitory effect of titrated NN increased with concentration in HMDMs (Figure A.5*C*). The inhibitory effect was also demonstrated with THP-1s, reducing the amount of TNF-α from approximately 7000pg/mL in SAC-stimulated alone controls to 4000pg/mL with 25% NN (Figure A.5*D*).

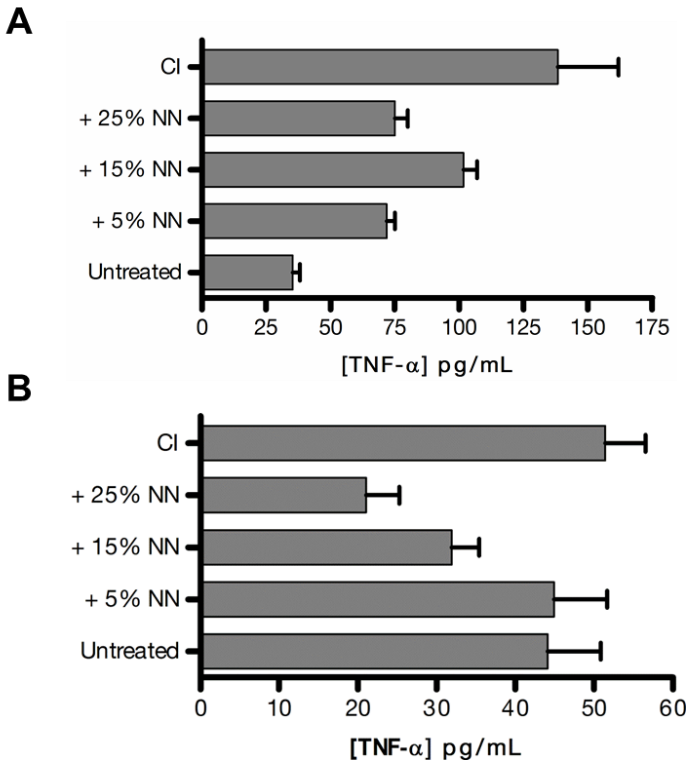

Figure A 1: Secreted TNF-α in CI stimulated buffy coat HMDMs treated with NN

ELISA results obtained from 18hrs incubation in two HMDM donors (**A** and **B**) stimulated with 3µg/mL CD40L and 5ng/mL IFN-γ alone or together with NN obtained from a single donor. Error bars are of the mean ±SD from treatments performed in triplicate.

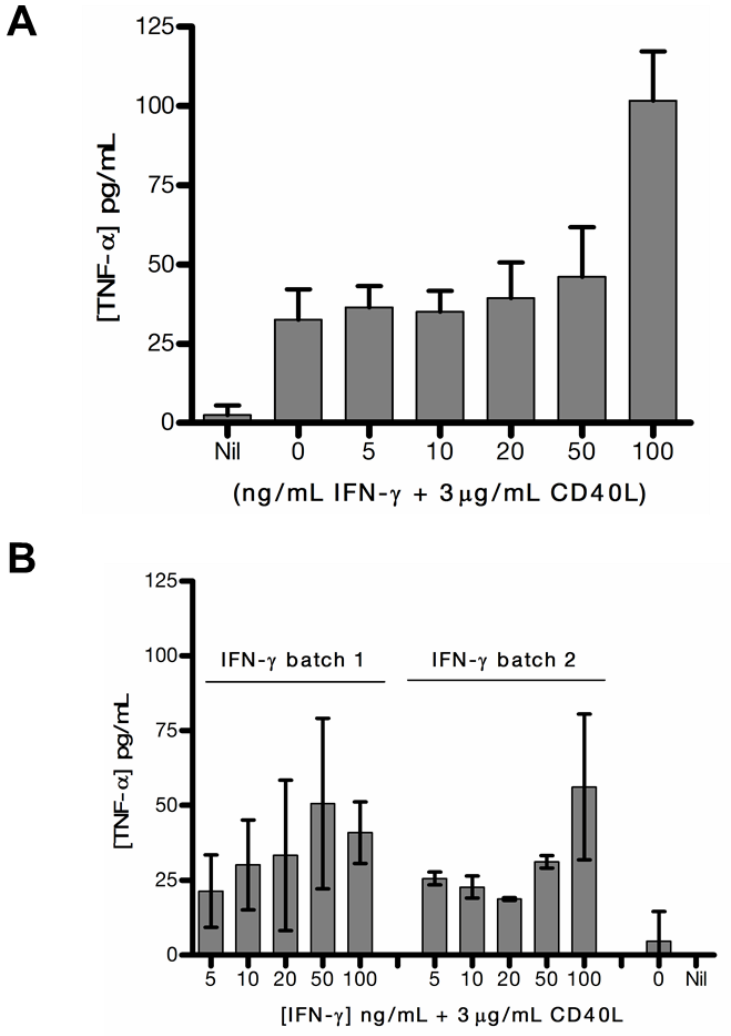

Figure A 2: CD40L stimulation of buffy coat HMDMs with titrated IFN-γ

Quantitated secreted TNF-α after overnight incubation of HMDMs stimulated with 3μg/mL CD40L and increasing amounts (ng/mL) of human IFN-γ alongside unstimulated negative controls (Nil). Error bars represented the mean ±SD from one experiment (**A**) and repeated using two batches of human IFN-γ (**B**). All treatments were performed in triplicate.

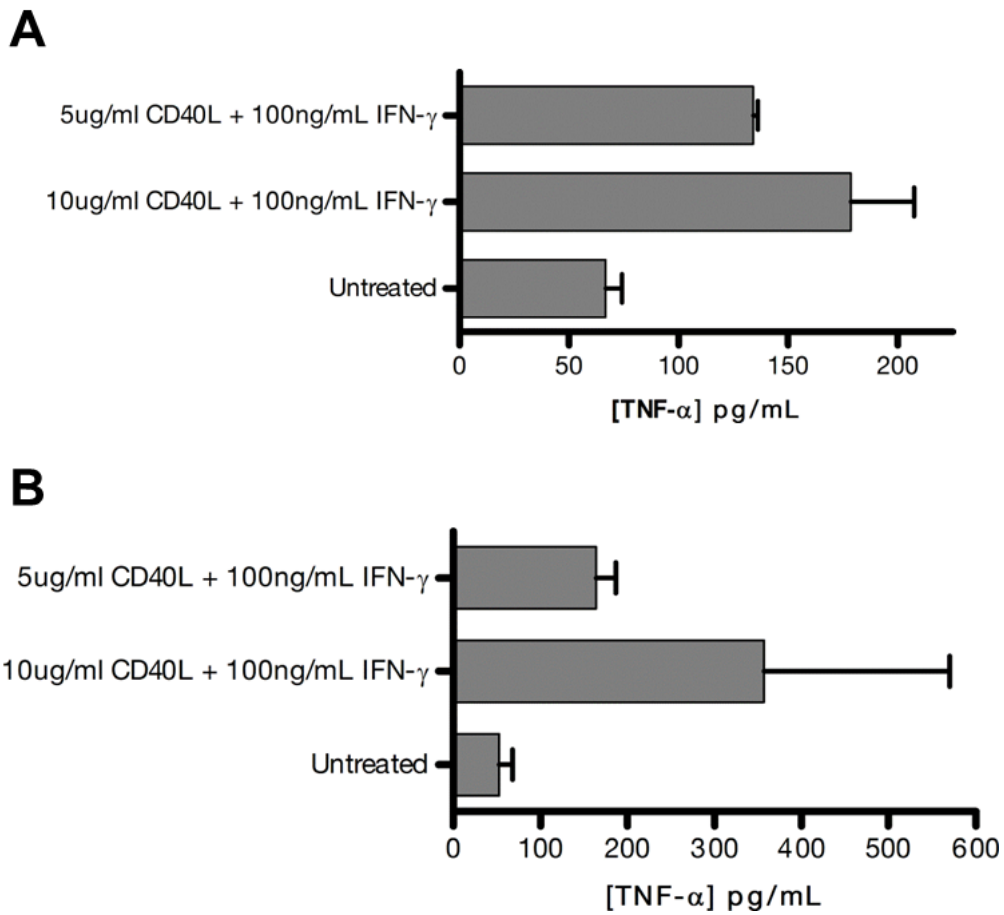

Figure A 3: CD40L optimisation for stimulation of buffy coat HMDMs and THP-1 cells

TNF-α ELISA quantitation of buffy coat HMDMs (**A**) and monocytic THP-1 cells (**B**) stimulated with two concentrations of CD40L with 100ng/mL IFN-γ at 18hrs incubation (alongside untreated control). Results represent the mean ±SD of single experiments with triplicate samples for each treatment.

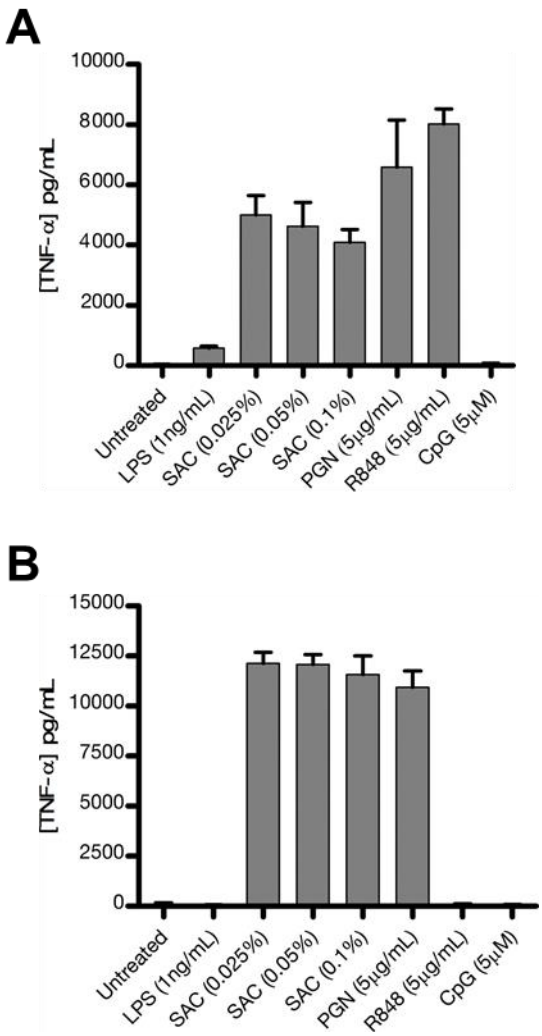

Figure A 4: Response of buffy coat HMDMs and THP-1 cells to a range of TLR agonists

TNF-α values quantified from ELISAs obtained after 18hrs incubation for buffy coat HMDMs (**A**) and THP-1s (**B**) from a single experiment. Error bars represent the mean ±SD of samples performed in triplicate.

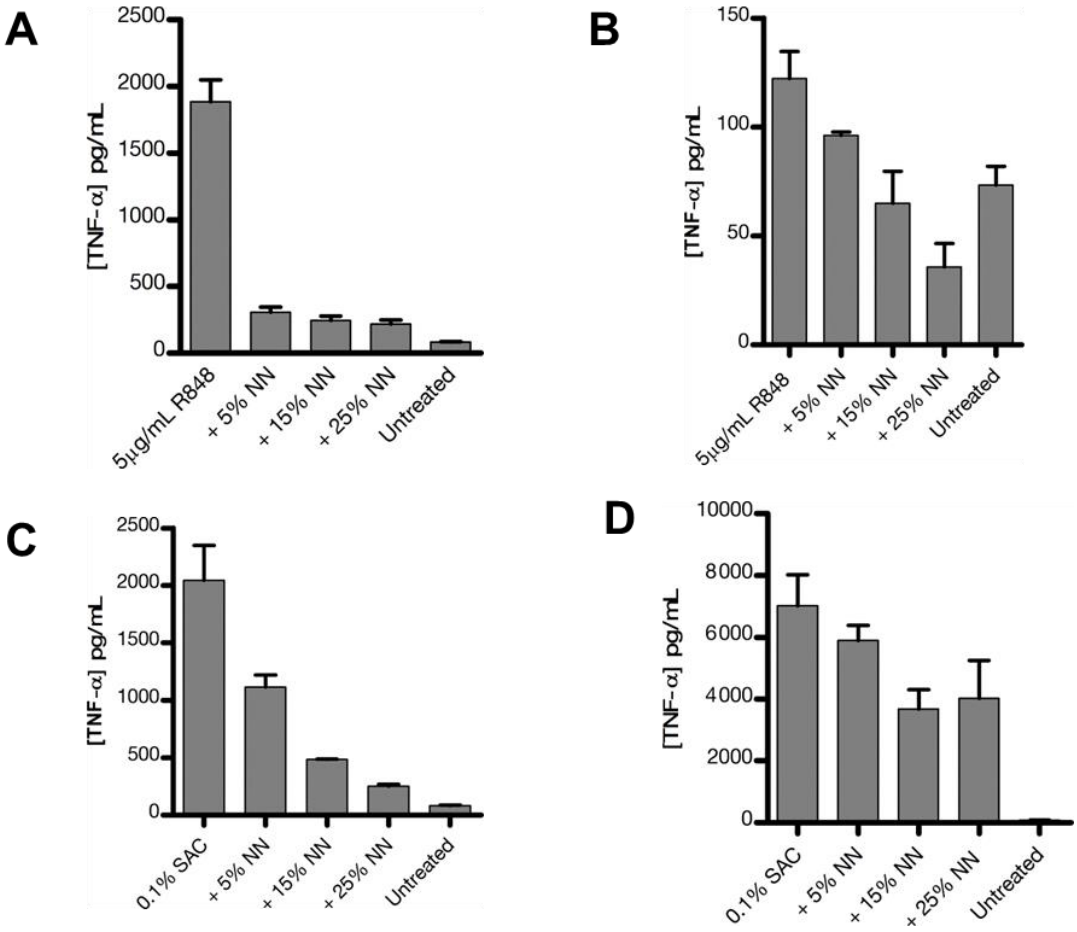

Figure A 5: NN effect on buffy coat HMDMs and THP-1 cells stimulated with R848 or SAC

TNF-α quantitation of HMDMs (**A**) and THP-1 cells (**B**) stimulated with 5µg/mL R848 in the presence of titrated necrotic neutrophils. Stimulation using 0.1% *Staphylococcus aureus* Cowan strain (SAC) was performed in HMDMs (**C**) and THP-1 cells (**D**). Error bars represent the mean ±SD of single experiments at 18hrs from triplicate repeats for all samples.

Appendix B

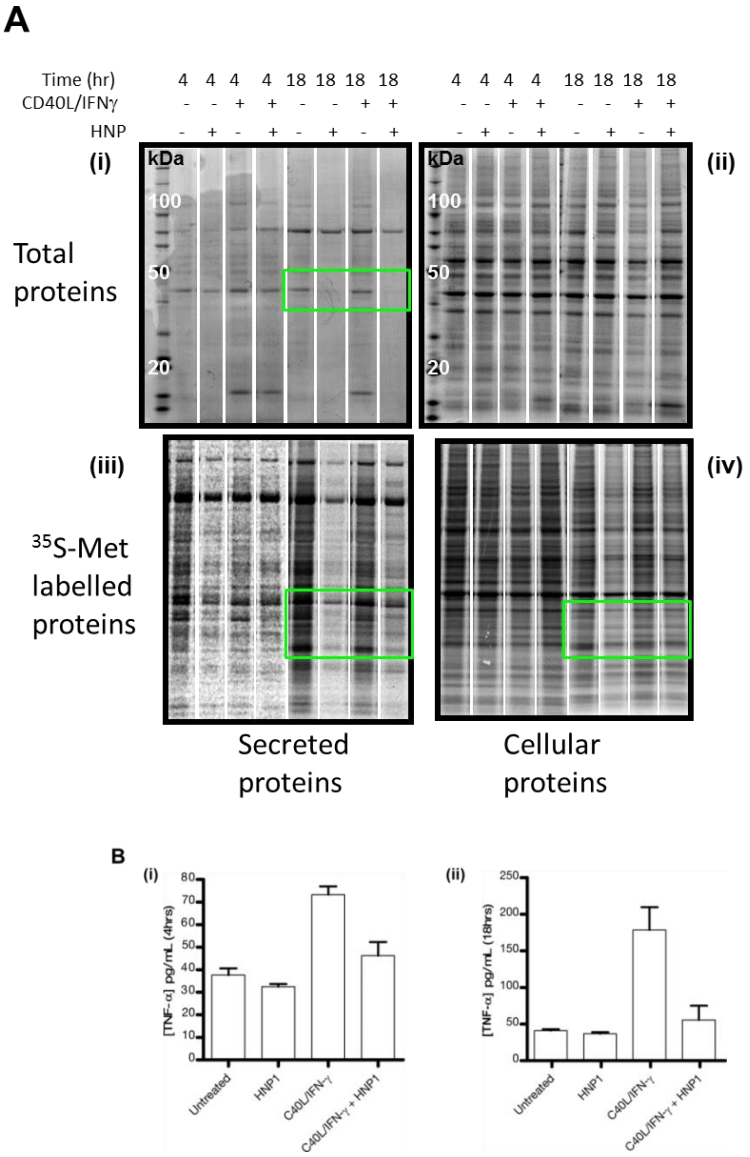

Figure B 1: HNP1 effect on secreted and intracellular HMDM protein synthesis (Run2)

A repeat experiment of Figure 4.3 (**A**) Gelcode Blue stained gels showing total secreted (**i**) and intracellular (**ii**) proteins. Radiolabelled protein images of *de novo* secreted (**iii**) and intracellular (**iv**) protein synthesis, with green boxes indicating areas of reduced or absent proteins. (**B**) TNF-α ELISAs of secreted proteins at 4hrs (**i**) and 18hrs (**ii**) with error bars of the mean ±SD of triplicate repeats. Experiment performed by Dr Matthew Brook.

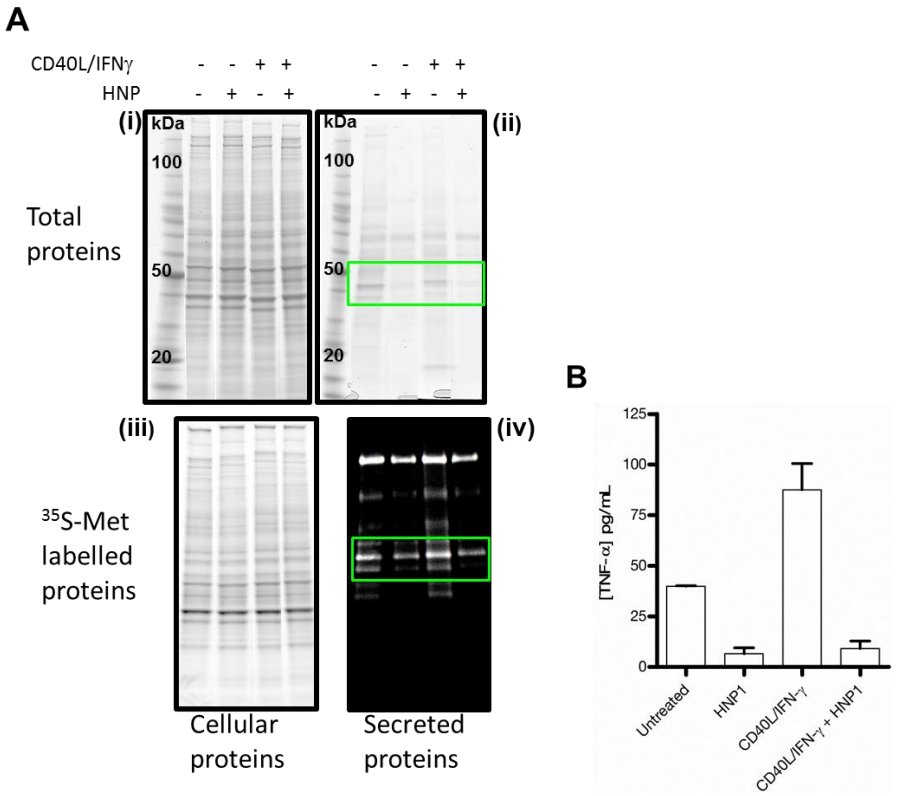

Figure B 2: HNP1 effect on secreted and intracellular HMDM protein synthesis (Run3)

Repeat experiment of Figure 4.3. (**A**) Gelcode Blue stained gels showing total secreted (**i**) and intracellular (**ii**) proteins at 18hrs incubation. Radiolabelled protein images of *de novo* secreted (**iii**) and intracellular (**iv**) protein synthesis, with green boxes indicating areas of reduced or absent proteins. (**B**) TNF-α ELISAs of secreted proteins at 18hrs with error bars of the mean ±SD of triplicate repeats. Experiment co-performed with Dr Matthew Brook.

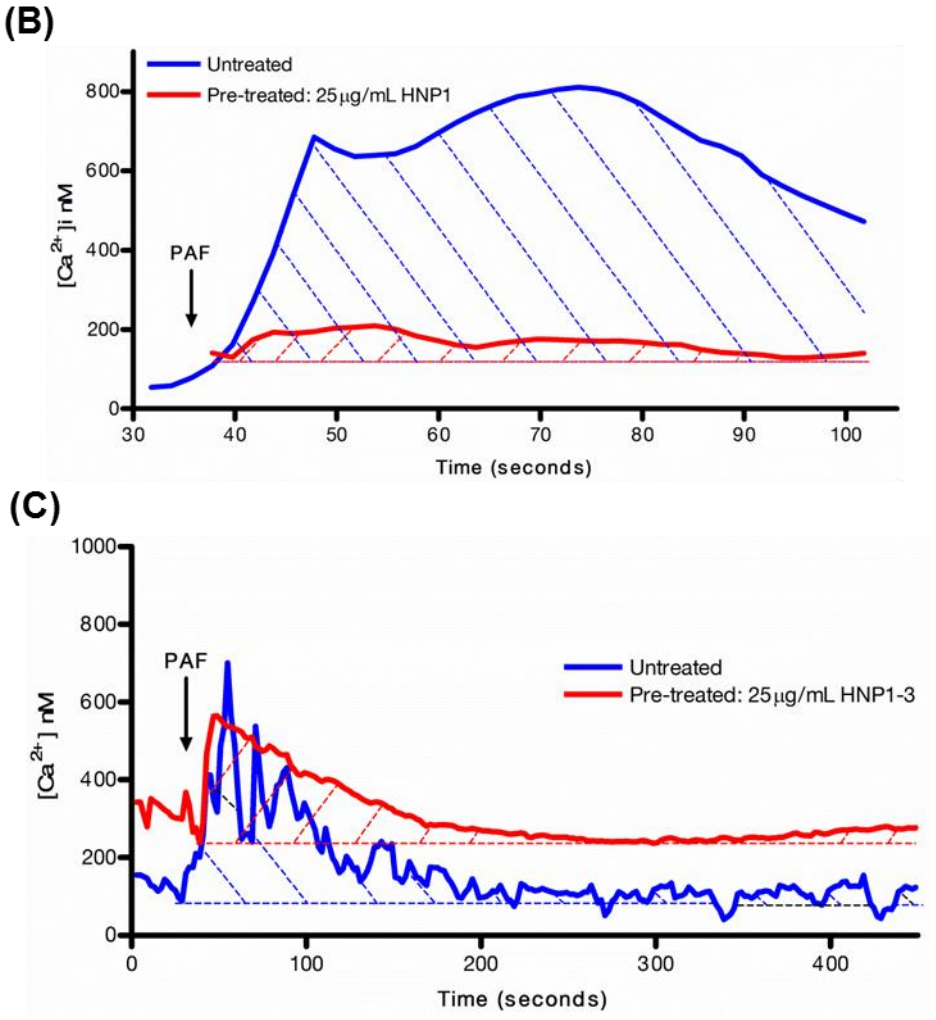

Figure B 3: Calcium mobilisation in HNP treated HMDMs (with external Ca2+ ions)

(**B** and **C**) Two repeat experiments of Figure 4.6. Calcium flux was induced using 1μM Platelet-Activating Factor (PAF) on buffy coat HMDMs treated overnight with HNP in Ca^{2+}-containing HBSS buffer. Cytoplasmic calcium was measured in real-time and total amounts were calculated using the area under each curve (See Table 4.2.1).

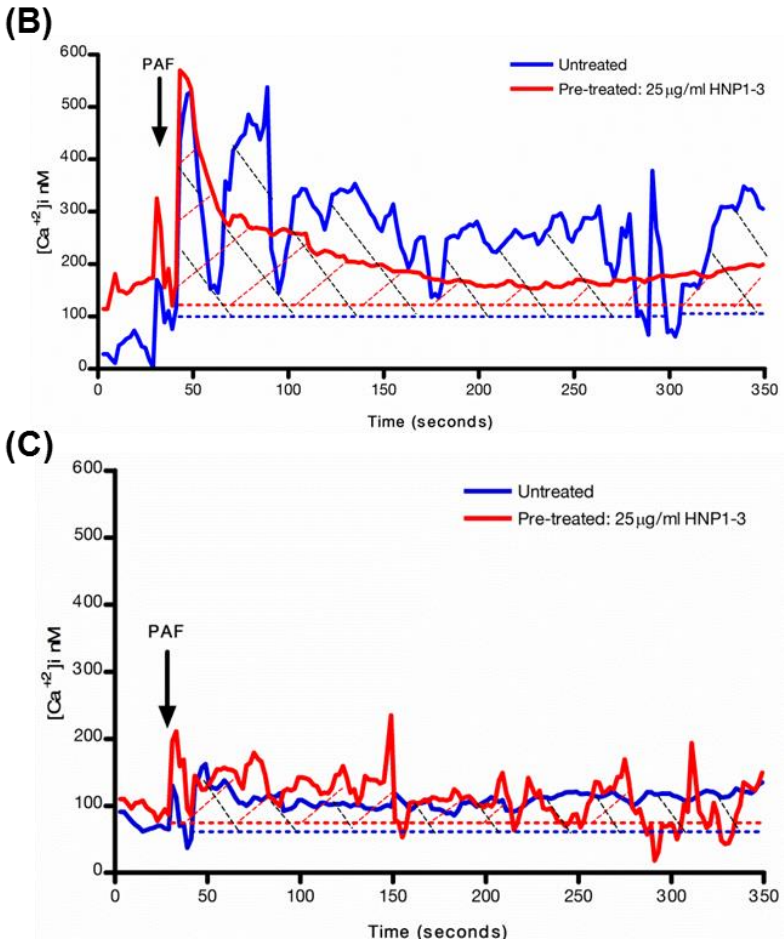

Figure B 4: Calcium mobilisation in HNP treated HMDMs (without external Ca2+ ions)

Calcium flux was induced using 1µM Platelet-Activating Factor (PAF) on buffy coat HMDMs treated overnight with HNP in HBSS buffer free of Ca^{2+} ions. Cytoplasmic calcium was measured in real-time and total amounts were calculated using the area under each curve for all three independent experiments.

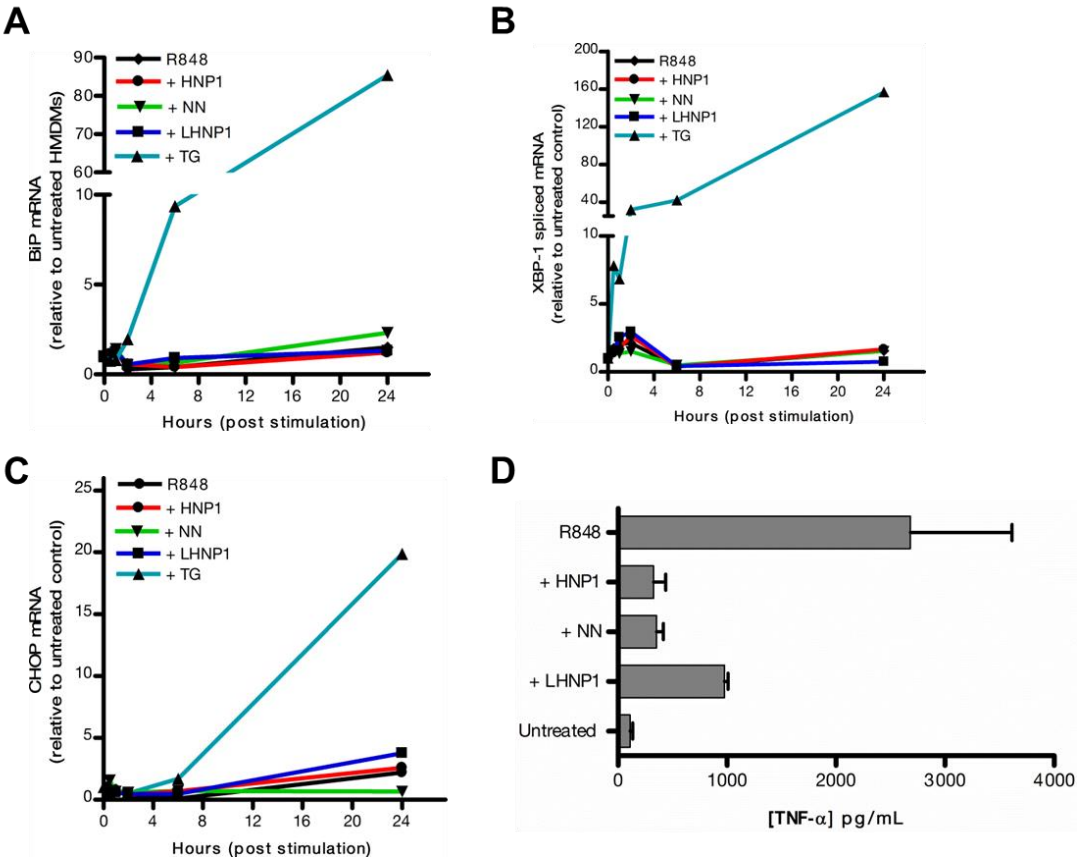

Figure B 5: Gene expression of ER stress markers BiP, spliced XBP-1 and CHOP with α-defensins (Run2)

Repeat of Figure 4.14 with BiP (**A**), spliced XBP-1 (**B**) and (**C**) CHOP mRNA expression normalised to basal levels in untreated cells. Buffy coat HMDMs were stimulated with R848 alone or in co-culture with 25% NN, 12.5µg/mL HNP1, LHNP1, or 1uM thapsigargin. (**D**) Secreted TNF-α quantified by ELISA at 24hrs. Error bars represent the mean ± SD of samples performed in triplicate. Results co-performed in conjunction with the Professor Pieter Hiemstra research lab (Leiden University, The Netherlands).

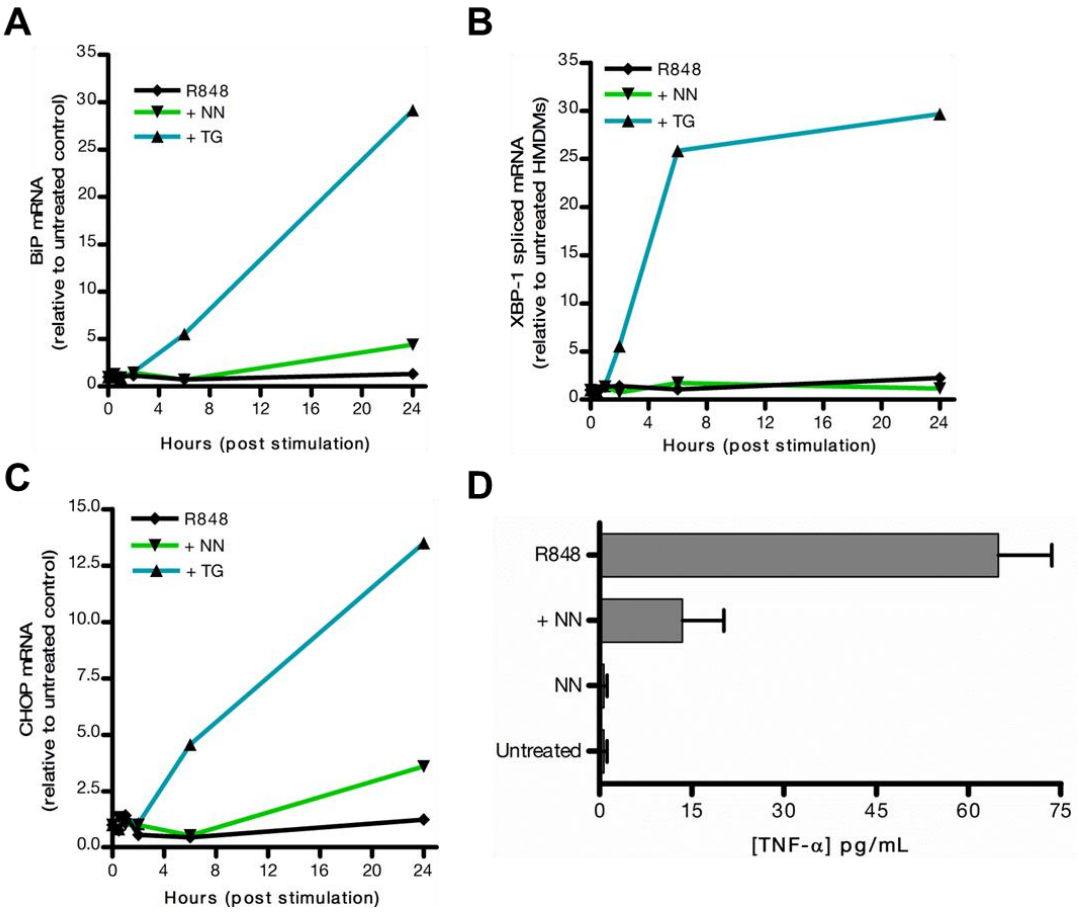

Figure B 6: Gene expression of ER stress markers BiP, spliced XBP-1 and CHOP with α-defensins (Run3)

A repeat of Figure 4.14: qPCR quantitation over 24hrs of ER stress markers BiP (**A**), spliced XBP-1 (**B**) and (**C**) CHOP normalised to basal levels in untreated cells. Buffy coat HMDMs were stimulated with 2.5µg/mL R848 either alone or in co-culture with 25% NN or 100nM thapsigargin as a positive control. (**D**) Quantitated secreted TNF-α by ELISA at 24hrs. Values obtained are from triplicate repeats for all samples with mean ± SD for error bars. Results co-performed in conjunction with the Professor Pieter Hiemstra research lab (Leiden University, The Netherlands).

Chemically-induced calcium manipulations in α-defensin treated HMDMs

Bryostatin-1 does not rescue TNF-α secretion in defensin-treated HMDMs

Around the same period in the research, the inhibition of calcium mobilisation with HNP was linked to the ongoing debate as to whether TNF-α mRNA stability was accountable for the inhibition of the secreted cytokine. It was postulated that there perhaps was a link between irregular calcium levels in HNP-treated HMDMs and the rapid decline in TNF-α mRNA (Chapter 3, section 3.2.3). The family of kinase enzymes known as Protein Kinase C (PKC) form part of the AGC kinase group, one of eight super-kinase families within the cell[186]. PKC enzymes are important mediators of the immune signalling response which direct cell growth, differentiation and gene expression. One PKC mediated signalling pathway is the Mitogen Activated Pathway (MAPK) which regulates cytokine gene expression. The conventional PKC isoforms (PKCα and β) require calcium alongside cell membrane-bound Diacylglycerol (DAG) for full enzymatic activity. This isoform has previously been implicated in mRNA stability by regulating the shuttling of the stimulus-dependant mRNA stabilizing factor HuR from the nucleus to the cytoplasm[187]. HuR forms part of the embryonic lethal abnormal vision (ELAV) protein family which act by binding to the 3'-untranslated mRNA regions, preventing their degradation by *trans*-acting destabilizing factors[188].

The hypothesis was that decreased calcium mobilisation through the actions of α-defensins may result in incomplete cPKC activation. This could imply a decrease in TNF-α mRNA stability, possibly mediated by limited or no HuR shuttling into the cytoplasm. To establish if PKC activation could reverse TNF-α mRNA stability and restore secreted cytokine in α-defensin treated HMDMs, the macrolactone Bryostatin-1 was used to artificially activate PKC.

For this buffy coat HMDMs were pretreated with bryostatin-1 at 5nM (Figure B 7) and 10nM (Figure B 8) for 30min. Cells were then stimulated with R848 alone or together with 12.5μg/mL HNP1, LHNP1, or 25% NN for 24hrs and TNF-α ELISA performed on the supernatants.

Secreted TNF-α in stimulated HMDMs with HNP1 treatment remained attenuated in bryostatin-1 pretreated HMDMs at both time points, with inhibition similar to that observed in cells that were not pretreated with bryostatin-1. Stimulated cells with 25% NN showed partial TNF-α inhibition at 4hrs which became largely inhibited at 24hrs incubation, again being similar to controls that were not pretreated with bryostatin-1. Linearised HNP1 (LHNP1) again had no effect on TNF-α secretion. Levels of TNF-α secreted were approximately doubled with Bryostatin-1 pre-treatment compared to their untreated alternatives, suggesting a priming of the PKC/MAPK pathway prior to the inhibitory actions of α-defensins ensued.

This result suggests that although PKC activation is linked to enhanced TNF-α production, this activation alone is not sufficient to rescue the effects of α-defensins. It was discovered in retrospect that α-defensins inhibit PKC activity by direct binding[152,189,190]. This direct binding effect could neutralise PKC activation by Bryostatin-1. Thus future PKC activity studies in macrophages would look to address how α-defensin-mediated PKC inhibition might affect downstream signal transduction pathways (if at all).

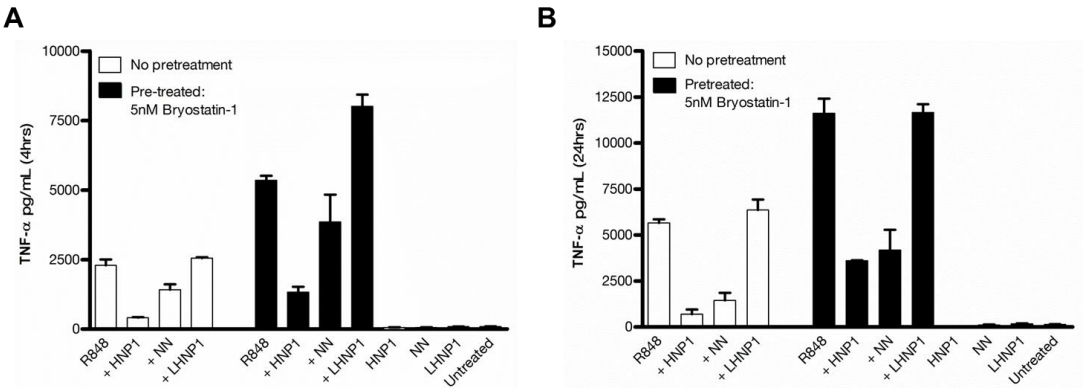

Figure B 7: The anti-inflammatory effect of α-defensin on HMDMs pretreated with 5nM Bryostatin 1

Secreted TNF-α of buffy coat HMDMs stimulated with 2.5μg/mL R848 alone or in the presence of 12.5μg/mL HNP1, LHNP1 or 25% NN and quantitated by ELISA at 4hrs (**A**) and 24hrs (**B**) alongside unstimulated controls. Results represent the mean ± SEM of two independent experiments.

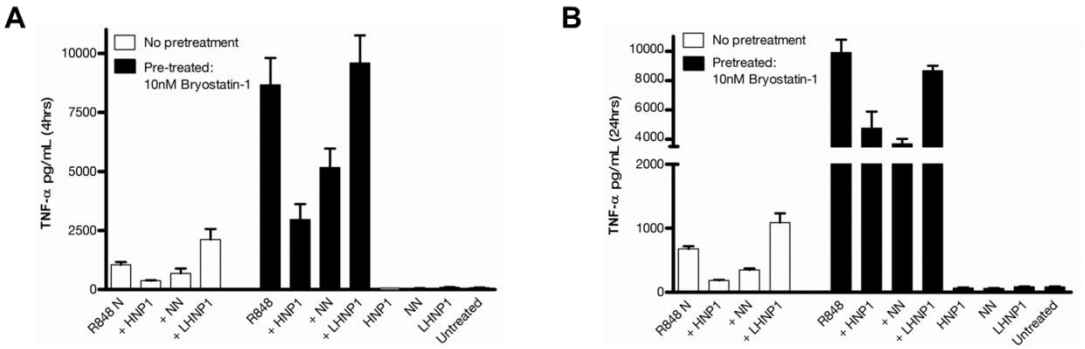

Figure B 8: The anti-inflammatory effect of α-defensin on HMDMs pretreated with 10nM Bryostatin 1

Secreted TNF-α of buffy coat HMDMs stimulated with 2.5μg/mL R848 alone or in the presence of 25μg/mL HNP1, LHNP1 or 25% NN and quantitated by ELISA at 4hrs (**A**) and 24hrs (**B**) alongside unstimulated controls. Results represent the mean ± SD of one experiment.

Artificial calcium replacement enhances inhibitory effect of α-defensins

Up to this point, two clear patterns were beginning to emerge on the cell biology of α-defensin treated macrophages; proteins synthesis was being inhibited and cells were displaying irregular calcium mobilisation regulation. These two symptoms were suggestive of the most common diagnosis, endoplasmic reticulum stress. The emerging hypothesis was that, through irregular intracellular calcium homeostasis, the optimal functioning of the ultra-sensitive endoplasmic reticulum was impaired resulting in the possible accumulation of unfolded or misfolded proteins. If ER stress was implicated, it would explain the reduction in translation as the cell undergoes a rescue response termed the Unfolded Protein Response (UPR) pathway. In an attempt to reverse this process, calcium was artificially introduced into these α-defensin treated HMDMs by way of a calcium ionophore (the name of which remains undisclosed due to potential patent application violations).

Figure B 9 shows the first attempt at rescuing the inhibitory effect of 25% NN in R848 stimulated buffy coat HMDMs with ionophore at 10μM. The results were in direct contrast to what was anticipated; the ionophore synergistically inhibited secreted TNF-α, IL-6 and IL-8 with NN after 18hrs incubation and on its own the inhibitory effects were similar to NN (albeit different in mechanism).

The effect of the ionophore was also tried at a concentration of 20μM. As an added control for the effects of calcium-mediated inhibition, culture media chelated of calcium with 1mM EGTA was used (Figure B 10). The inhibitory effects of NN, calcium ionophore, and the synergistic effects of the two were confirmed in two HMDMs donors after 24hrs incubation stimulated with R848. The inhibitory effects of the ionophore were, however, partially prevented in calcium-depleted culture media. The inability to completely restore pro-inflammatory potential in these cells was possibly due to incomplete calcium chelation (i.e. higher EGTA concentrations were required) or due to the influx of other cations which this ionophore is known to transport to a lesser extent (magnesium). The delicate balance of calcium homeostasis was further highlighted as EGTA on its own had a mild inhibitory effect on stimulated HMDMs. This is possibly attributed to the efflux of calcium from intracellular stores, also resulting in a calcium imbalance.

Since it was observed that basal levels of calcium were higher after 24hrs in HNP treated HMDMs compared to controls (Figure 4.6), it was thought that this elevated calcium concentration might be the catalyst to the downstream effects of calcium homeostasis and protein synthesis. In an attempt to prevent this increase in calcium brought on by α-defensin treatment, R848 stimulated HMDMs were treated with 12.5μg/mL HNP1 or LHNP1 in culture media depleted of calcium (using 1mM EGTA) and compared to HMDMs in conventional culture media over 24hrs (Figure B 11). Results show that calcium depletion had no reverse effect on the inhibitory actions of α-defensins, with only a mild recovery of secreted TNF-α in ionophore-treated control cells as a comparison.

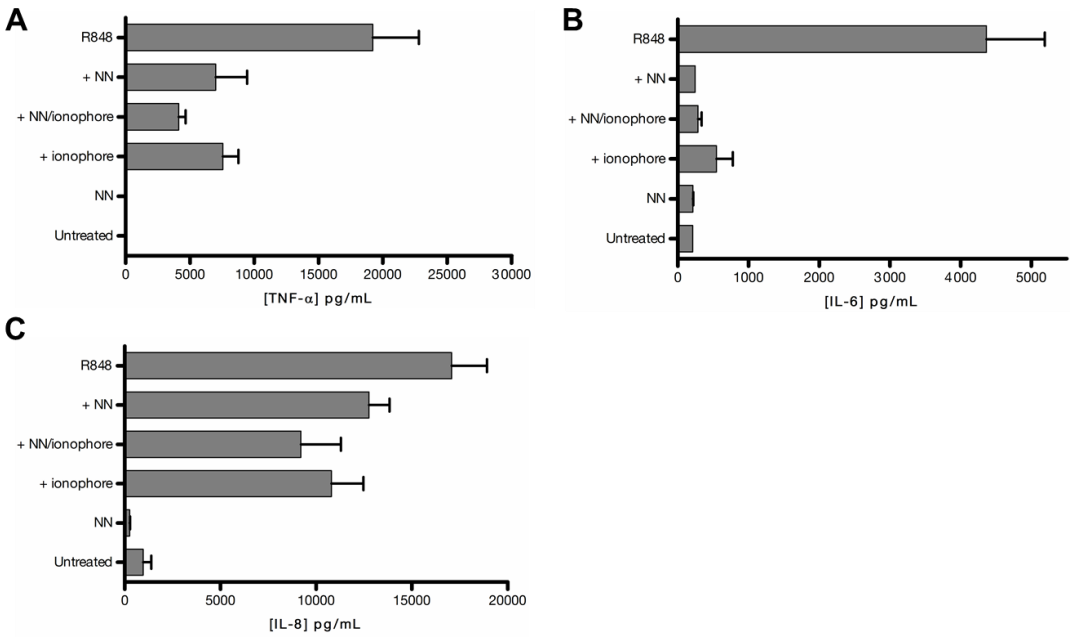

Figure B 9: Treatment of NN-treated HMDMs with a calcium ionophore (Run1)

Quantitated secreted TNF-α (**A**), IL-6 (**B**) and IL-8 (**C**) at 18hrs of R848-stimulated buffy coat HMDMs in co-culture with NN (25%), 10µM calcium ionophore (ionophore), or in combination. Untreated and NN controls were included. Results represent the mean ± SD of one experiment.

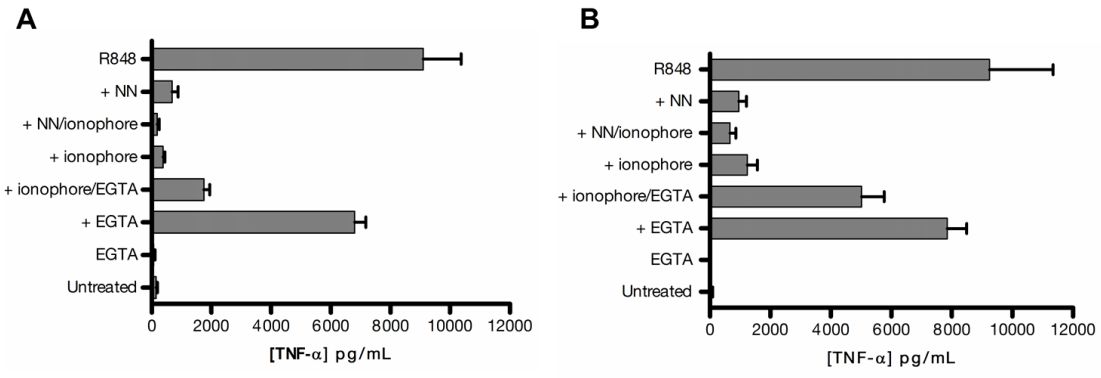

Figure B 10: Treatment of NN-treated HMDMs with a calcium ionophore (Run2)

Secreted TNF-α at 24hrs of buffy coat HMDM from two donors (**A** and **B**) stimulated with R848 in the presence of either 25% NN, 20µM calcium ionophore (ionophore), or in combination. EGTA (1mM) was added to stimulated cells treated with ionophore as a control. Negative controls included EGTA alone samples and untreated cells. Error bars represent the mean ± SD.

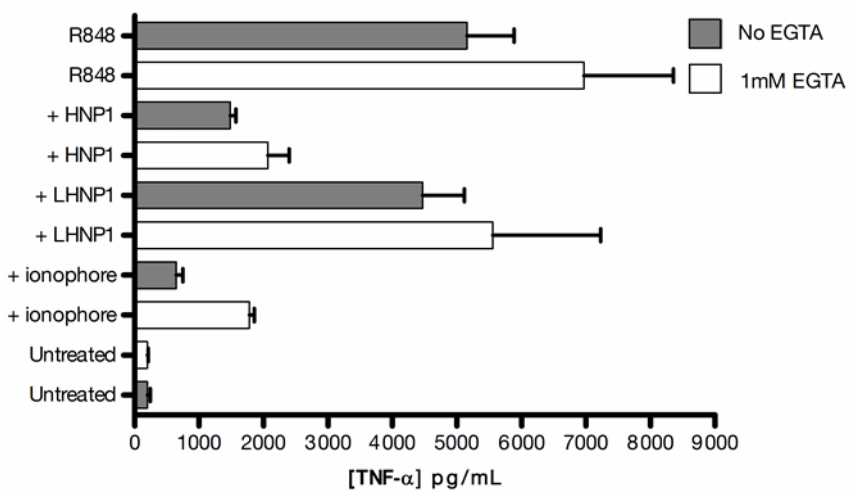

Figure B 11: EGTA addition in HNP1 treated HMDMs

TNF-α values quantitated by ELISA after 24hrs incubation of 2.5μg/mL R848 stimulated buffy coat HMDMs with 12.5μg/mL HNP1, LHNP1 or 10μM calcium ionophore (ionophore) in IMDM media with or without 1mM EGTA. Untreated controls for both media conditions were included. Error bars represent the mean ± SD of a single experiment.

The activation of L-type calcium channels does not rescue NN inhibitory effect

Since calcium influx was stunted in α-defensin-treated HMDMs upon plate-activating factor, it was thought that α-defensins might have impaired the opening of outer membrane dihydropyridine-sensitive calcium channels, also known as termed L-type calcium channels. It was postulated that, if impaired calcium channels are linked to the inhibitory effects of α-defensins on secreted TNF-α, could the chemically-induced opening of this channel restore HMDM function. This study was likened to the blocking of the L-type calcium channel in peripheral blood-derived human dendritic cells by exogenous human immunodeficiency virus, type 1 Tat protein[191]. By the addition of dihydropyridine calcium channel agonist, Bay K8644 (100nM), inhibition of IL-12 and apoptotic body engulfment was reversed in these dendritic cells.

In the first of these experiments, HMDMs were R848 stimulated and simultaneously treated with 25% NN either alone or with 1μM Bay K8644 for 24hrs (Figure B 12*A*). As an added control, external calcium concentration was increased with the addition of 1mM $CaCl_2$. Results from a single experiment showed no reversal in the inhibitory actions of NN on secreted TNF-α. To pre-empt the potential inhibition of L-type calcium channels by α-defensins, the next experiment allowed for the pretreatment of HMDMs with Bay K8644 4hrs prior to stimulation and 25% NN addition (Figure B 12*B*). There remained no reversal of the inhibitory actions of NN when compared to control cells that did not receive Bay K8644 pretreatment. In these limited experiments, no implication could be made on the connection between α-defensins and impaired calcium channel function. Although the positive effect of Bay K8644 was observed in other leukocytes obtained from human peripheral blood[191], no validation experiments were performed to confirm their activity on HMDMs. The use of Fura-2/AM within Bay K8644 treated cells could have been one such validation method to quantitate enhanced calcium uptake using this dihydropyridine.

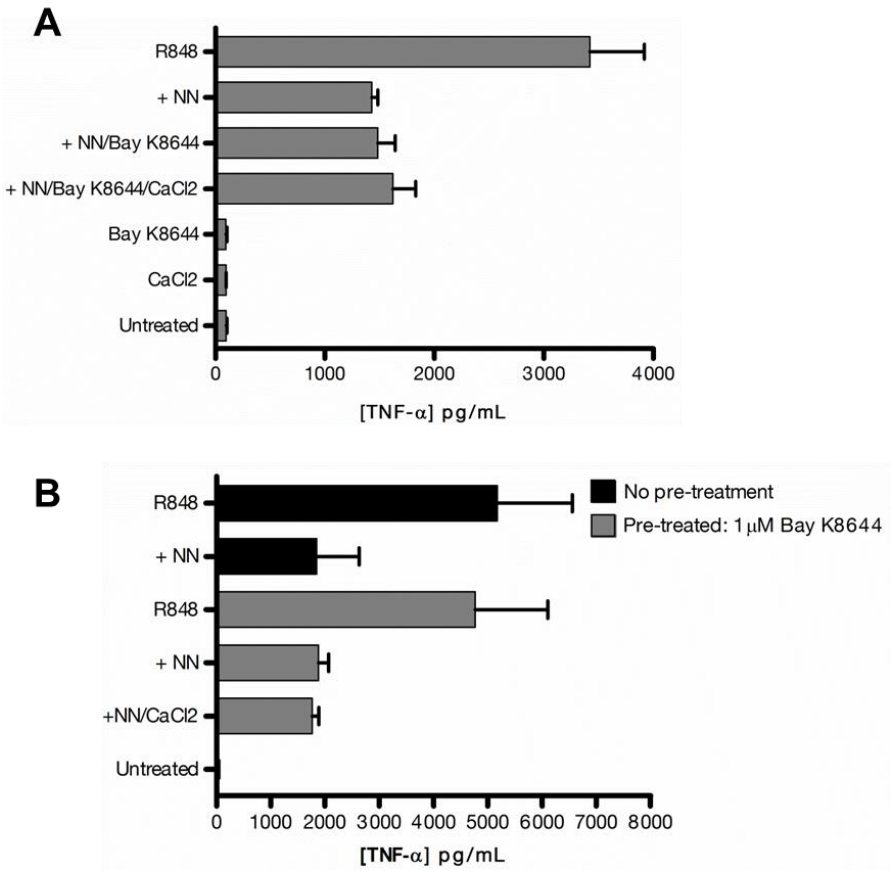

Figure B 12: The effect of calcium channel agonist Bay K8644 in NN-treated HMDMs

Secreted TNF-α quantified by buffy coat ELISA after 24hrs.(**A**) R848 stimulated HMDMs co-cultured with 25% NN, 1μM Bay K8644 or both. 1mM $CaCl_2$ was added in a separate test sample. (**B**) HMDMs pre-incubated with Bay K8644 (30min) prior to stimulation in co-culture with 25% NN alone or 1mM $CaCl_2$. Results represent the mean ± SD of one experiment.

Appendix C

Techniques addressing molecular interactions failed to confirm HNP1/rps20 binding

The confocal data gave a suggestion of HNP1/rps20 aggregate formation in HMDMs, particularly after 24hrs treatment. As evidential as this data was, it did not conclusively prove HNP1 binding to ribosomes. With limited time restrictions on the remaining research period, considerations turned to performing downstream molecular techniques in order to provide greater evidence of a binding event. Two approaches were taken to address this question.

Firstly, it was decided to utilize the system that provided the strongest results of HNP1-mediate translation inhibition, specifically the *in vitro* translation assay. Using 25µg/mL HNP1 and W26A treated rabbit reticulocytes as before, the protocol was modified to separate out and detect ribosomes using sucrose density ultracentrifugation as performed for polysome analysis. Following manual fractionation of centrifuged sucrose gradients, RNA extraction (by TRIzol method) and subsequent agarose electrophoresis meant it was possible to identify the rRNA-containing fractions (Figure C 1*A*). The residual organic phase from the TRIzol extraction process corresponding to the rRNA-containing fractions were pooled in order to perform protein precipitation and subsequent SDS-PAGE and Western blotting to positively identify the presence of HNP1 (Figure C 1*B*). Details on the methodology can be found in Chapter, section 2.15.

Resulting Western blots were unable to detect the presence of HNP1 or W26A in both rRNA-containing fractions (F6-10) and fractions which did not contain rRNA (F1-5). As a positive control for the detection of both HNP1 and W26A by Western blotting, amounts of pure peptide corresponding to the starting amount added to reticulocyte mixtures were added alongside test samples for electrophoresis (Figure C 1*C*). Monoclonal mouse anti-HNP1-3 antibody confirmed the positive immuno-detection of both peptide forms. Antibody sensitivity for both HNP1 and W26A was performed using titrated amounts of pure peptides, which displayed sensitivity down to 20ng by Western blotting.

Since neither fractions pooled were able to detect any peptide, this assay was not able to provide any further positive identification of HNP1 association with ribosomes. The most likely cause could be attributed to the unrefined protein precipitation method described for purifying proteins from TRIzol extraction, possibly losing peptide during the extraction process. Alternative methods considered included protein purification by dialysis. Factoring in the starting microgram amounts of peptide, this method would have been too cumbersome to effectively process and identify HNP1/W26A.

The second method attempted to prove HNP1-ribosome binding was by immunoprecipitation (IP). In this experiment (which was attempted twice without success) the rabbit reticulocyte system was again utilized to perform an *in vitro* translation as previously performed in Chapter 5 (section 5.2.1). After 90min incubation with 25μg/mL HNP1, W26A or vehicle control samples (performed in duplicate for each samples), rabbit reticulocyte mixtures were incubated in IP reaction buffer (detailed methodology described in Chapter 2, section 2.10.6). For duplicate samples, mixtures either contained 500ng anti-HNP1-3 antibody or an $IgG_{1,\kappa}$ isotype control antibody which were incubated for 2hrs prior to the addition of Protein G sepharose beads and subsequent overnight incubation. Following Protein G bead washing and purification by centrifugation, boiled bead samples were electrophoresed alongside eluents from the first washing stage, of which a portion of the volume was protein precipitated corresponding to ~0.5μL of pure rabbit reticulocyte lysate. The inclusion of the eluent was to ideally to determine the fraction of rps20 'pulled-down' by HNP1 bound to Protein G beads relative to residual the amount of rsp20 remaining in the lysate.

SDS-PAGE and Western blotting for rps20 (~13kDa) was unable to detect ribosomes in the purified bead fractions (Figure C 2*A-i*). The secondary antibody detected non-specific bands on the blot, which was unusual considering that a Cleanblot reagent was used designed specifically for IP assays to detect native primary antibody conformations (i.e. the primary antibody to rps20 immunoblotted for) as opposed to denatured antibody used in the pull-down stage of the assay. This was contrary to the

preceding validation assay using Cleanblot which successfully detected titrated amounts of pure reticulocyte lysate following immunoblotting using anti-rps20 primary antibody (Figure C 2*B*). It is possible that the polyclonal anti-rps20 primary antibody could have non-specifically bound to the high amounts of IgG used in the pull-down stage and this would require further optimisation. Eluted volumes from the bead washing step, equivalent to 0.5µL of pure rabbit reticulocyte were unable to be detected (Figure C 2*A-ii*). In addition, both blots contained a positive control sample of 0.5µL pure reticulocyte lysate included for Western blotting which failed to be completely detected. This indicated an overall error with the experiment which required further optimisation and repeating.

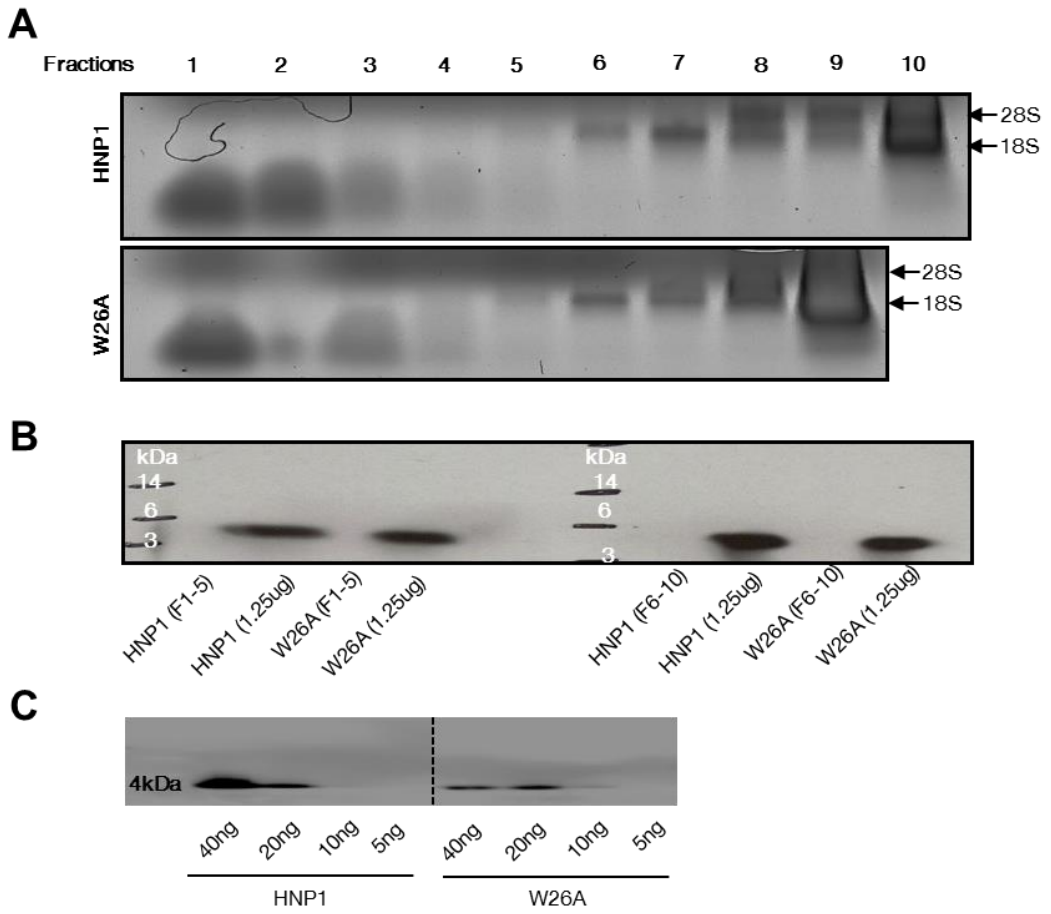

Figure C 1: Detection of HNP1 in sucrose density gradient centrifugation assay

Collected fractions post sucrose density ultracentrifugation of rabbit reticulocyte lysates treated with 25µg/mL HNP1 or W26A and processed using TRIzol extraction.

(**A**) RNA agarose electrophoresis of collected fractions. Increasing sucrose density resulted in the presence of 28S- and 18S rRNA (fractions 6-10).

(**B**) By-product volumes from RNA extraction process containing proteins were processed by pooling volumes from rRNA-containing fractions (F6-10) and fractions without (F1-5). Proteins were precipitated, electrophoresed (12% SDS-PAGE) and immunoblotted using anti-HNP1-3 antibody. Original assay amounts of peptides were included as controls positive detection of peptides (1.25µg).

(**C**) Antibody validation assay by Western blotting of titrated HNP1 and W26A using anti-HNP1-3 antibody.

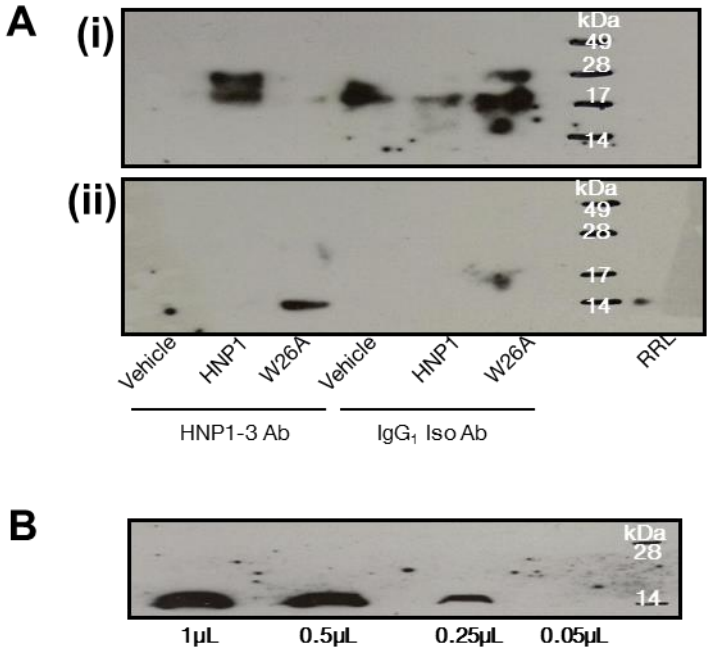

Figure C 2: Rps20 expression by western blotting following immunoprecipitation

(**A**) Western blot results for ribosomal protein S20 expression in rabbit retic lysates treated with 25µg/mL HNP1 or W26A as per *in vitro* translation protocol. Following immunoprecipitation bead-depleted fractions were electrophoresed by 12% SDS-PAGE (**i**). Supernatant volumes separated from bead fractions were also electrophoresed, with volumes loaded equivalent to 0.5µL of pure rabbit reticulocyte lysate (**ii**). A positive control lane was added for the detection of rps20 in RRL, with 0.5µL of pure rabbit reticulocyte lysate added (RRL).

(**B**) Validation of rps20 detection using titrated volumes of rabbit reticulocyte lysate.

References

1. Nathan C. Points of control in inflammation. *Nature.* 2002;420(6917):846-852.

2. Office NA. Health and social care - Services for people with rheumatoid arthritis. 15 July 2009. http://www.nao.org.uk/report/services-for-people-with-rheumatoid-arthritis/. Accessed 24 July 2013.

3. Medzhitov R. Toll-like receptors and innate immunity. *Nature Reviews Immunology.* 2001;1(2):135-145.

4. Hoffmann JA, Kafatos FC, Janeway CA, Ezekowitz RAB. Phylogenetic Perspectives in Innate Immunity. *Science.* 1999;284(5418):1313-1318.

5. Geering B, Stoeckle C, Conus S, Simon H-U. Living and dying for inflammation: neutrophils, eosinophils, basophils. *Trends in Immunology.* 2013.

6. Zhang Q, Raoof M, Chen Y, Sumi Y, Sursal T, Junger W, Brohi K, Itagaki K, Hauser CJ. Circulating mitochondrial DAMPs cause inflammatory responses to injury. *Nature.* 2010;464(7285):104-107.

7. Garg AD, Nowis D, Golab J, Vandenabeele P, Krysko DV, Agostinis P. Immunogenic cell death, DAMPs and anticancer therapeutics: An emerging amalgamation. *Biochimica et Biophysica Acta - Reviews on Cancer.* 2010;1805(1):53-71.

8. Luster AD. Chemokines — Chemotactic Cytokines That Mediate Inflammation. *New England Journal of Medicine.* 1998;338(7):436-445.

9. Ortega-Gómez A, Perretti M, Soehnlein O. Resolution of inflammation: an integrated view. *EMBO Molecular Medicine.* 2013;5(5):661-674.

10. Cowland JB, Borregaard N. Isolation of neutrophil precursors from bone marrow for biochemical and transcriptional analysis. *Journal of Immunological Methods.* 1999;232(1–2):191-200.

11. Pillay J, den Braber I, Vrisekoop N, Kwast LM, de Boer RJ, Borghans JAM, Tesselaar K, Koenderman L. In vivo labeling with 2H2O reveals a human neutrophil lifespan of 5.4 days. *Blood.* 2010;116(4):625-627.

12. Dale DC, Boxer L, Liles WC. The phagocytes: neutrophils and monocytes. *Blood.* 2008;112(4):935-945.

13. Muller WA. Leukocyte-endothelial cell interactions in the inflammatory response. *Laboratory Investigation; A Journal Of Technical Methods And Pathology.* 2002;82(5):521-533.

14. Nathan CF. Neutrophil activation on biological surfaces. Massive secretion of hydrogen peroxide in response to products of macrophages and lymphocytes. *The Journal of Clinical Investigation.* 1987;80(6):1550-1560.

15. Baggiolini M, Clark-Lewis I. Interleukin-8, a chemotactic and inflammatory cytokine. *FEBS Letters.* 1992;307(1):97-101.

16. Timár C, Lőrincz Á, Ligeti E. Changing world of neutrophils. *Pflugers Arch - Eur J Physiol.* 2013:1-13.

17. Nagaoka I, Tamura H, Hirata M. An Antimicrobial Cathelicidin Peptide, Human CAP18/LL-37, Suppresses Neutrophil Apoptosis via the Activation of Formyl-Peptide Receptor-Like 1 and P2X7. *The Journal of Immunology.* 2006;176(5):3044-3052.

18. Bowdish DME, Davidson DJ, Speert DP, Hancock REW. The Human Cationic Peptide LL-37 Induces Activation of the Extracellular Signal-

Regulated Kinase and p38 Kinase Pathways in Primary Human Monocytes. *The Journal of Immunology.* 2004;172(6):3758-3765.

19. Yang D, Chen Q, Schmidt AP, Anderson GM, Wang JM, Wooters J, Oppenheim JJ, Chertov O. LL-37, the Neutrophil Granule – And Epithelial Cell – Derived Cathelicidin, Utilizes Formyl Peptide Receptor–Like 1 (Fprl1) as a Receptor to Chemoattract Human Peripheral Blood Neutrophils, Monocytes, and T Cells. *The Journal of Experimental Medicine.* 2000;192(7):1069-1074.

20. Jaillon S, Peri G, Delneste Y, Frémaux I, Doni A, Moalli F, Garlanda C, Romani L, Gascan H, Bellocchio S, Bozza S, Cassatella MA, Jeannin P, Mantovani A. The humoral pattern recognition receptor PTX3 is stored in neutrophil granules and localizes in extracellular traps. *The Journal of Experimental Medicine.* 2007;204(4):793-804.

21. Bournazou I, Pound JD, Duffin R, Bournazos S, Melville LA, Brown SB, Rossi AG, Gregory CD. Apoptotic human cells inhibit migration of granulocytes via release of lactoferrin. *The Journal of Clinical Investigation.* 2009;119(1):20-32.

22. Rotondo R, Bertolotto M, Barisione G, Astigiano S, Mandruzzato S, Ottonello L, Dallegri F, Bronte V, Ferrini S, Barbieri O. Exocytosis of azurophil and arginase 1-containing granules by activated polymorphonuclear neutrophils is required to inhibit T lymphocyte proliferation. *Journal of Leukocyte Biology.* 2011;89(5):721-727.

23. Cassatella MA. The production of cytokines by polymorphonuclear neutrophils. *Immunology Today.* 1995;16(1):21-26.

24. Mantovani A, Cassatella MA, Costantini C, Jaillon S. Neutrophils in the activation and regulation of innate and adaptive immunity. *Nature Reviews Immunology.* 2011;11(8):519-531.

25. Hamilton T, Li X, Novotny M, Pavicic PG, Datta S, Zhao C, Hartupee J, Sun D. Cell type- and stimulus-specific mechanisms for post-transcriptional control of neutrophil chemokine gene expression. *Journal of Leukocyte Biology.* 2012;91(3):377-383.

26. Seko Y. The role of cytokine mRNA stability in the pathogenesis of autoimmune disease. *Autoimmunity Reviews.* 2006;5:299 - 305.

27. Scapini P, Bazzoni F, Cassatella MA. Regulation of B-cell-activating factor (BAFF)/B lymphocyte stimulator (BLyS) expression in human neutrophils. *Immunology Letters.* 2008;116(1):1-6.

28. Brinkmann V, Reichard U, Goosmann C, Fauler B, Uhlemann Y, Weiss DS, Weinrauch Y, Zychlinsky A. Neutrophil extracellular traps kill bacteria. *Science (New York, N.Y.).* 2004;303(5663):1532-1535.

29. Simon D, Simon HU, Yousefi S. Extracellular DNA traps in allergic, infectious, and autoimmune diseases. *Allergy.* 2013;68(4):409-416.

30. Garcia-Romo GS, Caielli S, Vega B, Connolly J, Allantaz F, Xu Z, Punaro M, Baisch J, Guiducci C, Coffman RL, Barrat FJ, Banchereau J, Pascual V. Netting Neutrophils Are Major Inducers of Type I IFN Production in Pediatric Systemic Lupus Erythematosus. *Science Translational Medicine.* 2011;3(73):73ra20.

31. Théry C, Ostrowski M, Segura E. Membrane vesicles as conveyors of immune responses. *Nature Reviews Immunology.* 2009;9:581 - 593.

32. György B, Szabó T, Pásztói M, Pál Z, Misják P, Aradi B, László V, Pállinger É, Pap E, Kittel Á, Nagy G, Falus A, Buzás E. Membrane vesicles, current state-of-the-art: emerging role of extracellular vesicles. *Cell. Mol. Life Sci.* 2011;68(16):2667-2688.

33. Hong Y, Eleftheriou D, Hussain AAK, Price-Kuehne FE, Savage CO, Jayne D, Little MA, Salama AD, Klein NJ, Brogan PA. Anti-Neutrophil Cytoplasmic Antibodies Stimulate Release of Neutrophil Microparticles. *Journal of the American Society of Nephrology.* 2012;23(1):49-62.

34. Boxer LA. How to approach neutropenia. *ASH Education Program Book.* 2012;2012(1):174-182.

35. Schmidt S, Moser M, Sperandio M. The molecular basis of leukocyte recruitment and its deficiencies. *Molecular Immunology.* 2013;55(1):49-58.

36. Kuijpers T, Lutter R. Inflammation and repeated infections in CGD: two sides of a coin. *Cell. Mol. Life Sci.* 2012;69(1):7-15.

37. Ganz T, Lehrer RI. Antimicrobial peptides of vertebrates. *Current Opinion in Immunology.* 1998;10(1):41-44.

38. Lehrer RI, Lu W. α-Defensins in human innate immunity. *Immunological Reviews.* 2011;245(1):84-112.

39. Ganz T. Defensins: Antimicrobial peptides of innate immunity. *Nature Reviews.* 2003;3.

40. Zhao C, Wang I, Lehrer RI. Widespread expression of beta-defensin hBD-1 in human secretory glands and epithelial cells. *FEBS Letters.* 1996;396(2-3):319-322.

41. Das S, Nikolaidis N, Goto H, McCallister C, Li J, Hirano M, Cooper MD. Comparative Genomics and Evolution of the Alpha-Defensin Multigene Family in Primates. *Molecular Biology and Evolution.* 2010;27(10):2333-2343.

42. Liu L, Zhao C, Heng HHQ, Ganz T. The Human β-Defensin-1 and α-Defensins Are Encoded by Adjacent Genes: Two Peptide Families with Differing Disulfide Topology Share a Common Ancestry. *Genomics.* 1997;43(3):316-320.

43. Zhao L, Tolbert WD, Ericksen B, Zhan C, Wu X, Yuan W, Li X, Pazgier M, Lu W. Single, Double and Quadruple Alanine Substitutions at Oligomeric Interfaces Identify Hydrophobicity as the Key Determinant of Human Neutrophil Alpha Defensin HNP1 Function. *PLoS ONE.* 2013;8(11):e78937.

44. Lehrer RI, Lichtenstein A, Ganz T. Defensins: Antimicrobial and Cytotoxic Peptides of Mammalian Cells. *Annual Review of Immunology.* 1993;11.

45. Fellermann K, Stange EF. Defensins - innate immunity at the epithelial frontier. *European Journal of Gastroenterology & Hepatology.* 2001;13(7):771-776.

46. Lehrer RI, Barton A, Daher KA, Harwig SS, Ganz T, Selsted ME. Interaction of human defensins with Escherichia coli. Mechanism of bactericidal activity. *The Journal of Clinical Investigation.* 1989;84(2):553-561.

47. Kagan BLS, M. E.; Ganz, T.; Lehrer; R.I. Antimicrobial defensin peptides form voltage-dependent ion-permeable channels in planar lipid bilayer membranes

Proceedings of the National Academy of Sciences U.S.A. 1990;87:210-214.

48. Rice W, Ganz T, Kinkade JJ, Selsted M, Lehrer R, Parmley R. Defensin-rich dense granules of human neutrophils. *Blood.* 1987;70(3):757-765.

49. Demirkhanyan LH, Marin M, Padilla-Parra S, Zhan C, Miyauchi K, Jean-Baptiste M, Novitskiy G, Lu W, Melikyan GB. Multifaceted Mechanisms of HIV-1 Entry Inhibition by Human α-Defensin. *Journal of Biological Chemistry.* 2012;287(34):28821-28838.

50. Lehrer RI, Jung G, Ruchala P, Andre S, Gabius HJ, Lu W. Multivalent Binding of Carbohydrates by the Human α-Defensin, HD5. *The Journal of Immunology.* 2009;183(1):480-490.

51. Doss M, White MR, Tecle T, Gantz D, Crouch EC, Jung G, Ruchala P, Waring AJ, Lehrer RI, Hartshorn KL. Interactions of α-, β-, and θ-Defensins with Influenza A Virus and Surfactant Protein D. *The Journal of Immunology.* 2009;182(12):7878-7887.

52. Smith JG, Silvestry M, Lindert S, Lu W, Nemerow GR, Stewart PL. Insight into the Mechanisms of Adenovirus Capsid Disassembly from Studies of Defensin Neutralization. *PLoS Pathog.* 2010;6(6):e1000959.

53. Lehrer RI, Jung G, Ruchala P, Wang W, Micewicz ED, Waring AJ, Gillespie EJ, Bradley KA, Ratner AJ, Rest RF, Lu W. Human α-Defensins Inhibit Hemolysis Mediated by Cholesterol-Dependent Cytolysins. *Infection and Immunity.* 2009;77(9):4028-4040.

54. Kim C, Gajendran N, Mittrücker H-W, Weiwad M, Song Y-H, Hurwitz R, Wilmanns M, Fischer G, Kaufmann SHE. Human α-defensins neutralize anthrax lethal toxin and protect against its fatal consequences. *Proceedings of*

the National Academy of Sciences of the United States of America. 2005;102(13):4830-4835.

55. Wei G, de Leeuw E, Pazgier M, Yuan W, Zou G, Wang J, Ericksen B, Lu W-Y, Lehrer RI, Lu W. Through the Looking Glass, Mechanistic Insights from Enantiomeric Human Defensins. *Journal of Biological Chemistry.* 2009;284(42):29180-29192.

56. Leeuw Ed, Li C, Zeng P, Li C, Buin MD-d, Lu W-Y, Breukink E, Lu W. Functional interaction of human neutrophil peptide-1 with the cell wall precursor lipid II. *FEBS Letters.* 2010;584(8):1543-1548.

57. de Leeuw E, Burks SR, Li X, Kao JPY, Lu W. Structure-dependent functional properties of human defensin 5. *FEBS Letters.* 2007;581(3):515-520.

58. Wei G, Pazgier M, de Leeuw E, Rajabi M, Li J, Zou G, Jung G, Yuan W, Lu W-Y, Lehrer RI, Lu W. Trp-26 Imparts Functional Versatility to Human α-Defensin HNP1. *Journal of Biological Chemistry.* 2010;285(21):16275-16285.

59. Pazgier M, Wei G, Ericksen B, Jung G, Wu Z, de Leeuw E, Yuan W, Szmacinski H, Lu W-Y, Lubkowski J, Lehrer RI, Lu W. Sometimes it takes two to tango: Contributions of dimerization to functions of human α-defensin HNP1 peptide. *Journal of Biological Chemistry.* 2012;287(12):8944-8953.

60. van Furth R, Cohn ZA. The Origin and Kinetics of Mononuclear Phagocytes. *The Journal of Experimental Medicine.* 1968;128(3):415-435.

61. Romani N, Gruner S, Brang D, Kämpgen E, Lenz A, Trockenbacher B, Konwalinka G, Fritsch PO, Steinman RM, Schuler G. Proliferating dendritic

cell progenitors in human blood. *The Journal of Experimental Medicine.* 1994;180(1):83-93.

62. Mosser DME, J. P. Exploring the full spectrum of macrophage activation. *Nature Reviews.* 2008;8.

63. Chen C-J, Kono H, Golenbock D, Reed G, Akira S, Rock KL. Identification of a key pathway required for the sterile inflammatory response triggered by dying cells. *Nature Medicine.* 2007;13(7):851-856.

64. Rao KMK. MAP kinase activation in macrophages. *Journal of Leukocyte Biology.* 2001;69.

65. Huang Q. Differential regulation of interleukin 1 receptor and Toll-like receptor signaling by MEKK3. *NATURE IMMUNOLOGY.* 2003;5(1).

66. Mantovani A, Sica A, Sozzani S, Allavena P, Vecchi A, Locati M. The chemokine system in diverse forms of macrophage activation and polarization. *Trends in Immunology.* 2004;25(12):677-686.

67. Hesse M, Modolell M, La Flamme AC, Schito M, Fuentes JM, Cheever AW, Pearce EJ, Wynn TA. Differential Regulation of Nitric Oxide Synthase-2 and Arginase-1 by Type 1/Type 2 Cytokines In Vivo: Granulomatous Pathology Is Shaped by the Pattern of l-Arginine Metabolism. *The Journal of Immunology.* 2001;167(11):6533-6544.

68. Mosser DM, Edwards JP. Exploring the full spectrum of macrophage activation. *Nature Reviews. Immunology.* 2008;8(12):958-969.

69. McInnes IB, Schett G. The Pathogenesis of Rheumatoid Arthritis. *New England Journal of Medicine.* 2011;365(23):2205-2219.

70. McGeer PL, McGeer EG. The inflammatory response system of brain: Implications for therapy of Alzheimer and other neurodegenerative diseases. *Brain Res. Rev.* 1995;21(2):195-218.

71. Richardson VR, Smith KA, Carter AM. Adipose tissue inflammation: Feeding the development of type 2 diabetes mellitus. *Immunobiology.* 2013(0).

72. Hoffmann A, Xia Y, Verma IM. Inflammatory Tales of Liver Cancer. *Cancer Cell.* 2007;11(2):99-101.

73. Libby P, Ridker PM, Maseri A. Inflammation and Atherosclerosis. *Circulation.* 2002;105(9):1135-1143.

74. Levy BD, Clish CB, Schmidt B, Gronert K, Serhan CN. Lipid mediator class switching during acute inflammation: signals in resolution. *NATURE IMMUNOLOGY.* 2001;2(7):612-619.

75. Serhan CN. Novel Lipid Mediators and Resolution Mechanisms in Acute Inflammation: To Resolve or Not? *The American Journal of Pathology.* 2010;177(4):1576-1591.

76. Dalli J, Serhan CN. Specific lipid mediator signatures of human phagocytes: microparticles stimulate macrophage efferocytosis and pro-resolving mediators. *Blood.* 2012;120(15):e60-e72.

77. Henson PM, Hume DA. Apoptotic cell removal in development and tissue homeostasis. *Trends in Immunology.* 2006;27(5):244-250.

78. Savill J, Dransfield I, Gregory C, Haslett C. A blast from the past: clearance of apoptotic cells regulates immune responses. *Nat Rev Immunol.* 2002;2(12):965-975.

79. Fadok VA, Bratton DL, Konowal A, Freed PW, Westcott JY, Henson PM. Macrophages that have ingested apoptotic cells in vitro inhibit proinflammatory cytokine production through autocrine/paracrine mechanisms involving TGF-beta, PGE2, and PAF. *The Journal of Clinical Investigation.* 1998;101(4):890-898.

80. Perruche S, Zhang P, Liu Y, Saas P, Bluestone JA, Chen W. CD3-specific antibody-induced immune tolerance involves transforming growth factor-beta from phagocytes digesting apoptotic T cells. *Nature Medicine.* 2008;14(5):528-535.

81. Morelli AE, Larregina AT, Shufesky WJ, Zahorchak AF, Logar AJ, Papworth GD, Wang Z, Watkins SC, Falo LD, Thomson AW. Internalization of circulating apoptotic cells by splenic marginal zone dendritic cells: dependence on complement receptors and effect on cytokine production. *Blood.* 2003;101(2):611-620.

82. Ravichandran Kodi S. Beginnings of a Good Apoptotic Meal: The Find-Me and Eat-Me Signaling Pathways. *Immunity*. 2011;35(4):445-455.

83. Fadok VA, Bratton DL, Rose DM, Pearson A, Ezekewitz RAB, Henson PM. A receptor for phosphatidylserine-specifc clearance of apoptotic cells. *Nature*. 2000;405:85-90.

84. Fadok VA, Bratton DL, Guthrie L, Henson PM. Differential Effects of Apoptotic Versus Lysed Cells on Macrophage Production of Cytokines: Role of Proteases. *The Journal of Immunology.* 2001;166(11):6847-6854.

85. Mevorach D, Zhou JL, Song X, Elkon KB. Systemic Exposure to Irradiated Apoptotic Cells Induces Autoantibody Production. *The Journal of Experimental Medicine.* 1998;188(2):387-392.

86. Napirei M, Karsunky H, Zevnik B, Stephan H, Mannherz HG, Möröy T. Features of systemic lupus erythematosus in Dnase1-deficient mice. *Nature Genetics.* 2000;25(2):177-181.

87. Miles K, Clarke DJ, Lu W, Sibinska Z, Beaumont PE, Davidson DJ, Barr TA, Campopiano DJ, Gray M. Dying and Necrotic Neutrophils Are Anti-Inflammatory Secondary to the Release of α-Defensins. *The Journal of Immunology.* 2009;183(3):2122-2132.

88. Brown KL, Poon GFT, Birkenhead D, Pena OM, Falsafi R, Dahlgren C, Karlsson A, Bylund J, Hancock REW, Johnson P. Host Defense Peptide LL-37 Selectively Reduces Proinflammatory Macrophage Responses. *The Journal of Immunology.* 2011;186(9):5497-5505.

89. Komatsu M, Waguri S, Ueno T, Iwata J, Murata S, Tanida I, Ezaki J, Mizushima N, Ohsumi Y, Uchiyama Y, Kominami E, Tanaka K, Chiba T. Impairment of starvation-induced and constitutive autophagy in Atg7-deficient mice. *The Journal of Cell Biology.* 2005;169(3):425-434.

90. Sanjuan MA, Dillon CP, Tait SWG, Moshiach S, Dorsey F, Connell S, Komatsu M, Tanaka K, Cleveland JL, Withoff S, Green DR. Toll-like receptor signalling in macrophages links the autophagy pathway to phagocytosis. *Nature.* 2007;450(7173):1253-1257.

91. Saitoh T, Akira S. Regulation of innate immune responses by autophagy-related proteins. *Journal of Cell Biology.* 2010;189(6):925-935.

92. Cuervo AM, Macian F. Autophagy, nutrition and immunology. *Molecular Aspects of Medicine.* 2012;33(1):2-13.

93. Kabeya Y, Mizushima N, Ueno T, Yamamoto A, Kirisako T, Noda T, Kominami E, Ohsumi Y, Yoshimori T. LC3, a mammalian homologue of yeast Apg8p, is localized in autophagosome membranes after processing. *The EMBO Journal.* 2000;19(21):5720-5728.

94. Kabeya Y, Mizushima N, Yamamoto A, Oshitani-Okamoto S, Ohsumi Y, Yoshimori T. LC3, GABARAP and GATE16 localize to autophagosomal membrane depending on form-II formation. *Journal of Cell Science.* 2004;117(13):2805-2812.

95. Cadwell K, Liu JY, Brown SL, Miyoshi H, Loh J, Lennerz JK, Kishi C, Kc W, Carrero JA, Hunt S, Stone CD, Brunt EM, Xavier RJ, Sleckman BP, Li E, Mizushima N, Stappenbeck TS, Virgin Iv HW. A key role for autophagy and the autophagy gene Atg16l1 in mouse and human intestinal Paneth cells. *Nature.* 2008;456(7219):259-263.

96. Choi AMK, Ryter SW, Levine B. Autophagy in Human Health and Disease. *New England Journal of Medicine.* 2013;368(7):651-662.

97. Barton GM. Viral recognition by Toll-like receptors. *Seminars in Immunology.* 2007;19(1):33-40.

98. Diebold SS, Kaisho T, Hemmi H, Akira S, Reis e Sousa C. Innate Antiviral Responses by Means of TLR7-Mediated Recognition of Single-Stranded RNA. *Science.* 2004;303(5663):1529-1531.

99. Heil F, Hemmi H, Hochrein H, Ampenberger F, Kirschning C, Akira S, Lipford G, Wagner H, Bauer S. Species-Specific Recognition of Single-

Stranded RNA via Toll-like Receptor 7 and 8. *Science.* 2004;303(5663):1526-1529.

100. Hiscott J, Kwon H, xE, nin P. Hostile takeovers: viral appropriation of the NF-kB pathway. *The Journal of Clinical Investigation.* 2001;107(2):143-151.

101. Hemmi H, Kaisho T, Takeuchi O, Sato S, Sanjo H, Hoshino K, Horiuchi T, Tomizawa H, Takeda K, Akira S. Small anti-viral compounds activate immune cells via the TLR7 MyD88-dependent signaling pathway. *Nature Immunology* Feb 2002;3(2):196-200.

102. Jurk M, Heil F, Vollmer J, Schetter C, Krieg AM, Wagner H, Lipford G, Bauer S. Human TLR7 or TLR8 independently confer responsiveness to the antiviral compound R848. *Nature Immunology.* 2002;3(6):499-499.

103. Marshak-Rothstein A. Toll-like receptors in systemic autoimmune disease. *Nature Reviews. Immunology.* 2006;6(11):823-835.

104. Consortium WTCC. Genome-wide association study of 14,000 cases of seven common diseases and 3,000 shared controls. *Nature.* 2007;447(7145):661-678.

105. Symmons DPM, Bankhead CR, Harrison BJ, Brennan P, Barrett EM, Scott DGI, Silman AJ. Blood transfusion, smoking, and obesity as risk factors for the development of rheumatoid arthritis - Results from a primary care-based incident case-control study in Norfolk, England. *Arthritis and Rheumatism.* 1997;40(11):1955-1961.

106. Ballanti E, Perricone C, di Muzio G, Kroegler B, Chimenti MS, Graceffa D, Perricone R. Role of the complement system in rheumatoid arthritis and

psoriatic arthritis: Relationship with anti-TNF inhibitors. *Autoimmunity Reviews.* 2011;10(10):617-623.

107. Feldmann M, Maini SRN. Role of cytokines in rheumatoid arthritis: an education in pathophysiology and therapeutics. *Immunological Reviews.* 2008;223(1):7-19.

108. Solomon S, Rajasekaran N, Jeisy-Walder E, Snapper SB, Illges H. A crucial role for macrophages in the pathology of K/B × N serum-induced arthritis. *European Journal of Immunology.* 2005;35(10):3064-3073.

109. Kim ND, Chou RC, Seung E, Tager AM, Luster AD. A unique requirement for the leukotriene B4 receptor BLT1 for neutrophil recruitment in inflammatory arthritis. *The Journal of Experimental Medicine.* April 17, 2006 2006;203(4):829-835.

110. Wipke BT, Allen PM. Essential Role of Neutrophils in the Initiation and Progression of a Murine Model of Rheumatoid Arthritis. *The Journal of Immunology.* 2001;167(3):1601-1608.

111. Adan N, Guzman-Morales J, Ledesma-Colunga MG, Perales-Canales SI, Quintanar-Stephano A, Lopez-Barrera F, Mendez I, Moreno-Carranza B, Triebel J, Binart N, Martinez de la Escalera G, Thebault S, Clapp C. Prolactin promotes cartilage survival and attenuates inflammation in inflammatory arthritis. *Journal of Clinical Investigation.* 2013;123(9):3902-3913.

112. Kim H-R, Kim K-W, Kim B-M, Jung HG, Cho M-L, Lee S-H. Reciprocal activation of CD4+T cells and synovial fibroblasts by SDF-1 promotes RANKL expression and osteoclastogenesis in rheumatoid arthritis. *Arthritis & Rheumatism.* 2013:n/a-n/a.

113. Feldmann M, Maini RN. Lasker Clinical Medical Research Award. TNF defined as a therapeutic target for rheumatoid arthritis and other autoimmune diseases. *Nature Medicine.* 2003;9(10):1245-1250.

114. Williams RO, Feldmann M, Maini RN. Anti-tumor necrosis factor ameliorates joint disease in murine collagen-induced arthritis. *Proceedings of the National Academy of Sciences.* 1992;89(20):9784-9788.

115. Shi J, Aono S, Lu W, Ouellette AJ, Hu X, Ji Y, Wang L, Lenz S, van Ginkel FW, Liles M, Dykstra C, Morrison EE, Elson CO. A Novel Role for Defensins in Intestinal Homeostasis: Regulation of IL-1β Secretion. *The Journal of Immunology.* 2007;179(2):1245-1253.

116. Haslett C, Guthrie LA, Kopaniak MM, Johnston RBJ, Henson PM. Modulation of Multiple Neutrophil Functions by Preparative Methods or Trace Concentrations of Bacterial Lipopolysaccharide. *American Journal of Pathology.* 1985;119:101-110.

117. Park EK, Jung HS, Yang HI, Yoo MC, Kim C, Kim KS. Optimized THP-1 differentiation is required for the detection of responses to weak stimuli. *Inflammation Research.* 2007;56(1):45-50.

118. Wu Z, Ericksen B, Tucker K, Lubkowski J, Lu W. Synthesis and characterization of human α-defensins 4-6. *The Journal of Peptide Research.* 2004;64(3):118-125.

119. Pace CN, Vajdos F, Fee L, Grimsley G, Gray T. How to measure and predict the molar absorption coefficient of a protein. *Protein Science.* 1995;4(11):2411-2423.

120. Lowry OH, Rosebrough NJ, Farr AL, Randall RJ. Protein Measurement with the Folin Phenol Reagent *Journal of Biological Chemistry.* 1951;193(1):265-275.

121. Potapova TA, Sivakumar S, Flynn JN, Li R, Gorbsky GJ. Mitotic progression becomes irreversible in prometaphase and collapses when Wee1 and Cdc25 are inhibited. *Molecular Biology of the Cell.* 2011;22(8):1191-1206.

122. Smith RWP, Anderson RC, Smith JWS, Brook M, Richardson WA, Gray NK. DAZAP1, an RNA-binding protein required for development and spermatogenesis, can regulate mRNA translation. *RNA.* 2011;17(7):1282-1295.

123. Gallie DR. The cap and poly(A) tail function synergistically to regulate mRNA translational efficiency. *Genes and Development.* 1991;5(11):2108 - 2116.

124. Park CB, Kim HS, Kim SC. Mechanism of Action of the Antimicrobial Peptide Buforin II: Buforin II Kills Microorganisms by Penetrating the Cell Membrane and Inhibiting Cellular Functions. *Biochemical and Biophysical Research Communications.* 1998;244(1):253-257.

125. Sladic RT, Lagnado CA, Bagley CJ, Goodall GJ. Human PABP binds AU-rich RNA via RNA-binding domains 3 and 4. *European Journal of Biochemistry.* 2004;271(2):450-457.

126. van Schadewijk A, van't Wout E, Stolk J, Hiemstra P. A quantitative method for detection of spliced X-box binding protein-1 (XBP1) mRNA as a measure of endoplasmic reticulum (ER) stress. *Cell Stress and Chaperones.* 2012;17(2):275-279.

127. Vandesompele J, De Preter K, Pattyn F, Poppe B, Van Roy N, De Paepe A, Speleman F. Accurate normalization of real-time quantitative RT-PCR data by geometric averaging of multiple internal control genes. *Genome Biology.* 2002;3(7).

128. Ganz T. Extracellular release of antimicrobial defensins by human polymorphonuclear leukocytes. *Infection and Immunity.* 1987;55(3):568-571.

129. Territo MC, Ganz T, Selsted ME, Lehrer R. Monocyte-chemotactic activity of defensins from human neutrophils. *The Journal of Clinical Investigation.* 1989;84(6):2017-2020.

130. Liu C-Y, Lin H-C, Yu C-T, Lin S-M, Lee K-Y, Chen H-C, Chou C-L, Huang C-D, Chou P-C, Liu W-T, Wang C-H, Kuo H-P. The concentration-dependent chemokine release and pro-apoptotic effects of neutrophil-derived α-defensin-1 on human bronchial and alveolar epithelial cells. *Life Sciences.* 2007;80(8):749-758.

131. Rodríguez-García M, Oliva H, Climent N, Escribese MM, García F, Moran TM, Gatell JM, Gallart T. Impact of α-defensins1–3 on the maturation and differentiation of human monocyte-derived DCs. Concentration-dependent opposite dual effects. *Clinical Immunology.* 2009;131(3):374-384.

132. Lichtenstein A, Ganz T, Selsted M, Lehrer R. In vitro tumor cell cytolysis mediated by peptide defensins of human and rabbit granulocytes. *Blood.* 1986;68(6):1407-1410.

133. Lichtenstein AK, Ganz T, Nguyen TM, Selsted ME, Lehrer RI. Mechanism of target cytolysis by peptide defensins. Target cell metabolic activities,

possibly involving endocytosis, are crucial for expression of cytotoxicity. *The Journal of Immunology.* 1988;140(8):2686-2694.

134. Soehnlein O, Kai-Larsen Y, Frithiof R, Sorensen OE, Kenne E, Scharffetter-Kochanek K, Eriksson EE, Herwald H, Agerberth B, Lindbom L. Neutrophil primary granule proteins HBP and HNP1–3 boost bacterial phagocytosis by human and murine macrophages. *The Journal of Clinical Investigation.* 2008;118(10):3491-3502.

135. Dean JLE, Sarsfield SJ, Tsounakou E, Saklatvala J. p38 Mitogen-activated Protein Kinase Stabilizes mRNAs That Contain Cyclooxygenase-2 and Tumor Necrosis Factor AU-rich Elements by Inhibiting Deadenylation. *Journal of Biological Chemistry.* 2003;278(41):39470-39476.

136. Tudor C, Marchese FP, Hitti E, Aubareda A, Rawlinson L, Gaestel M, Blackshear PJ, Clark AR, Saklatvala J, Dean JLE. The p38 MAPK pathway inhibits tristetraprolin-directed decay of interleukin-10 and pro-inflammatory mediator mRNAs in murine macrophages. *FEBS Letters.* 2009;583(12):1933-1938.

137. Kleeff J, Kornmann M, Sawhney H, Korc M. Actinomycin D induces apoptosis and inhibits growth of pancreatic cancer cells. *International Journal of Cancer.* 2000;86(3):399-407.

138. Rajabi M, de Leeuw E, Pazgier M, Li J, Lubkowski J, Lu W. The Conserved Salt Bridge in Human α-Defensin 5 Is Required for Its Precursor Processing and Proteolytic Stability. *Journal of Biological Chemistry.* 2008;283(31):21509-21518.

139. Khine AA, Del Sorbo L, Vaschetto R, Voglis S, Tullis E, Slutsky AS, Downey GP, Zhang H. Human neutrophil peptides induce interleukin-8 production through the P2Y6 signaling pathway. *Blood.* 2006;107(7):2936-2942.

140. Sakamoto N, Mukae H, Fujii T, Ishii H, Yoshioka S, Kakugawa T, Sugiyama K, Mizuta Y, Kadota J-i, Nakazato M, Kohno S. Differential effects of α- and β-defensin on cytokine production by cultured human bronchial epithelial cells. *American Journal of Physiology - Lung Cellular and Molecular Physiology.* 2005;288(3):L508-L513.

141. Ahn JK, Huang B, Bae E-K, Park E-J, Hwang J-W, Lee J, Koh E-M, Cha H-S. The role of α-defensin-1 and related signal transduction mechanisms in the production of IL-6, IL-8 and MMPs in rheumatoid fibroblast-like synoviocytes. *Rheumatology.* 2013;52(8):1368-1376.

142. Jackson RJ, Hellen CUT, Pestova TV. The mechanism of eukaryotic translation initiation and principles of its regulation. *Nature Reviews. Molecular Cell Biology.* 2010;11(2):113-127.

143. Cooper GM. *The Cell: A Molecular Approach. 2nd Edition*: Sunderland (MA): Sinauer Associates; 2000.

144. Eisner DA, Diaz ME, Li Y, O'Neill SC, Trafford AW. Stability and instability of regulation of intracellular calcium. *Experimental Physiology.* 2005;90(1):3-12.

145. Roy B, Li WW, Lee AS. Calcium-sensitive Transcriptional Activation of the Proximal CCAAT Regulatory Element of the grp78/BiP Promoter by the

Human Nuclear Factor CBF/NF-Y. *Journal of Biological Chemistry.* 1996;271(46):28995-29002.

146. Aoki T, Koike T, Nakano T, Shibahara K, Kondo S, Kikuchi H, Honjo T. Induction of Bip mRNA upon Programmed Cell Death of Differentiated PC12 Cells as Well as Rat Sympathetic Neurons. *Journal of Biochemistry.* 1997;121(1):122-127.

147. Rutkowski DT, Kaufman RJ. A trip to the ER: coping with stress. *Trends in cell biology.* 2004;14(1):20-28.

148. Yan W, Frank CL, Korth MJ, Sopher BL, Novoa I, Ron D, Katze MG. Control of PERK eIF2α kinase activity by the endoplasmic reticulum stress-induced molecular chaperone P58IPK. *Proceedings of the National Academy of Sciences.* 2002;99(25):15920-15925.

149. Ron D, Walter P. Signal integration in the endoplasmic reticulum unfolded protein response. *Nature Reviews. Molecular Cell Biology.* 2007;8(7):519-529.

150. Yoshida H, Matsui T, Yamamoto A, Okada T, Mori K. XBP1 mRNA Is Induced by ATF6 and Spliced by IRE1 in Response to ER Stress to Produce a Highly Active Transcription Factor. *Cell.* 2001;107(7):881-891.

151. Kagan BL, Selsted ME, Ganz T, Lehrer RI. Antimicrobial defensin peptides form voltage-dependent ion-permeable channels in planar lipid bilayer membranes. *Proceedings of the National Academy of Sciences.* 1990;87(1):210-214.

152. Nassar T, Akkawi Se, Bar-Shavit R, Haj-Yehia A, Bdeir K, Al-Mehdi A-B, Tarshis M, Higazi AA-R. Human α-defensin regulates smooth muscle cell

contraction: a role for low-density lipoprotein receptor–related protein/α2-macroglobulin receptor. *Blood.* 2002;100(12):4026-4032.

153. Proud CG. eIF2 and the control of cell physiology. *Seminars in Cell & Developmental Biology.* 2005;16(1):3-12.

154. Gao Y-d, Hanley PJ, Rinné S, Zuzarte M, Daut J. Calcium-activated K+ channel (KCa3.1) activity during Ca2+ store depletion and store-operated Ca2+ entry in human macrophages. *Cell Calcium.* 2010;48(1):19-27.

155. Hsu C-H, Chen C, Jou M-L, Lee AY-L, Lin Y-C, Yu Y-P, Huang W-T, Wu S-H. Structural and DNA-binding studies on the bovine antimicrobial peptide, indolicidin: evidence for multiple conformations involved in binding to membranes and DNA. *Nucleic Acids Research.* 2005;33(13):4053-4064.

156. Dever TE, Green R. The Elongation, Termination, and Recycling Phases of Translation in Eukaryotes. *Cold Spring Harbor Perspectives in Biology.* 2012;4(7).

157. Kieft J. The structure-based mechanism of translation initiation in bacteria and eukaryotes", in Steitz, T. (ed.), The Mechanisms of Ribosome Function: Insights into protein synthesis. *The Biomedical & Life Sciences Collection, Henry Stewart Talks Ltd, London.* 2008.

158. Warner JR, Knopf PM, Rich A. A Multiple Ribosomal Structure in Protein Synthesis *Proceedings of the National Academy of Sciences.* 1963;49(1):122-129.

159. Gu W, Kwon Y, Oko R, Hermo L, Hecht NB. Poly (A) binding protein is bound to both stored and polysomal mRNAs in the mammalian testis. *Molecular Reproduction and Development.* 1995;40(3):273-285.

160. Brogden KA. Antimicrobial peptides: pore formers or metabolic inhibitors in bacteria? *Nature Reviews. Microbiology.* 2005;3(3):238-250.

161. Ryder S, Recht M, Williamson J. Quantitative Analysis of Protein-RNA Interactions by Gel Mobility Shift. In: Lin R-J, ed. *RNA-Protein Interaction Protocols.* Vol 488: Humana Press; 2008:99-115.

162. Tan Z-J, Chen S-J. Salt Contribution to RNA Tertiary Structure Folding Stability. *Biophysical Journal.* 2011;101(1):176-187.

163. Bowman JC, Lenz TK, Hud NV, Williams LD. Cations in charge: magnesium ions in RNA folding and catalysis. *Current Opinion in Structural Biology.* 2012;22(3):262-272.

164. Melnikov S, Ben-Shem A, Garreau de Loubresse N, Jenner L, Yusupova G, Yusupov M. One core, two shells: bacterial and eukaryotic ribosomes. *Nature Structural & Molecular Biology* 2012;19(6):560-567.

165. Verschoor A, Srivastava S, Grassucci R, Frank J. Native 3D structure of eukaryotic 80s ribosome: morphological homology with E. coli 70S ribosome. *The Journal of Cell Biology.* 1996;133(3):495-505.

166. McCallum FS, Maden BEH. Human 18 S ribosomal RNA sequence inferred from DNA sequence. Variations in 18 S sequences and secondary modification patterns between vertebrates. . *Biochemical Journal.* 1985;232(3):725-733.

167. Gonzalez IL, Gorski JL, Campen TJ, Dorney DJ, Erickson JM, Sylvester JE, Schmickel RD. Variation among human 28S ribosomal RNA genes. *Proceedings of the National Academy of Sciences.* 1985;82(22):7666-7670.

168. Muller-McNicoll M, Neugebauer KM. How cells get the message: dynamic assembly and function of mRNA-protein complexes. *Nature Reviews Genetics.* 2013;14(4):275-287.

169. Paine PL, Moore LC. Nuclear envelope permeability. *Nature.* 1975;254(5496):109 -114.

170. Kim J, Izadyar A, Nioradze N, Amemiya S. Nanoscale Mechanism of Molecular Transport through the Nuclear Pore Complex As Studied by Scanning Electrochemical Microscopy. *Journal of the American Chemical Society.* 2013;135(6):2321-2329.

171. Adam SA, Marr RS, Gerace L. Nuclear protein import in permeabilized mammalian cells requires soluble cytoplasmic factors. *The Journal of Cell Biology.* 1990;111(3):807-816.

172. Mizushima N, Yoshimori T. How to Interpret LC3 Immunoblotting. *Autophagy.* 2007;3(6):542-545.

173. Thoreen CC, Kang SA, Chang JW, Liu Q, Zhang J, Gao Y, Reichling LJ, Sim T, Sabatini DM, Gray NS. An ATP-competitive Mammalian Target of Rapamycin Inhibitor Reveals Rapamycin-resistant Functions of mTORC1. *Journal of Biological Chemistry.* 2009;284(12):8023-8032.

174. Zou G, de Leeuw E, Li C, Pazgier M, Li C, Zeng P, Lu W-Y, Lubkowski J, Lu W. Toward Understanding the Cationicity of Defensins: ARG AND LYS VERSUS THEIR NONCODED ANALOGS. *Journal of Biological Chemistry.* 2007;282(27):19653-19665.

175. Jenssen H, Hamill P, Hancock REW. Peptide Antimicrobial Agents. *Clinical Microbiology Reviews.* 2006;19(3):491-511.

176. Calnan BJ, Tidor B, Biancalana S, Hudson D, Frankel AD. Arginine-Mediated RNA Recognition: The Arginine Fork. *Science.* 1991;252(5009):1167-1171.

177. Gordon GW, Berry G, Liang XH, Levine B, Herman B. Quantitative Fluorescence Resonance Energy Transfer Measurements Using Fluorescence Microscopy. *Biophysical Journal.* 1998;74(5):2702-2713.

178. Lamark T, Johansen T. Aggrephagy: Selective Disposal of Protein Aggregates by Macroautophagy. *International Journal of Cell Biology.* 2012;2012.

179. Scott MG, Vreugdenhil ACE, Buurman WA, Hancock REW, Gold MR. Cutting Edge: Cationic Antimicrobial Peptides Block the Binding of Lipopolysaccharide (LPS) to LPS Binding Protein. *The Journal of Immunology.* 2000;164(2):549-553.

180. Van Wetering S, Mannesse-Lazeroms SP, Dijkman JH, Hiemstra PS. Effect of neutrophil serine proteinases and defensins on lung epithelial cells: modulation of cytotoxicity and IL-8 production. *Journal of Leukocyte Biology.* 1997;62(2):217-226.

181. McKeown STW, Lundy FT, Nelson J, Lockhart D, Irwin CR, Cowan CG, Marley JJ. The cytotoxic effects of human neutrophil peptide-1 (HNP1) and lactoferrin on oral squamous cell carcinoma (OSCC) in vitro. *Oral Oncology.* 2006;42(7):685-690.

182. Panyutich AV, Panyutich EA, Krapivin VA, Baturevich EA, Ganz T. Plasma defensin concentrations are elevated in patients with septicemia or bacterial

meningitis *Journal of Laboratory and Clinical Medicine.* 1993;122(2):202-207.

183. Soong LB, Ganz T, Ellison A, Caughey GH. Purification and characterization of defensins from cystic fibrosis sputum. *Inflammation Research.* 1997;46(3):98-102.

184. Chou RC, Kim ND, Sadik CD, Seung E, Lan Y, Byrne MH, Haribabu B, Iwakura Y, Luster AD. Lipid-Cytokine-Chemokine Cascade Drives Neutrophil Recruitment in a Murine Model of Inflammatory Arthritis. *Immunity.* 2010;33(2):266-278.

185. Gómez-Reino J. Biologic monotherapy as initial treatment in patients with early rheumatoid arthritis. *Rheumatology.* 2012;51(suppl 5):v31-v37.

186. Pearce LR, Komander D, Alessi DR. The nuts and bolts of AGC protein kinases. *Nature Reviews. Molecular Cell Biology.* 2010;11(1):9-22.

187. Doller A, Huwiler A, Müller R, Radeke HH, Pfeilschifter J, Eberhardt W. Protein Kinase Cα-dependent Phosphorylation of the mRNA-stabilizing Factor HuR: Implications for Posttranscriptional Regulation of Cyclooxygenase-2. *Molecular Biology of the Cell.* 2007;18(6):2137-2148.

188. Li H, Park S, Kilburn B, Jelinek MA, Henschen-Edman A, Aswad DW, Stallcup MR, Laird-Offringa IA. Lipopolysaccharide-induced Methylation of HuR, an mRNA-stabilizing Protein, by CARM1. *Journal of Biological Chemistry.* 2002;277(47):44623-44630.

189. Chang TL, Vargas J, Jr., DelPortillo A, Klotman ME. Dual role of α-defensin-1 in anti–HIV-1 innate immunity. *The Journal of Clinical Investigation.* 2005;115(3):765-773.

190. Charp PA, Rice WG, Raynor RL, Reimund E, Kinkade Jr JM, Ganz T, Selsted ME, Lehrer RI, Kuo JF. Inhibition of protein kinase C by defensins, antibiotic peptides from human neutrophils. *Biochemical Pharmacology*. 1988;37(5):951-956.

191. Poggi A, Rubartelli A, Zocchi MR. Involvement of Dihydropyridine-sensitive Calcium Channels in Human Dendritic Cell Function: COMPETITION BY HIV-1 TAT. *Journal of Biological Chemistry*. 1998;273(13):7205-7209.